The Use of *In Vitro* Unbound Drug Fraction and Permeability in Predicting Central Nervous System Drug Penetration

A thesis submitted to the University of Manchester for the degree of Doctor of Philosophy (PhD) in the Faculty of Medical and Human Sciences

2010

Lucy Claudine Bentham

School of Pharmacy and Pharmaceutical Sciences

Contents

Total word count 70,927

List of Figures

Chapter 5: Species Comparison of Nonspecific Drug Binding in Blood and Brain Tissue

Chapter 6: The use of a Physiologically Based Pharmacokinetic Model of the Rat Central Nervous System to Predict Extent of Drug Penetration

List of Tables

Abbreviations

A-B	Apical to basolateral
ABC	Adenosine 5′-triphosphate binding cassette
ACM	Astrocyte-conditioned medium
AEBSF	4-(2-aminoethyl) benzenesulfonyl fluoride
ATP	Adenosine 5'- triphosphate
AUC	Area under the curve
B-A	Basolateral to apical
BBB	Blood-brain barrier
BCRP	Breast cancer resistance protein
BCSFB	Blood-cerebral spinal fluid barrier
bFGF	Basic fibroblastic growth factor
Br:Bl	Brain:blood concentration ratio
BSA	Bovine serum albumin
C	Celsius
Calcein-AM	Calcein acetoxymethyl ester
cAMP	Cyclic adenosine monophosphate
CAPS	*N*-cyclohexyl-3-aminopropanesulphonic acid
C_{blood}	Total blood concentration
C_{brain}	Total brain concentration
C_D	Concentration in donor compartment
C_d^{final}	Concentration in the donor compartment at end of the incubation period
CEC	Cerebral endothelial cell
CL	Clearance
cm	Centimetre
CNS	Central nervous system
CO_2	Carbon dioxide
CP	Choroid plexus
CPT-cAMP	Chlorophenylthio- cyclic adenosine monophosphate
C_R	Concentration in receiver compartment

C_r^{final}	Cumulative receiver concentration at end of the incubation period
CSF	Cerebral spinal fluid
C(t)	Average system concentration
C_u	Unbound concentration
$C_{u,blood}$	Unbound blood concentration
$C_{u,brain}$	Unbound brain concentration
$C_{u,total}$	Total concentration
C_0	Initial concentration in donor compartment
D	Dilution factor
Da	Daltons
DAPI	4, 6-diamidino-2-phenylindole
dc/dt	Change in receiver chamber concentration over time
DMEM	Dulbecco's modified eagle medium
DMPK	Drug metabolism and pharmacokinetics
DMSO	Dimethylsulfoxide
DNA	Deoxyribonucleic acid
DPBS	Dulbecco's phosphate buffered saline
°	Degree
EBM-2	Endothelial basal medium-2
EC	Endothelial cells
ECACC	European collection of animal cell cultures
EDTA	Potassium ethylenediaminetetraacetic acid
EGF	Epidermal growth factor
EMP1	Epithelial membrane protein
ER	Efflux ratio
EVOM	Ep/endothelial voltohmmeter
FBS	Foetal bovine serum
FITC	Fluorescein iso-thiocyanate
g	Gram
x g	Gravity
fu	Fraction unbound

fu_{CSF}	Fraction unbound cerebral spinal fluid
fu_{blood}	Fraction unbound in blood
fu_{brain}	Fraction unbound in brain
fu(apparent)	Measured fraction unbound of drug in diluted blood and brain homogenate
GDNF	Glial-derived neurotrophic factor
GSK	GlaxoSmithKline
h	Hour
hCMEC	Human cerebral microvascular endothelial cells
HBSS	Hank's buffered salt solution
HEPES	4-(2-hydroxyethyl)-1-piperazineethanesulfonic acid
HPLC	High-performance liquid chromatography
HTS	High throughput screening
H_2O	Water
IB4	Isolectin–B4
ICF	Intracellular fluid
IGF	Insulin-like growth factor
IgG	Immunoglobulin G
IMSERN	Institut National de la Santé et de la Recherche Médicale
IS	Internal standard
ISF	Interstitial fluid
IVS	Intravascular space
JAM	Junctional adhesion molecule
Kbb	*In vitro* brain:blood partition coefficient
Kg	Kilogram
K_p	Total brain to blood concentration ratio
$K_{p,uu}$	Unbound brain to unbound blood concentration ratio
l	Litre
LC-MS/MS	Liquid chromatography- Mass spectroscopy/mass spectroscopy
L-DOPA	L-3,4-dihydroxphenylalanine
L-15	Leibovitz-15 medium

mA	Milliamp
MDCK	Madin-Darby Canine Kidney
MDCKwt	Madin-Darby Canine Kidney wild type
MEM	Minimal Essential Medium
mg	Milligram
$MgCl_2$	Magnesium chloride
min	Minute
µl	Microlitre
ml	Millilitre
µM	Micromolar
mM	Millimolar
MRP	Multidrug resistance associated protein
MTT	Methylthiazolyldiphenyl-tetrazolium bromide **(**3-(4, 5-dimethylthiazol-2-yl)-2, 5-diphenyltetrazolium bromide,
MW	Molecular weight
MWCO	Molecular weight cut off
NaOH	Sodium hydroxide
NEAA	Non essential amino acids
nm	Nanometer
nmol	Nanomole
Ω	Ohm
P	*In situ* brain permeability product
P_{app}	Apparent permeability coefficient
PBEC	Porcine brain endothelial cell
PBPK	Physiologically based pharmacokinetic
PBS	Phosphate-buffered saline
PDGF	Platelet-derived growth factor
PDS	Plasma derived serum
PET	Positron emission tomography
P_{exact}	Exact permeability coefficient
P-gp	P-glycoprotein

PSA	Polar surface area
PS_{bbb}	Bi-directional permeability-surface area product at the blood-brain barrier
PS_{cp}	Bi-directional permeability-surface area product of the choroid epithelium of the choroid plexus
PSe_{bbb}	Efflux permeability-surface area product from blood-brain barrier to blood
PSe_{cp}	Efflux permeability-surface area product from choroid epithelium of the choroid plexus into the systemic circulation
PSe_{cp1}	Efflux PS area product type 1 (efflux from choroid epithelium of choroid plexus into the systemic circulation)
PSe_{cp2}	Efflux PS area product type 2 (efflux from choroid epithelium of the choroid plexus into CSF)
PVDF	Polyvinylidene fluoride
PXR	Pregnane X receptor
Q_{bbb}	Blood flow to the BBB
Q_{bf}	Bulk flow of ISF
Q_{cp}	Blood flow to the CP
$R_{cell\ monolayer}$	Resistance across Transwell® insert with cell monolayer
R_{filter}	Resistance across Transwell® insert without cell monolayer
RFU	Relative fluorescence units
RMT	Receptor mediated transcytosis
RNA	Ribonucleic acid
RO-20-1724	4-(3-Butoxy-4-methoxybenzyl)-2-imidazlidinone
rpm	Revolutions per minute
RT	Room temperature
s	Second
SDS	Sodium dodecyl sulphate
SDS-PAGE	Sodium dodecyl sulphate polyacrylamide
t	Time
T-25	25 cm^2 tissue culture flask

T-75	75 cm^2 tissue culture flask
T-175	175 cm^2 tissue culture flask
T-225	225 cm^2 tissue culture flask
TBS-T	Tris-buffered saline Tween 20
TEM	Transmission electron microscopy
TEMED	Tetramethylethylenediamine
TER	Transcellular electrical resistance
TGFß	Transforming growth factor-ß
TJ	Tight junctions
U	Units
UK	United Kingdom
V	Volts
v	Volume
V_d	Volume of distribution
V_D	Donor chamber volume
VEGF	Vascular endothelial growth factor
V_R	Receiver chamber volume
$V_{u,brain}$	Unbound volume of distribution in the brain
w	Weight
ZO	Zona-occluden

The University of Manchester
Lucy Claudine Bentham
Degree title: Doctor of Philosophy
19/08/2010
PhD Title: The Use of *In Vitro* Unbound Drug Fraction and Permeability in Predicting Central Nervous System Drug Penetration

Abstract

The permeation of drugs across the blood-brain barrier (BBB) is a prerequisite for central nervous system (CNS) drug penetration. The BBB, possessing efflux transporters and tight junctions, limits drug penetration to the brain. Consequently, the discovery of novel drugs to treat CNS diseases remains problematic and is lagging behind other therapeutic areas.

In vitro assays have progressed understanding of the factors that govern brain penetration. Central nervous system drug penetration is now thought to be modulated by three main processes, namely BBB permeability, active transport at the BBB and drug binding in blood and brain tissue. A more integrated approach to CNS drug discovery programmes is emerging which encompasses these processes in order to examine the rate and extent of drug brain penetration across species and improve predictions in human.

A primary porcine *in vitro* BBB model was developed and characterised for the prediction of CNS drug permeability *in vivo*. Characterisation confirmed that the model exhibited physiologically realistic cell architecture, the formation of tight junction protein complexes, transcellular electrical resistance consistently >2000 $\Omega.cm^2$, functional expression the P-gp efflux transporter and γ-glutamyl transpeptidase and alkaline phosphatase activities.

Transport of 12 centrally acting test drugs was investigated across four *in vitro* BBB models in order make comparisons between models and to generate *in vitro* permeability and efflux measurements. Blood-brain barrier permeability and active efflux processes are two major influences on the rate of drug penetration across the BBB.

Species differences in fu_{blood} and fu_{brain}, two prime influences on the extent of drug penetration, were investigated using equilibrium dialysis. Fraction unbound in brain was shown to be comparable across species suggesting that species differences in brain penetration could be due to variation in fu_{blood} for drugs that cross the BBB by passive diffusion, and/or species differences in transporter characteristics for drugs that are subject to active transport processes at the BBB.

An in-house hybrid-PBPK rat CNS model was used to predict calculated rat $K_{p,uu}$ using *in vitro* permeability, efflux, fu_{blood} and fu_{brain} parameters generated during this work. The predicted $K_{p,uu}$ generated using the rat CNS hybrid-PBPK model were within 3-fold of calculated $K_{p,uu}$. The rat CNS hybrid-PBPK model has potential use, as a tool for drug discovery scientists to aid the prediction of the extent of drug penetration in the early stages of drug discovery.

This work has demonstrated that *in vitro* permeability and unbound drug fraction can be used to predict CNS drug penetration.

Declaration

No portion of the work referred to in the thesis has been submitted in support of an application for another degree or qualification of this or any other university or other institute of learning.

Lucy Bentham

Copyright and Intellectual Property Rights

The Author

Lucy Bentham is a practicing pharmacist. She graduated from Cardiff University in 2004 with a Master of Pharmacy, first class honours. Following this she completed her pre-registration year at Wythenshawe Hospital, Manchester and became a member of the Royal Pharmaceutical Society in 2005. In order to gain competency in the profession, Lucy spent six months as a locum pharmacist in the community, followed by six months as a locum pharmacist in hospital, prior to commencing her PhD in 2006. Lucy was initially inspired to embark on a PhD after gaining an interest in drug delivery during her Masters research project, based on transdermal drug delivery. Consequently, a PhD based on central nervous system drug delivery was of great interest to her. Lucy has enjoyed locuming as a community pharmacist throughout her PhD and working part time as a hospital pharmacist during the write up period.

Acknowledgements

Writing a thesis is a very challenging and overwhelming experience. Writing this thesis would not have been made possible without the help and support from my supervisors, colleagues, family and friends.

I wish to thank my supervisors Professor Brian Houston, Dr Jeffrey Penny at the University of Manchester and Dr Phil Jeffrey and Dr Caroline Peet my supervisors at GSK for their expertise, advice, interesting feedback and encouragement. I would like to say a special thank you to Dr Caroline Peet (Cal) and Alex Peet for their generous hospitality during my stay with them whilst completing my placement at GSK in Harlow, Essex. I would also like to acknowledge Cal for her enthusiasm, meticulous and thorough eye, valuable suggestions, interesting discussions and continued support despite leaving GSK prior to the completion of this thesis. I would also like to acknowledge the funding from GlaxoSmithKline (GSK) that helped to make this thesis possible.

I am grateful for the support and fun times that I have shared with my fellow PhD students in 'Team Jeff' Angkana Saovapakhiran, Sergio Mares, Hayley McGlynn, Ben Staley, Louise Taylor, Kanin Rungsardthong and Bo Kangwantas. However, I owe my deepest gratitude to my fabulous friend Carina Cantrill (aka Dr C) for being a wonderful, understanding, inspiring and positive person, who always had time for me no matter how busy she was, in order to help and listen to PhD and personal problems and whom I also have shared many hilarious and fun times.

It is a pleasure to thank the people who have made this thesis possible by sharing their expertise, Dr Raj Badhan, Dr Alan Curry, Dr John McLaughlin, Dr Trudy Rodgers Dr Kaye Ogungbenro, Carol Marshall, Shiyam Mohamed, Adam Lucas, Lindsay Mulligan, Sue Murby and Gordon for his kind words and positivity

I am forever indebted to my parents for their love and kindness during my education from 1986-2010 and brother Max for always being so funny. My thanks and appreciation also goes to Gee Gee, Pa, Shooby, Ray, Aunty Lizzy and especially to my Uncle Leo for his time and incredible editorial input in proof reading my thesis.

I would like to thank Henry for his enduring patience, understanding, kindness and for caring for me when I needed a bit of help and also for all the printing and treats.

I want to express my warmest gratitude to my amazing friends and housemates for their insurmountable patience, respect for my commitment to my work and for being there on the bad days Kate (Kaaatie) and Solomon Bader. Also to my oldest friend Hannah for our weekly lunch/moan dates where we have put the world to rights. In addition, to all my girls who still invited me to every outing during my write up knowing that I would not be able come but just so that I didn't feel left out of the group. I promise we will definitely have that holiday very soon.

Lastly, but certainly not least I would like to thank Rita for her kind nature, listening to me and for her valuable help which removed so many pressures from my life.

For Mummy, Daddy and Max

Chapter 1
Introduction

1.0 Chapter 1: Introduction

1.1 Background

Central nervous system (CNS) diseases are prevalent, dramatically decrease quantity of life and can be fatal. It has been proposed by the World Health Organisation that CNS diseases account for 35% of the total disease burden in Europe (Olesen et al. 2003) with annual costs estimated at around £300 billion of which approximately £11 billion is spent on drug treatment (Andlin-Sobocki et al. 2005).

Currently, there are shortages of efficacious drugs to treat CNS diseases, for instance, Alzheimer's, Parkinson's and Huntington's disease, whereas many non-CNS diseases, for example, cardiovascular diseases can be controlled using drug treatment.

The incidence of CNS diseases increases with age and it has been predicted that by 2020 the number of people older than 65 years will increase by 50% (Pardridge 2007) highlighting an urgent need for more drugs to treat CNS disorders.

Development times for CNS drugs (12-16 years) are significantly longer, compared to those for non-CNS drugs (10-12 years) (Palmer et al. 2005) and success rates of CNS drugs candidates (~8%) are much lower than most other therapeutic areas such as cardiovascular disease (~20%) (Kola et al. 2004). Despite immense endeavour from the pharmaceutical industry to discover and develop novel CNS active drugs to meet the current demand, attrition rates still remain higher than in any other therapeutic area (Pangalos et al. 2007).

Successful CNS drug disposition is hindered by the complex anatomy, physiology and disease pathology of the brain (Abbott 2005) and also by the high degree of protection afforded to the brain via the blood-brain barrier (BBB) (Begley et al. 2003). The effect of disease on the integrity of the BBB, transporter function and expression is relatively unknown (Palmer 2009) and consequently clinical symptoms are often used for diagnosis instead of disease mechanisms.

The use of *in vitro* assays has aided understanding of the factors that govern brain penetration. Central nervous system drug penetration is now thought to be modulated by three main processes; BBB permeability, active transport at the BBB and drug binding in blood and brain tissue (Jeffrey et al. 2010). A more integrated approach to CNS drug discovery programmes is now emerging which encompasses these processes in order to examine the rate

and extent of drug brain penetration across species and improve predictions in humans (Hammarlund-Udenaes et al. 2008; Reichel 2009).

In vitro assays are routinely employed to screen and eliminate compounds prior to *in vivo* studies helping to reduce attrition rates (Jeffrey et al. 2007). However, most *in vitro* and *in vivo* assays to date have been rodent based, due to difficulties in obtaining human measurements, thus impeding human predictions.

Drug metabolism and pharmacokinetics have become an important predictive tool for use in drug discovery (Summerfield et al. 2006). The ability to more accurately predict drug penetration across the BBB is integral to aiding drug discovery and development. Therefore, a physiologically based pharmacokinetic model (PBPK) of the CNS to predict the extent of drug brain penetration in the early stages of drug discovery is highly desirable. This would reduce cost, decrease time from drug discovery through development to the market, and most importantly lead to more successful treatments for patients with CNS disorders.

1.2 The blood-brain barrier

1.2.1 History of the blood-brain barrier

Studies performed by German microbiologist Paul Ehrlich in 1885 (Ehrlich 1885; Pardridge 1983) initially introduced the concept of a barrier existing between the blood and brain. Injecting a vital dye systemically into laboratory animals revealed uptake of the dye in all parts of the body except the CNS. Ehrlich interpreted these findings as lack of adsorption of the dye in the CNS. In 1909 Edwin Goldman (Ehrlich's student) demonstrated adsorption of a vital dye by the CNS via direct injection into the tissue, whilst the rest of the body remained unstained. Subsequently Goldmann concluded the existence of a blood-brain barrier (Goldmann 1913).

1.2.2 Protection of the brain

The brain is the control centre of the body. It regulates functions vital for life, for example, the control of muscles such as the heart, respiration and hormone production. Neuronal cell division is limited in adult brains (Lennington et al. 2003) and cell death causes neurodegeneration and neuropathological diseases. A high level of protection of the brain is therefore crucial for human survival.

The CNS is protected by three physiological barriers; the BBB, the blood-cerebrospinal fluid barrier formed by the epithelial cells of the choroid plexus, and the arachnoid epithelium of the meninges which forms an avascular barrier between the extracellular fluids of the CNS and the rest of the body (Abbott et al. 2006).

The BBB has the largest surface area of all three interfaces (9-15 $m^2.kg^{-1}$ brain) (Abbott 2005), creating an extremely high density capillary network throughout the brain parenchyma, providing almost every neurone with an individual blood supply (Reichel 2009). Hence, the BBB is considered to be the primary interface of the brain and forms the focus of this research.

The BBB controls the transport of material into and out of the brain, and maintains the neural microenvironment required for optimum synapse signalling (Abbott 2002). The BBB protects the brain from potentially neurotoxic, physiological metabolites, peripheral neurotransmitters (e.g. glutamate) (Abbott 2002), xenobiotics from diet or environment (Begley et al. 2003) and pathogens (Wolburg et al. 2002). The BBB also permits the entry of nutrients such as glucose via specific influx transporters (Abbott 2005) and allows the free diffusion of small molecules, such as oxygen and carbon dioxide and the exit of waste products (Ballabh et al. 2004).

1.2.3 Physiology of the blood-brain barrier

The BBB (Figure 1.1) consists of a continuous monolayer of cerebral endothelial cells (CECs) that compose the walls of the cerebral microvascular capillaries present throughout the brain parenchyma. In addition to CECs, neighbouring cells namely astrocytes, pericytes and neurones, as well as a capillary-secreted basement membrane constitute the functional unit of the BBB and in combination are often referred to as the neurovascular unit.

The CECs are highly specialised for their protective barrier function and are characterised by:-

- Tight junctions (*zonulae occludentes*) between adjacent CECs creating a restrictive paracellular pathway (Reese et al. 1967).
- Sparse pinocytotic vesicular transport which limits fluid phase uptake (Bauer et al. 2000).
- The absence of fenestrations (Gaillard et al. 2005).
- Numerous influx and efflux transporters (Abbott et al. 2009)
- High density of mitochondria in the cytosol (de Vries et al. 1997).
- The presence of protective enzymes, for example, cytochrome P450 (Dauchy et al. 2009) and monoamine oxidase (Abbott 2002).

These specific features distinguish CECs from peripheral endothelial cells found in the rest of the body, and describe the term 'BBB phenotype'.

Figure 1.1 The blood-brain barrier

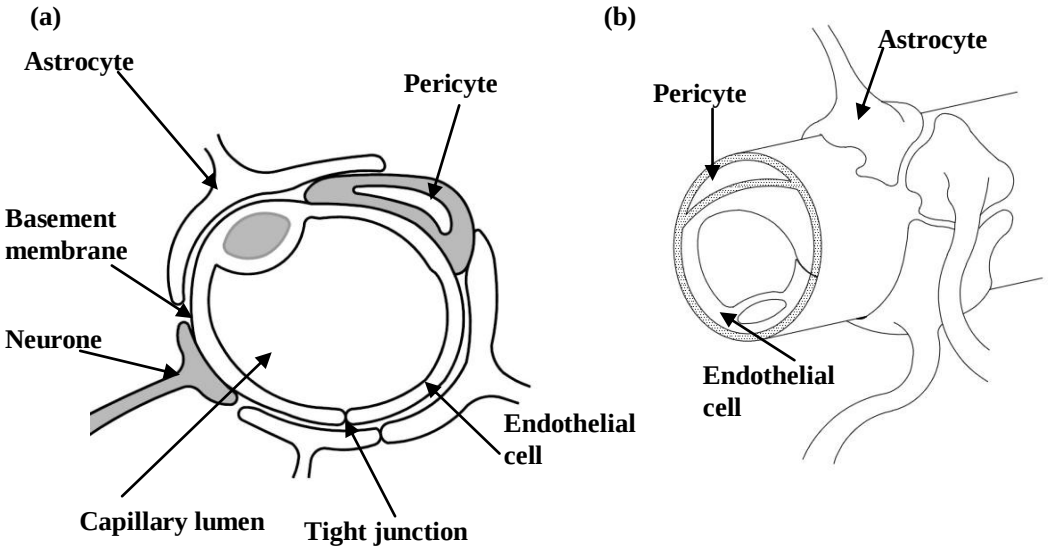

(a) Cross section of the neurovascular unit of the BBB formed by cerebral endothelial cells, astrocytes, pericytes, neurones and a basement membrane. The cerebral endothelial cells form tight junctions at their boundaries. Adapted from (Abbott et al. 2008) (b) Three dimension schematic of the BBB components, CECs, astrocytes and pericytes. Adapted from (Abbott et al. 2008).

1.2.3.1 The role of astrocytes at the blood-brain barrier

Astrocytes, located within the brain parenchyma, have end foot processes which surround the CECs (Kacem et al. 1998) and play an important role in the induction of the 'BBB phenotype' (Janzer et al. 1987). In 1981, Stewart and Wiley (Stewart et al. 1981) transplanted brain tissue from quail embryos into the gut of chick embryos. The brain tissue became vascularised by chick endothelial cells and the capillaries formed were reported to exhibit BBB properties. However, when the experiment was reversed and avascular tissue from embryonic quail gut was transplanted into embryonic chick brain, the chick endothelial vessels which invaded the quail gut tissue grafts were found to be permeable. This suggested that the barrier properties of the BBB were not intrinsic to CECs, although, it was not concluded which other cells were responsible. A continuation of this work (Janzer et al. 1987) which involved transplanting neonatal rat brain astrocytes into the rat eye and chick placenta provided evidence that astrocytes contributed to the formation of non-leaky junctions between endothelial cells from origins other than the CNS, strongly suggesting induction of tight junction properties and improved barrier function of the BBB.

1.2.3.2 The role of pericytes at the blood-brain barrier

Pericytes are multifunctional perivascular cells morphologically situated closest to CECs sharing a basement membrane (Correale et al. 2009). The role of pericytes at the BBB is still being elucidated.

Pericytes are thought to provide mechanical stability to CECs (von Tell et al. 2006). Pericytes may also aid regulation of capillary blood flow, expression of the smooth muscle isoform of actin (α-SM actin, a contractile protein), has been found in pericytes but no expression has been found in CECs (Bandopadhyay et al. 2001). In addition, pericytes are thought to play a regulatory role in the formation of new cerebral blood vessels during the initiation, proliferation, differentiation and branching out of the vessels (Smith et al. 2006). Further, platelet-derived growth factor produced by CECs is thought to aid the association of pericytes to CECs, and studies using platelet-derived growth factor knock out mice have reported increased BBB permeability and edematous phenotype, which was suggested to be caused through the absence of pericytes (Hellstrom et al. 2001). Additionally, the up regulation of the tight junction protein occludin has been demonstrated using *in vitro* BBB

models cultured with pericyte-conditioned medium, suggesting that pericytes play a role in the formation of a restrictive paracellular properties of the BBB (Hori et al. 2004).

1.2.3.3 The role of neurones at the blood-brain barrier

There is currently little in-depth understanding of the role of neurones in the formation of the BBB phenotype (Cardoso et al. 2010). Neurones are electrically excitable cells that play a role in the induction and regulation of BBB properties by electrical and chemical signalling (Bauer et al. 2000). Cerebral endothelial cells cultured with cortical neurones have been shown to increase the expression of the BBB marker enzyme γ-glutamyl transpeptidase demonstrating that neurones can induce BBB properties (Tontsch et al. 1991). However, the BBB plays a reciprocal role in maintaining the neural microenvironment which is required for optimum synapse signalling.

1.2.3.4 The role of the basement membrane at the blood-brain barrier

The basement membrane is composed of collagen type IV, heparan sulphate, fibronectin and laminin (Scherrmann 2002) and connects the CECs with astrocytes, pericytes and neurones, constituting an essential part of the BBB. The basement membrane supports the CECs, and is thought to influence drug transport as some of its components form a negatively charged interface, discriminating against negatively charged molecules (Vorbrodt 1989).

1.2.4 Protective functions of the blood-brain barrier

1.2.4.1 The physical element of the blood-brain barrier– tight junction proteins

Tracer experiments with the electron dense probe horseradish peroxidase (Reese et al. 1967) first revealed that CECs formed a restrictive barrier between the blood and the brain due to the presence of tight junctions between adjacent CECs.

Tight junctions are the main physical barrier component of the BBB restricting paracellular penetration of ions, polar solutes and macromolecules from blood to brain. The restriction of ion transport results in high transcellular electrical resistance (TER) across the BBB *in vivo* >1000 $\Omega.cm^2$ (Crone et al. 1982; Butt et al. 1990).

Over recent years, significant advances have been made in understanding the formation of tight junctions (Figure 1.2) and the identification of their individual components. Tight

junctions are composed of three integral transmembrane proteins, occludin (Furuse et al. 1993), claudins (Furuse et al. 1998) and junction adhesion molecules (JAM) (Martin-Padura et al. 1998). Occludin, claudin and JAM possess extracellular domains responsible for limiting paracellular permeability and intracellular domains which form a junctional complex with cytoplasmic proteins such as ZO-1 (Martin-Padura et al. 1998), ZO-2 (Gumbiner et al. 1991), ZO-3 (Haskins et al. 1998) and cingulin (Citi et al. 1988) which connect the integral membrane proteins to actin within the cytoskeleton.

Most recently, a novel tight junction protein, called epithelial membrane protein (EMP1) has been discovered at the BBB (Bangsow et al. 2008). Epithelial membrane protein 1 is structurally similar to occludin and claudin, and is thought to play a role in the formation of the tight junction between adjacent endothelial cells and limit paracellular permeability across the BBB.

Figure 1.2 Composition of a tight junction between two adjacent cerebral endothelial cells

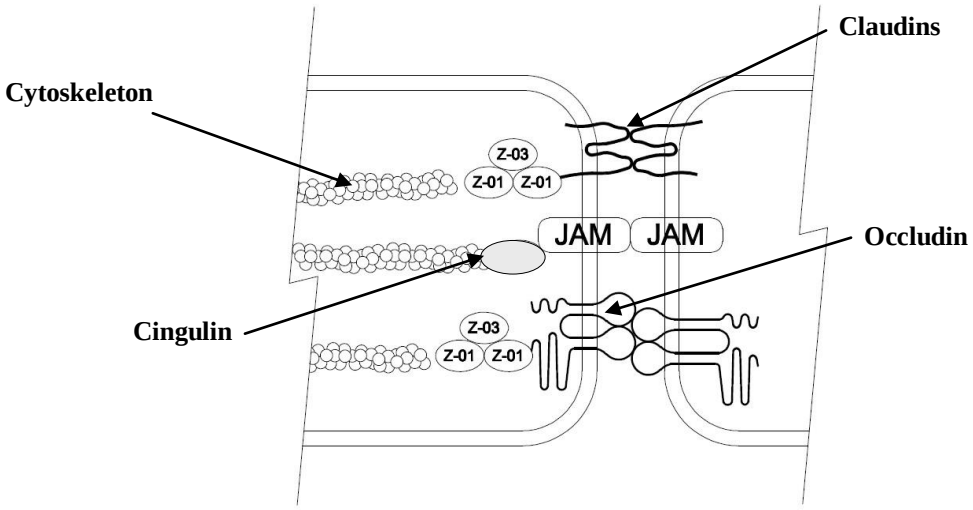

The tight junction between two adjacent CECs is composed of integral membrane proteins occludin, claudin and JAM forming a complex with ZO-1, ZO-2, ZO-3 and cingulin which are connected to actin within the cytoskeleton. The tight junctional complex limits paracellular transport of molecules across the BBB. Adapted from (Abbott et al. 2009).

1.2.4.2 Adenosine 5'-triphosphate binding cassette transporters at the blood-brain barrier

In addition to tight junctions, the BBB possess adenosine 5′-triphosphate (ATP) binding cassette (ABC) efflux transporters, situated in the cell membrane of CECs. These ABC efflux transporters serve as an additional defence mechanism of the brain, excluding harmful lipophilic substances (Abbott 2005). Adenosine 5′-triphosphate binding cassette efflux transporters have broad substrate specificity and can limit efficacy of novel CNS active drugs because potential drug candidates are often substrates of these efflux transporters (Potschka 2009). Previously, drug discovery programmes have increased the lipophilicity of novel compounds in an attempt to enhance BBB permeation. However, this has not always proven successful as this strategy can also increase the chance of the compound becoming a substrate of an efflux transporter (Abbott et al. 2009), hence limiting brain penetration.

Adenosine 5′-triphosphate binding cassette efflux transporters are a superfamily of multidomain integral membrane proteins classified into seven sub families, *ABCA-ABCG* (Dean et al. 2001), that can transport solutes across cell membranes. P-glycoprotein (P-gp, ABCB1), multidrug resistance-associated proteins (MRPs, *ABCC1, 2, 4, 5* and possibly *3* and *6*) and breast cancer resistance protein (BCRP, *ABCG2*) are currently thought to be the principle efflux transporters at the BBB (Begley 2004; Dauchy et al. 2008). The mechanism of action of ABC efflux transporters involves the binding of a substrate molecule to two transmembrane domains of the ABC efflux transporter molecule. This stimulates binding of ATP to two cytosolic nucleotide-binding domains. Adenosine 5′-triphosphate is consequently hydrolysed providing energy to translocate the substrate across the membrane (Linton 2007). To date, the impact of ABC efflux transporters in relation to drug disposition in the brain is still being elucidated (Ward 2008; Potschka 2009).

Good knowledge and understanding of ABC efflux transporters is extremely useful during drug discovery and development because efflux transporters can reduce brain penetration (Dorner et al. 2009) of drugs which are substrates of efflux transporters. Additionally, over expression of efflux transporters at the BBB can lead to drug resistance in some CNS disorders including depression and epilepsy (Bauer et al. 2010). Induction or inhibition of efflux transporters at the BBB by one drug can alter the pharmacokinetics and efficacy of another drug resulting a drug-drug interaction (Zhou 2008).

1.2.4.2.1 P-glycoprotein (*ABCB1*)

P-glycoprotein was the first ABC efflux transporter to be discovered in 1976 (Juliano et al. 1976). P-glycoprotein is a phosphorylated glycoprotein of 170 kDa encoded by the human multidrug resistance gene (*MDR1* also known as *ABCB1*) and was originally discovered with the occurrence of multidrug resistant tumours (Juliano et al. 1976; Kartner et al. 1983). P-glycoprotein is also expressed in various non-malignant human tissues including placenta, kidney and intestine (Zhou 2008) and was the first ABC transporter to be detected in CECs of the human BBB in 1989 (Cordon-Cardo et al. 1989; Thiebaut et al. 1989).

P-glycoprotein excludes drugs from the brain by either preventing molecules from entering the brain from the systemic circulation (gatekeeper function) or by effluxion of drugs that have entered the CECs, back out into the lumen of the capillary (Demeule et al. 2002; Hammarlund-Udenaes et al. 2008).

P-glycoprotein is currently deemed the most understood and clinically relevant ABC efflux transporter at the BBB in drug discovery programmes due to its wide range of substrates (Schinkel 1999) varying in size (range from 300 - 4000 Da) and structure (Miller et al. 2008) which makes it difficult to define accurate structure activity relationships for P-gp. Identification of the structural features of typical P-gp substrates could be a useful tool for drug development scientists during lead optimisation, in order to obtain the desired interaction of the drug with the efflux transporter for example no interaction, inhibition or interaction (non-CNS drugs) (Zhou 2008).

In vivo studies comparing brain penetration of drugs in genetically modified knock out mice and wild type mice have demonstrated that P-gp at the BBB can limit brain penetration of drugs, which are substrates of this efflux transporter, highlighting the importance of P-gp at the BBB (Doran et al. 2005).

Brain uptake of P-gp substrates in humans has been investigated using positron emission tomography (PET) using the P-gp substrate radiotracer ^{11}C-N-*desmethyl*-loperamide, (Kreisl et al. 2010). The study showed low brain uptake of ^{11}C-N-*desmethyl*-loperamide. However, brain uptake was increased 4-fold when a sufficient dose of the P-gp inhibitor tariquidar (6 mg.kg^{-1}) was co-administered with ^{11}C-N-*desmethyl*-loperamide demonstrating that P-gp can limit brain uptake of P-gp substrates in humans.

Up regulation of P-gp can occur in response to drug treatment (for example phenobarbital (Volk et al. 2005), hence reducing efficacy of drug therapy. A P-gp substrate (unnamed) labeled with ^{11}C has recently shown potential to detect upregulation of P-gp function, using PET, in response to drug treatment (van Waarde et al. 2009) allowing further investigation into P-gp function and expression in relation to CNS diseases.

Positron emission tomography has emerged as a useful non-invasive *in vivo* tool to aid understanding of the role P-gp at the BBB. Positron emission tomography has potential application for *in vivo* assays employed in drug discovery programmes after high throughput *in vitro* screening assays in order to investigate the affinity of novel drugs for P-gp at the BBB in humans (Elsinga et al. 2005).

The literature has highlighted the importance of P-gp at the BBB in respect to drug penetration. Hence, the P-gp efflux transporter is the ABC efflux transporter of interest during this study.

1.2.4.2.2 Multidrug resistance-associated protein (*ABCC*)

Multidrug resistance-associated protein was first discovered in the human lung cancer cell line, H69AR (Cole et al. 1992). Multidrug resistance-associated protein is expressed in the intestine, kidney, liver and at the BBB (Liu et al. 2010). At the BBB MRP is principally expressed at the basolateral membrane (Soontornmalai et al. 2006). Expression of MRP has been reported in isolated CECs from a range of species for example, rat (Regina et al. 1998), porcine (Zhang et al. 2006; Smith et al. 2007) bovine (Bachmeier et al. 2006), and humans, where it has been shown to limit drug penetration (Potschka et al. 2003).

1.2.4.2.3 Breast cancer resistance protein (*ABCG2*)

The ABC transporter BCRP was recently discovered on the apical membrane of a multidrug resistance breast cancer cell line (Doyle et al. 1998). Breast cancer resistance protein has also been detected on the apical membrane of human CECs (Cooray et al. 2002). The development of *Abcg2*$^{-/-}$ knock out mice have demonstrated how BCRP limits drug brain penetration at the BBB (Vlaming et al. 2009).

1.2.4.3 The enzymatic element of the blood-brain barrier

In addition to the metabolism of drugs in the liver, further metabolism may take place at the BBB. The presence of enzymes expressed on the plasma membrane of the CECs forming the BBB (Joo 1993) constitute the protective metabolic element of the 'BBB phenotype' limiting penetration of exogenous and endogenous substrates (El-Bacha et al. 1999).

The presence of metabolising enzymes at the BBB, for example phase 1 cytochrome P450 enzymes (Dauchy et al. 2009), may also limit drug penetration to the brain. The presence of cytochrome P450 enzymes have been characterised in the hCMEC/D3 cell line and human brain microvessels (Dauchy et al. 2009). The hCMEC/D3 cell line expressed genes encoding for cytochrome P450 isoforms including CYP2U1 and CYP2S1 which showed the strongest expression. The genes of the other isoforms were either weakly expressed (6 isoforms) or barely detectable (4 isoforms). Expression of 11 of the 12 genes encoding isoforms expressed in the hCMEC/D3 cell line were also expressed in the human brain microvessels and included CYP2U1 and CYP2S1, however their role in drug metabolism remains to be elucidated.

Genes for 16 cytochrome P450 isoforms were also detected in human CECs isolated from healthy human brains including genes that encoded for CYP1A1, CYP1B1 and CYP3A4 (Ghosh et al. 2010). The expression of 11 of these genes, including CYP3A4, known to metabolise antiepileptic drugs, was significantly increased in human CECs isolated from brains of drug–resistant epileptic patients, compared to human CECs isolated from healthy human brains.

Other metabolising enzymes, including monoamine oxidases, which have been shown to metabolise the antidepressant citalopram (Kosel et al. 2001), have also been characterised at the human BBB (Kalaria et al. 1987).

1.3 Drug transport across the blood-brain barrier

Drugs are transported across the BBB via two routes namely the paracellular route and the transcellular route (Figure 1.3). The paracellular route is highly restrictive due to the presence of tight junctions between adjacent CECs which prevent the penetration of even relatively small polar compounds, for example nutrients such as glucose and amino acids, across the

BBB. The dominant route of drug transport across the BBB is via the transendothelial route which involves the following processes:-

1. Passive diffusion
2. Receptor-mediated transcytosis
3. Adsorptive mediated transcytosis
4. Carrier mediated influx

Figure 1.3 Routes of drug transport cross the blood-brain barrier

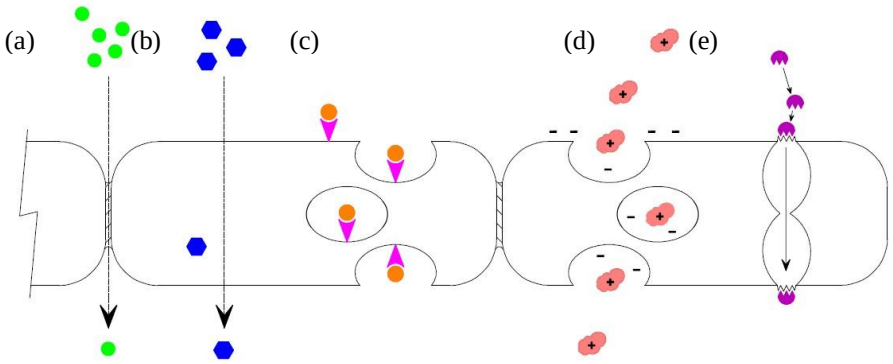

(a) Paracellular route, drugs permeate the BBB between adjacent CECs of BBB. (b) Passive diffusion of drugs through the CECs from the blood into the brain. (c) Receptor-mediated transcytosis involving specific interaction of the drug at a receptor on the cell membrane triggering internalisation of the extracellular material and drug and transportation of it across the CECs (d) Adsorptive medium transcytosis, cationic drugs bind to the negatively charged glycocalyx on the cell surface inducing internalisation and transfer of drug across the cell (e) Carrier medium influx transporters transport drugs across the CECs from the blood into the brain. Adapted from (Begley et al. 2003).

Drugs can passively diffuse from the polar environment of the blood directly through the CECs into the brain. Physicochemical drug properties can be related to the ability of a drug to passively permeate the BBB, although these properties are not always indicative of CNS penetration (e.g. drugs that are substrates of efflux transporters may still be excluded from the CNS). A general trend between lipophilicity and CNS drug penetration exists where the rate of BBB penetration increases with increasing lipophilicity of the drug (Levin 1980; Liu et al. 2004; Summerfield et al. 2006; Summerfield et al. 2007). However, optimum lipophilicity has been shown to correspond to a logD of approximately 2-3 (van de Waterbeemd et al. 2001; Summerfield et al. 2007).

Other physiochemical properties of drugs that are considered optimum for passive drug diffusion across the BBB are a MW <400-600 (Pardridge 1998), polar surface area (PSA) <70 $Å^2$ (Kelder et al. 1999) and formation of <6 hydrogen bonds with water (Pardridge 1998). Basic drugs passively diffuse across the BBB more easily than acidic drugs because bases are cationic and interact with negatively charged glycocalyx and the phospholipid heads of the cerebral cell membranes (Abbott et al. 2009).

Transcytosis is the main route of transport across the BBB for drugs with large molecular weight such as proteins like insulin (Banks 1999). Transcytosis is a process that involves the invagination of the cell membrane which forms a free vesicle that internalises both extracellular fluid and drug molecules. The free vesicle then travels through the cell where it fuses with the opposite membrane and releases the contents (Begley et al. 2003). Receptor-mediated transcytosis involves a specific interaction of the drug at a receptor on the cell membrane which triggers internalisation of the extracellular material and drug and transports them across the CECs (Smith et al. 2006). Adsorptive-mediated transcytosis is a less specific process where a cationic drug binds to the negatively charged glycocalyx on the cell surface inducing internalisation and transfer of drug across the CEC into the brain (Abbott et al. 2009).

Essential polar nutrients such as glucose and amino acids are unable to passively diffuse across the BBB into the CNS. More than 20 specific solute carriers for a range of different solutes have now been identified at the BBB (Zhang et al. 2002). For example, the glucose transporter, large neutral amino acid transporter and organic cation transporters (Abbott et al. 2009). Transporters may be located on either the apical or basolateral membrane or both, meaning that solutes may be transported across the CECs from the blood to the brain or from the brain to the blood. Carrier mediated transport may be utilised for drug delivery for example L-DOPA and gabapentin which are substrates for the large neutral amino acid transporter and lidocaine, imipramine and propranolol which are substrates for the cationic transporter (OCT) (Begley 2004).

1.4 Methods for studying central nervous system brain penetration

Numerous *in vitro* and *in vivo* models and techniques exist to study brain penetration. The main *in vitro* and *in vivo* techniques commonly applied in CNS drug discovery are discussed below.

1.4.1 *In vitro* blood-brain barrier models for studying blood-brain barrier penetration

Since the discovery of the BBB around 100 years ago (Goldmann 1913), its permeability function has been the main focus of BBB research. A variety of *in vitro* BBB models from a range of species cell types and tissues have been employed since the 1970s generating vast amounts of literature within this field and making comparisons between different models extremely difficult. Currently, there is no single *in vitro* BBB model that is considered to be the 'gold standard'.

The main aims of a valid *in vitro* BBB model are to mimic the BBB *in vivo* and predict *in vivo* permeability. The model should display *in vivo* BBB characteristics such as similar cell architecture, tight junctions forming a restrictive paracellular pathway, reproducible solute permeability, functional expression of key transporters, such as P-gp, and expression of BBB marker enzymes, for example alkaline phosphatase and γ-glutamyl transpeptidase (Gumbleton et al. 2001). Additionally, the model should be low cost, allow ease of culture and high throughput screening (Gumbleton et al. 2001). *In vitro* BBB models carry some advantages over *in vivo* BBB models, in that they permit the examination of the BBB in isolation, can eliminate compounds prior to *in vivo* studies thereby reducing animal experimentation and are more cost effective.

In general, *in vitro* BBB models consist of a confluent monolayer of cells grown on a filter representing the CECs of the *in vivo* BBB. Either side of the cell monolayer is a buffer filled compartment, one representing the blood (apical) and the other representing the brain (basolateral) (Figure 1.4). *In vitro* studies are performed to measure the rate of drug transport from the apical (A) compartment across the cell monolayer into the basolateral (B) compartment and *vice versa*.

Apparent permeability (P_{app} Equation 1.1) is the traditional measure of rate of drug transport across an *in vitro* BBB model. Equation 1.1 is accurate when drug transport is linear over time, <10% of the drug is transported across the cell monolayer, there is inappreciable

backflow and good mass balance (Youdim et al. 2003). More recently, an alternative measurement of permeability, called exact permeability, has been derived (P_{exact} Equation 1.2a and 1.2b) (Tran et al. 2004). The exact permeability measurement is thought to provide a more accurate measure of rate of drug transport because it provides a mathematical solution for the whole transport curve not just the linear phase unlike the apparent permeability solution. Additionally, the exact permeability solution can be applied when >10% of the drug is transported across the cell monolayer and when there are mass balance problems. Both apparent and exact permeability solutions were used in this work in order to make comparisons between the two solutions.

$$P_{app}(cm.s^{-1}) = (dc/dt).(V/AC_0)$$ Equation 1.1

dc/dt = Change in receiver compartment concentration over time (mol.l^{-1}.s^{-1})

V = Volume in the receiver compartment (cm^3)

A = Surface area of Transwell® insert (cm^2)

C_0 = Initial concentration in the donor compartment (mol.l^{-1})

$$P = -\left(\frac{V_R V_D}{(V_R + V_D)At}\right)\ln\left\{1 - \frac{\langle C_R(t)\rangle}{\langle C(t)\rangle}\right\}$$

Equation 1.2a

V_D = Donor compartment volume (cm^3)

V_R = Receiver compartment volume (cm^3)

A = Surface area of the permeability barrier (cm^2)

t = Time of measurement (s)

C_R = Drug concentration in the receiver compartment (mol.l^{-1}) at time t

$\langle C(t)\rangle$ = Average system concentration of drug defined by Equation 1.2b

$$\langle C(t)\rangle = \frac{V_D C_D(t) + V_R C_R(t)}{V_D + V_R}$$

Equation 1.2b

C_D = Drug concentration in the donor compartment (mol.l^{-1}) at time t

The rate of drug transport is often determined from both the apical to the basolateral compartment and from the basolateral to the apical compartments in order to determine an efflux ratio (ER) (B-A/A-B) for the drug. These studies are also performed with a potent transporter inhibitor, for example the P-gp inhibitor GF120918. For a drug with a high efflux ratio, if the efflux ratio returns to unity in the presence of the inhibitor, it is likely that the efflux observed without the inhibitor is due to the efflux transporter P-gp and hence the drug could be a substrate of P-gp.

Figure 1.4 Schematic of an *in vitro* blood-brain barrier model

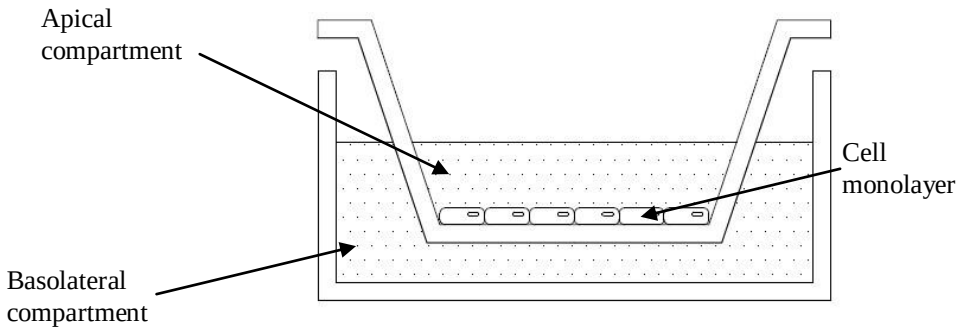

The upper compartment (apical) represents the blood side of the BBB. A cell monolayer is grown on a filter at the base of the apical compartment which is suspended in the lower (basolateral) compartment which represents the brain side of the BBB.

Cell monolayer integrity, reflecting the extent of paracellular and transcellular permeation of ions across the cell monolayer of an *in vitro* BBB model, can be assessed by measuring transcellular electrical resistance (TER). The literature reports a wide variation of TER between *in vitro* BBB models, ranging from very low TER values, for example 300 $\Omega.cm^2$ obtained with an immortalised porcine cell line co-cultured with the C6 glioma cell line (Lauer et al. 2004), to much higher TER values for example 1650 $\Omega.cm^2$ obtained using primary porcine CECs co-cultured with primary rat astrocytes (Cohen-Kashi Malina et al. 2009). An ideal model would display TER representative of the BBB *in vivo* which has been reported to be between 1490 $\Omega.cm^2$ (across the rat BBB) (Butt et al. 1990) and 1870 $\Omega.cm^2$ (across the frog BBB) (Crone et al. 1982).

1.4.1.1 *In vitro* blood-brain barrier models using primary cultured cells

Ferenc Joo and co-workers were the first to successfully isolate viable brain capillaries from rat brains in 1973 (Joo et al. 1973). Bowman et al. improved and modified this work and were the first to use an *in vitro* BBB model containing a filter, by culturing bovine endothelial cells on a collagen coated nylon mesh insert (Bowman et al. 1983). Since then the literature reports numerous *in vitro* BBB models using primary cell culture based on rodents (Lundquist et al. 2002; Calabria et al. 2006; Nakagawa et al. 2009), bovine (Rubin et al. 1991; Gaillard et al. 2000) and porcine (Franke et al. 2000; Zhang et al. 2006; Smith et al. 2007) as difficulties in obtaining human tissue limits the use of human CECs for primary cell culture. Although, most recently a primary human *in vitro* BBB model demonstrating high TER and expression of tight junction proteins, the efflux transporter P-gp and endothelial cell markers such as von Willebrand factor has been reported (Bernas et al. 2010).

The main advantage of using primary CECs is that they exhibit the closest phenotypic resemblance to the *in vivo* BBB retaining *in vivo* characteristics such as tight junctions (Rubin et al. 1991), expression of transporters (Zhang et al. 2006) and BBB enzymes (Smith et al. 2007). However, drawbacks include difficulties in obtaining pure cultures and isolation of primary cells and cell culture can be labour intensive (Gumbleton et al. 2001). Despite primary CEC cultures providing the closest phenotypic resemblance to the *in vivo* BBB, down regulation or loss of *in vivo* BBB characteristics can still occur on isolation from brain tissue (DeBault et al. 1980).

1.4.1.1.1 Modulation of *in vitro* blood-brain barrier model properties

The correct culturing techniques and conditions can help to maintain BBB characteristics of primary cultured CECs which are often down regulated or lost on isolation. These include co-culture with astrocytes or culture with astrocyte-conditioned medium (ACM), adding supplements to the medium, removing serum from the medium and purification of CECs using puromycin treatment.

Co-culture of primary CECs with astrocytes or culturing in ACM typically improves barrier properties of *in vitro* BBB models (Abbott 2002; Abbott et al. 2006). Co-culture with astrocytes has been shown to induce BBB properties such as tight junction formation and decreased permeability (Dehouck et al. 1990; Rubin et al. 1991; Sobue et al. 1999). Co-culture

with astrocytes has also been shown to induce BBB-associated enzymes such as alkaline phosphatase (Sobue et al. 1999; Smith et al. 2007) and γ-glutamyl transpeptidase (El Hafny et al. 1996) and the expression of the efflux transporter P-gp (El Hafny et al. 1997; Gaillard et al. 2000). A large increase in the expression of the efflux transporter P-gp in bovine CECs co-cultured with astrocytes compared to bovine CECs cultured alone has been reported (Cecchelli et al. 1999). As P-gp is currently deemed the most important transporter regarding drug penetration at the *in vivo* BBB, co-culture with astrocytes can provide an *in vitro* BBB model more representative of the *in vivo* BBB and potentially provide an accurate permeability screen.

The components of the cell culture medium can also enhance the restrictive nature of *in vitro* BBB models. Supplements added to the medium have been shown to enhance tight junction protein expression between adjacent cells of *in vitro* BBB models. Hydrocortisone has been shown to increase TER and decrease cell monolayer sucrose permeability (Hoheisel et al. 1998; Calabria et al. 2006). Supplementing medium with cyclic adenosine monophosphate (cAMP) has also been shown to increase TER across an *in vitro* BBB model (Rubin et al. 1991), since cAMP is thought to act as a second messenger which induces phosphorylation of tight junction proteins and therefore tightens the barrier. Additionally, agents that increase intracellular cAMP levels, for example chlorophenylthio-cyclic adenosine monophosphate (CPT-cAMP) and RO-20-1724, have also been shown to increase TER (Igarashi et al. 1999).

The role of serum in cell culture is to provide the cells with nutrients, hormones, growth factors, proteins and trace minerals to aid cell proliferation (Nitz et al. 2003). However, PBEC monolayers were reported to exhibit lower TER and higher sucrose permeability when cultured with serum-containing medium compared to serum-free medium (Hoheisel et al. 1998; Nitz et al. 2003). The serum in the cell culture medium was thought to inhibit CEC differentiation and reduce barrier tightness of established confluent cell monolayers. The serum-derived factors responsible for this and their mode of action are still to be elucidated, although it has been hypothesised that vascular endothelial growth factor (VEGF) and lysophosphatidic acid could play a role along with other serum-derived factors (Nitz et al. 2003).

Contamination of CECs from cells such as astrocytes and pericytes is an inevitable problem associated with the isolation of primary CECs. Contamination can result in incomplete barrier formation of the cultured cell monolayers (Parkinson et al. 2005) and low reproducibility between isolations. A recent study showed that addition of the P-gp substrate puromycin to isolated primary CECs eliminated contaminating cells and showed no toxic effects towards CECs (Perriere et al. 2005). Another study using primary cultured rat CECs repeatedly achieved purities of 99.8% using a similar approach (Calabria et al. 2006).

1.4.1.2 Immortalised cell lines employed as *in vitro* blood-brain barrier models

To overcome the problems encountered with harvesting and maintaining primary cultured CECs, immortalised CEC lines have been developed. The literature documents a large variety of *in vitro* BBB model based on immortalised cell lines using various cell types which employ a range of culturing techniques and conditions, for example co-culture with astrocytes (Sobue et al. 1999) and addition of supplements to the culture medium (Muruganandam et al. 1997). Immortalised brain capillary cell lines have been documented from a range of species, for example the rat GPNT cell line (Regina et al. 1999) and RBEC1 cell line (Kido et al. 2000), the mouse MBEC cell line (Tatsuta et al. 1992), the bovine cell line SV-BEC (Durieu-Trautmann et al. 1991), the porcine cell line PBMEC/C1-2 (Lauer et al. 2004) and the human cell line hCMEC/D3 (Weksler et al. 2005).

In vitro BBB models based on immortalised CEC lines retain some *in vivo* characteristics such as expression of key transporters (Wang et al. 2005) and BBB marker enzymes such as alkaline phosphatase (Sobue et al. 1999). The main advantages of these *in vitro* BBB models are ease of culture and their potential use in high throughput screening. However, a major disadvantage is that they demonstrate insufficient barrier properties (Reichel et al. 2003). As a result, drug discovery groups within the pharmaceutical industry tend to use *in vitro* BBB models based on cell lines from non-cerebral origins, such as the MDR1–MDCKII and Caco-2 cell line, for BBB permeability screening, which demonstrate better barrier properties. Several immortalised cell lines were employed as *in vitro* BBB models in this thesis and will now be discussed in more detail.

1.4.1.2.1 The hCMEC/D3 cell line

The development of a well characterised human endothelial *in vitro* BBB model would be the ultimate model for studying human *in vivo* BBB penetration. However, healthy human brain tissue for primary cell culture is extremely difficult to routinely obtain. The main source of human brain tissue is from surgical procedures or post mortems, but the tissue is often damaged or diseased.

To overcome the limitations of primary culture, and reduce variation in tissue composition/expression levels of transporters, several immortalised human endothelial cell lines have been established, for example the BB19 cell line which is flawed by high sucrose permeability (Kusch-Poddar et al. 2005) and the NKIM-6 cell line (Ketabi-Kiyanvash et al. 2007) which offers no permeability data at present.

The hCMEC/D3 cell line is the first example of an extensively characterised human brain endothelial cell line. The hCMEC/D3 cell line was developed by infection of primary endothelial cultures by lentiviral vectors encoding hTERT and SV40 large T antigen (T-SV40) (Weksler et al. 2005). The hCMEC/D3 cell line retains most morphological and functional characteristics of the *in vivo* BBB even without co-culture with astrocytes and shows no indication of phenotypic drift up to passage 35. The hCMEC/D3 cell line expresses, the tight junction proteins ZO-1, JAM-A and claudin-5 (Weksler et al. 2005) and functional ABC transporters P-gp, MRP1 and BCRP (Poller et al. 2008). However, this model is potentially flawed by high sucrose permeability $1.65 \pm 0.18 \times 10^{-3}$ cm.min^{-1} and extremely low TER (<40 Ω.cm^2 compared to 1490-1870 Ω.cm^2 *in vivo* (Crone et al. 1982; Butt et al. 1990)). Modification of culture conditions with the addition of human serum reduced passive sucrose permeability by up to 39% (Poller et al. 2008). The authors suggested that the observed reduction in passive sucrose permeability made the *in vitro* BBB model suitable for drug transport studies, however, this is questionable. Further work using the hCMEC/D3 cell line has lead to the development of a humanised dynamic *in vitro* BBB model, where hCMEC/D3 cells were grown inside hollow microporous fibres and exposed to pulsatile flow. Transcellular electrical resistances of hCMEC/D3 cells grown dynamically (approximately 1200 Ω.cm^2) were greater than hCMEC/D3 grown on Transwell® inserts (60-80 Ω.cm^2 in this study) (Cucullo et al. 2008) and were hence, more representative of the *in vivo* BBB.

1.4.1.2.2 The MDCK cell line

The Madin-Darby canine kidney (MDCK) cell line is a canine epithelial cell line that has previously been used as an *in vitro* BBB model (Veronesi 1996; Wang et al. 2005; Summerfield et al. 2006; Summerfield et al. 2007) despite being epithelial not endothelial, from kidney not from brain and derived from dog and not from human. Madin-Darby canine kidney wild type cells express low levels of P-gp. However, MDCK type II cells can be transfected with the human *MDR1* cDNA to produce the MDR1-MDCKII cell line which exhibits polarised expression of P-gp (Pastan et al. 1988). An advantage of the MDR1-MDCKII cell line is that it can be used in automated high throughput screening, requiring only 3-4 days of culture prior to use and monolayers demonstrate very low sucrose permeability ($1\text{-}3 \times 10^{-6}$ $cm.s^{-1}$) (Gumbleton et al. 2001). Consequently, this cell line is often the *in vitro* BBB model of choice in CNS drug discovery programmes for estimation of drug permeability and identification of P-gp substrates. A relatively recent study investigating nine *in vitro* cell line-based BBB models for their suitability as a BBB permeability screen concluded that the MDCK cell line transfected human *MDR1* was the most promising used in the study (Garberg et al. 2005). Wang et al. also conclude the MDR1-MDCKII cell line employed as an *in vitro* BBB model is suitable for use in high throughput drug discovery programmes (Wang et al. 2005).

1.4.1.2.3 The Caco-2 cell line

The Caco-2 cell line is a well characterised human colorectal adenocarcinoma cell line developed by the Sloan-Kettering Institute for Cancer Research. The Caco-2 cell line possess tight junctions (Hilgers et al. 1990) and expresses the efflux transporters P-gp (Hunter et al. 1993), MRP2 (Gutmann et al. 1999), MRP3, MRP1 (low levels) and MRP5 (low levels) (Hirohashi et al. 2000) and BCRP (Xia et al. 2005). Traditionally, the Caco-2 cell line has been used as a model of the human intestine because *in vitro* intestinal permeability has been shown to correlate with *in vivo* data (Yee 1997). The literature also reports the use of the Caco-2 cell line as an *in vitro* BBB model (Kalvass et al. 2002; Garberg et al. 2005). However, the cell line expresses some transporters and enzymes that are not present at the BBB *in vivo* (Sun et al. 2008) and takes approximately 21 days in culture to form confluent cell monolayers (Sun et al. 2008), which are limitations to its use as an *in vitro* BBB model.

1.4.2 *In vivo* techniques for studying central nervous system drug penetration

In vivo techniques are the most reliable techniques for studying CNS drug penetration as they use living tissue and they examine the overall effect of the whole body on an experiment. *In vivo* techniques are also important for validating *in vitro* techniques that can then be used for higher throughput studies. However, drawbacks include the requirement of large numbers of live animals, low throughput, the need for expensive equipment and experimental expertise and the highly invasive nature (apart from some imaging studies) of the studies. Additionally, *in vivo* techniques have limited application in humans and consequently extrapolation of data from preclinical species to humans is often required, which can be subject to problems regarding species differences.

1.4.2.1 Measurements of total blood and brain tissue drug concentration

Traditionally, brain penetration *in vivo* is determined from the total brain to blood concentration ratio (also known as the partition coefficient K_p) in rodents. Rodents are acutely dosed orally, subcutaneously or intraperitoneally, blood and brain samples are then taken at 3-5 time points. Alternatively, rodents are dosed via intravenous infusion and blood and brain samples are taken at one time point (Doran et al. 2005; Summerfield et al. 2006).

1.4.2.2 The *mdr1a/1b (-/-)* knock out mouse model

Humans possess one gene (*MDR1*) that encodes the P-gp efflux transporter whereas rodents possess two genes (*mdr1a* and *mdr1b*). The development of genetically modified *mdr1a/1b* (-/-) knock out mice has provided a suitable *in vivo* model for studying the effect of P-gp on CNS drug disposition, as in combination the *mdr1a* and *mdr1b* genes are thought to execute the equivalent function as the *MDR1* gene in humans (Schinkel 1999). The 'gold standard' assay for P-gp substrate identification, involves determination of the fold difference of a drugs K_p in wild type and *mdr1a/1b* (-/-) knock out mice (Summerfield et al. 2006). An alternative *in vivo* mouse model is the chemical knock out mouse in which mice are pre-treated prior to studies with an optimal dose of a potent P-gp inhibitor, for example GF120918, which allows the role of P-gp in CNS drug distribution to be studied (Cutler et al. 2006).

1.4.2.3 Microdialysis

Microdialysis is the only *in vivo* technique that can directly measure unbound concentrations of drugs simultaneously in the blood and brain tissue (Hammarlund-Udenaes 2000). The technique is semi-invasive and involves the insertion of a microdialysis probe into the tissue or fluid being examined. The technique can be used in pre-clinical studies (Xie et al. 1998) and in the clinic (Ederoth et al. 2004). However, poor recovery of lipophilic compounds and low throughput limit its use in drug discovery programmes (Hammarlund-Udenaes et al. 2008).

1.4.2.4 *In situ* brain perfusion

The *in situ* rat brain perfusion technique was developed by Takasato et al. to study transport of drugs into the brain (Takasato et al. 1984). The technique involves inserting a cannula into the carotid artery of an anaesthetised animal, the cardiac blood supply is cut off and the brain circulation is taken over by infusing the animal with blood or buffer containing the drug of interest (Summerfield et al. 2007). After perfusion the animal is sacrificed and the brain is removed for analysis.

1.4.2.5 Positron emission tomography

Positron emission tomography (PET) is a non invasive *in vivo* tracer technique (Cunningham et al. 2004) that can be used to give quantitative information on the biodistribution and receptor occupancy of drug and P-gp function and expression within the CNS of humans with high sensitivity and resolution (Summerfield et al. 2008). Positron emission tomography also has applications in the clinic, for example to monitor tumor progression (Grosu et al. 2010), as well as in a drug discovery setting.

In drug discovery PET can be used to investigate P-gp functionality (Elsinga et al. 2005) at the BBB in disease states, for example investigation of depression using probes such as [^{11}C]verapamil (de Klerk et al. 2009), P-gp interactions at the BBB, intra brain distribution of novel drugs, and to make direct comparisons between preclinical species and humans (Syvanen et al. 2009) in order to investigate species differences. However, this technique is not currently widely applicable because it requires expensive specialist equipment, radiolabelling of substrates with short half lives on site and expertise.

1.4.3 Equilibrium dialysis

In addition to the role of the BBB, nonspecific drug binding in blood and brain tissue is another important factor to be considered in the brain penetration of drugs. Drug fraction unbound in blood (fu_{blood}) is important because it determines the amount of free drug available to cross the BBB. Drug fraction unbound in brain (fu_{brain}) tissue is important because it determines the amount of free drug able to interact with target sites and the amount of drug available for potential efflux out of the CNS.

Equilibrium dialysis is an *in vitro* technique that can be used to determine the drug fraction unbound in blood and brain tissue. Equilibrium dialysis is often chosen over other methods such as ultrafiltration and ultracentrifugation because it is less prone to experimental artifacts (Kariv et al. 2001). The 96-well format equilibrium dialysis plate enables multiple compounds with replicates to be screened simultaneously and is made of Teflon® which reduces nonspecific binding to the apparatus (Banker et al. 2003). The technique is easy to perform, low cost, and is more comparable to the *in vivo* situation as results are obtained under equilibrium. The literature mainly reports equilibrium dialysis studies using rodent blood and brain tissue (Kalvass et al. 2002; Maurer et al. 2005; Summerfield et al. 2006; Kalvass et al. 2007; Summerfield et al. 2007). However, more recently, the use of porcine and human blood and porcine, marmoset, cynomolgous monkey and dog brain tissue in equilibrium dialysis studies (Summerfield et al. 2008; Read et al. 2010) has been documented.

1.4.4 Brain slice

The brain slice technique is an alternative *in vitro* technique to equilibrium dialysis for determining the drug fraction unbound in brain tissue (Becker et al. 2006; Friden et al. 2009). The fundamental difference between the two techniques is that equilibrium dialysis requires homogenisation of brain tissue with a buffer prior to dialysis, whereas the brain slice technique maintains the cellular structure of the brain tissue. The validity of using homogenised brain tissue has caused debate because homogenisation destroys tissue components and may expose binding sites that would otherwise not be available for drug binding with intact tissue (Becker et al. 2006) and could lead to an underestimation of fu_{brain}. However, this is of more relevance for compounds that are highly bound to brain tissue (>99 %) (Read et al. 2010). Additionally, the disruption of acidic organelles, for example

lysosomes, could alter the distribution of basic lipophilic drugs (Clausen et al. 1993) and also differences between interstitial fluid drug concentration and intracellular drug concentration may not be reflected in the fraction unbound (Reichel 2009). However, studies have shown agreement between unbound fractions when the brain homogenate method was compared to the brain slice method (Becker et al. 2006).

1.5 The challenge of effective drug penetration across the blood-brain barrier

Appearances can often be deceptive and the BBB is a prime example of this. Although the BBB has a short diffusional pathway, a large surface area (100-200 $cm^2.g^{-1}$ brain (Begley 2003)) and is a dense capillary network with high blood flow, it remains an excellent barrier and effective drug delivery to the brain is still a massive challenge for scientists.

Central nervous system drug penetration is thought to be modulated by three main processes (Jeffrey et al. 2010):-

1. Blood-brain barrier permeability
2. Facilitated transport at the BBB
3. Drug binding in blood and brain tissue

These three processes act in concert to determine three separate but inter-related facets of CNS drug delivery, namely the rate and extent of brain penetration and brain distribution of compounds (Hammarlund-Udenaes et al. 2008; Reichel 2009).

1.5.1 The role of the blood-brain barrier in modulating brain drug penetration

1.5.1.1 Blood brain barrier permeability

Cell barrier permeability has been shown to be a factor that can differentiate between drugs that permeate the BBB and drugs that do not. *In vitro* permeability was investigated, using MDR1-MDCKII cells, for a group of CNS active drugs (n = 48) and a group of non-CNS active drugs (n = 45) (Mahar Doan et al. 2002). The CNS active drug group was predominantly (46 out of 48 drugs) characterised by passive permeability (described using the apparent permeability coefficient P_{app}) > 150 $nm.s^{-1}$. In the non-CNS active group, P_{app} for 13

out of 45 drugs were < 150 $nm.s^{-1}$ compared to 2 (sumitriptan and zolmitriptan, both antimigraine drugs) out of 48 for the CNS active drug group. Furthermore, it has been suggested that sumitriptan and zolmitriptan may not have to cross the BBB to exert a clinical effect (Goadsby 2000).

In a similar study Wang et al. used MDR1-MDCKII cells to compare the passive permeability of CNS active and non-CNS active drugs (Wang et al. 2005). Central nervous system active drugs were also characterised by greater P_{app} values (> 30 $nm.s^{-1}$) compared to non-CNS active drugs. However, CNS active drugs were characterised by P_{app} > 30 $nm.s^{-1}$ which was lower than P_{app} >150 $nm.s^{-1}$ (Mahar Doan et al. 2002) reported previously.

A comparison of 14 drugs (Jeffrey et al. 2007) common to both studies (Mahar Doan et al. 2002; Wang et al. 2005) revealed a poor correlation between apical to basal (A-B) permeability between the two data sets which highlights the difficulties in comparing data from different groups and the impact of different assay conditions.

1.5.1.2 P-glycoprotein efflux at the blood-brain barrier

P-glycoprotein is currently deemed the most understood and clinically relevant ABC efflux transporter at the BBB in drug discovery programmes (Zhou 2008) due to its wide range of substrates (Schinkel 1999). To date, P-gp is also the only efflux transporter at the BBB that has been shown to reduce, although not entirely prohibit, CNS drug penetration (Doran et al. 2005). *In vitro* assays are routinely employed ahead of *in vivo* studies (with key compounds) to screen for P-gp substrates as an integral component of CNS drug discovery (Jeffrey et al. 2007). *In vitro* efflux ratios have been shown to correlate with *in vivo* data obtained from *mdr1a/1b* (-/-) knock out mice (Summerfield et al. 2006). Despite this, Doran et al. have observed some inconsistencies where compounds were found to be substrates of P-gp using the *mdr1a/1b* (-/-) knock out mice model but were not found to be substrates using *in vitro* P-gp assays (Doran et al. 2005). Substrates of P-gp may exhibit a reduced therapeutic window due to the effect of P-gp and require higher free blood concentrations to compensate, running the risk of peripheral toxicity (Liu et al. 2008).

One study evaluated brain penetration of 32 CNS active drugs using the *mdr1a/1b* (-/-) knock out mouse and wild type mouse model (Doran et al. 2005). The majority (27 of 32) of CNS active drugs possessed an efflux ratio significantly greater than unity, although only 4 of

32 were greater than 2-fold, suggesting that P-gp substrates can still penetrate the brain. However, it must be noted that despite most of the drugs in this study being subjected to P-gp active efflux, the US Food and Drug Administration does not consider a drug to be a substrate unless it has an efflux ratio greater than 2 (Zhang et al. 2008).

P-gp substrates have been shown to penetrate the CNS (Summerfield et al. 2006) suggesting that, although P-gp may limit CNS penetration of substrates, it does not entirely preclude it. Summerfield et al. summarised effective CNS drug penetration as a balance between good passive permeability, low P-gp efflux, correct physicochemical properties and sufficient brain tissue binding (which was suggested to provide a concentration gradient to overcome some of the affects of P-gp and thereby favour CNS penetration). Hence, although low P-gp efflux is beneficial, it is important not exclude all P-gp substrates during drug discovery, especially if they exhibit other properties considered favourable for CNS penetration or are particularly potent so even small amounts at the active site in the brain can have the desired efficacious outcome.

1.5.2 Fraction unbound in blood and brain tissue and blood-brain barrier penetration

Drug-protein binding is the reversible interaction of drugs with proteins in blood and tissues. It is only the fraction of drug that is unbound (fu Equation 1.3) that is able to pharmacologically interact at a target site (Banker et al. 2003).

$$Free\ drug + free\ protein \leftrightarrow drug\text{-}protein\ complex$$

Fraction unbound is defined as the extent to which a drug is bound to proteins in plasma, blood or tissues:

$$Fraction\ unbound(fu) = \frac{unbound\ drug}{total\ drug} \qquad \text{Equation 1.3}$$

The fraction of drug unbound is dependent upon the affinity of the drug for the binding protein, the concentration of the binding protein(s) and the concentration of the drug relative to the concentration of the binding protein(s) (Birkett 2006). Knowledge of the extent of

binding of a drug is important in terms of predicting the pharmacokinetics, pharmacodynamics and pharmacological interaction of a drug with the target site. The major drug binding blood proteins are albumin, alpha$_1$-acid glycoprotein and lipoproteins (Maurer et al. 2005). Knowledge of the proteins involved in drug tissue binding is lacking, however, it is thought that the overall extent of nonspecific tissue binding can be used to obtain pharmacokinetic information (Maurer et al. 2005).

As drugs penetrate the brain, several equilibrium drug distribution processes between the bound and unbound drug molecules occur concomitantly within the brain compartments (Figure 1.5). Equilibrium takes place across the BBB between the blood and the brain interstitial fluid, within the brain interstitial fluid, across cell membranes between the brain interstitial fluid and the intracellular fluid and within the brain cells. All equilibrium processes effect how fast steady state between blood and brain is reached (Hammarlund-Udenaes et al. 2008).

Figure 1.5 Equilibrium processes between bound and unbound drug within brain compartments

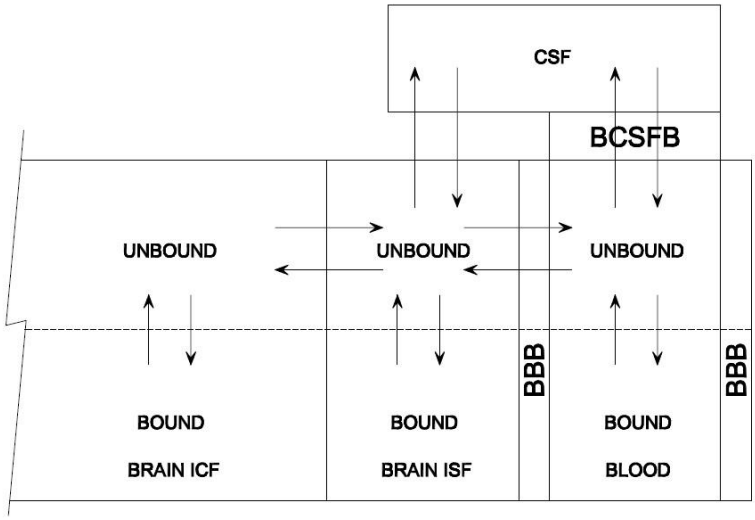

Equilibrium processes between bound and unbound drug within brain compartments. BBB is the blood-brain barrier, ISF is the interstitial fluid, ICF is the intracellular fluid, BCSFB is the blood cerebral spinal fluid barrier and CSF is the cerebral spinal fluid. Adapted from (Hammarlund-Udenaes et al. 2008).

Equilibrium dialysis is an *in vitro* technique used to measure drug-protein binding in blood and brain tissue which has become a recent addition to traditional *in vitro* BBB models for studying CNS brain penetration**.** Fraction unbound in blood and brain tissue determined by

using equilibrium dialysis can be used to calculate the *in vitro* blood to brain partition coefficient (fu_{blood}:fu_{brain}) also known as Kbb (Summerfield et al. 2006), which has previously been used as an *in vitro* measure of brain penetration for drugs that passively diffuse (Kalvass et al. 2002; Maurer et al. 2005).

Since

$$C_{u,blood} = C_{u,brain} \qquad \text{Equation 1.4}$$

And

$$C_u = fu \ x \ C_{total} \qquad \text{Equation 1.5}$$

Therefore

$$fu_{blood} \ x \ C_{blood} = fu_{brain} \ x \ C_{brain} \qquad \text{Equation 1.6}$$

And

$$\frac{C_{brain}}{C_{blood}} = \frac{fu_{blood}}{fu_{brain}} \qquad \text{Equation 1.7}$$

Where, C_u is the unbound concentration, C_{total} is the total concentration, $C_{u,blood}$ and $C_{u,brain}$ are the unbound concentration in blood and brain respectively, C_{blood} and C_{brain} are the total concentration in blood and brain respectively, fu is the fraction unbound, and fu_{blood} and fu_{brain} are the fraction unbound in blood and brain respectively.

Kalvass et al. investigated the relationship between Kbb and K_p (*in vivo* total brain to blood concentration ratio) in mice (Kalvass et al. 2002). For compounds that showed no evidence of P-gp efflux an excellent correlation (R^2 = 0.98) between Kbb and K_p was observed. For compounds that were considered to be P-gp substrates, Kbb over predicted K_p in every case. For one P-gp substrate (unnamed in the study) Kbb over predicted K_p in FVB mice suggesting that the over prediction was a function of P-gp efflux. Kbb also over predicted K_p in *mdr1a/1b* (+/+) mice to the same extent as the ratio of K_p *mdr1a/1b* (-/-) mice to K_p *mdr1a/1b* (+/+) mice showing the influence of P-gp at the BBB on relative tissue binding in plasma and brain tissue. Analogous to the finding of Kalvass and Maurer, Summerfield et al. found Kbb to predict K_p for non-P-gp substrates (Summerfield et al. 2006). The prediction of

K_p in rats using Kbb was improved for P-gp substrates when the P-gp efflux ratio was incorporated into the Kbb estimate (i.e. Kbb/ER) where Kbb represents the distribution of the compound into the brain tissue and the efflux ratio represented the effect of the BBB on drug brain penetration. A further study (Maurer et al. 2005) has also shown Kbb to predict K_p in mice for drugs that passively diffuse across the BBB, confirming that fraction unbound in blood and brain tissue can be used to examine CNS brain penetration.

1.6 Integrated concept of central nervous system drug penetration

The literature reports various measures and models of CNS drug penetration. However, the parameters that describe 'good CNS penetration' are still under debate. Traditionally, brain penetration was most often determined from the total brain to blood concentration ratio (also known as the partition coefficient, K_p) (Kalvass et al. 2002; Maurer et al. 2005; Summerfield et al. 2006; Summerfield et al. 2008). However, a lot of criticism now surrounds the use of K_p as a measure of brain penetration. A study performed by Doran et al (Doran et al. 2005) highlights a good example of this, where a range of K_p values (0.06-24) were determined in mouse for a group of 34 CNS active drugs. These findings suggest that a high K_p is not always a prerequisite for effective CNS penetration. However, a high K_p can be an indication of a high degree of nonspecific binding to brain tissue, potentially reducing the amount of free drug available for pharmacological interaction with receptors. It has been suggested that K_p may only represent a measure of inert partitioning of a drug into lipid material (van de Waterbeemd et al. 2001) such as the brain. The differences in protein and lipid composition may be used to explain this, since in brain the weight fraction of lipid and protein are comparable (0.11 and 0.079 respectively) whereas in blood the weight fraction of protein (0.18) is substantially greater than that of lipid (0.0065) (Jeffrey et al. 2007). Another limitation of the K_p parameter is that it represents a combination of all processes that govern CNS brain penetration including BBB permeability, active transport processes, relative drug binding between brain and blood, metabolism and bulk flow and does not permit the effect of each process on CNS brain penetration to be individually examined (Jeffrey et al. 2007).

It is now accepted that CNS drug penetration can no longer be defined by a single parameter and a more holistic view to CNS drug discovery is now emerging. The new

integrated concept to CNS drug discovery focuses on three individual but inter-related components of CNS penetration:-

- Rate of drug transport
- Extent of drug penetration concentration equilibrium between blood and brain tissue
- Drug distribution within brain tissue

The new approach puts more emphasis on free drug concentrations at the site of action within the brain (Hammarlund-Udenaes et al. 2008; Liu et al. 2008; Reichel 2009). All aspects of this new approach can be addressed using current *in vitro* and *in vivo* methods.

1.6.1 Rate of drug penetration across the blood-brain barrier

The rate of drug penetration across the BBB is determined by BBB permeability which is a function of passive permeability related to physicochemical properties of drugs, active transport processes at the BBB, blood protein binding which determines the amount of free drug available to cross the BBB and, cerebral blood flow (Reichel 2009). *In vitro* BBB models are used to generate permeability measurements to represent the rate of drug transport across the *in vivo* BBB. *In vivo*, the rate of drug transport across the BBB can be determined from several methods including microdialysis and *in situ* permeability studies.

1.6.2 Extent of drug penetration across the blood-brain barrier

The use of K_p to determine the extent of CNS drug penetration is limited because it is a composite of all processes influencing brain penetration. Instead, the concentration ratio of unbound drug in the brain to unbound drug in the blood ($K_{p,uu}$ Equation 1.8) is a much more useful parameter, which can be used as a measure of the extent of brain penetration (Hammarlund-Udenaes et al. 2008).

When the K_p of the drugs used in a study by Doran *et al* (Doran et al. 2005) was compared to the $K_{p,uu}$ (Liu et al. 2008), the fold difference was reduced from 240-fold between the K_p values to 34-fold between the $K_{p,uu}$ values, demonstrating the effect of nonspecific binding on determination of K_p.

When the K_p and $K_{p,uu}$ of the S- and R-enantiomers of certirizine were characterised (Gupta et al. 2006), K_p values of 0.22 and 0.04 were determined for S- and R-enantiomers respectively, initially suggesting that the S-enantiomer would preferentially penetrate the brain. However, the $K_{p,uu}$ values (0.17 and 0.14 for S- and R-enantiomers respectively) were similar for both enantiomers, suggesting no stereoselective brain penetration. Differences in plasma protein binding were found to be the cause of stereoselective K_p values, highlighting the affect of drug binding in plasma (or blood) and brain tissue on this parameter.

$K_{p,uu}$ is derived from the relationship between influx and efflux clearances and describes the affect of passive permeability and active transport processes at the BBB on the extent of CNS drug penetration (Hammarlund-Udenaes et al. 2008). When $K_{p,uu}$ is close to unity passive diffusion across the BBB is assumed, when $K_{p,uu} < 1$ efflux at the BBB is assumed and when $K_{p,uu} > 1$ influx at the BBB is assumed. $K_{p,uu}$ has been suggested to be the most pertinent parameter for predicting which drugs will be CNS active (Hammarlund-Udenaes et al. 2008), with a high $K_{p,uu}$ being most desirable (Liu et al. 2008).

Microdialysis is currently the only *in vivo* method for directly determining $K_{p,uu,}$ (Hammarlund-Udenaes 2000) however, this approach has limited use in a drug discovery setting. A more practical approach is to calculate $K_{p,uu}$ (Equation 1.9) using fu_{blood} and fu_{brain} determined using equilibrium dialysis and K_p determined from *in vivo* studies. A strong correlation between $K_{p,uu}$ determined from microdialysis and calculated $K_{p,uu}$ has recently been described (Liu et al. 2008).

$$K_{p,uu} = \frac{AUC_{u,brain}}{AUC_{u,blood}}$$ Equation 1.8

Where $AUC_{u,brain}$ is the area under the concentration-time curve for unbound concentration in brain tissue and $AUC_{u,blood}$ the area under the concentration-time curve for unbound concentration in blood.

$$K_{p,uu} = K_p \times \frac{fu_{brain}}{fu_{blood}}$$ Equation 1.9

Where K_p is the total brain to blood concentration ratio, fu_{brain} is the fraction unbound in brain tissue and fu_{blood} is the fraction unbound in blood.

1.6.3 Drug distribution within brain tissue

The unbound volume of distribution in the brain ($V_{u,brain}$ Equation 1.10) describes the relationship between the total drug concentration in the brain and the unbound drug concentration and is used to measure the extent of drug distribution in the brain (Hammarlund-Udenaes et al. 2008; Reichel 2009). Unbound volume of distribution in brain is dependent upon the affinity of drugs for brain tissue components and indicates whether a drug is distributed solely in the interstitial fluid ($V_{u,brain}$ approx 0.2 $ml.g^{-1}$ brain), throughout the interstitial fluid and intercellular fluid ($V_{u,brain}$ approx 0.8 $ml.g^{-1}$ brain) or if the drug mainly nonspecifically binds to brain tissue ($V_{u,brain}$ > 0.8 $ml.g^{-1}$ brain) (Hammarlund-Udenaes et al. 2008; Reichel 2009). Microdialysis can be used to determine $V_{u,brain}$ *in vivo*, though this is an experimentally complex, low throughput approach. Unbound volume of distribution can also be estimated *in vitro* using fu_{brain} obtained from brain slice (Friden et al. 2007) or equilibrium dialysis (Reichel 2009).

$$V_{u,brain} = 1 + D\left(\left(\frac{1}{fu(apparent)}\right) - 1\right)$$ Equation 1.10

D = the dilution factor in diluted brain homogenate

$fu\ (apparent)$ = Measured fraction unbound of drug in diluted brain homogenate

To summarise, the methods used to determine the delivery of novel CNS active drugs to the brain has surmounted enormous uncertainty and debate. It has now been established that effective drug delivery to the brain can not be defined by a single parameter and instead is a multifactorial concept. The pharmacokinetic parameters required to describe drug delivery to the brain, using the newer integrated approach are:

1. A measure of the rate (P_{app} and P_{exact} in this work) of drug transport across the BBB.
2. A measure of the extent of drug penetration across the BBB (K_p and $K_{p,uu}$ calculated from K_p and fu_{blood} and fu_{brain} in this work).
3. A measure of the distribution within the brain ($V_{u,brain}$, calculated using fu_{brain} from equilibrium dialysis in this work).

High BBB permeability, a low propensity for transporter-mediated efflux, high $K_{p,uu}$, high fu_{blood} and high fu_{brain} in relation to fu_{blood} are favourable drug properties for effective drug delivery to the brain. However, drugs with low BBB permeability, drugs that are substrates of efflux transporter and drugs with low fu_{blood} or low fu_{brain} in relation to fu_{blood} can still exert a therapeutic effect since it is a balance between all of these factors which determine effective drug delivery to the brain. It is also important to remember that favourable pharmacokinetic properties must also be combined with appropriate physicochemical properties, good pharmacological and toxicology data in order for novel CNS active drug candidates to be successful in the clinic.

1.7 Physiologically based pharmacokinetic modelling

An ability to be able to predict the extent of drug brain penetration in the early stages of drug discovery would be a valuable tool for the selection of novel CNS active drugs.

However, at present there is a lack of mathematical predictive models that can use *in vitro* parameters to accurately predict CNS drug penetration *in vivo* in order to reduce the quantity of expensive, complicated and time consuming *in vivo* studies required. Recently, a hybrid-PBPK model of the rat CNS has been developed and validated, using *in vivo* parameters, by Dr Raj Badhan (manuscript in preparation) to predict rat *in vivo* CNS drug penetration. The use of *in vitro*-derived parameters, unbound drug fraction and permeability as input parameters for this hybrid-PBPK model of the rat CNS will be investigated during this thesis in order to establish whether *in vitro* parameters can be used in the early stages of drug discovery to predict CNS drug penetration.

1.8 Pre-clinical animal species and central nervous system drug discovery

Rodent models have historically been used widely throughout CNS drug discovery programmes to predict outcomes in humans. However, positive effects observed with rodents in the laboratory have not been mirrored in clinical trials. The exciting development of transgenic mouse models in the 1990s (Schinkel et al. 1997) have failed to reduce attrition rates of novel CNS active drugs and added to the surmounting uncertainty regarding the use of rodent models in CNS drug discovery. Currently, there is limited knowledge concerning the reasons for species differences in CNS drug penetration.

In vitro studies using cell lines transfected with P-gp from a range of species have demonstrated species differences in P-gp functionality (Ohe et al. 2003; Katoh et al. 2006; Xia et al. 2006; Baltes et al. 2007) despite close amino acid homology across species (Kim et al. 2008). In one example different efflux ratios were obtained from monolayer efflux assays for several compounds out of a compound set with mouse (L-mdrla) and human (L-MDR1) P-gp-transfected cell lines, suggesting that *in vitro* mouse studies did not always provide a good prediction of the effect of human P-gp upon drug penetration *in vivo* (Yamazaki et al. 2001).

In another example antiepileptic drugs including phenytoin and levetiracetam did not exhibit an efflux ratio using MDR1-MDCK and LLC-MDR1 cell lines (cell lines that expressed human P-gp) in monolayer efflux assays whereas studies using the LLC-mdrla (cell line that expressed mouse P-gp) classed phenytoin and levetiracetam as substrates suggesting species differences in substrate recognition or P-gp transport efficacy (Baltes et al. 2007).

Positron Emission Tomography (PET) is an *in vivo* technique that permits drug interaction with P-gp to be directly compared between preclinical species and humans (Syvanen et al. 2009). *In vivo* studies using PET radioligands to study P-gp activity have shown differences in brain uptake of the PET radioligands in human compared to rodents suggesting species differences in P-gp function (Yasuno et al. 2006; Liow et al. 2007; Zhang et al. 2007; Syvanen et al. 2009).

A recent PET study using three radiolabelled P-gp substrates demonstrated species differences in K_p values, with a higher brain uptake of the radiolabelled substrates observed in humans, monkey and minipig compared to guinea pig and rat suggesting the possibility of species differences in P-gp transport (Syvanen et al. 2009). However, in the presence of a P-gp inhibitor (cyclosporin A; this part of the study did not include humans) species differences in brain uptake were still observed, suggesting that species differences in P-gp alone were not responsible.

Species differences observed in the presence of the P-gp inhibitor could suggest differences in the expression of other active transporters such as MRPs and BCRP, active transporters unidentified currently but present at the BBB or differences in plasma protein or brain tissue binding across species.

Higher concentrations of the P-gp inhibitor GF120918 in guinea pig have been reported to achieve full P-gp inhibition compared to mice and rat (Cutler et al. 2006) again suggesting differences in P-gp functionality. Species differences in P-gp functionality between rodents and higher species such as monkeys and human must therefore be taken into account when extrapolating data from animal studies to human.

The pregnane X receptor (PXR) plays a vital role in the regulation of P-gp expression, since xenobiotics bind to PXR and induce expression of P-gp (Ott et al. 2009). Functional similarities between pig and human pregnane X receptors have been documented (Ott et al. 2009). Xenobiotics that induced P-gp expression in human, for example hyperforin and rifampicin, also induced P-gp expression in porcine brain endothelial cells (PBECs) but not in rat CECs, proposing the use of a porcine model for the prediction of xenobiotic-PXR interactions in human.

Species differences in drug binding in plasma has been reported and may also account for differences observed in CNS efficacy between different species. Drug efficacy has been

demonstrated for one compound class in guinea pig whilst not in rat (Summerfield et al. 2006). Species differences in pharmacology and active transporters were ruled out and fu_{brain} was found to be comparable in guinea pig and rat. However, higher drug plasma binding was reported in rat compared guinea pig resulting in lower free fraction available to penetrate the BBB leading the authors to postulate that BBB penetration was restricted as a result of relative drug binding in blood exceeding that in brain.

Species differences have been demonstrated at the BBB in relation to P-gp functionality and also in drug plasma protein binding which are both factors thought to govern CNS drug penetration and will be examined further during this thesis.

Species differences have been highlighted between rodent and human which emphasises the problem of using rodent models to predict human CNS drug penetration. A preclinical species that is more representative of human would therefore be highly advantageous. As difficulties still remain in using a human primary cell model in research, the use of a porcine (a higher species) model will be examined during this work. Important similarities between humans and pigs have been illustrated such as extent of brain drug penetration (Syvanen et al. 2009), functional similarities between pig and human PXR (Ott et al. 2009) and drug binding in blood and brain (Summerfield et al. 2008). Porcine models have been considered the gold standard in cardiovascular (Hughes 1986) and wound healing research (Simon et al. 2000) for many years due to their similarities to humans. Their use in CNS research may be just as valuable.

1.9 Aim and objectives

The overall aim of this work is to use *in vitro* unbound drug fraction and permeability in order to predict CNS drug penetration.

The specific objectives of this work are:-

1. To develop and characterise a primary porcine *in vitro* BBB model to predict CNS drug permeability *in vivo*.
2. To compare *in vitro* BBB models regarding their potential for the prediction of *in vivo* BBB permeability.
3. To determine species differences in drug binding in blood and brain tissue.
4. Employ *in vitro*-derived parameters, unbound drug fraction and permeability, in an in-house a hybrid-PBPK model of the rat CNS to predict CNS drug penetration.

Chapter 2
Materials and Methods

2.0 Chapter 2: Materials and methods

2.1 Materials

2.1.1 Chemicals, solutions and media composition

An alphabetical list of all chemicals used and their suppliers is documented in Appendix 1. Solutions and media composition are documented in Appendix 2.

2.1.2 Blood and brain tissue

Rat blood and brain tissue were collected from male Sprague Dawley rats (approximately 250 g) (Charles Rivers Laboratories, Tranent, Scotland). Rats were sacrificed via cervical dislocation. Blood was collected by cardiac puncture and potassium ethylenediaminetetraacetic acid (EDTA) stabilised (final concentration 1.8 mg per ml blood) to prevent coagulation. Brains (1.8-2.0 g) were removed and placed in phosphate buffered saline (PBS, 137.0 mM NaCl, 2.7 mM KCl, 10.0 mM Na_2HPO_4 and 2.0 mM KH_2PO_4, pH 7.4) containing penicillin G sodium (100 $U.ml^{-1}$) and streptomycin sulphate (100 $\mu g.ml^{-1}$) on ice.

Porcine blood and brain tissue from Landrace pigs (80-90 kg) were collected from a local abattoir (C.S Morphets and Sons Ltd, Widnes, UK) immediately after sacrifice. Blood was collected from the jugular vein and carotid artery and stabilised with potassium EDTA (final concentration 1.8 mg per ml of blood). Brains (170-190 g) were isolated and transported in Leibovitz-15 medium (L-15) containing penicillin G sodium (100 $U.ml^{-1}$) and streptomycin sulphate (100 $\mu g.ml^{-1}$) on ice.

Dog blood and brain tissue from male Swiss Beagles (10-15 kg) were supplied in-house at GlaxoSmithKline (GSK, New Frontiers Science Park, Harlow, Essex, UK). The dogs were sacrificed by terminal anaesthesia with sodium pentobarbitone and death was confirmed by the cutting of the brachial artery. Blood was collected by jugular puncture and potassium EDTA (final concentration 1.8 mg per ml of blood) stabilised. Brains were removed and placed in PBS containing penicillin G sodium (100 $U.ml^{-1}$) and streptomycin sulphate (100 $\mu g.ml^{-1}$) on ice.

Human blood was collected from volunteers (staff at University of Manchester, Manchester, UK) into plastic Vacutainer tubes lined with potassium EDTA (final concentration 1.8 mg per ml of blood).

2.1.3 Test drug selection

Twelve centrally-acting test drugs were chosen by GSK for use in equilibrium dialysis and transport studies. All the drugs chosen have a molecular weight < 505 and liphophilicities, cLogP, that range from 0.4-6.1. The drugs studied are amprenavir, carbamazepine, chlorpromazine, citalopram, clozapine, haloperidol, mesoridazine, primidone, quetiapine, risperidone, ziprasidone. Their physicochemical properties are documented in Appendix 3.

2.2 Methods

2.2.1 Culture of cell lines

The Caco-2 cell line was obtained from European Collection of Animal Cell Cultures (ECACC, Salisbury, Wiltshire, UK). Cell stocks were rapidly thawed at 37 °C in a water bath and seeded in a 25 cm^2 tissue culture flask (T-25) using Caco-2 culture medium (Dulbecco's Modified Eagle Medium (DMEM) containing 10 % (v/v) foetal bovine serum (FBS), 100 $U.ml^{-1}$ penicillin G sodium, 100 $\mu g.ml^{-1}$ streptomycin sulphate, 2 mM L-glutamine and 1 % (v/v) non-essential amino acids (NEAA)).

The medium was replaced on alternate days until the cells reached confluency, typically 5 to 7 days post-seeding. Upon confluency, the medium was aspirated, the cells were washed twice with PBS pre-warmed to 37 °C, and incubated with enough 0.25 % (w/v) trypsin-EDTA solution to cover the entire cell layer (0.5 ml for a T-25 flask).

The flask was incubated at 37 °C in a humidified atmosphere of 5 % CO_2 in air with occasional agitation. Once the cells had detached, Caco-2 culture medium was immediately added to prevent the further action of trypsin-EDTA. The resulting cell suspension was transferred to a 25 ml universal tube and centrifuged at 1000 x g for 5 min.

The pellet was resuspended in culture medium and either reseeded in flasks for further culture or seeded onto Transwell® inserts (seeding density of 1.2 x 10^5 $cells.cm^{-2}$). Cells were cultivated for at least 3 passages prior to experimental use in order to stabilise the phenotype (Polli et al. 2001). Cells with a defined interval of passage were used (50-60) as the phenotype of low and high passage cells can vary.

The human cerebral microvascular endothelial cell line hCMEC/D3 (passage 25) was obtained under license from INSERM, France. Cell stocks were rapidly thawed at 37 °C in a water bath and seeded in T-25 flasks (pre-coated with rat tail collagen type 1 (100 $\mu g.ml^{-1}$ in

1 mM acetic acid) as were all hCMEC/D3 tissue culture surfaces, (section 2.2.3.1) and maintained in hCMEC/D3 culture medium (EBM2 basal medium containing 2.5 % (v/v) FBS, 100 $U.ml^{-1}$ penicillin G sodium, 100 $\mu g.ml^{-1}$ streptomycin sulphate, 125 µl VEGF, 125 µl IGF, 125 µl EGF, 50 µl hydrocortisone (from EGM-2 MV bullet kit), 1 mM 4-(2-hydroxyethyl)-1-piperazineethanesulfonic acid (HEPES) and 200 $ng.ml^{-1}$ bFGF) at 37 °C in a humidified atmosphere of 5 % CO_2 in air.

Culture medium was removed and replaced with fresh culture medium on alternate days. The cells were subcultured as described above for Caco-2 cells and cultivated for at least 3 passages prior to experimental use in order to stabilise the phenotype. The cells were passaged twice a week (INSERM recommend use of cells until passage 35 without loss of BBB properties).

Two different Madin-Darby Canine Kidney Cells (MDCK) cell lines were used in this study, the human-MDR1-transfected MDCK cell line (MDR1-MDCKII) and its corresponding non-transfected parent wild-type (MDCKwt). Both cell lines were obtained from The Netherlands Cancer Institute (Amsterdam, Netherlands), at a concentration of 1×10^7 cells per vial (passage 33).

Each vial was rapidly thawed at 37 °C and seeded onto a 175 cm^2 tissue culture flask (T-175) in 50 ml of MDCK culture medium (DMEM with Glutamax containing 10 % (v/v) FBS, 100 $U.ml^{-1}$ penicillin G sodium and 100 $\mu g.ml^{-1}$ streptomycin sulphate). The medium was replaced 24 h post-seeding and on alternate days thereafter. The cells were cultured at 37 °C in a humidified atmosphere of 5 % CO_2 and passaged at 80-90 % confluence (every 3-4 days) using 0.5 % (w/v) trypsin-EDTA solution. Cells were passaged for two weeks from frozen before use, in order to stabilise the phenotype and establish a growth pattern.

The rat astrocyte cell line CTX-TNA2 (passage 8) was received as a gift from the laboratory of Professor Dame Nancy Rothwell (University of Manchester, Manchester, UK). Cell stocks were revived and cells were routinely cultured in astrocyte culture medium (DMEM containing 10 % (v/v) FBS, 100 $U.ml^{-1}$ penicillin G sodium and 100 $\mu g.ml^{-1}$ streptomycin sulphate) as described above. Cells were passaged twice a week and the culture medium was harvested from the astrocytes for use in subsequent studies and referred to as astrocyte conditioned medium (ACM).

2.2.1.1 Trypan blue assay

A trypan blue assay was used to determine the number of viable cells for use in subsequent studies. Cells were detached from growth surfaces (section 2.2.1) and resuspended in 1 ml of culture medium. A 20 µl volume of cell suspension and 20 µl of 0.4 % (w/v) trypan blue were mixed together in an Eppendorf tube and incubated for approximately 5 min at room temperature in order to allow the dye to traverse the membrane of non-viable cells. A cover slip was placed on top of the haemocytometer, 10 µl of trypan blue-cell suspension was placed in each of the two chambers of the haemocytometer and the number of viable cells (cells which were not stained blue) were counted. The estimated number of viable cells per ml was calculated as follows:

Viable cells (cell.ml^{-1}) = Average count (unstained cells) per grid square x dilution factor x 10^{4}

Equation 2.1

2.2.1.2 Cryopreservation of cell stocks

After harvesting cells, as described in section 2.2.1, the cell pellet was resuspended in freezing medium (90 % (v/v) FBS, 10 % (v/v) DMSO) for all cell lines except hCMEC/D3 (95 % (v/v) FBS, 5 % (v/v) DMSO) for cryopreservation. Cells were frozen down at a concentration 2 million cells.ml^{-1}. A 1 ml volume of cell suspension was aliquoted into cryovials and stored overnight at -80 °C in a cell cooling box (Nalgene® Labware Roskilde, Denmark). This allows controlled cell freezing at a rate of -1 °C.min^{-1}, prior to long term storage in liquid nitrogen (-196 °C).

2.2.2 Culture of primary rat astrocytes

Primary rat astrocytes were received as a gift from the laboratory of Professor Dame Nancy Rothwell (University of Manchester, Manchester, UK). Mixed glial cell cultures were prepared using a method previously described (McCarthy et al. 1980).

In brief, 0-to 2-day-old rat pups were sacrificed and the cerebral cortices were removed and rolled on a piece of sterile filter paper to remove the meninges. Cortices were dissociated

through an 80 µm nylon mesh (Plastok Associates Ltd, Birkenhead, UK), the filtrate collected and centrifuged at 200 x g for 10 min (Mistral 3000i, MSE Ltd, Loughborough, UK).

The remaining pellet was resuspended in 10 ml of DMEM containing 10 % (v/v) FBS, penicillin G sodium (100 $U.ml^{-1}$) and streptomycin sulphate (100 $\mu g.ml^{-1}$). Cells were counted and seeded at 5 x 10^5 $cells.ml^{-1}$ in 75 cm^2 tissue culture flasks (T-75) pre-coated with poly-D-lysine and grown at 37 °C in a humidified atmosphere of 5 % CO_2 in air.

The culture medium was initially changed 5 days post-seeding and then every third day until the cells reached confluency (approximately 12-13 days post-seeding). Upon confluency, mixed glial cultures were incubated overnight at 37 °C in a humidified atmosphere of 5% CO_2 in air. They were shaken at 245 rpm (Orbital incubator S150 with shaker, Stuart Scientific, Staffordshire, UK), in order to detach contaminating progenitor cells whilst the astrocytes remained adhered to the flask.

The astrocytes were harvested by treatment with 0.25 % (w/v) trypsin-EDTA solution (section 2.2.1), centrifuged (200 x g, 5 min) (Mistral 30001, MSE Ltd, Loughborough, UK) and seeded onto 12 well plates at 1 x 10^5 cells per well and maintained in astrocyte culture media (DMEM containing 10 % (v/v) FBS, 100 $U.ml^{-1}$ penicillin G sodium, 100 $\mu g.ml^{-1}$ streptomycin sulphate) for 10 days at 37 °C in a humidified atmosphere of 5 % CO_2 in air. The medium was harvested and replaced with fresh medium on alternate days and the ACM was stored at -20 °C for use in subsequent studies.

2.2.3 Isolation of porcine cerebral microvascular capillaries

Porcine brain endothelial cells (PBECs) were isolated based on a method by Rubin et al (Rubin et al. 1991), with adaptations. Fresh porcine brain hemispheres (10-12) were collected and any bruised or damaged hemispheres were rejected.

The hemispheres were washed in PBS and placed on ice. Using curved forceps, the meninges were removed and discarded. The resulting hemispheres were placed in ice-cold PBS containing penicillin G sodium (100 $U.ml^{-1}$) and streptomycin sulphate (100 $\mu g.ml^{-1}$).

White matter was removed, carefully in order not to remove cortical grey matter using curved forceps, and discarded. The remaining cortical grey matter was dissected and passed through a 50 ml syringe into a 225 cm^2 tissue culture flask (T-225) containing Minimal Essential Medium (MEM) with 25 mM HEPES supplemented with 10 % (v/v) FBS, penicillin

G sodium (100 $U.ml^{-1}$) and streptomycin sulphate (100 $\mu g.ml^{-1}$) and placed on ice. Final composition brain tissue:medium was 1:4 (w/v).

Cortical grey matter was homogenised (Dounce Homogeniser 40 ml, Jencons, UK) in MEM/HEPES supplemented with 10% (v/v) FBS, penicillin G sodium (100 $U.ml^{-1}$) and streptomycin sulphate (100 $\mu g.ml^{-1}$). Homogenisation commenced with a loose pestle (89-127 µm clearance) for 15 strokes followed by homogenisation with a tight pestle (25-76 µm clearance) for a further 15 strokes.

Homogenate (100 ml per nylon mesh filter) was sequentially filtered under vacuum, initially through a 150 µm pore size nylon mesh (Plastok Associates Ltd, Wirral, UK) followed by 60 µm pore size nylon mesh (Plastok Associates Ltd, Wirral, UK). The material retained on the 60 µm pore nylon mesh was digested in 15 cm diameter cell culture grade petri dishes containing 80 ml of digest mix (Appendix 2) with incubation at 1 h at 37 °C on an Orbital Incubator S150 Shaker (Stuart Scientific, Staffordshire, UK) at 100 rpm.

Material retained on the filters was then washed off with MEM/HEPES, the digest mix centrifuged at 1000 x g (Mistral 3000i, MSE Ltd, Loughborough, UK) for 10 min. The pellet containing the cerebromicrovessels was washed twice in MEM/HEPES supplemented with 10 % (v/v) FBS, penicillin G sodium (100 $U.ml^{-1}$) and streptomycin sulphate (100 $\mu g.ml^{-1}$).

The remaining pellet was re-suspended in 10 ml of 90 % (v/v) FBS and 10 % (v/v) DMSO). A proportion (usually 1 ml) of the microvessels and freezing medium suspension was diluted in 11 ml PBEC culture media (Appendix 2) and 2 ml was added to each well of a pre-coated (section 2.2.3.1) 6-well plate.

The remainder of the suspension was transferred into cryogenic vials (1 ml per vial) and maintained at -80 °C overnight in a cell-freezing container (-1 $°C.min^{-1}$ cooling rate), before transfer to liquid nitrogen (-196 °C) for long term storage until use.

2.2.3.1 Coating cell culture surfaces with collagen and fibronectin

Porcine brain endothelial cells do not demonstrate optimum growth on plastic surfaces. In order to overcome this problem, the surfaces of 6-well plates were coated to aid attachment and proliferation. Each well was initially coated with 1 ml of rat tail collagen type 1 (100 $\mu g.ml^{-1}$ in 1 mM acetic acid) and incubated for 2 h at room temperature under gentle agitation to ensure homogeneous surface coating. The collagen was aspirated away and the

wells were washed twice with PBS to remove any excess collagen. The surface of Transwell® inserts were also coated in a similar manner.

Each well was then treated with 1 ml of human fibronectin (7.5 $\mu g.ml^{-1}$ in sterile distilled water) and incubated overnight at 4 °C, followed by 1 h at room temperature under gentle agitation. The fibronectin was aspirated and the wells were washed twice with PBS. To prevent the wells from drying out, the final PBS wash was left in the wells until cell seeding.

The coating process was performed on all surfaces used to grow PBECs including Transwell® inserts and 96-well plates. The volume of collagen and fibronectin used to treat other surfaces was adjusted for the surface area, based upon the volume used to treat 6-well plates. The hCMEC/D3 cell line was seeded onto surfaces coated only with collagen as described above.

2.2.3.2 Culture of primary porcine brain endothelial cells

Aliquots of cerebromicrovascular suspension were removed from liquid nitrogen, rapidly thawed at 37 °C, resuspended in PBEC culture medium at 37 °C and seeded onto pre-coated 6-well plates (section 2.2.3.1).

The cerebromicrovessels were maintained at 37 °C in a humidified atmosphere of 5 % CO_2 in air for 24 h to ensure that the cells had adhered to the plates. One vial of cerebromicrovascular suspension was seeded onto two pre-coated 6-well plates (2 ml culture medium per well).

In order to eradicate contaminating cells such as pericytes, 24 h post-seeding, the cells were treated with puromycin dihydrochloride (3 $\mu g.ml^{-1}$) in PBEC culture medium:CTX-TNA2 ACM (1:1) for three days. Medium containing puromycin was then removed and the cells were maintained in PBEC culture medium: CTX-TNA2 ACM (1:1) at 37 °C in a humidified atmosphere of 5 % CO_2 in air, until 70-80 % confluent (approximately seven days post-seeding). Culture medium was replaced on alternate days (Figure 2.1).

At 70-80 % confluency culture medium was aspirated away and the cells were washed twice with PBS pre-warmed to 37 °C and then once with PBS containing 0.2 $mg.ml^{-1}$ EDTA. Each well was incubated with 300 µl of 0.5 % (w/v) trypsin-EDTA solution at 37 °C in a humidified atmosphere of 5 % CO_2 in air for 10 min. An equal volume of PBEC culture medium was then added to each well to inactivate the trypsin.

The resulting cell suspension was centrifuged at 1500 x g (Mistral 3000i, MSE Ltd, Loughborough, UK) for 5 min, the remaining cell pellet was resuspended in PBEC culture medium:CTX-TNA2 ACM (1:1) and used in subsequent studies.

Figure 2.1 Culture of primary porcine brain endothelial cells

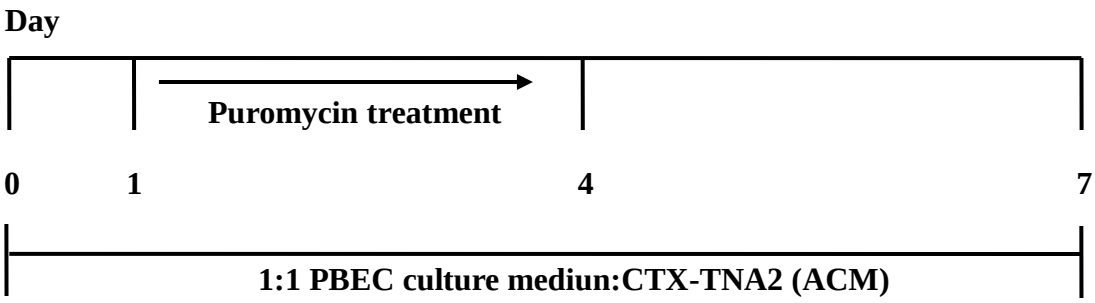

Porcine brain endothelial cell were revived from frozen on day 0 and maintained in 1:1 PBEC culture medium:CTX-TNA2 until day 7 when the PBECs were approximately 70-80 % confluent. On day 1, 24 h post seeding, the PBECs were treated with puromycin (3 $\mu g.ml^{-1}$) until day 4 to eradicate contaminating cells.

2.2.3.3 Seeding porcine brain endothelial cells onto 96-well plates

96-well plates were coated with collagen and fibronectin as described in section 2.2.3.1. Cells were homogeneously resuspended in PBEC culture medium:CTX-TNA2 ACM (1:1) at a density of 100,000 $cell.ml^{-1}$, 200 µl (20,000 cells per well of the suspension was added to each well) and plates maintained at 37 °C in a humidified atmosphere of 5 % CO_2 in air.

2.2.4 Primary porcine *in vitro* blood-brain barrier model

The primary porcine *in vitro* blood-brain barrier model (Figure 2.2) consisted of a monolayer of PBECs grown on pre-coated (section 2.2.3.1) Transwell® polycarbonate inserts (pore size 0.4 µm, diameter 12 mm, growth area 1.12 cm^2, 12-well cell culture cluster) in non-contact co-culture with the rat astrocyte cell line CTX-TNA2 (section 2.2.1).

Porcine brain endothelial cells were seeded at a density 8 x 10^4 cells per insert and maintained in PBEC culture medium:CTX-TNA2 ACM (1:1), for six days. The medium was replaced on alternate days when transcellular electrical resistance (TER) measurements were taken (section 2.2.5). Inserts containing PBEC monolayers were placed into the wells of 12

well plates containing confluent monolayers of astrocytes and the co-culture was maintained for 3 days (from day 4 to day 6 post-seeding of PBECs onto Transwell® inserts). Twenty four hours (day 6) prior to transport studies the medium was replaced with PBEC transport medium (DMEM containing, 100 $U.ml^{-1}$ penicillin G sodium, 100 $\mu g.ml^{-1}$ streptomycin sulphate, 125 µM heparin, 2 mM L-glutamine, 312.5 µM cAMP, 17.5 µM RO-20-1724 and 550 nM hydrocortisone).

Porcine brain endothelial cells were maintained at 37 °C in a humidified atmosphere of 5 % CO_2 in air throughout growth on Transwell® inserts. Inserts contained 0.5 ml medium in the apical compartment and 1.5 ml in the basolateral compartment. During medium changes, medium was aspirated first from the basolateral compartment of all wells and then carefully and slowly from the apical compartment to ensure monolayer maintenance. Fresh medium was initially replaced in the apical compartment followed by the basolateral compartment.

Porcine brain endothelial cell monolayer with TER<1000 $ohm.cm^2$ were discarded and not used for experiments.

Figure 2.2 Primary porcine *in vitro* blood-brain barrier model

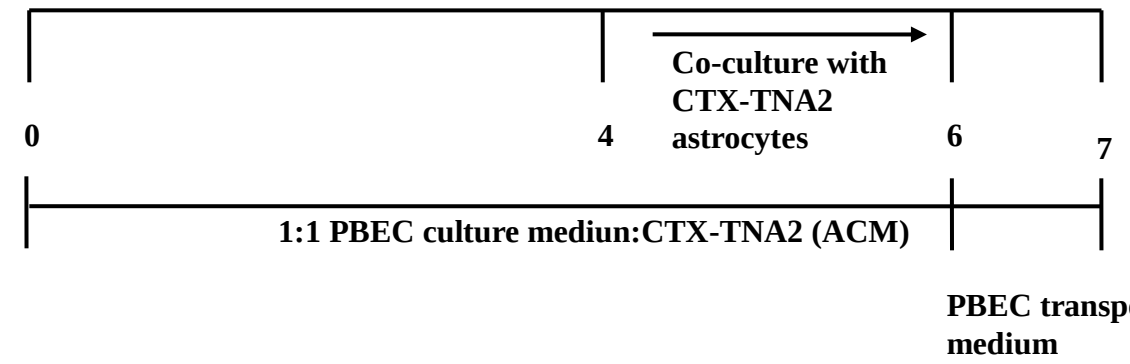

Porcine brain endothelial cells were seeded at a density of 8 x 10^4 cells per insert and maintained in 1:1 PBEC culture medium:CTX-TNA2 until day 6. Porcine brain endothelial cells were maintained in co-culture with CTX-TNA2 astrocytes from day 4 to day 6. On day 6 the PBECs were removed from co-culture and the medium was switched to PBEC transport medium.

2.2.5 Measurement of transcellular electrical resistance

During growth on Transwell® inserts, and directly before and after all transport studies, the integrity (reflecting the extent of paracellular and transcellular permeation of ions) of cell monolayers was assessed, using a voltohmmeter (EVOM) (World Precision Instruments, Aston, Stevenage, UK), to measure TER.

The 'chop-stick' electrodes were placed with the current-passing electrode in the apical compartment and the voltage-measuring electrode in the basolateral compartment of each filter unit and well in order to measure the resistance across the filter and cell monolayer.

Control measurements were also taken using a filter with no cells seeded (blank filter). Transcellular electrical resistance was calculated (Equation 2.2) by subtraction of the electrical resistance of the blank filter from the electrical resistance of the filter with the cell monolayer, followed by correction for the filter surface area.

$$TER(ohm.cm^2) = A(R_{cell\ monolayer} - R_{filter})$$

Equation 2.2

$R_{cell\ \ monolayer}$ = Resistance across Transwell® insert with cell monolayer (Ohm)

R_{filter} = Resistance across Transwell® insert without cell monolayer (Ohm)

A = Surface area of Transwell® insert (cm^2)

2.2.6 Transmission electron microscopy of confluent cell monolayers

Transmission electron microscopy (TEM) was used for qualitative assessment of PBEC monolayers grown on Transwell® inserts. Medium was aspirated from inserts containing confluent cell monolayers and the cells were washed twice with PBS.

The filters were carefully cut out of the Transwell® inserts, removed from the Transwell® supports and fixed overnight in sodium cacodylate buffer containing 0.1 M gluteraldehyde. The filters were then washed for 20 min with sodium cacodylate buffer and post-fixed in 1 % (w/v) osmium tetroxide in 0.1 M in sodium cacodylate for 30 min. The fixed cells were washed in sodium cacodylate buffer and dehydrated in an increasing concentration

series of ethanolic solutions 70 % (v/v) [20 min], 90 % (v/v) [20 min] and 100 % (v/v) [30 min x 2].

The cells were then treated twice with propylene oxide for 30 min and infiltrated with epoxy resin (Araldite), 50 % (v/v) [40 min at 40 ^{o}C] and 100 % (v/v) for 1 h at 40 ^{o}C. The cells were then embedded into fresh Araldite resin, by positioning the filters into the embedding moulds containing a layer of prepolymerized resin to lift the filter away from the bottom of the mould so that transverse sections of the filter could be cut.

Sections, 100 nm thick, of the resin-embedded filters were cut using a diamond knife on a Reichert OMU 4 Ultracut Ultramicrotome (Vienna, Austria) and collected onto 400-mesh copper grids (Agar, Scientific, UK). The Sections were stained with 1 % (w/v) uranyl acetate for 40 min at room temperature (DNA and RNA stain), washed with distilled water and then stained with Reynolds lead citrate for 10 min at room temperature before a final wash with water. Sections were examined using a transmission electron microscope (Philips CM10, Cambridge, UK) and digital images were recorded on an AMT LR44 digital camera (Deben, UK).

Transmission electron microscopy studies were carried out by Dr Alan Curry at the Department of Clinical Sciences, Manchester Royal Infirmary.

2.2.7 Immunocytochemical detection of tight junction proteins in primary porcine brain endothelial cell monolayers

Porcine brain endothelial cell monolayers cultured on Transwell® inserts (section 2.2.4) were immunostained for the detection of tight junction proteins. The culture medium was gently aspirated taking care not to disrupt the PBEC monolayer and the cells were washed twice with PBS warmed to 37 °C.

The PBECs were fixed in ice-cold methanol:acetone solution (1:1 v/v) for 2 min on ice, then washed twice with PBS warmed to 37 °C. The cell monolayers were incubated with 250 µl per well blocking solution (10 % (v/v) horse serum in PBS) in order to block nonspecific binding sites, for 1 h at room temperature with gentle agitation.

The blocking solution was aspirated, the cell monolayers washed with PBS warmed to 37 °C and incubated with rabbit anti-human occludin (1:100), or rabbit anti human-ZO-1 (1:100) primary antibody in blocking solution for 1 h at room temperature.

The primary rabbit antibody was aspirated and the cell monolayers washed four times with PBS warmed to 37 °C and incubated with secondary antibody, fluorescein iso-thiocyanate (FITC) -labeled mouse anti-rabbit IgG (1:200) in blocking solution, for 45 min at room temperature in the dark. The secondary antibody was aspirated and the cell monolayers were washed four times in PBS warmed to 37 °C.

The filters were then cut from the Transwell® inserts using a scalpel, rinsed with distilled water, mounted onto a glass microscopy slide and enclosed with a cover slip. Specimens were viewed using the Leica DM IRBE confocal microscope (Leica Microsystems, Milton Keynes, UK) using a FITC filter, excitation λ 494 nm and emission λ 521 nm.

2.2.8 Cell staining using fluorescein iso-thiocyanate conjugated isolectin B4 for examination of porcine brain endothelial cell morphology

Porcine brain endothelial cells were grown to confluence on Transwell® inserts (section 2.2.4). The cells were washed twice with PBS. FITC-conjugated isolectin B4 (IB4 1:200 dilution) was added to the donor compartment of the insert for 30 min in the dark. The cells were then washed twice with PBS warmed to 37 ºC and fixed with 4 % (v/v) paraformaldehyde and mounted using ProLong® mounting media containing DAPI.

The filters were then cut from the Transwell® inserts using a scalpel, rinsed with distilled water, mounted onto a glass microscopy slide and enclosed with a cover slip. Specimens were viewed using a fluorescent microscope (Olympus, Middlesex, UK) attached to a digital camera. The images were captured using METAVUE imaging software (Nikon, Kingston Upon Thames) and processed using Adobe Photoshop.

2.2.9 Assessment of paracellular permeability across the *in vitro* porcine blood brain barrier model

In order for the primary porcine *in vitro* BBB model to act as a permeability screen, it is essential that it displays a restrictive paracellular pathway. Lucifer yellow was used to assess paracellular permeability and integrity of the *in vitro* primary porcine BBB model. Paracellular permeability was measured in both the apical to basolateral (A-B) and basolateral to apical (B-A) directions.

Porcine brain endothelial cells were grown to confluence on Transwell® inserts (section 2.2.4) for seven days prior to assessment of paracellular permeability. Transcellular electrical resistance of cell monolayers was measured using an EVOM chopstick electrode (section 2.2.5) before and after the study. The growth medium was replaced with PBEC transport medium containing 100 µM of Lucifer yellow in the donor compartment and PBEC transport medium alone in the acceptor compartment (n=5, 12 replicate determinants).

The PBEC monolayers were incubated at 37 °C in a humidified atmosphere of 5 % CO_2 in air for 60 min. Samples of 150 µl were removed from both the donor and acceptor compartments after 60 min and transferred to black flat bottom 96-well plates. Lucifer yellow in the samples was quantified by fluorescence spectroscopy (Tecan Safire, Männedorf, Switzerland) excitation λ 425 nm and emission λ 515 nm. Each plate contained a Lucifer yellow calibration curve.

Apparent permeability coefficient (P_{app}) was determined using the following equation:

$$P_{app}(cm.s^{-1}) = (dc/dt).(V/AC_0) \qquad \text{Equation 2.3}$$

dc/dt = Change in receiver compartment concentration over time (mol.l^{-1}.s^{-1})
V = Volume in the receiver compartment (cm^3)
A = Surface area of Transwell® insert (cm^2)
C_0 = Initial concentration of probe in the donor compartment (mol.l^{-1})

2.2.10 Measurement of P-glycoprotein efflux activity in porcine and human brain endothelial cells using the calcein accumulation assay

The calcein acetoxymethyl ester (calcein-AM) intracellular accumulation assay was adapted from previous methods reported in the literature (Liminga et al. 1994; Tiberghien et al. 1996). Porcine brain endothelial cells were seeded (section 2.2.3.3) at 2 x 10^4 cells per well on clear 96-well flat bottom plates, with the appropriate pre-treatment (section 2.2.3.1), and maintained in culture medium. The assay was performed once the cells had reached confluency (3-4 days post-seeding).

Upon confluency, the medium was carefully aspirated away and the cells were washed twice with PBS warmed to 37 °C. Cells were then equilibrated in 200 µl of appropriate transport medium (PBEC transport medium: DMEM containing 100 $U.ml^{-1}$ penicillin G sodium, 100 $\mu g.ml^{-1}$ streptomycin sulphate, 125 µM heparin, 2 mM L-glutamine, 312.5 µM cAMP, 17.5 µM RO-20-1724 and 550 nM hydrocortisone) for 30 min at 37 °C in a humidified atmosphere of 5 % CO_2 in air.

The cells were then incubated for a further 30 min 37 °C in either transport medium or transport medium containing the P-glycoprotein (P-gp) inhibitor GF120918 (2 µM). The P-gp substrate calcein-AM was added to all wells (final concentration 0.25 µM) and the plate incubated at 37 °C for 30 min (n= 3 independent studies each with 8 replicates). The medium was aspirated away and the cells washed with PBS warmed to 37 °C to remove any calcein-AM which had not been internalised. Intracellular calcein accumulation was measured by fluorescence spectroscopy using a multi-plate reader (Tecan Safire, Männedorf, Switzerland) excitation λ 484 nm and emission λ 530 nm.

2.2.11 Determination of P-glycoprotein expression by western blotting

2.2.11.1 Preparation of cell lysates for sodium dodecyl sulfate polyacrylamide gel electrophoresis and western blotting

Cells from frozen stocks were rapidly thawed at 37 °C, resuspended in 1 ml PBS and centrifuged at 1000 *x* g (Centaur 2, Sanyo, IL, USA) for 10 min. The supernatant was discarded and the remaining pellet was resuspended in 1 ml PBS and the above step repeated. The cell pellet was then resuspended in 1 ml of lysis buffer with protease inhibitor cocktail (50 mM Tris-HCl pH 7.8, 5 mM EDTA, 2 $\mu l.ml^{-1}$ protease inhibitor cocktail (4-(2-aminoethyl) benzenesulfonyl fluoride (AEBSF), pepstatin A, E-64, bestatin, leupeptin, and aprotinin)) and centrifuged at 2000 *x* g (Centaur 2, Sanyo, IL, USA) for 10 min. The remaining pellet was resuspended in 500 µl of lysis buffer with protease inhibitor and centrifuged at 165,000 *x* g (Beckman TLX-120 Optima Ultracentrifuge, rota TLA120.2, Beckman Coulter, High Wycombe, UK) for 90 min at 4 °C. The final pellet was resuspended in 1 ml lysis buffer (without protease inhibitor) and stored at -80 °C until required. The protein concentration of the cell membrane preparation was quantified using the Bradford protein assay (Bradford 1976), section 2.2.11.6.

2.2.11.2 Sodium dodecyl sulphate polyacrylamide gel electrophoresis

A standard 6 % (w/v) sodium dodecyl sulphate polyacrylamide (SDS-PAGE) gel was used to separate proteins on a Bio-Rad Mini Protean II Dual Slab Cell (Biorad Laboratories Ltd, Hemel Hempstead, UK). The glass plates were cleaned with 70 % (v/v) ethanol in distilled water and air dried. For gel preparation, a small and a large glass plate were separated by rubber spacers and clamped together in the casting cassette.

The resolving and stacking gels were prepared as outlined in Tables 2.1 and 2.2 respectively. The components were added in the order stated in the tables and mixed in a beaker by gently swirling in order to prevent the addition of air which hinders polymerisation.

Table 2.1 Composition of sodium dodecyl sulphate polyacrylamide resolving gel (5 ml, 6 % (w/v) gel)

Materials	Ml
Deionised H_2O	2.700
1.5 M Tris-HCl pH 8.8, 0.4 % (w/v) SDS	1.250
30 % (v/v) acrylamide/bisacrylamide (30:1) in deionised H_2O	1.000
10 % (w/v) APS in deionised H_2O	0.050
TEMED	0.004

Table 2.2 Composition of sodium dodecyl sulphate polyacrylamide stacking gel (5 ml, 5 % (w/v) gel)

Materials	Ml
Deionised H_2O	2.870
0.5 M Tris-HCl pH 6.8, 0.4 % (w/v) SDS	1.250
30 % (v/v) acrylamide/bisacrylamide (30:1) in deionised H_2O	0.830
10 % (w/v) APS in d H_2O	0.050
TEMED	0.005

After the addition of TEMED the resolving gel was gently poured into the casting cassette of the Bio-Rad Mini Protean II Dual Slab Cell until the gel reached 1 cm from the bottom of the comb position. A small volume of water was immediately and gently poured on top of the resolving gel to prevent oxygen diffusing into the gel. The gel was left for approximately 45 min at room temperature to set. The water was removed and the top of the

gel was dried with blotting paper. The stacking gel was then cast on top of the resolving gel in the casting cassette, and the Teflon® comb inserted. The stacking gel was left to set for approximately 45 min at room temperature. The comb was removed and the wells were washed out with running buffer (deionised H_2O containing 3.75 $mg.ml^{-1}$ Tris base, 17.63 $mg.ml^{-1}$ glycine, 1.25 $mg.ml^{-1}$ SDS).

The glass plates were assembled in the electrophoresis tank, the central reservoir was filled with running buffer and running buffer was added to the external chamber to cover the bottom of the plates and complete the electrical circuit.

Protein samples were added to SDS-sample buffer (1:4 v/v) (composition of 8 ml SDS-sample buffer: 1.0 ml Tris base 0.025 M, 3.8 ml deionised H_2O, 0.8 ml glycerol, 1.6 ml 10 % (vv) SDS, 0.4 ml mercaptoethanol, 0.4 ml bromophenol blue 1 % (w/v)) and loaded into the wells of the stacking gel (30 µg protein per lane).

The molecular weight marker was heated to 95-100 °C for 3-5 min prior to loading onto stacking gel. Electrophoresis was carried out at 7 $V.cm^{-1}$ until the bromophenol blue (present in the sample buffer) reached 1 cm above the bottom of the gel.

2.2.11.3 Electrotransfer of proteins

The Bio-Rad Mini Trans-Blot Cell System (Biorad Laboratories Ltd, Hemel Hempstead, UK) was used to transfer the proteins from the SDS-PAGE gel to Hybond™-P polyvinylidene fluoride (PVDF) membrane.

Following electrophoresis, the SDS-PAGE gel was immersed in chilled transfer buffer (10 mM CAPS, pH 11) for 15 min to equilibrate. The PVDF membrane was cut to size and soaked in methanol for 10 s followed by deionised water for 5 min and finally in transfer buffer for 10 min. Gels were then placed onto the PVDF membranes and sandwiched between blotting paper and fibre pads, both previously soaked in transfer buffer.

Protein transfer took place in ice-cold transfer buffer at 200 mA for 2 h. Following transfer, the membranes were placed in blocking buffer (TBS-T containing 50 $mg.ml^{-1}$ Marvel® milk) at 4 °C overnight. The membranes were then washed three times in TBS-T for 10 min each time prior to immunological detection of P-gp.

2.2.11.4 Immunological detection of P-glycoprotein

The PVDF membranes containing electrotransferred proteins were incubated with either C219 anti-P-gp monoclonal antibody (Abcam, Cambridge, UK) 1:100 dilution in TBS-T or with TBS-T alone for 2 h at room temperature with gentle agitation. The membranes were then washed three times in excess TBS-T for 10 min and then incubated for 2 h at room temperature with horse radish peroxidise-conjugated sheep anti-mouse secondary IgG antibody (GE Healthcare Buckinghamshire, UK) 1:2000 dilution in TBS-T. The PVDF membranes were washed three times in excess TBS-T for 10 min followed by a final wash in TBS-T for 15 min.

2.2.11.5 Chemiluminescent detection of P-glycoprotein

Chemiluminescent protein detection was carried out in a dark room. ECL Plus® Western Blotting Detection System (GE Healthcare, Buckinghamshire, UK) was used for protein detection. Solutions A and B were mixed together (40:1) to generate the detection solution.

Excess wash buffer was drained from the PVDF membranes, the detection solution applied to the protein side of the membranes, and the membranes were incubated for 5 min at room temperature. The membranes were drained of detection solution and exposed to film (Hyperfilm™ ECL, Amersham Pharmacia Biotech, Buckinghamshire, UK) in an x-ray film cassette for 3-5 min.

Developer (Kodak Developer, Sigma-Aldrich Chemical Company, Poole, Dorset, UK) was then applied for approximately 3-5 min. The membranes were then rinsed in deionised water and fixed (Kodak Fixer, Sigma-Aldrich Chemical Company, Poole, Dorset, UK) for approximately 3-5 min.

2.2.11.6 Determination of protein concentration in cell lysates using the Bradford protein assay

Prior to use, working Bradford reagent was prepared by diluting Bradford dye reagent with distilled water (1:4 v/v). The solution was filtered through a Whatman grade I filter paper and equilibrated to room temperature. Bovine serum albumin (BSA) was used as the protein standard.

Serial dilutions of 1, 2, 4, 6, 8 and 10 µg.ml^{-1} BSA in PBS were prepared from a stock solution of 1 mg.ml^{-1} BSA in PBS. One ml working Bradford reagent was added directly to 20 µl of the sample to be quantified (either diluted BSA solution or cell lysate) in a cuvette. The solution was gently mixed and incubated at room temperature for 5 min. Absorbance was measured at 595 nm using A WPA UV1101 Biotech Photometer (Pharmacia Biotech, Cambridge, UK).

The protein content of the samples was determined using a standard curve derived from BSA serial dilutions. The experimental blank contained 20 µl of PBS instead of protein solution.

2.2.12 Determination of protein concentration of primary porcine brain endothelial cell monolayers in 96-well plates using the Bradford protein assay

Primary porcine brain endothelial cells were grown on clear 96-well flat bottom plates (section 2.2.3.3) to confluency in either PBEC culture medium alone, PBEC culture medium:CTX-TNA2 ACM (1:1), or PBEC culture medium:primary rat ACM (1:1 v/v).

Cell monolayers were washed with PBS warmed to 37 °C. A volume of 160 µl PBS was then added to each well followed by 40 µl of concentrated Bradford reagent dye and the plate was incubated for 5 min at room temperature. Absorbance was measured as described in section 2.2.11.6.

The protein content of the samples was determined using a standard curve derived from BSA (10, 20, 40, 60, 80, 100, 120 µg.ml^{-1}) within the 96-well plate.

2.2.13 Measurement of alkaline phosphatase activity in primary porcine brain endothelial cells

Alkaline phosphatase activity was determined as previously described by Sobue et al. 1999 with modifications (Sobue et al. 1999). Briefly, PBECs were grown on clear 96-well flat bottom plates (section 2.2.3.3) to confluency in either PBEC culture medium alone, PBEC culture medium:CTX-TNA2 ACM (1:1) or PBEC culture medium:primary rat ACM (1:1). Cell monolayers were washed with PBS warmed to 37 °C and incubated in the dark with 275 µl per well of assay buffer comprising of 0.7 M 2-amino-2-methyl-1-propanol, 1 mM

$MgCl_2$ and 10 mM *p*-nitrophenyl phosphate pH 10.2, for 10 min at 37 °C in a humidified atmosphere of 5 % CO_2 in air. The reaction was stopped by the addition of 55 µl 1 N NaOH.

The amount of *p*-nitrophenol product formed by the cells was determined spectrophotometrically using a multi-plate reader (Tecan Safire, Männedorf, Switzerland) at 410 nm using a molar extinction coefficient (ε) of 17,000 $M^{-1}.cm^{-1}$. Enzyme activity was expressed as specific enzyme activity ($nmol.min^{-1}.mg\ protein^{-1}$). The protein content of the cells was determined by the method described by Bradford 1976 (Bradford 1976) (section 2.2.12).

2.2.14 Measurement of γ-glutamyl transpeptidase activity in primary porcine brain endothelial cells

γ-glutamyl transpeptidase activity in PBECs was assessed according the method previously document by (William B 1981). In brief, PBECs were grown to confluence on 96-well plates under the same conditions described in section 2.2.3.3. The cells were washed with PBS warmed to 37 °C followed by incubation with 275 µl per well of assay buffer comprising of 0.1 M Tris-HCl pH 8, 20 mM glycylglycine and 1 mM L-γ-glutamyl-*p*-nitroanilide. The plates were incubated at 37 °C in a humidified atmosphere 5 % CO_2 in air for 40 min. The reaction was stopped by the addition of 55 µl of 1 N NaOH.

The amount of *p*-nitroanilide product formed by the cells was determined spectrophotometrically using a multi-plate reader (Tecan Safire, Männedorf, Switzerland) at 410 nm, using a ε of 8,800 $M^{-1}.cm^{-1}$. Enzyme activity was expressed as specific enzyme activity ($nmol.min^{-1}.mg\ protein^{-1}$). The protein content of the cells was determined as described in section 2.2.12.

2.2.15 Assessment of test drug concentration on cell viability

2.2.15.1 Determination of optimal seeding density for the cell viability (methylthiazolyldiphenyl-tetrazolium bromide) assay

Cells were required to remain in the exponential growth phase throughout the cell viability (methylthiazolyldiphenyl-tetrazolium bromide **(**3-(4, 5-dimethylthiazol-2-yl)-2, 5-diphenyltetrazolium bromide, MTT) assay to avoid underestimating drug toxicity. Therefore, it was important to determine optimal seeding density for each cell type used in these studies.

Cells were plated in a 96-well plate at a range of densities from 625-20,000 cells per well in quadruplicate. Cells were incubated at 37 °C in a humidified atmosphere of 5 % CO_2 for 48 h and a MTT assay was then performed (section 2.2.15.3). The seeding density that gave an absorbance of approximately 1 (at 570 nm) was chosen for subsequent MTT studies.

2.2.15.2 Test drug preparation

Four sterile dilutions (stock made in DMSO) of each test drug (30 µM, 3 µM, 0.3 µM and 0.03 µM) were freshly prepared on the day of the study. Culture medium was used as the diluent and the final solvent concentrations in all test drug concentrations did not exceed 1 % (v/v).

2.2.15.3 Cell viability (methylthiazolyldiphenyl-tetrazolium bromide) assay

Each cell type was seeded at the optimal density determined from a preliminary study (section 2.2.15.1) onto clear flat bottom 96-well plates until cells were approximately 70-80 % confluent, ensuring optimal sensitivity of the assay. Sterile water was dispensed into the outer most wells of each plate to reduce uneven evaporation of the culture medium during incubation which could produce erroneous results.

The MTT assay was performed under sterile conditions. Prior to commencing the assay the cells were inspected with a microscope to ensure that they were evenly distributed between wells and appeared to be healthy. Culture medium was changed to the corresponding transport medium for each cell type (Appendix 2) 30 min prior to the start of the assay to allow the cells to equilibrate.

The cells were washed with PBS pre-warmed to 37 °C and 200 µl of transport medium containing the test drug at the desired concentration was added. Four concentrations of each test drug in quadruplicate, in the presence and absence of the P-gp inhibitor GF120918A (2 µM), were assessed. The plates were incubated as described above for 60 min.

The medium was removed and the cells were carefully washed twice with PBS pre-warmed to 37 °C and incubated with fresh culture medium (200 µl per well) for 24 h at 37 °C in a humidified atmosphere of 5 % CO_2 in air. Methylthiazolyldiphenyl-tetrazolium bromide powder was dissolved in PBS (5 $mg.ml^{-1}$) and filtered through a 0.2 µm pore size Nalgene filter to sterilise the solution and to remove insoluble residues. Pre-warmed (37 °C) MTT

solution, 20 µl, was added to each well, the plates were protected from light and incubated at 37 °C in a humidified atmosphere of 5 % CO_2 in air for 4 h. The medium was removed and 100 µl of DMSO was added to all wells to stop the reaction and solubilise the purple formazan reaction product. The plates were incubated for a further 90 min at room temperature on an Orbital Incubator S150 Shaker (Stuart Scientific, Staffordshire, UK) at 100 rpm.

The absorbance of the samples was measured on a multi-plate reader (MRX, Dynatech Laboratories, Guernsey UK) using 570 nm as the test wavelength and 630 nm as the reference wavelength.

Percentage cell viability was determined using the following:

% cell viability = (absorbance of sample) / (absorbance of control) x 100

Equation 2.4

The mean blank absorbance was subtracted from the absorbance of each of the samples and controls before the percentage cell viability was calculated.

2.2.15.4 Quality control of the cell viability (methylthiazolyldiphenyl-tetrazolium bromide) assay

The solvent control (control containing no drug) corresponded to a cell viability of 100 %. Solvent controls were placed on both the left and the right side of the plates in order to detect systematic errors. The assay was considered acceptable if the means of each of the two solvent controls did not vary by more than ± 15 %. Growth controls (cells not exposed to drug) were present to detect the effect of solvent. As a positive control, DMSO (no growth medium) was added to kill the cells to demonstrate that the assay was working as expected.

2.2.16 *In vitro* cell monolayer permeability studies

2.2.16.1 The Caco-2 *in vitro* blood-brain barrier model

The Caco-2 *in vitro* BBB model consisted of Caco-2 cells seeded onto Transwell® polycarbonate inserts (pore size 0.4 µm, diameter 12 mm, growth area 1.12 cm^2, 12-well cell culture cluster). Cells were seeded at a density of 1.2 x 10^5 $cell.cm^{-2}$ and were cultured for 21-29 days in Caco-2 culture medium (DMEM containing 10 % (v/v) FBS, 2 mM L-glutamine,

1 % (v/v) NEAA, 100 $U.ml^{-1}$ penicillin G sodium and 100 $\mu g.ml^{-1}$ streptomycin sulphate). Inserts contained 0.5 ml in the apical compartment and 1.5 ml in the basolateral compartment, and were maintained at 37 °C in a humidified atmosphere of 5 % CO_2 in air. The medium was initially changed 24 h post-seeding to remove non-adherent cells and reduce the risk of multilayer formation. Thereafter, the medium was changed on alternate days and TER measurements were taken as described in section 2.2.5.

2.2.16.2 The hCMEC/D3 *in vitro* blood-brain barrier model

The hCMEC/D3 cells were seeded at a density of 5 x 10^4 $cells.cm^{-2}$ onto Transwell® polycarbonate inserts (pore size 0.4 µm, diameter 12 mm, growth area 1.12 cm^2, 12-well cell culture cluster), pre-coated with rat tail collagen type 1 (100 $\mu g.ml^{-1}$ in 1 mM acetic acid) (section 2.2.3.1). The cells were cultured for 7 days and maintained at 37 °C in a humidified atmosphere of 5 % CO_2 in air. Medium was replaced every third day when TER measurements were taken (section 2.2.5).

2.2.16.3 The MDR-1 MDCKII *in vitro* blood-brain barrier model

The MDR-1 MDCKII *in vitro* BBB consisted of MDR-1 MDCKII cells grown on a BD Falcon™ HTS 24-Multiwell Insert System for automated high throughput screening assays. The insert system consisted of a cell culture insert assay platform, composed of a multiwell insert plate with microporous polyethylene terephthalate membrane (1.0 µM pore size, diameter 6.5 mm, growth area 0.31 cm^2, 24 well clusters), a feeder tray and a lid. The MDR-1 MDCKII and the corresponding wild type cells were seeded at a density of 7.5 x 10^4 cells per well. The medium was changed 24 h post-seeding and the day before the study. Cells were ready for use 3-4 days post-seeding.

2.2.17 Measure of apparent permeability, exact permeability and P-glycoprotein efflux activity

Transport assays were conducted using all of the *in vitro* BBB models described in section 2.2.4 and 2.2.16. The permeability of centrally-acting test drugs (section 2.1.3) was assessed bi-directionally by measuring A-B and B-A transport, in the presence and absence of the P-gp inhibitor, GF120918 (2 µM). To assess cell monolayer integrity Lucifer yellow

(100 µM) was added to the donor compartment of all wells. All test drugs were assayed in duplicate, in three independent experiments.

Transport assays using PBEC, hCMEC/D3 and Caco-2 *in vitro* BBB models were performed at University of Manchester as follows; the cell monolayers were carefully washed with PBS and equilibrated in the appropriate transport medium/solution (Appendix 2) for 30 min at 37 °C. For incubations containing inhibitor, the cell monolayers were pre-incubated for 30 min in transport medium containing 2 µM GF120918 (in both apical and basolateral compartments). Cells were incubated with 3 µM of test drug (and 100 µM Lucifer yellow) in transport medium in the donor compartment. Transport across the confluent cell monolayer was measured in both A-B and B-A directions in the presence and absence of GF120918. The *in vitro* BBB models were incubated for 60 min at 37 °C. At a single 60 min sampling time point, 25 µl was taken from the apical and basolateral compartment of each Transwell® insert. A blank (no cells seeded) plate with the same insert coating (section 2.2.3.1) as the corresponding *in vitro* BBB model was prepared containing 0.5 ml of dose solution in the apical compartment, from which a 25 µl sample was taken at t=0 min and t=60 min to factor possible nonspecific binding to the plate over time. Samples were transferred to a 96-deep well block containing an internal standard (SB243213) and analysed using liquid chromatography-tandem mass spectroscopy (LC-MS/MS) as described in section 2.2.17.1. The drug peak area to internal standard ratio was used to calculate P_{app} (Equation 2.3) and P_{exact} (Equation 2.5 and 2.6) in both directions, efflux ratios (fold difference between B-A rate of drug transport across *in vitro* BBB model relative to A-B rate of drug transport) and test drug recoveries (Equation 2.7).

At 60 min, 150 µl was removed from the apical and basolateral compartments to assess Lucifer yellow levels fluorometrically: excitation λ 425 nm and emission λ 515 nm, on a multi-plate reader (MRX, Dynatech Laboratories, Guernsey UK). Transcellular electrical resistance was also measured before and after each transport assay.

$$P = -\left(\frac{V_R V_D}{(V_R + V_D)At}\right)\ln\left\{1 - \frac{\langle C_R(t)\rangle}{\langle C(t)\rangle}\right\}$$

Equation 2.5

V_D = Donor compartment volume (cm^3)

V_R = Receiver chamber volume (cm^3)

A = Surface area of the permeability barrier (cm^2)

t = Time of measurement (s)

C_R = Drug concentration in the receiver compartment ($mol.L^{-1}$) at time t

$\langle C(t)\rangle$ = Average system concentration of drug defined by Equation 2.6

$$\langle C(t)\rangle = \frac{V_D C_D(t) + V_R C_R(t)}{V_D + V_R}$$

Equation 2.6

C_D = Drug concentration in the donor compartment ($mol.L^{-1}$) at time t

$$\text{Percentage Recovery} = 100\ x\left(\frac{\left(V_r x C_r^{\ final}\right) + \left(V_d x C_d^{\ final}\right)}{V_d x C_0}\right)$$

Equation 2.7

V_r = Volume in the receiver compartment (cm^3)

V_d = Volume in the donor compartment in (cm^3)

C_0 = Concentration of dosing solution (µM)

$C_r^{\ final}$ = Cumulative receiver concentration at the end of the incubation period (µM)

$C_d^{\ final}$ = Concentration in the donor compartment at end of the incubation period (µM)

Transport assays using MDR1-MDCKII and MDCKwt in vitro BBB models were performed at GSK (New Frontiers Science Park, Harlow, Essex, UK) (using Dulbecco's phosphate buffered saline (DPBS) containing 1 mM HEPES as transport solution) as above

with modifications. The assays were carried out using a Packard Multiprobe 2 HT ex-robot (Perkin Elmer, Massachusetts, USA) for high throughput screening in 24 Transwell® clusters, under gentle agitation. An acceptance criteria for Lucifer yellow P_{exact} was employed for this assay, where $P_{exact} < 80$ nm.s^{-1}. If more than five wells on a 24-well plate failed, the run failed and was repeated.

The efflux substrate amprenavir (also a test drug) was included in every assay performed at GSK as a positive control. MDR-1 MDCKII cells were expected to exhibit functional P-gp activity whereas MDCKwt were not. Amprenavir being one of the twelve test drugs was also used in all transport studies using the other *in vitro* BBB models.

2.2.17.1 Analysis of test drugs using liquid chromatography-tandem mass spectroscopy

Samples were analysed by LC-MS/MS on a Quattro Ultima (Waters Ltd, Herts, UK) mass spectrometer, employing an electrospray interface in positive mode at a source temperature of 125 °C. Each drug was initially tuned to give specific mass transitions to monitor (Appendix 4). Samples, 10 µl, were injected into a 2795 HPLC system (Waters Ltd, Herts, UK) onto a Luna C18 50 x 4.6 mm 3 µm column (Phenomenex, Cheshire, UK) operated at 40 °C and at an eluent flow rate of 1 ml.min^{-1}, which was split by an accurate splitter (Presearch, Hampshire, UK) to deliver 0.25 ml.min^{-1} to the mass spectrometer. Gradient elution of each analyte was achieved over a 5 min runtime.

2.2.18 Equilibrium dialysis measurement of nonspecific drug binding

Equilibrium dialysis methodology was adapted from Summerfield et al. (Summerfield, Stevens et al. 2006). Fraction unbound drug in blood and brain for each test drug was determined using 96-well equilibrium dialysis equipment (HT dialysis LLC, Gales Ferry, CT) (Banker et al. 2003).

Dialysis membrane strips (molecular weight cut off (MWCO) 6-8-kDa) were conditioned sequentially in deionised water for 40 min followed by deionised water:ethanol 80:20 (v/v) for 20 min. The membranes were gently separated and maintained in the ethanolic solution until required. Prior to use, membranes were rinsed twice in deionised water and excess water removed.

Brains were weighed, added to PBS (brain:PBS 1:2 (w/v)) and homogenised (Dounce Homogeniser, Jencons, UK). Homogenisation commenced using a loose pestle (89-127 µm clearance) for 15 strokes followed by a tight pestle (25-76 µm clearance) for 15 strokes. Alternatively, brains were homogenised (brain:PBS 1:2 (w/v)) with a Heidolph Silent Crusher M (Heidolph Instruments GmbH & Co, Walpersdorfer, Schwabach) at 26,000 rpm. Blood was diluted (1:1 (v/v)) with PBS. Both diluted blood and brain homogenate were mixed continuously prior to dialysis studies on an orbital plate micro shaker (Orbital incubator S150 with shaker, Stuart Scientific, Staffordshire, UK) at 125 rpm.

Diluted blood and brain homogenate were spiked with each of the test drugs to give a final concentration of 1 $\mu g.ml^{-1}$ and 100 µl aliquots of spiked diluted blood and brain homogenate were loaded into the 96-well equilibrium dialysis equipment (6 replicate determinants in each study, n of at least 3 for all drugs). Diluted blood and brain homogenate were dialysed against 100 µl PBS on an orbital plate micro shaker (Orbital incubator S150 with shaker, Stuart Scientific, Staffordshire, UK) at 125 rpm at 37 °C for 5 h.

The plate (Figure 2.3) was sealed to eliminate evaporation. A positive control compound (GW633104) (n=6 in blood or brain or both) was present in every equilibrium dialysis study. For the equilibrium dialysis plate to be accepted the results from the control compound in blood and brain were within 2-fold of the mean replicate data.

Figure 2.3 A schematic of the equilibrium dialysis study using 96-well equilibrium dialysis equipment

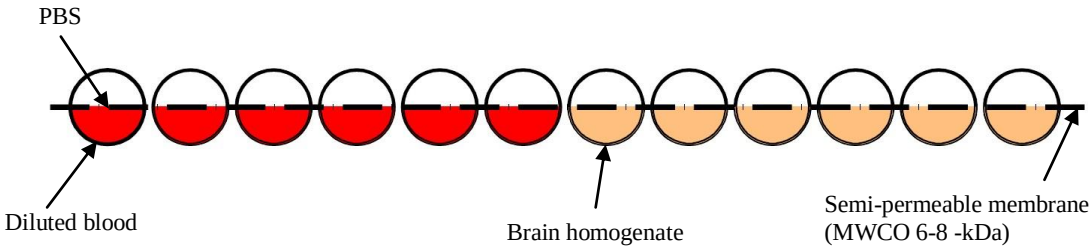

A 100 µl volume of diluted blood and brain homogenate spiked with centrally-acting test drug was dialysed against 100 µl PBS for 5 h at 37 °C, n of at least 3, 6 replicate determinants.

Following 5 h incubation, 50 µl PBS, 20 µl diluted blood and 20 µl of brain homogenate were transferred from the 96-well equilibrium dialysis equipment to SreenMate tubes (Matrix Technologies, Hudson, NH, USA). A 20 µl volume of control diluted blood (diluted blood containing no drug) or control brain homogenate (brain homogenate containing no drug) was added to the corresponding 50 µl PBS sample, 50 µl of control PBS was added to the 20 µl diluted blood sample and 50 µl of control PBS added to the 20 µl brain homogenate sample to produce the same matrix composition for analysis (Figure 2.4). Test drugs were extracted by the addition of 200 µl of acetonitrile containing an internal standard (SB243213, 50 $ng.ml^{-1}$). Samples were allowed to mix for 15 min, centrifuged at 2465 x g for 20 min (Mistral 3000i, MSE Ltd, Loughborough, UK) and the supernatant assayed using LC-MS/MS section 2.2.17.1.

Figure 2.4 Flow diagram of matrix matching in equilibrium dialysis studies

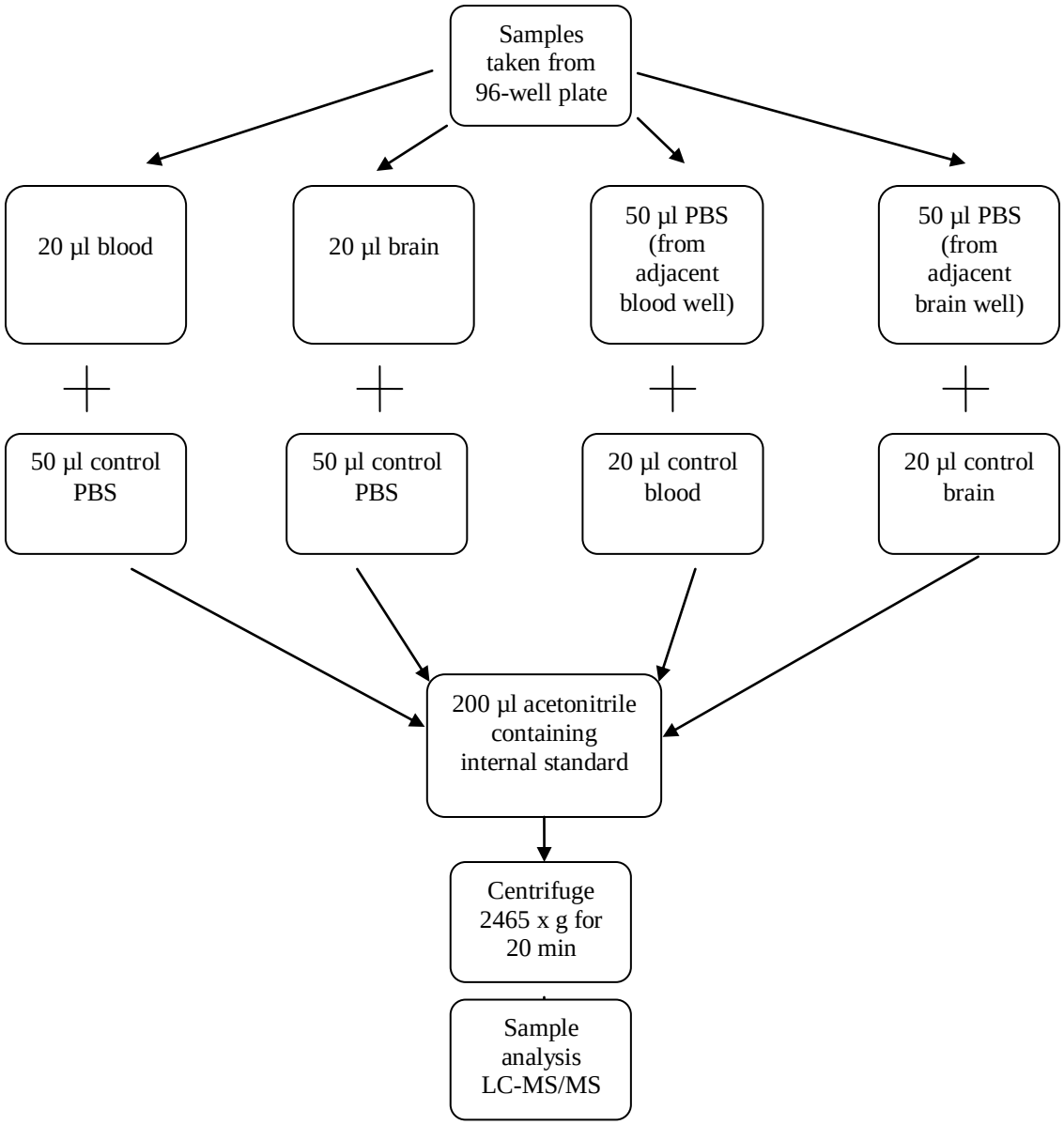

A PBS, blood or brain sample was taken from each well of the 96-well plate and matrix matched with the corresponding PBS, blood or brain control. Samples were then extracted with acetonitrile containing an internal standard, centrifuged and analysed by LC-MS/MS.

Fraction unbound was determined as the ratio of the test drug peak area to internal standard peak area in PBS divided by the ratio of the test drug peak area to internal standard

peak area in diluted blood or brain homogenate with correction for dilution factor according to Equation 2.8 (Summerfield et al. 2006).

$$fu = \frac{(1/D)}{(1/fu(apparent) - 1) + (1/D)}$$

Equation 2.8

D = the dilution factor in diluted blood and brain homogenate

$fu\ (apparent)$ = Measured fraction unbound of drug in diluted blood and brain homogenate.

2.2.19 Determination of the extent of test drug penetration in rat

The extent of test drug penetration in rat described as the total brain to blood concentration ratio (K_p) was supplementary data, determined by GSK, at GSK (New frontiers Science Park, Harlow, Essex, UK) and remains the property of GSK. In brief, rats were dosed via intravenous infusion. At the end of the infusion period rats were sacrificed and blood and brain tissue were removed and analysed.

2.2.20 Physiologically based pharmacokinetic modelling

An in-house hybrid-physiologically-based pharmacokinetic (PBPK) model of the rat CNS (Appendix 7) was developed by Dr Raj Badhan using MATLAB Version 7.5b (manuscript in preparation) to predict the extent of drug penetration *in vivo*. The model was generated using literature derived physiological parameters for Sprague-Dawley rats.

The ratio of unbound drug concentration in the brain to unbound drug concentration in the blood ($K_{p,uu}$) was the parameter that was predicted to quantify the extent of drug penetration. The model has been validated by Dr Raj Badhan using drug-specific parameters of 7 model compounds. The predicted $K_{p,uu}$ of the 7 model compounds was within 3-fold of observed values reported in microdialysis studies.

In the current studies, simulations using the rat CNS hybrid-PBPK model were ran for 5 test drugs used throughout this work, namely chlorpromazine, citalopram, clozapine, haloperidol and risperidone in order to predict the extent of CNS drug penetration, as

described by $K_{p,uu}$ using *in vitro* unbound drug fraction and permeability and *in situ* permeability.

The drug-specific pharmacokinetic input parameters were rat volume of distribution (V_d) and clearance (CL) obtained from the literature (see Table 6.1). The drug-specific permeability input parameters were *in vitro* permeability generated from transport studies using MDR1-MDCKII (Chapter 4) and porcine *in vitro* BBB models (Chapter 4), rat *in situ* permeability data sourced from the literature (Summerfield et al. 2007) and efflux ratios derived from knock out mice studies obtained from the literature (Doran et al. 2005). The drug-specific fraction unbound input parameters were rat fu_{blood} and fu_{brain} obtained using equilibrium dialysis (Chapter 5).

The model predictions were compared to $K_{p,uu}$ values calculated (Equation 2.9) using rat K_p (supplementary data, determined by GSK and the property of GSK) and rat fu_{blood} and fu_{brain} determined using equilibrium dialysis (Chapter 5). Predictions were considered to be similar to calculated $K_{p,uu}$ if they were within 3-fold of the calculated values.

$$K_{p,uu} = K_p \times \frac{fu_{brain}}{fu_{blood}} \qquad \text{Equation 2.9}$$

Where K_p is the total brain to blood concentration ratio, fu_{brain} is the fraction unbound in brain and fu_{blood} is the fraction unbound in blood.

Chapter 3

Characterisation of a Primary Porcine *In Vitro* Blood-Brain Barrier Model

3.0 Chapter 3: Characterisation of a primary porcine *in vitro* blood-brain barrier model

3.1 Background

The development of novel drugs to treat disorders of the CNS is the fastest growing sector within the modern drug discovery paradigm (Summerfield et al. 2007). A well characterised, physiologically-representative *in vitro* BBB model that is able to predict *in vivo* BBB permeability is a valuable tool to aid the discovery of new centrally acting drug candidates.

A primary porcine *in vitro* BBB model was characterised, for use, as a drug permeability screen. For the model to be used as a permeability screen it must exhibit physiologically realistic cell architecture, tight junction protein complexes between adjacent cells, a restrictive paracellular pathway, functionally active efflux transporters and BBB marker enzymes.

The primary porcine *in vitro* BBB model was characterised by; studying endothelial cell morphology, expression of tight junction proteins, measurement of γ-glutamyl transpeptidase and alkaline phosphatase marker enzyme activity and functional expression of P-gp, since this efflux transporter is a major contributor to BBB barrier properties *in vivo*.

It is essential to demonstrate that a robust *in vitro* model possesses many of the key *in vivo* characteristics if it is to be used successfully in BBB permeability studies.

3.2 Results

3.2.1 Isolation of porcine brain microvascular capillaries

Porcine brain microvascular capillaries were successfully isolated (section 2.2.3), seeded onto 6-well plates pre-coated with collagen and fibronectin (section 2.2.3.1) and maintained in culture (section 2.2.3.2) until the porcine brain endothelial cells (PBECs) had reached confluency, approximately 10 days post-seeding. The morphology of the PBECs was examined using a light microscope (Olympus CK30, Olympus Europa, Hamburg, Germany).

Initially, the isolated capillaries were observed as short, occasionally branched, microvascular capillary fragments, although, contaminating cells for example pericytes were also present. The capillary fragments attached quickly in clusters to the surfaces of the 6-well plates 2 to 4 h post-seeding. Once attached, the PBECs grew out from the capillary fragments forming islands of cells.

The capillary fragments and cells were treated with puromycin (section 2.2.3.2) 24 h post-seeding to purify the PBECs (the presence of contaminating glial cells are inevitable in primary isolated cultures). Three to 5 days post-seeding the PBECs had differentiated to exhibit typical, elongated, spindly, fusiform morphology, characteristic of CECs. By day 7 the PBECs were approximately 70 % confluent and free from contaminating cells.

Phase contrast photographs of the PBECs on day 10 revealed a uniform, tightly packed, confluent monolayer (Figure 3.1). The morphology of the PBECs was consistent both within and between isolations.

Figure 3.1 Phase contrast photograph of a confluent porcine brain endothelial cell monolayer

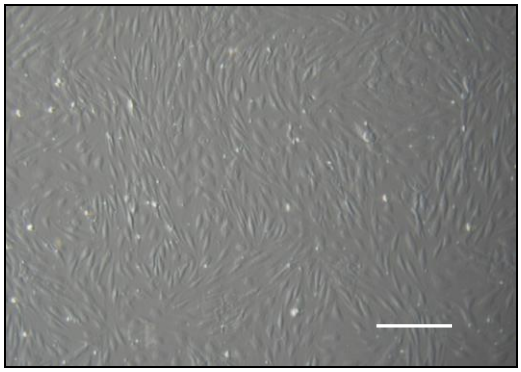

Porcine brain endothelial cells exhibited typical elongated, spindly, fusiform morphology characteristic of CECs and formed a uniform, tightly packed, confluent monolayer. Scale bar 50 µm. Magnification x 40.

3.2.2 Effect of culture conditions on porcine brain endothelial cell monolayer transcellular electrical resistance and morphology

Previous studies have shown culture conditions significantly modulate the properties of *in vitro* BBB models (Dehouck et al. 1990; Rubin et al. 1991; El Hafny et al. 1996; El Hafny et al. 1997; Sobue et al. 1999; Gaillard et al. 2000; Gumbleton et al. 2001; Nitz et al. 2003; Haseloff et al. 2005; Calabria et al. 2006). Consequently, the effects of supplements (312.5 µM cAMP, 17.5 µM RO-20-1724 and 550 nM hydrocortisone) and co-culture with primary rat astrocytes on PBEC monolayer TER (Figure 3.2) and cellular morphology (Figure 3.3) was investigated in order to determine the TER and morphology most representative of BBB *in vivo*.

Porcine brain endothelial cells monolayers maintained in medium containing supplements (cAMP, RO-20-1724 and hydrocortisone) and co-cultured with primary rat astrocytes achieved significantly higher TER, 385 ± 28 $\Omega.cm^2$ (Figure 3.2 yellow bar), compared to all other culture conditions.

Porcine brain endothelial cell monolayers maintained in mono-culture (i.e. without astrocytes) in medium containing supplements achieved TER of 233 ± 32 $\Omega.cm^2$ (Figure 3.2 red bar). Porcine brain endothelial cell monolayers maintained in medium containing no supplements and co-cultured with astrocytes, achieved TER of 200 ± 17 $\Omega.cm^2$ (Figure 3.2 green bar). Porcine brain endothelial cells maintained in medium containing no supplements and without astrocytes achieved the lowest TER of 40 ± 10 $\Omega.cm^2$ (Figure 3.2 blue bar).

Figure 3.2 **Effect of culture conditions on transcellular electrical resistance of porcine brain endothelial cell monolayers**

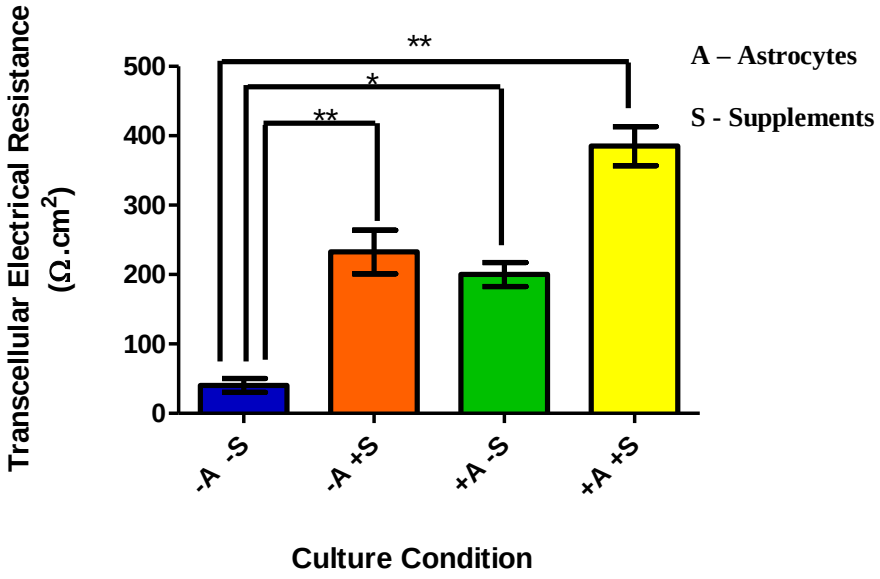

Porcine brain endothelial cells were maintained on Transwell® inserts for 7 days. The PBECs were maintained in PBEC growth medium (DMEM containing 10 % (v/v) plasma-derived serum, 100 $U.ml^{-1}$ penicillin G sodium, 100 $\mu g.ml^{-1}$ streptomycin sulphate, 125 µM heparin and 2 mM L-glutamine) until day 6 and in mono-culture (no astrocytes) (blue, red) or in co-culture with primary rat astrocytes in a non-contact model for 3 days (from days 4 to 6) (green, yellow). On day 6 the astrocytes were removed from the monolayers in co-culture and PBEC growth medium was replaced (in all Transwell® inserts) with transport medium (DMEM containing, 100 $U.ml^{-1}$ penicillin G sodium, 100 $\mu g.ml^{-1}$ streptomycin sulphate, 125 µM heparin, 2 mM L-glutamine) with (red, yellow) or without supplements (312.5 µM cAMP, 17.5 µM RO-20-1724 and 550 nM hydrocortisone) (blue, green) 24 h before TER was measured, on day 7. Data are expressed as mean TER ± standard deviation of at least 4 Transwell® inserts from one PBEC isolation employing 10-12 pooled brains. Statistical significance was determined using a Mann-Whitney test: * = $P< 0.05$ and ** = $P< 0.01$.

Figure 3.3 Effect of culture conditions on porcine brain endothelial cell morphology

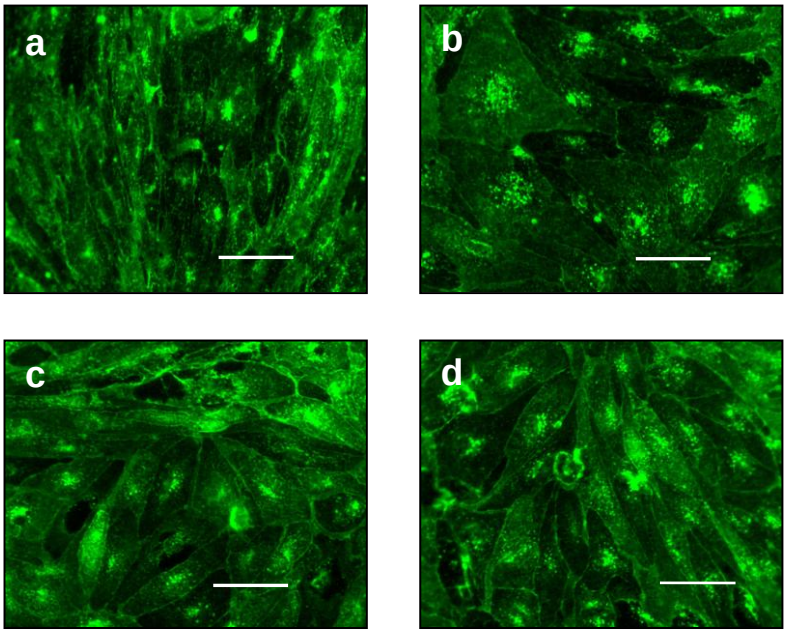

Porcine brain endothelial cells were maintained on Transwell® inserts for 7 days in either mono-culture (a, b) or co-culture with primary rat astrocytes (c, d) and maintained with (b, d) or without (a, c) supplements (312.5 µM cAMP, 17.5 µM RO-20-1724 and 550 nM hydrocortisone). The cells were labeled with isolectin B4 and examined by fluorescent microscopy. Scale bar: 10 µm and magnification x 100.

Porcine brain endothelial cells maintained in co-culture with primary rat astrocytes exhibited a more discrete spindle-like morphology (Figure 3.3c and 3.3d), indicative of the *in vivo* BBB phenotype, compared to PBECs maintained in mono-culture (Figure 3.3a and 3.3b**).** Porcine brain endothelial cells maintained in medium containing supplements and co-cultured with astrocytes (Figure 3.3d) demonstrated a spindle-shaped morphology similar to PBECs maintained without supplements and co-cultured with astrocytes (Figure 3.3c) suggesting that co-culture with astrocytes had a greater influence on the morphology of the PBECs compared to supplements.

3.2.3 Purification of porcine brain endothelial cells with puromycin treatment.

Porcine brain endothelial cell monolayer maintained in transport medium containing supplements and co-cultured with primary rat astrocytes have been shown to achieve the highest TER (385 ± 28 $\Omega.cm^2$, section 3.2.2) compared to PBEC monolayers maintained in

other culture conditions. To optimise culture conditions and increase TER further, purification of PBECs prior to seeding onto Transwell® inserts was investigated.

Endothelial cells are known to be more sensitive to trypsin than pericytes (and other contaminating cells) and detach from 6-well plates before contaminating cells during trypinisation. By monitoring the plates closely under the microscope, approximately 3 min after the addition of trypsin, the majority of the PBECs detached first and were collected leaving pericytes and other contaminating cells adhered to the culture matrix. However, this step was difficult to carry out and standardise between each 6-well plate.

To increase purity of PBECs, treatment with puromycin was investigated (Perriere et al. 2005). Isolated porcine brain microvascular capillaries were treated with 3 $\mu g.ml^{-1}$ puromycin for 3 days 24 h post-seeding onto 6-well plates (section 2.2.3.2). Puromycin, a P-gp substrate, is toxic to contaminating glial cells that either lack or express P-gp at lower levels than PBECs.

Figure 3.4 **Effect of puromycin treatment on transcellular electrical resistance of porcine brain endothelial cell monolayers**

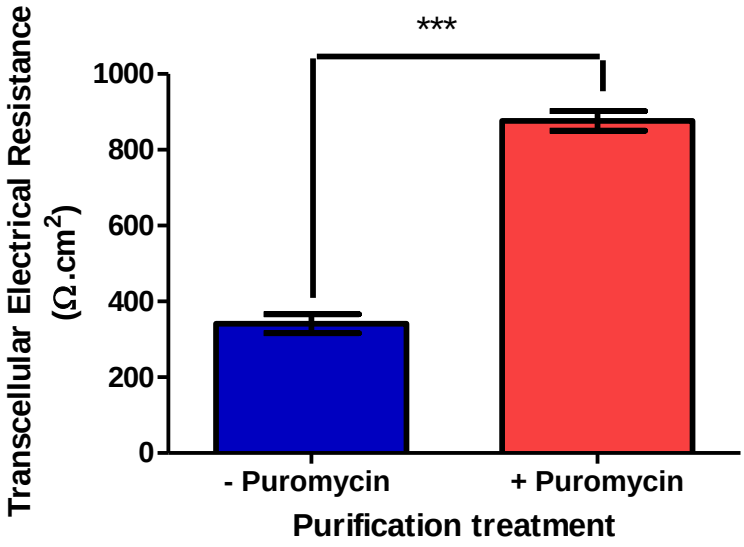

Porcine brain endothelial cells grown on 6-well plates were treated with puromycin (3 µg.ml^{-1} for 3 days 24 h post-seeding (red)) or no puromycin treatment (blue). Porcine brain endothelial cells were harvested, seeded onto Transwell® inserts and maintained in PBEC growth medium and in co-culture with primary rat astrocytes for 3 days (from day 4-6). On day 6 PBEC growth medium was replaced with transport medium containing supplements (312.5 µM cAMP, 17.5 µM RO-20-1724 and 550 nM hydrocortisone) 24 h before TER was measured, on day 7. Data are expressed as mean TER ± standard deviation, of 8 Transwell® inserts from one PBEC isolation employing 10-12 pooled brains. Statistical significance was determined using a Mann-Whitney test: *** = P<0.001.

Transcellular electrical resistance of PBEC monolayers was significantly increased from 341 ± 71 Ω.cm^2 (P< 0.001) for PBEC monolayers not treated with puromycin to 867 ± 74 Ω.cm^2 for PBEC monolayers treated with puromycin (Figure 3.4).

The presence of contaminating cells appears to reduce the TER of the PBEC monolayers. Purification with puromycin treatment has standardised and enhanced the purification step, whilst producing PBEC monolayers with significantly greater TER.

3.2.4 Effect of astrocyte cell type on transcellular electrical resistance of primary porcine brain endothelial cell monolayers

It is widely reported in the literature that glial cells, in particular astrocytes, play a role in the induction the BBB phenotype of CECs. Astrocytes have been shown to up-regulate the expression of tight junction proteins (Dehouck, Meresse et al. 1990), the BBB marker enzyme

γ-glutamyltranspeptidase (El Hafny et al. 1996) and several specific transport systems (El Hafny et al. 1997).

Parallel studies in our laboratory have shown that PBEC monolayers co-cultured with the CTX-TNA2 rat astrocyte cell line and maintained in PBEC growth medium:CTX-TNA2, ACM (1:1) (CTX-TNA2, ACM is DMEM containing 10 % (v/v) FBS, 100 $U.ml^{-1}$ penicillin G sodium and 100 $\mu g.ml^{-1}$ streptomycin harvested from CTX-TNA2 rat astrocytes) routinely demonstrate TER > 2000 $\Omega.cm^2$ (personal communication with Dr Carina Cantrill). Such TERs are substantially higher than PBEC monolayers maintained in co-culture with primary rat astrocytes and are similar to electrical resistances reported for the *in vivo* BBB (Crone et al. 1982; Butt et al. 1990).

3.2.5 Time course of transcellular electrical resistance across the primary porcine *in vitro* blood-brain barrier

Following the results obtained from previous studies (section 3.2.2 and 3.2.3) and personal communication with Dr Carina Cantrill, PBEC monolayer TER (pre-treated with puromycin and co-cultured with CTX-TNA astrocytes) was examined over a time course of 7 days.

Figure 3.5 **Transcellullar electrical resistance of the primary porcine *in vitro* blood-brain barrier model over a time course of seven days**

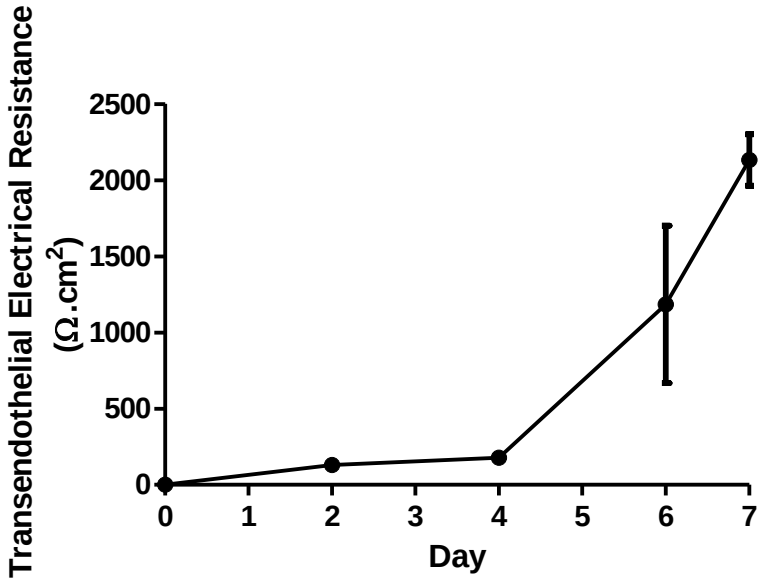

Porcine brain endothelial cells treated with puromycin were seeded onto Transwell® inserts and maintained in PBEC growth medium:ACM (CTX-TNA2 rat astrocyte cell line) (1:1). Porcine brain endothelial cells were co-cultured with the CTX-TNA2 rat astrocyte cell line in a non-contact model for 3 days (from day 4-6). On day 6 the astrocytes were removed and the medium changed to transport medium containing supplements (312.5 µM cAMP, 17.5 µM RO-20-1724 and 550 nM hydrocortisone) 24 h before TER was measured. Transcellular electrical resistance was routinely measured on days 2, 4, 6 and 7. Each data point represents the mean TER ± standard deviation of 8 Transwell® inserts from one typical PBEC isolation employing 10-12 pooled brains.

The TER of the PBEC monolayers co-cultured with the CTX-TNA2 rat astrocyte cell line and maintained in PBEC growth medium:CTX-TNA2, ACM (1:1) and supplements consistently achieved TER>2000 $\Omega.cm^2$ seven days post-seeding (Figure 3.5) (TER 2132 ± 169 $\Omega.cm^2$ typical example from one isolation), compared to the TER of PBEC monolayers co-cultured with primary rat astrocytes and maintained in PBEC supplemented growth medium (TER 867 ± 74 $\Omega.cm^2$ section 3.2.3).

Porcine brain endothelial cell monolayers examined under these specific culture conditions achieved TER higher than was observed in other studies performed during this work (section 3.2.2 and 3.2.3). Porcine brain endothelial cells maintained under the conditions of this study will be referred to as the primary porcine *in vitro* BBB model throughout the rest of this work and will be used for subsequent transport studies (Chapter 4).

3.2.6 Ultrastructural morphology of the primary porcine *in vitro* blood-brain barrier model

Ultrastructural morphological features of the primary porcine *in vitro* BBB were qualitatively examined by transmission electron microscopy (section 2.2.6) seven days post-seeding onto Transwell® inserts (Figure 3.6a and 3.6b).

Figure 3.6 **Transmission electron micrographs of the primary porcine *in vitro* blood-brain barrier model**

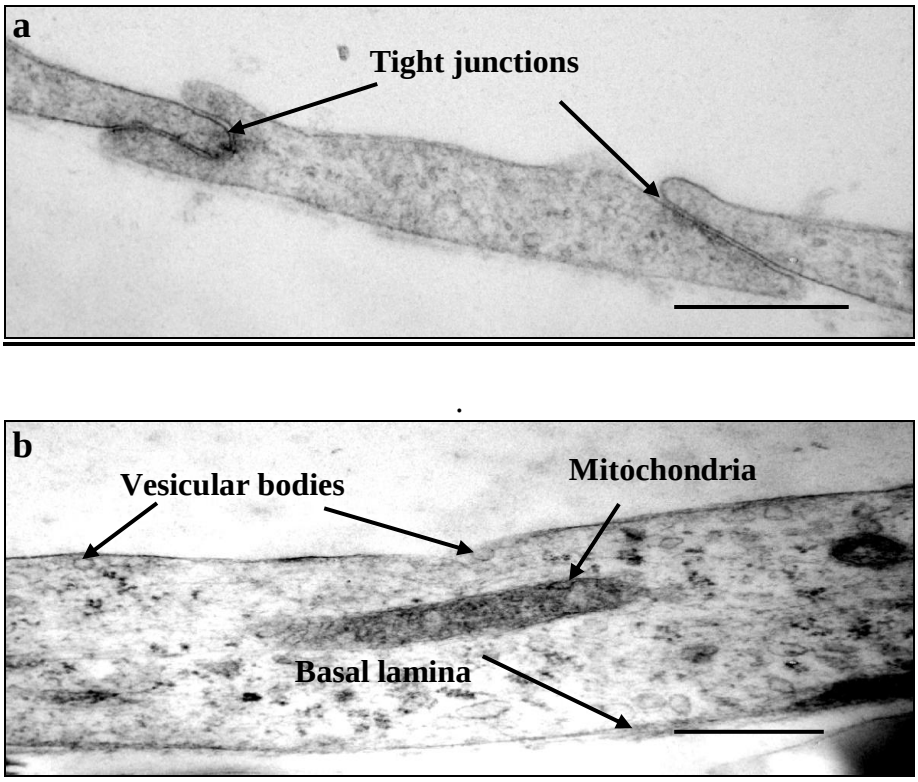

(a) Transmission electron micrograph of a cross section of the primary porcine *in vitro* BBB model, showing spindle-shaped morphology and the formation of tight junction complexes between adjacent cells. Bar is 1.25 µm. Magnification 17,000 x. (b) Transmission electron image showing preservation of mitochondria, a prominent basal lamina on the under-surface of the cells and a number of intracellular vesicles within the cell cytoplasm. Bar indicates 2.5 µm. Magnification 17,000 x.

Transmission electron micrographs confirmed the formation of PBEC monolayers. The PBECs retained the spindle-shaped morphology characteristic of endothelial cells (perinuclear cell diameter ~1.0 µm) which extended peripherally into thin attenuations (diameter ~0.1 µm).

Tight junction protein complexes appear as electron dense structures at contact points between adjacent cells (Figure 3.6a). Mitochondria and a prominent basal lamina were present, as well as vesicular bodies throughout the cells (Figure 3.6b).

3.2.7 Detection of the tight junction proteins occludin and ZO-1 in the primary porcine *in vitro* blood-brain barrier

Transmission electron micrographs of the primary porcine *in vitro* BBB model confirmed the presence of tight junctions between apposing cells (Figure 3.6a). To confirm the expression and localisation of tight junction proteins in PBEC cell monolayers, immunofluorescence studies were conducted.

Figure 3.7 Immunofluorescent detection of tight junction proteins in porcine brain endothelial cell monolayers

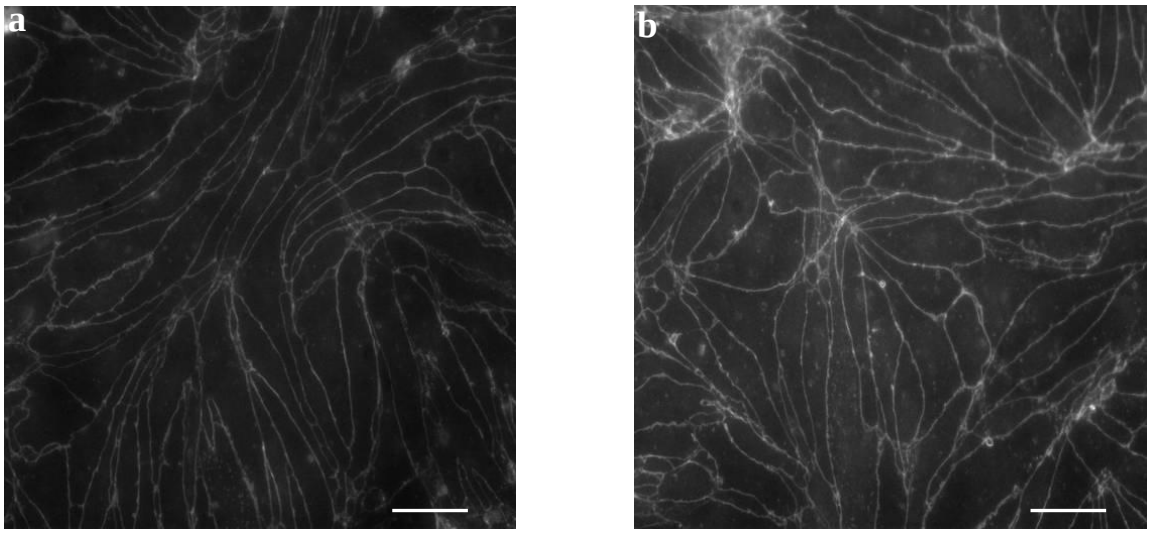

Porcine brain endothelial cell monolayers were washed with PBS warmed to 37 °C and fixed in ice cold methanol:acetone solution (1:1) for 2 min on ice followed by incubation with 10 % (v/v) horse serum in PBS, for 1 h at room temperature. Cell monolayers were washed with PBS and incubated with rabbit anti-human occludin (1:100) (a) or rabbit anti human-ZO-1 (1:100) (b) primary antibody for 1 h at room temperature. The cell monolayers were washed with PBS warmed to 37 °C and incubated with FITC labeled mouse anti-rabbit IgG (1:200) secondary antibody for 45 min at room temperature in the dark. The cell monolayers were washed with PBS, the filters cut from the Transwell® inserts using a scalpel, mounted onto a glass microscopy slide and enclosed with a cover slip. Specimens were viewed using a Leica DM IRBE confocal microscope (Leica Microsystems, Milton Keynes, UK) using FITC filter. Magnification x 200 scale bar 10µM.

Immunofluorescence studies confirmed the expression the tight junction proteins occludin (Figure 3.7a) and ZO-1 (Figure 3.7b) between the cells of the primary porcine *in vitro* BBB model. Both occludin and ZO-1 were localised at the points of membrane contact between the individual cells forming tight junction protein complexes around PBEC borders. Negative controls showed negligible fluorescence compared to samples.

Occludin and ZO-1 are vital components of tight junction protein complexes and a major contributor to the restrictive paracellular transport of molecules across the BBB *in vivo* (Furuse et al. 1993; Martin-Padura et al. 1998). These studies indicate that the primary porcine *in vitro* BBB model displays a BBB phenotype representative of the BBB *in vivo* with potential for low paracellular permeability, a necessity if the model is to serve as a permeability screen.

Lucifer yellow was used to assess paracellular permeability of the primary porcine *in vitro* BBB model. The apparent permeability coefficient (P_{app}) of Lucifer yellow across the primary porcine *in vitro* BBB model, from apical to basal compartments, was $2.16 \times 10^{-5} \pm 0.72 \times 10^{-5}$ $cm.s^{-1}$ (Data are the mean ± standard deviation of 5 independent experiments, with at least 12 replicates in each experiment).

3.2.8 Expression of P-glycoprotein in porcine brain endothelial cells

The P-gp efflux transporter is known to be highly expressed at the BBB and may limit entry of therapeutics into the CNS (Cordon-Cardo et al. 1989). In order for the primary porcine *in vitro* BBB model to be representative of the BBB *in vivo* it must possess functionally active P-gp. Expression of P-gp in PBECs was investigated by western blot analysis. Immunoblotting with the mouse monoclonal C219 antibody (P-gp specific) produced a single cross reactive band with an apparent molecular weight of approximately 170 kDa (Figure 3.8) confirming the expression of P-gp at the protein level in PBECs.

Figure 3.8 Expression of P-glycoprotein in porcine brain endothelial cells

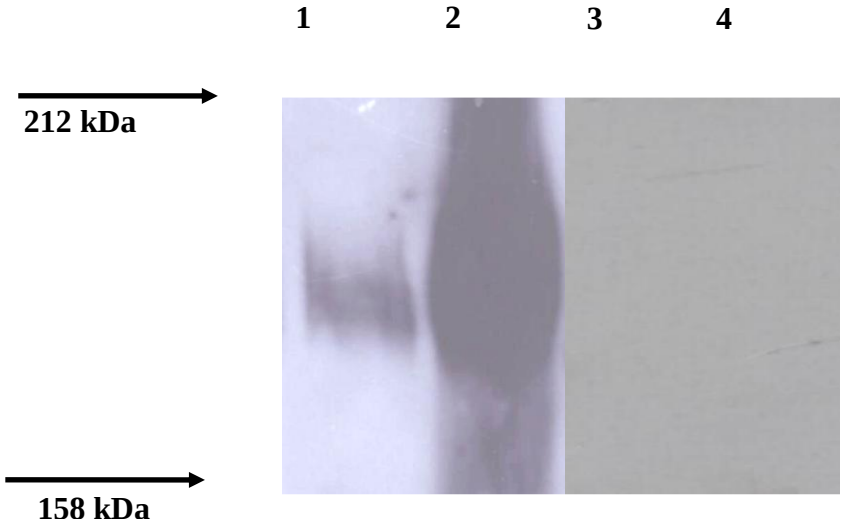

Caco-2 cell (lane 1 and lane 3) and porcine brain endothelial cell (lane 2 and lane 4) membranes were isolated by differential centrifugation. Solubilised proteins (30 µg protein per lane) were separated by SDS-polyacrylamide gel electrophoresis, electrotransfered to PVDF membrane, incubated with either mouse monoclonal C219 antibody and then with sheep anti-mouse horse radish peroxidase labelled IgG (lanes 1 and 2) or with sheep anti-mouse horse radish peroxidase labelled IgG alone (lanes 3 and 4). P-gp was detected by enhanced chemiluminescence.

Parallel western blot studies in our laboratory also confirmed expression of the efflux transporter BCRP in the PBECs (Personal communication with Sergio Mares-Samano).

3.2.9 Measurement of P-glycoprotein efflux activity in porcine brain endothelial cells

Calcein acetoxymethyl ester (calcein AM) is a non-fluorescent, membrane permeable compound which undergoes hydrolysis by intracellular esterases to produce calcein, a strongly fluorescent membrane impermeant compound which is retained within the cell. Calcein AM is a substrate of the P-gp efflux transporter (Tiberghien et al. 1996). P-glycoprotein activity in PBECs was assessed by measuring intracellular calcein accumulation with and without the P-gp inhibitors GF120918 (Figure 3.9).

Figure 3.9 **Intracellular accumulation of calcein in porcine brain endothelial cells with and without GF120918**

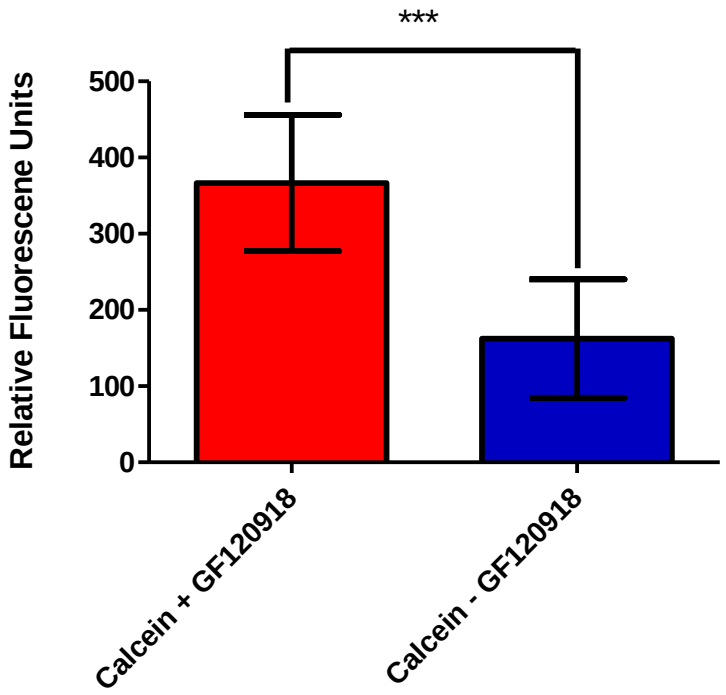

Porcine brain endothelial cells were pre-incubated in PBEC transport medium or PBEC transport medium containing 2 µM GF120918 (P-gp inhibitor) for 30 min prior to incubation with calcein AM (final concentration 0.25 µM) for 30 min. Intracellular calcein accumulation was measured by fluorescence spectroscopy (484 nm excitation and 530 nm emission). Data as relative fluorescence units are expressed as the mean ± standard deviation of at least 8 replicates, n=3 independent experiments. Statistical significance was determined using a Mann-Whitney test: *** = P<0.001.

A significantly greater (P<0.001) accumulation of intracellular calcein, 366.7 ± 89.3 RFU, was observed in the PBECs pre-incubated with the P-gp inhibitor GF120918 (Figure 3.9, red) compared to control (no pre-incubation with P-gp inhibitor GF120918 Figure 3.9, blue) at 162.4 ± 71.6 RFU. These findings indicate that P-gp is functionally active in the PBECs employed in our studies.

3.2.10 Monolayer efflux assay

A monolayer efflux assay was performed to confirm functional P-gp activity within the primary porcine *in vitro* BBB model. Amprenavir is a known P-gp substrate (Polli et al. 2004) and was used as a marker of efflux function. The ratio of the basolateral–apical (B-A) permeability versus the apical to basolateral (A-B) permeability of amprenavir was compared

to measure the efflux function of the primary porcine *in vitro* BBB model directly. The monolayer efflux assay was also performed with amprenavir and the P-gp inhibitor GF120918.

Figure 3.10 Directional permeability of amprenavir across the primary porcine *in vitro* blood-brain barrier model

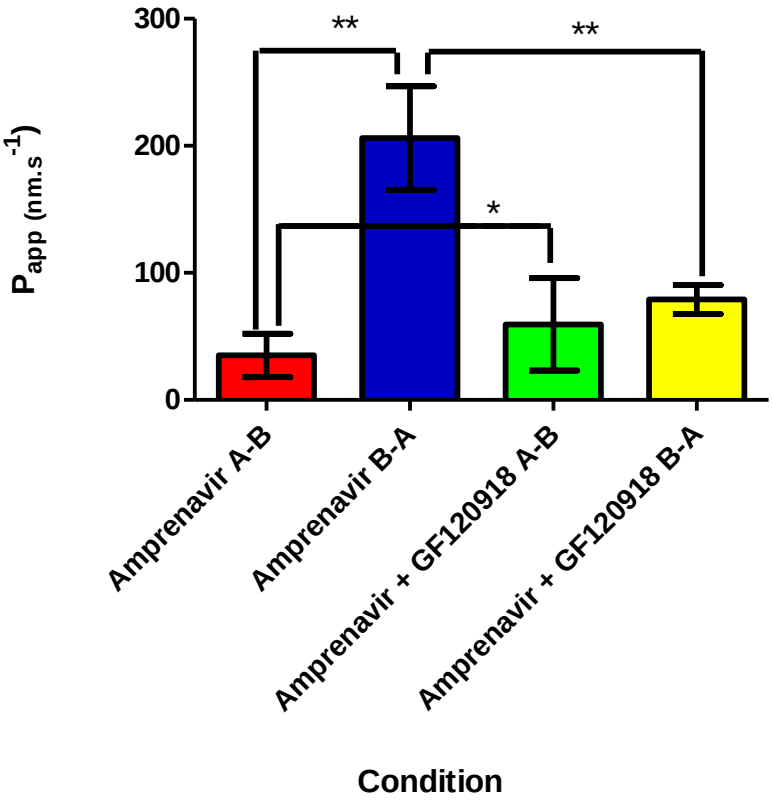

Permeability of amprenavir was measured in basolateral–apical (B-A) (blue) and apical to basolateral (A-B) (red) directions in the primary porcine *in vitro* blood-brain barrier model. Amprenavir permeability (B-A) (yellow) and (A-B) (green) permeability was also measured with GF120918. Data are presented as the mean P_{app} ($nm.s^{-1}$) ± standard deviation of duplicates n=3 independent experiments. Statistical significance was determined using a Mann-Whitney test: *= P<0.05, ** = P<0.01

The B-A apparent permeability (P_{app}) of amprenavir (206.0 ± 40.8 $nm.s^{-1}$ Figure 3.10, blue) is significantly greater (P<0.01) than A-B permeability (35.0 ± 17.2 $nm.s^{-1}$ Figure 3.10, red) suggesting that the primary porcine *in vitro* BBB model possesses functional P-gp which is pumping the amprenavir into the apical compartment.

Complete inhibition of P-gp activity would be expected to reduce B-A permeability and increase A-B such that there would be no appreciable difference between the two

measurements. In the presence of the P-gp inhibitor GF120918 B-A permeability was significantly reduced (from 206.0 ± 40.8 $nm.s^{-1}$ Figure 3.10 blue to 79.0 ± 11.3 $nm.s^{-1}$, Figure 3.10 yellow) and A-B permeability was significantly increased (from 35.0 ± 17.2 $nm.s^{-1}$ Figure 3.10 red to 59.49 $nm.s^{-1}$ ± 36.3 Figure 3.10 green).

The ratio of (B-A)/(A-B) apparent permeabilities is 5.91 in the absence of GF120918, compared to 1.33 (close to unity) with GF120918. An efflux ratio >2 is regarded to represent involvement of functional P-gp activity, and hence this confirms functional P-gp activity within the primary porcine *in vitro* BBB model.

3.2.11 Measurement of γ-glutamyl transpeptidase activity in primary porcine brain endothelial cells

In *vivo*, brain endothelial cells exhibit high levels of γ-glutamyltranspeptidase activity which can be used as a marker enzyme for brain CECs (Caspers et al. 1984). It has been reported that *in vitro* the enzyme activity is lost from the cells as they migrate outwards from isolated capillary fragments (DeBault et al. 1980).

Astrocytic growth factors have been widely reported to induce γ-glutamyltranspeptidase activity in brain endothelial cells (el Hafny, Bourre et al. 1996). To confirm the functional activity of γ-glutamyltranspeptidase in isolated PBECs and the effect of astrocytic growth factors, γ-glutamyltranspeptidase activity was measured spectrophotometrically.

Figure 3.11 **γ-glutamyl transpeptidase activity in porcine brain endothelial cells**

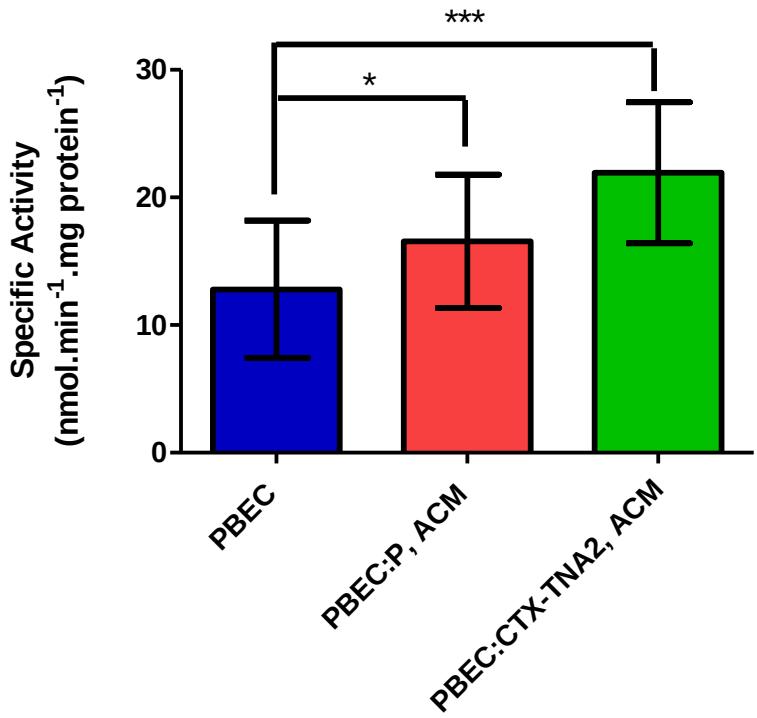

Porcine brain endothelial cells were grown to confluency on clear 96-well flat bottom plates in either PBEC culture medium (blue), PBEC culture medium:primary rat ACM, 1:1 (red) or PBEC culture medium:CTX-TNA2, ACM, 1:1 (green). Enzyme activity was determined spectrophotometrically by measuring production of *p*-nitroanilide at 410 nm, using ε = 8,800 $M^{-1}.cm^{-1}$. Enzyme activity is expressed as specific activity (nmol.min^{-1}.mg $protein^{-1}$). Data are expressed as mean ± standard deviation of 6 replicates, n=3 independent experiments. Statistical significance was determined using a Mann-Whitney test: * = P< 0.05 and *** = P < 0.001.

γ-glutamyl transpeptidase activity was detected in PBECs grown in all three culture conditions (Figure 3.11). The specific activity of γ-glutamyl transpeptidase in PBECs maintained in PBEC culture medium:primary rat, ACM (1:1) (16.6 ± 5.2 nmol.min^{-1}.mg $protein^{-1}$) and in PBEC culture medium:CTX-TNA2, ACM (1:1) (22.3 ± 6.1 nmol.min^{-1}.mg $protein^{-1}$) was significantly higher than PBECs maintained in PBEC culture medium (12.8 ± 5.4 nmol.min^{-1}.mg $protein^{-1}$). Thus, in these studies, γ-glutamyl transpeptidase activity was retained on isolation of PBECs from brain tissue and increased when cells were exposed to astrocytic growth factors.

3.2.12 Measurement of alkaline phosphatase activity in primary porcine brain endothelial cells

Alkaline phosphatase activity can be used as a BBB marker enzyme. The expression of alkaline phosphatase is often reduced in primary cultured endothelial cells, but has been shown to be restored by astrocytic factors (El Hafny et al. 1996). To confirm the functional expression of alkaline phosphatase in isolated PBECs and the effect of astrocytic growth factors on activity, the formation of *p*-nitrophenol in PBECs was measured spectrophotometrically.

Figure 3.12 **Alkaline phosphatase activity in primary porcine brain endothelial cells**

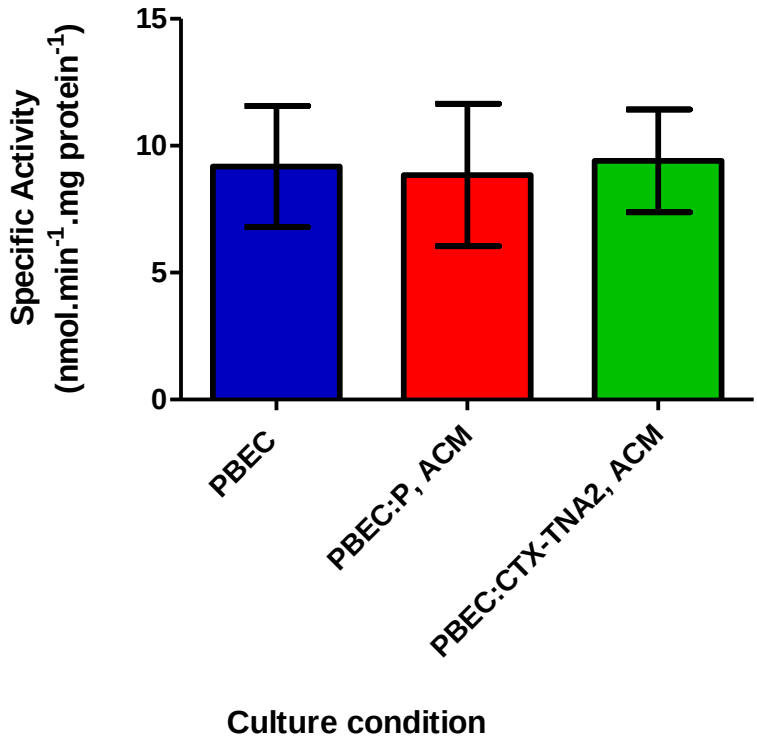

Porcine brain endothelial cells were grown on clear 96-well flat bottom plates to confluency in either; PBEC culture medium (blue), PBEC culture medium:primary rat ACM, 1:1 (red) or PBEC culture medium:CTX-TNA2, ACM, 1:1 (green).Enzyme activity was determined spectrophotometrically at 410 nm, using ε 17,000 $M^{-1}.cm^{-1}$. Enzyme activity is expressed as specific enzyme activity (nmol.min^{-1}.mg $protein^{-1}$). Data are expressed as mean ± standard deviation of 6 replicates, n=3 independent experiments. Statistical significance was determined using a Mann-Whitney test.

Although, specific enzyme activity was retained on isolation of PBECs maintained in PBEC culture medium, 9.1 ± 2.6 nmol.min^{-1}.mg protein^{-1} (Figure 3.12 blue), alkaline phosphatase activity was not significantly increased in PBECs maintained in either PBEC culture medium:primary rat, ACM 1:1 (9.3 ± 1.9 nmol.min^{-1}.mg protein^{-1}) or in PBEC culture medium:CTX-TNA2, ACM, 1:1 (9.2 ± 3.0 nmol.min^{-1}.mg protein^{-1}), suggesting astrocytic factors did not significantly affect specific activity of alkaline phosphatase in these *in vitro* studies.

3.3 Discussion

The primary aim of this chapter was to develop and characterise a primary porcine *in vitro* BBB model for the prediction of CNS drug permeability *in vivo*. Primary CEC cultures exhibit the closest phenotypic resemblance to the *in vivo* BBB, retaining *in vivo* characteristics such as tight junctions (Bowman et al. 1983; Rubin et al. 1991; Abbott et al. 1992), expression of transporters (Zhang et al. 2006; Smith et al. 2007) and BBB marker enzymes (El Hafny et al. 1996; Smith et al. 2007). Despite this, down regulation or loss of *in vivo* BBB characteristics can still occur on isolation from brain tissue (DeBault et al. 1980) although, the correct culturing techniques and conditions can help to maintain these characteristics.

For an *in vitro* BBB model to serve as a permeability screen it must display a restrictive paracellular pathway. Hence, the first part of this chapter focussed on determining the optimum culture conditions that would produce the greatest TER across PBEC monolayers and consequently develop a reproducible primary porcine *in vitro* BBB model.

The primary porcine *in vitro* BBB model was then characterised to demonstrate that the model exhibited other key *in vivo* characteristics required for use as a permeability screen including endothelial cell morphology, expression of tight junction proteins, measurement of γ-glutamyl transpeptidase and alkaline phosphatase enzyme activity and the presence of barrier functionality such as functional expression of P-gp (Gumbleton et al. 2001).

Porcine brain endothelial cells were successfully isolated from freshly harvested porcine brains and grown on 6-well plates before being seeded onto Transwell® inserts. The PBECs grown on the 6-well plates were fully confluent within ten days of isolation forming a uniform, tightly packed monolayer. Phase contrast images using light microscopy showed that the cells exhibited typical, elongated, spindly, fusiform morphology, characteristic of CECs.

These images were consistent with other isolated primary PBECs reported in the literature (Zhang et al. 2006; Smith et al. 2007).

Although, primary cultured CECs provide the closest phenotypic resemblance to CECs *in vivo*, down regulation or loss of *in vivo* BBB characteristics can still occur on isolation of CECs from brain tissue (DeBault et al. 1980). Co-culture with astrocytes or ACM has been shown to induce *in vivo* BBB properties for example tight junction formation and decreased permeability (Dehouck et al. 1990; Rubin et al. 1991; Sobue et al. 1999), expression of the efflux transporter P-gp (El Hafny et al. 1997; Gaillard et al. 2000) and BBB enzyme activity such as alkaline phosphatase (Sobue et al. 1999) and γ-glutamyl transpeptidase (El Hafny et al. 1996) which are necessary if the *in vitro* BBB model is to be used as a permeability screen.

Supplements added to the medium have also been shown to enhance tight junction protein expression between adjacent cells of *in vitro* BBB models (Rubin et al. 1991; Hoheisel et al. 1998; Igarashi et al. 1999; Calabria et al. 2006).

The effect of co-culture with primary rat astrocytes and the addition of supplements namely hydrocortisone, cAMP and RO-20-1724 to the culture medium on cellular morphology and PBEC monolayer TER was investigated in order to determine the conditions which produced morphology and TER most representative of BBB *in vivo*. Porcine brain endothelial cells monolayers co-cultured with primary rat astrocytes and maintained in medium containing supplements (cAMP, RO-20-1724 and hydrocortisone) achieved significantly higher TER (385 $\Omega.cm^2$) and the morphology most representative of the *in vivo* BBB compared to PBECs cultured alone and with no supplements, alone with supplements or in co-culture without supplements.

Astrocytes have been shown to secrete chemicals that are thought to induce BBB properties for example glial-derived neurotrophic factor (GDNF), basic fibroblast growth factor (bFGF) and transforming growth factor-ß (TGFß) (Tran et al. 1999; Abbott 2002; Haseloff et al. 2005; Abbott et al. 2006). Addition of supplements to culture medium has also been shown to increase TER (Rubin et al. 1991; Gaillard et al. 2001) explaining why the combination of co-culture with astrocytes and the addition of supplements to the medium resulted in the optimum culture conditions observed in this study.

There is still large speculation over which astrocytic factors induce the specific 'BBB phenotype'. However, GDNF in combination with CPT-cAMP and RO20-1724 has been

shown to synergistically decrease mannitol permeability and increase TER of PBECs (Igarashi et al. 1999). Chlorophenylthio-cyclic adenosine monophosphate and RO-20-1724 increase intracellular cAMP which is thought to induce phosphorylation of tight junction proteins and hence increase TER (Igarashi et al. 1999). In addition, bFGF has been shown to decrease L-glucose permeability and increase alkaline phosphatase activity in bovine brain endothelial cells (Sobue et al. 1999). Addition of hydrocortisone to culture medium has also resulted in increased TER and decreased cell monolayer sucrose permeability (Hoheisel et al. 1998; Calabria et al. 2006).

Although, co-culture with astrocytes and the use of supplemented medium were the culture conditions that produced the greatest PBEC monolayer TER, the TER (385 $\Omega.cm^2$) was still not representative of that reported *in vivo* 1490 $\Omega.cm^2$ and 1870 $\Omega.cm^2$ (Crone et al. 1982; Butt et al. 1990).

Contamination from astrocytes and pericytes during CEC isolation can result in the formation of an incomplete barrier of primary cultured CECs (Parkinson et al. 2005) and low reproducibility between studies. In order to optimise culture conditions and increase TER further, the method used to purify the PBECs prior to seeding them onto Transwell® inserts was investigated.

Porcine brain endothelial cells were treated with 3 $\mu g.ml^{-1}$ puromycin for 3 days 24 h post seeding onto 6-well plates. Transcellular electrical resistance across PBEC monolayers was significantly increased for PBEC monolayers treated with puromycin (867 $\Omega.cm^2$) compared to the control. These results were reproducible between PBEC isolations and puromycin treatment was found to be a simple way to standardise the purification step. Puromycin is an aminonucleoside antibiotic produced by *streptomyces alboniger* which prevents peptidyl transfer in the ribosome and hence prevents protein synthesis (Calabria et al. 2006). Endothelial cells can survive relatively large concentrations of puromycin which is a P-gp substrate, as they express the P-gp efflux transporter in contrast puromycin is cytotoxic to contaminating glial cells that either lack or express P-gp at lower levels than PBECs. These findings were consistent with previous studies.

Primary rat CECs, co-cultured with astrocytes, maintained in medium supplemented with cAMP and purified using puromycin treatment showed a reduction in sodium fluorescein permeability and an increase in TER across cell monolayers (Perriere et al. 2005).

Further validation of purification using puromycin treatment was documented, (Calabria et al. 2006) where puromycin treatment was used to purify primary rat CECs. Puromycin treatment was considered to be the best purification method in the study and cells treated with both puromycin and glucocorticoid attained higher TER than with glucocorticoid treatment alone.

Co-culture of primary cultured PBECs with primary cultured rat astrocytes have shown to induce BBB properties in this work. Parallel studies in our laboratory (personal communication with Dr Carina Cantrill) have shown that PBEC monolayers co-cultured with the CTX-TNA2 rat astrocyte cell line routinely demonstrate TER > 2000 $\Omega.cm^2$. These TER were substantially higher than TER obtained across PBEC monolayers maintained in co-culture with primary rat astrocytes and are similar to electrical resistances reported across the *in vivo* BBB (Crone et al. 1982; Butt et al. 1990).

The precise reasons why PBECs co-culture with the CTX-TNA2 rat astrocyte cell line resulted in higher TER values across cell monolayers than PBECs co-cultured with primary rat astrocytes are not known. However, it is possible that the CTX-TNA2 cell line could produce a variety of astrocytic factors, such as GDNF, bFGF and TGFß, or produce higher levels of astrocytic factors compared to the primary rat astrocytes, the levels of which may be more representative of the *in vivo* situation and hence, produce TER similar to *in vivo* TER. It is also possible that the primary cultured astrocytes may loose some of their phenotypic properties on isolation. Therefore, the CTX-TNA2 astrocytes in culture may be more representative of the astrocytes at the BBB *in vivo* and PBECs co-cultured with CTX-TNA2 astrocytes may produce higher TER than PBECs co-cultured with primary rat astrocytes.

Astrocytes used for co-culture (or ACM) are most often sourced from either the rat C6 glioma cell line (Lauer et al. 2004; Smith et al. 2007) or from primary rat astrocytes (Gaillard et al. 2000; Kido et al. 2002). However, TER of primary porcine *in vitro* BBB models co-cultured with the C6 glioma cell line have reported TER values of up to 900 $\Omega.cm^2$ (Smith et al. 2007) and, primary porcine *in vitro* BBB models co-cultured with primary rat astrocytes have reported TER up to 550 $\Omega.cm^2$ (Zhang et al. 2006). None of these TER values were as high as the TER values obtained in our laboratory when PBECs were co-cultured with the CTX-TNA2 cell line.

The literature documents numerous *in vitro* BBB models using primary and immortalised cell lines, from a range of species and tissues which are cultured under various conditions, some which have reported high TER, although, not as high as those achieved in our laboratory. The highest *in vitro* BBB model TER reported in the literature to date is 1650 $\Omega.cm^2$, and, like our model, was achieved using an *in vitro* BBB model composed of primary PBECs (purified with puromycin) but this model was co-cultured with primary rat astrocytes seeded onto the underside of the Transwell® insert and also onto the base of the well (Cohen-Kashi Malina et al. 2009).

As *in vitro* BBB models using primary PBECs have resulted in the highest model TER in the literature, the development of an *in vitro* BBB model using immortalised PBECs could be beneficial in terms of ease of culture and higher throughput of studies. However, *in vitro* BBB models using immortalised cell lines have been shown to exhibit much lower model TER. A porcine *in vitro* BBB model based upon the PBMEC/C1-2 cell line co-cultured with C6 glioma conditioned medium and maintained in medium supplemented with cAMP and R20-1724 (Lauer et al. 2004) obtained TER up to 300 $\Omega.cm^2$ despite similar conditions to the primary porcine *in vitro* BBB model in this thesis.

Following the results obtained from these studies and personal communication with Dr Carina Cantrill, purification using puromycin treatment, co-cultured with astrocytes from the CTX-TNA astrocyte cell line and the use of supplemented medium were deemed the optimum culture conditions for PBECS in the development of an *in vitro* BBB model for use as permeability screen. The primary porcine *in vitro* BBB model routinely attained TER >2000 $\Omega.cm^2$ 7 days post-seeding onto Transwell inserts®. Porcine brain endothelial cells cultured under these optimised conditions were referred to as the primary porcine *in vitro* BBB model and the rest of this work focussed on characterisation of this model in order to validate its use as a permeability screen.

Transmission electron micrographs showed that the PBECs of the porcine *in vitro* BBB retained spindly, attenuated morphology, characteristic of primary cultured CECs (Abbott et al. 1992; Zhang et al. 2006; Smith et al. 2007) and formed cell monolayers. These findings were consistent with the images taken of the PBECs on 6-well plates using the light microscope before seeding them onto Transwell® inserts. The presence of tight junction protein complexes between adjacent cells was also confirmed, using the electron microscope.

Tight junction protein complexes are imperative if the primary porcine *in vitro* BBB model is to serve as a permeability screen. Tight junction protein complexes are also indicative of the high TER values obtained across PBEC monolayers of the porcine *in vitro* BBB model in these studies.

The transmission electron micrographs in this study are comparable with transmission electron micrographs of PBEC monolayers reported in the literature (Zhang et al. 2006; Smith et al. 2007). Vesicular bodies, a basal lamina and mitochondria were also observed.

Supportive immunofluorescence studies confirmed the presence of the tight junction proteins occludin and ZO-1, at the points of membrane contact between the individual PBECs. The immunofluorescence images taken in these studies depicted fluorescence around the cell borders associated with the presence of occludin and ZO-1 between adjacent PBECs. These images were consistent with images documented in the literature from previous studies which also confirmed the presence of occludin and ZO-1 between CECs (Rubin et al. 1991; Neuhaus et al. 2008; Cohen-Kashi Malina et al. 2009).

In order to assess the restrictive nature of the porcine *in vitro* BBB model, Lucifer yellow was used to quantify the paracellular permeability of the model. The mean P_{app} of Lucifer yellow across the primary porcine *in vitro* BBB model was $2.16 \times 10^{-5} \pm 0.72 \times 10^{-5}$ $cm.s^{-1}$ reflecting low paracellular permeability of the model.

The permeability of Lucifer yellow across intact rat pial vessels has been reported in the literature as 31.6×10^{-6} $cm.s^{-1}$ (Easton et al. 1994) which is comparable with the Lucifer yellow permeability of 2.16×10^{-5} $cm.s^{-1}$ (21.6×10^{-6} $cm.s^{-1}$) obtained across the porcine *in vitro* BBB model in these studies. However, Lucifer yellow permeabilities across a primary bovine *in vitro* BBB model were reported to be 6.3×10^{-4} $cm.s^{-1}$ (Culot et al. 2008) which were greater than the permeabilities obtained in these studies. Lucifer yellow permeabilities of 2.22×10^{-5} $cm.s^{-1}$ have also been reported across the immortalised human cell line hCMEC/D3 (Poller et al. 2008) which are consistent with these studies, although TER values across cell monolayers were low (<40 $\Omega.cm^2$) (Weksler et al. 2005). For further discussion please refer to Chapter 4 discussion.

For the porcine *in vitro* BBB model to serve as a permeability screen it is important that it can discriminate between drugs of different permeabilities. Parallel studies in our laboratory (Cantrill 2009) reported a 10-fold difference between the permeabilities of fluorescent

dextrans (FD), FD4 (4,000 molecular weight) permeability was 10-fold greater than FD10 (10,000 molecular weight) permeability.

Transmission electron microscopy has depicted evidence of the presence of tight junction protein complexes, immunofluorescence studies have confirmed the presence of the tight junction proteins occludin and ZO-1 and Lucifer yellow permeability has been quantified and reflects low paracellular permeability of the model. Therefore, characterisation of the primary porcine *in vitro* BBB model has confirmed that it possesses a restrictive paracellular pathway and is suitable for use as a permeability screen.

P-glycoprotein, an efflux transporter expressed on the apical membrane of the CECs of the BBB (Cordon-Cardo et al. 1989), functions as a defence mechanism of the brain, expelling harmful substances (Abbott 2005), but can also limit the penetration of drugs across the BBB. Therefore, functional expression of P-gp is a requirement of the *in vitro* BBB model if it is to be physiologically representative of the *in vivo* BBB and to serve as a permeability screen, in order to integrate the effect of P-gp efflux into the overall permeability measurement.

Western blot analysis confirmed the expression of P-gp at the protein level in PBECs. The expression of P-gp appeared exceptionally large in the PBEC sample. Expression of P-gp has also been reported in primary PBECs documented in the literature at the protein level using western blotting (Smith et al. 2007) and at the mRNA level using RT-PCR (Zhang et al. 2006; Smith et al. 2007). Parallel western blot studies in our laboratory also confirmed expression of the efflux transporter BCRP in PBECs (Personal communication with Sergio Mares-Samano).

Once expression of P-gp in the PBECs was confirmed, it was important to ensure that the P-gp efflux transporter was functionally active. A calcein AM accumulation assay (Eneroth et al. 2001; Bauer et al. 2003) was used to assess P-gp activity in the PBECs. A significantly greater intracellular accumulation of calcein was observed in PBECs pre-incubated with the P-gp inhibitor GF120918 compared to control cells (no pre-incubation with GF120918), which suggested that the P-gp expressed in PBECs was functionally active.

Similar assays have been employed in the literature also confirming functional expression of P-gp in primary PBECs using rhodamine-123 as a P-gp substrate and using verapamil as a P-gp inhibitor (Smith et al. 2006).

After the functional expression of the P-gp in PBECs had been confirmed it was also important to ensure that the primary porcine *in vitro* BBB model demonstrated directional

P-gp activity. To investigate this, amprenavir was used as a P-gp substrate in a monolayer efflux assay. Amprenavir exhibited an efflux ratio significantly greater than unity suggesting functional P-gp activity of the model. However, a much greater efflux ratio would have been expected considering the large expression of P-gp exemplified by the western blot. However, it is possible that not all of the P-gp expressed in the PBECs was functionally active. P-gp activity was confirmed when the efflux ratio of amprenavir was reduced to almost unity with the addition of GF120918, a P-gp inhibitor used as a control.

To further characterise the primary porcine *in vitro* BBB model the functional expression of BBB marker enzymes γ-glutamyltranspeptidase and alkaline phosphatase were investigated as enzyme activity can be lost when cells are isolated (DeBault and Cancilla 1980). Although, astrocytic growth factors have been reported to induce enzyme activity in brain endothelial cells (El Hafny et al. 1996).

γ-glutamyl transpeptidase activity was detected in PBECs maintained in PBEC culture medium, PBEC culture medium:primary rat ACM (1:1) and PBEC culture medium:CTX-TNA2 ACM (1:1). However, γ-glutamyl transpeptidase activity was significantly greater in PBECs maintained in both PBEC culture medium:primary rat ACM (1:1) and PBEC culture medium:CTX-TNA2 ACM (1:1) compared to PBECs maintained in culture medium alone. This suggested up-regulation of γ-glutamyl transpeptidase activity, in response to astrocytic factors. This is consistent with previous studies in the literature which have shown induction of γ-glutamyl transpeptidase activity by astrocytic factors, for example, in the mouse ME-2 endothelial cell line co-cultured with the C6 glioma cell line (DeBault et al. 1980).

Alkaline phosphatase activity was detected in PBECs maintained in PBEC culture medium, PBEC culture medium:primary rat ACM (1:1) and PBEC culture medium:CTX-TNA2 ACM (1:1). However, no significant difference in activity was observed between the different culture conditions. The reasons for this are still to be elucidated and are contradictory to the literature as expression of alkaline phosphate has been shown to be upregulated in primary PBECS exposed to C6 glioma cell line conditioned media (Smith et al. 2007).

Optimised culture conditions for PBECs were shown to include purification with puromycin treatment to eliminate contaminating cells, co-culture with the CTX-TNA2 astrocyte cell line and the use of supplemented medium. These optimised culture conditions have been used to develop a primary porcine *in vitro* BBB model exhibiting an extremely

restrictive barrier representative of the BBB *in vivo*. The primary porcine *in vitro* BBB model has been characterised to confirm; physiologically realistic cell architecture, the formation of tight junction protein complexes, a restrictive paracellular pathway, functional expression of efflux transporters and BBB-associated marker enzymes. The primary porcine *in vitro* BBB model therefore possesses key physiological features of the BBB *in vivo* and can be used as a valid model for use in subsequent drug permeation studies and potentially as a permeability screen for use in drug discovery programmes.

Primary CECs provide the closest phenotype to the *in vivo* BBB and in general provide a more restrictive paracellular transport pathway compared to immortalised cell lines. Primary cell based *in vitro* BBB models, for routine use as a permeability screen in drug discovery settings may be limited due to the time and expertise required to set up the *in vitro* BBB model. However, the high yield of CECs from a porcine brain, which can also be cryopreserved, is a distinct advantage of this *in vitro* BBB model. Reproducibility is often a problem associated with primary cell culture, good reproducibility within and between batches was observed using this model. In order to investigate interlaboratory variation, future work using this model could involve repetition of the isolation and cell culture techniques of the model in other laboratories. Another limitation to the use of a porcine *in vitro* BBB model is species differences between porcine and human. Although, the literature reports similarities between porcine and human in terms of brain uptake and differences between human and rat (Syvanen et al. 2009).

Finally, further characterisation of active transporters at the primary porcine *in vitro* BBB model would be beneficial. For example, characterisation of the MRP efflux transporter which has been shown to be expressed at other primary porcine CECs (Gutmann et al. 1999; Zhang et al. 2006) and influx transporters such as GLUT1 and LAT1 (Zhang et al. 2006; Smith et al. 2007) would be useful as the purpose of this model is to serve as a permeability screen.

Chapter 4

Transport of a Series of Centrally Acting Test Drugs Across *In Vitro* Blood-Brain Barrier Models

4.0 Chapter 4: Transport of a series of centrally acting test drugs across *in vitro* blood-brain barrier models

4.1 Background

A well characterised, physiologically-representative *in vitro* BBB model for the prediction of *in vivo* BBB permeability is a valuable tool to aid the discovery of novel centrally acting drugs. *In vitro* BBB models can be used to obtain permeability measurements of novel CNS drug candidates in drug discovery programmes which can be used as a surrogate for rate of drug brain penetration and can also give information on the potential of a drug to be a substrate of an efflux transporter(s) highlighting possible limitations to BBB penetration.

The literature documents numerous *in vitro* cell-based BBB models, using primary and immortalised cells, different cell types and cells from a range of species and tissues making it difficult to combine and compare data. All of these *in vitro* BBB models have advantages and limitations but none to date have been deemed the 'gold standard' for the prediction of *in vivo* BBB permeability. A set of 12 centrally-acting test drugs of interest, (based on in-house studies by GSK) were used in transport studies employing five *in vitro* BBB models which include examples of primary and immortalised cells, cells from cerebral and non-cerebral origin, and cells from different species (dog, pig and human). Data obtained using the caco-2 *in vitro* BBB model can be found in Appendix 5 because only a small number of studies were conducted using this *in vitro* BBB model.

The overall objective of these studies was to compare *in vitro* BBB models regarding their potential for the prediction of *in vivo* BBB permeability. The individual aims were to; determine a suitable test drug concentration for use in subsequent transport studies across *in vitro* BBB models, perform transport studies across five *in vitro* BBB models in order to investigate the relationship between *in vitro* BBB model permeabilities and investigate the relationship between *in vitro* BBB model permeability and rat *in situ* permeability surface product.

4.2 Results

4.2.1 Methylthiazolyldiphenyl-tetrazolium bromide assay

4.2.1.1 Determination of optimum seeding density of cells employed as *in vitro* blood-brain barrier models for the methylthiazolyldiphenyl-tetrazolium bromide assay

Preliminary studies were carried out to determine the optimum seeding density of each cell type (employed as *in vitro* BBB models) to be used in a methylthiazolyldiphenyl-tetrazolium bromide (3-(4, 5-dimethyl-2-thiazolyl)-2, 5-diphenyl-tetrazolium bromide, MTT) assay. Optimum sensitivity of the assay is achieved using near confluent cells that are in the exponential growth phase to avoid underestimating drug toxicity. Following 48 h in culture, the seeding density for each cell type that gave an absorbance of approximately 1 was chosen as the optimum seeding density for subsequent MTT assays. Optimum seeding densities chosen were as follows; PBEC 15,000 cells/well, hCMEC/D3 15,000 cells/well, MDR1-MDCKII 12,500 cells/well and MDCKwt 15,000 cells/well.

4.2.1.2 Assessment of test drug concentration for use in transport studies across *in vitro* blood-brain barrier models

Prior to conducting transport studies with each *in vitro* BBB model, an MTT assay was performed to examine the effect of test drug concentration (3 µM was a desirable concentration to remain consistent with in-house studies at GSK) on the viability of each cell type. A range of test drug concentrations were used in the assay for each cell type in order to obtain an alternative test drug concentration if required.

Figure 4.1 Effect of test drug concentration on cell viability

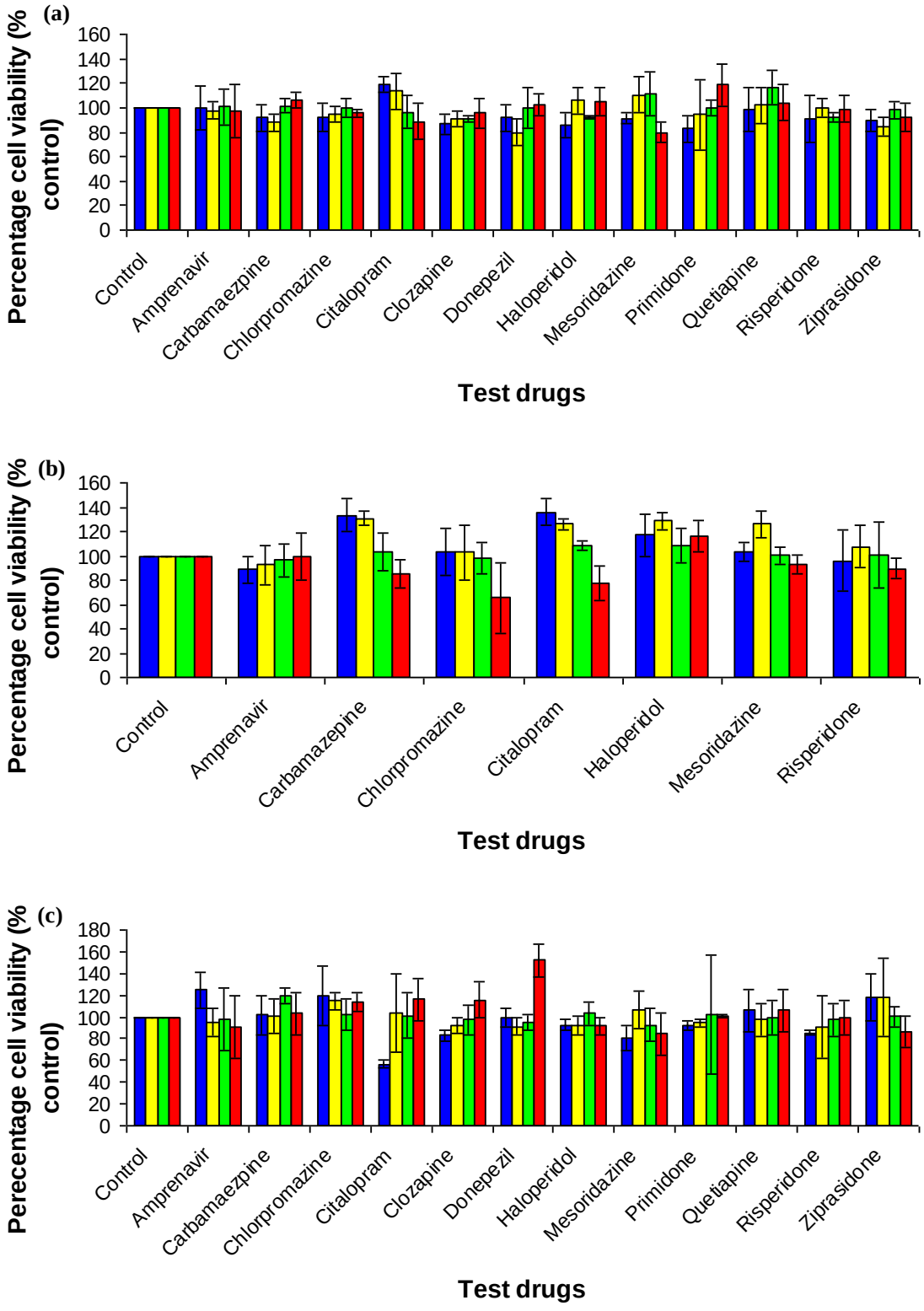

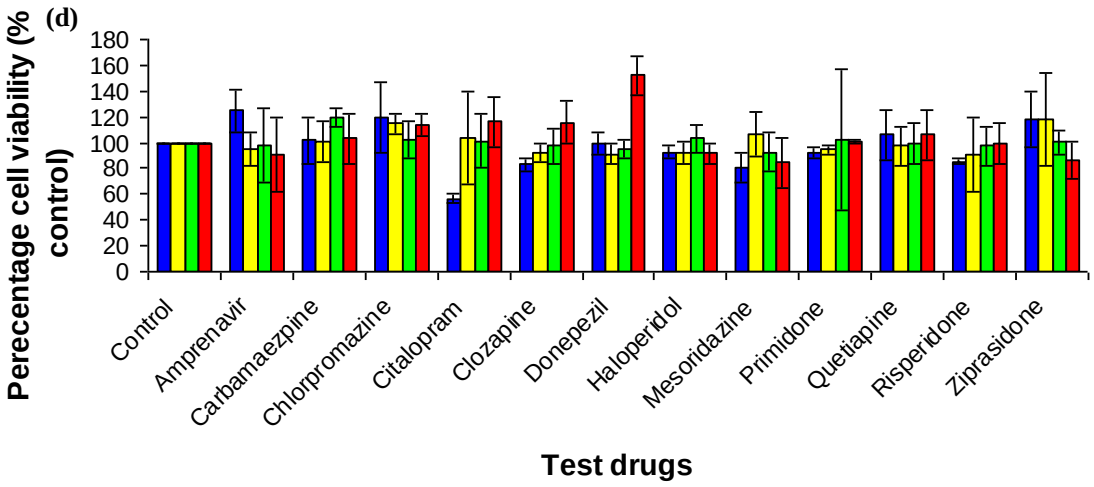

Each cell type (a) PBEC, (b) hCMEC/D3, (c) MDR1-MDCKII, and (d) MDCKwt were seeded onto 96-well plates at a pre-determined cell density and incubated for 24 h. Cells were then incubated with test drugs at 0.03 µM (blue), 0.3 µM (yellow), 3 µM (green) and 30 µM (red) for 60 min, washed with PBS and incubated for 24 h in growth medium. Methylthiazolyldiphenyl-tetrazolium bromide in PBS (5 $mg.ml^{-1}$) was added to all wells (10 µl per 100 µl medium) and the cells were incubated for 4 h. The MTT-formazan produced was solubilised and quantified colourmetrically using a spectrophotometer. The control (cells exposed to solvent at the same concentration as all test drug solutions) corresponded to a cell viability of 100 %. Data are expressed as mean ± standard deviation of 4 replicates from one independent experiment.

Figure 4.2 Effect of test drug concentration and GF120918 on cell viability

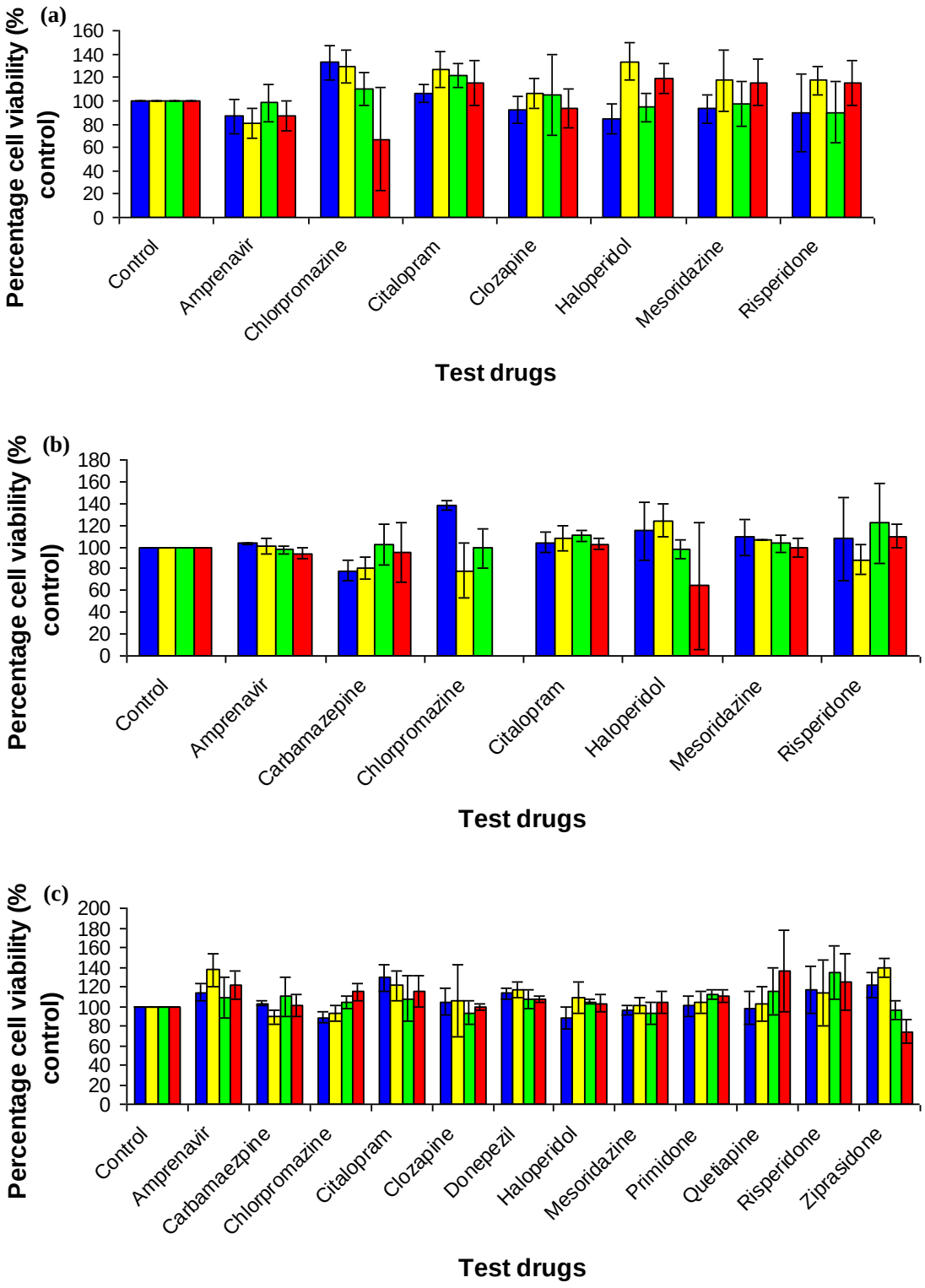

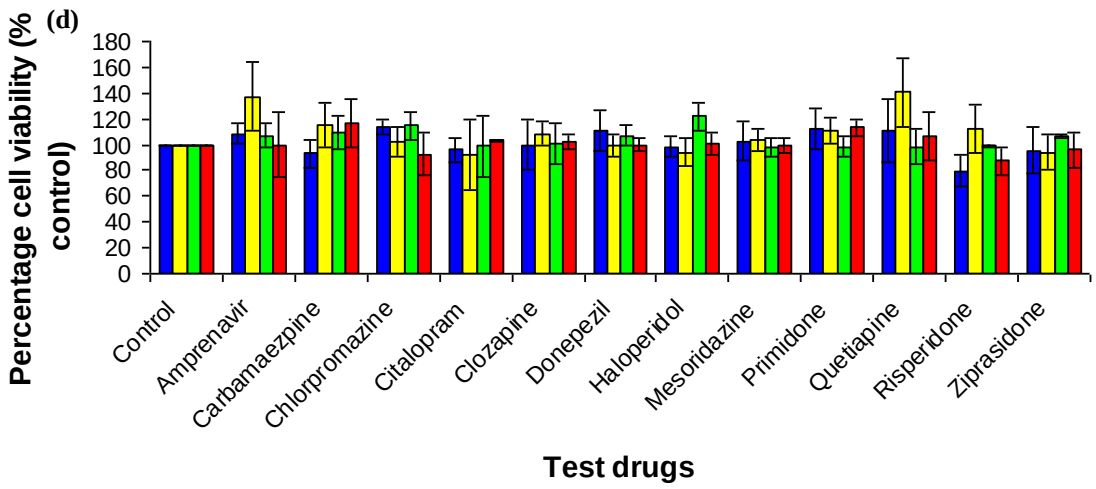

Each cell type (a) PBEC, (b) hCMEC/D3, (c) MDR1-MDCKII and (d) MDCKwt were seeded at a pre-determined density and incubated for 24 h. Each cell type was then co-incubated with the test drugs that were to be used in subsequent transport studies at a range of concentrations (blue 0.03 µM, yellow 0.30 µM, green 3.00 µM and red 30.00 µM) and GF120918 (2 µM) for 60 min. The cells were washed and incubated for 24 h in growth medium. Methylthiazolyldiphenyl-tetrazolium bromide in PBS (5 $mg.ml^{-1}$), was added to all wells (10 µl per 100 µl medium) and the cells were incubated for 4 h. The MTT-formazan produced was solubilised and quantified colourmetrically using a spectrophotometer. The control (cells exposed to solvent at the same concentration as all test drugs solutions) corresponded to a cell viability of 100 %. Data are expressed as mean ± standard deviation of 4 replicates from one independent experiment.

None of the test drugs at the desired test concentration (3 µM) were shown to substantially decrease the viability of any cell type (Figure 4.1) compared to control cells. Analogous findings were obtained when cell viability was measured following exposure of each cell type to both test drug and the P-gp inhibitor GF120918 (Figure 4.2). The paracellular marker Lucifer yellow (100 µM) alone, employed in all studies to monitor cell monolayer integrity, did not appreciably affect cell viability of any cell type (PBEC 100.72 %, hCMEC/D3 99.43 %, MDR1-MDCKII 124.21 % and MDCKwt 109.33 %) compared to control cells (100 %). Similarly, there was no appreciable effect on cell viability when cells were exposed to GF120918 (2 µM) alone (PBEC 128.88 %, hCMEC/D3 95.97 %, MDR1-MDCKII 102.52 %, and MDCKwt 100.05 %) or exposed to a combination of Lucifer yellow (100 µM) and GF120918 (PBEC 160.81 %, hCMEC/D3 111.44 %, MDR1-MDCKII 111.85 % and MDCKwt 100.38 %) compared to control cells. This study confirmed that a test drug concentration of 3 µM, the P-gp inhibitor GF120918 (2 µM) and the paracellular marker

Lucifer yellow (100 µM) did not substantially decrease cell viability of any cell type and were therefore suitable to be used in subsequent transport studies.

4.2.2 Characterisation of *in vitro* blood-brain barrier model integrity and efflux function

The integrity and efflux function of all *in vitro* BBB model monolayers was characterised, in order to identify differences between the models and similarities of the models to the BBB *in vivo*. Paracellular permeability, expressed as apparent permeability (P_{app} nm.s^{-1}) and exact permeability (P_{exact} nm.s^{-1}) and TER (Ω.cm^2) were used as markers of monolayer integrity. Amprenavir a known P-gp substrate (Polli et al. 1999) was used as a marker of functional P-gp activity.

Table 4.1 Markers of monolayer integrity and efflux function

In vitro BBB model	Lucifer yellow P_{app} (nm.s^{-1})	Lucifer yellow P_{exact} (nm.s^{-1})	TER (Ω.cm^2)	Efflux ratio (P_{app})	Efflux ratio (P_{exact})
Porcine	216.2 ± 72.2	230.0 ± 76.8	2000-2200	5.9	5.6
hCMEC/D3	54.5 ± 29.4	60.1 ± 31.3	20-40	1.2	0.8
MDR1-MDCKII	25.0 ± 12.0	26.4 ± 12.6	100-140	12.0	12.8
MDCKwt	28.5 ± 13.3	30.1 ± 14.0	40-50	2.0	2.0

The table shows A-B apparent permeability (P_{app} nm.s^{-1}) and exact permeability (P_{exact} nm.s^{-1}) of Lucifer yellow (100 µM), transcellular electrical resistance (Ω.cm^2) and efflux ratio (B-A/A-B) of amprenavir determined from both apparent permeability (P_{app} nm.s^{-1}) and exact permeability (P_{exact} nm.s^{-1}) across porcine, hCMEC/D3, MDR1-MDCKII and MDCKwt *in vitro* BBB models. Lucifer yellow data are expressed as mean ± standard deviation of at least 6 replicates, n=3 independent experiments, transcellular electrical resistance data are expressed as range of at least 12 replicates, n=3 independent experiments and efflux ratios (B-A/A-B) (P_{app} and P_{exact}) for amprenavir are calculated from mean of duplicates, n=3 independent experiments.

Lucifer yellow permeability (P_{app} and P_{exact}) (Table 4.1) was similar across hCMEC/D3, MDR1-MDCKII, and MDCKwt *in vitro* BBB models, whereas for the porcine model, Lucifer yellow permeability was an order of magnitude greater. No substantial differences were observed between Lucifer yellow P_{app} and P_{exact} for all *in vitro* BBB models.

The porcine *in vitro* BBB model displayed the greatest TER (2000-2200 Ω.cm^2) compared to all other *in vitro* BBB models in the study (Table 4.1) which was comparable to estimated *in vivo* TER (1490-1870 Ω.cm^2) (Crone et al. 1982; Butt et al. 1990). In comparison, the TER values of hCMEC/D3, MDR1-MDCKII and MDCKwt and were relative low and not representative of the BBB *in vivo*. Low Lucifer yellow permeability did not correlate with

high TER which would be expected if these parameters were connected, for example the porcine model displayed the highest Lucifer yellow permeability and also the highest TER.

A test drug with an efflux ratio greater than, or the same as 2, and, where efflux is inhibited by a potent P-gp inhibitor will be considered as a potential P-gp substrate during this work (Zhang et al. 2008), in keeping with FDA guidelines on identification of Pgp substrates. The porcine and MDR1-MDCKII *in vitro* BBB models both showed functional P-gp activity, the MDCKwt model exhibited borderline P-gp activity (efflux ratio = 2) and the hCMEC/D3 *in vitro* BBB model did not demonstrate any functional P-gp activity (Table 4.1).

This study has shown that the porcine and MDR1-MDCKII *in vitro* BBB models exhibit markers of monolayer integrity and P-gp efflux function which are desirable properties of an *in vitro* BBB model and representative of the BBB *in vivo*.

4.2.3 Transport studies

4.2.3.1 Permeability measurements of test drugs across the porcine *in vitro* blood-brain barrier model

Test drugs were used in permeability studies across the porcine *in vitro* BBB model. Tables 4.2 and 4.3 detail apparent permeability and exact permeability respectively, with and without the P-gp inhibitor GF120918 across the porcine *in vitro* BBB model for amprenavir, carbamazepine, chlorpromazine, citalopram, clozapine, donepezil, haloperidol, mesoridazine and risperidone. Percentage recoveries for all test drugs were similar.

Table 4.2 **Apparent permeability and efflux ratio of test drugs across the porcine *in vitro* blood-brain barrier model**

	With out inhibitor			With inhibitor		
Test Drug	**P_{app} A-B**	**P_{app} B-A**	**ER**	**P_{app} A-B**	**P_{app} B-A**	**ER**
Amprenavir	35.0 ± 17.2	206.9 ± 40.8	5.9	59.5 ± 36.3	79.4 ± 11.3	1.3
Carbamazepine	49.3	198.1	4.0	ND	ND	ND
Chlorpromazine	56.0 ± 20.0	17.6 ± 6.5	0.3	31.5 ± 8.3	43.8 ± 9.3	1.4
Citalopram	24.8 ± 12.4	63.3 ± 12.8	2.6	16.8 ± 8.4	18.0 ± 2.7	1.1
Clozapine	38.5 ± 3.7	55.9 ± 39.2	1.5	55.8	42.4	0.8
Donepezil	41.4	384.3	9.3	ND	ND	ND
Haloperidol	70.9 ± 32.4	108.2 ± 31.4	1.5	65.2 ± 15.6	73.7 ± 19.7	1.1
Mesoridazine	49.3 ± 13.0	55.2 ± 14.5	1.1	53.2 ± 21.2	88.9 ± 7.0	1.7
Risperidone	47.9 ± 14.4	62.4 ± 19.5	1.3	54.3 ± 11.1	93.3 ± 22.1	1.7

Apparent permeability of amprenavir, carbamazepine, chlorpromazine, citalopram, clozapine, donepezil, haloperidol, mesoridazine and risperidone (3 µM) across the porcine *in vitro* BBB model in both A-B and B-A directions, with and without the potent P-gp inhibitor GF120918 (2 µM), was measured over 60 min. The apparent permeability (P_{app} $nm.s^{-1}$) and efflux ratio (ER) were calculated. Apparent permeability data are expressed as mean ± standard deviation of duplicates, n=3 independent experiments for all test drugs apart from carbamazepine, clozapine (with inhibitor only) and donepezil where data are expressed as the mean of duplicates from one independent experiment. Efflux ratios (B-A/A-B) were calculated from mean apparent permeability values. ND denotes not determined.

Table 4.3 **Exact permeability and efflux ratio of test drugs across the porcine *in vitro* blood-brain barrier model**

	With out inhibitor			With inhibitor		
Test Drug	**P_{exact} A-B**	**P_{exact} B-A**	**ER**	**P_{exact} A-B**	**P_{exact} B-A**	**ER**
Amprenavir	33.7 ± 15.8	189.7 ± 45.0	5.6	45.1 ± 21.2	65.4 ± 10.4	1.5
Carbamazepine	44.9	164.5	3.7	ND	ND	ND
Chlorpromazine	91.8 ± 13.5	17.1 ± 6.1	0.2	59.6 ± 22.1	45.5 ± 10.4	0.8
Citalopram	22.2 ± 8.8	72.6 ± 17.1	3.3	34.8 ± 14.6	51.9 ± 31.5	1.5
Clozapine	81.3 ± 47.1	57.5 ± 33.2	0.7	90.8	42.5	0.5
Donepezil	39.3	383.9	9.8	ND	ND	ND
Haloperidol	66.2 ± 29.5	67.9 ± 13.5	1.0	67.5 ± 7.0	64.3 ± 19.1	1.0
Mesoridazine	42.6 ± 9.4	66.8 ± 24.2	1.6	64.6 ± 15.4	78.3 ± 14.9	1.2
Risperidone	61.8 ± 21.6	74.3 ± 19.7	1.2	68.0 ± 5.8	105.3 ± 22.0	1.6

Exact permeability of amprenavir, carbamazepine, chlorpromazine, citalopram, clozapine, donepezil, haloperidol, mesoridazine and risperidone (3 µM) across the porcine *in vitro* BBB model in both A-B and B-A directions, with and without the potent P-gp inhibitor GF120918 (2 µM), was measured over 60 min. The exact permeability (P_{exact} $nm.s^{-1}$) and efflux ratio (ER) were calculated. Exact permeability data are expressed as mean ± standard deviation of duplicates, n=3 independent experiments for all test drugs apart from carbamazepine clozapine (with inhibitor only) and donepezil where data are expressed as the mean of duplicates from one independent experiment. Efflux ratios (B-A/A-B) were calculated from mean exact permeability values. ND denotes not determined.

The P_{app} A-B ranged from 24.8-70.9 $nm.s^{-1}$ and the P_{app} B-A ranged from 17.6-384.3 $nm.s^{-1}$ without inhibitor. The P_{exact} A-B ranged from 22.2-91.8 $nm.s^{-1}$ and P_{exact}

B-A ranged from 17.1-383.9 $nm.s^{-1}$ without inhibitor. No appreciable difference between P_{app} B-A and P_{exact} B-A was observed which would be expected given that percentage recoveries of all test drugs were good and thus had little impact on the two permeability calculations.

Efflux ratios ranged from 0.3-9.3 (calculated using P_{app}) and 0.2-9.8 (calculated using P_{exact}) indicating that the porcine *in vitro* BBB model can identify substrates of efflux transporters. Amprenavir, carbamazepine, citalopram and donepezil (ER P_{app} 5.9, 4.0. 2.6 and 9.3, P_{exact} 5.6, 3.7, 3.3 and 9.8 respectively) were all identified as substrates of an efflux transporter(s) using the porcine *in vitro* BBB model. Efflux ratios were less than 2 (P_{app} 0.8-1.7, and P_{exact} 0.5-1.6) for all test drugs with the inhibitor suggesting that any efflux observed could potentially be due to P-gp (ER for carbamazepine and donepezil with GF120918 was unavailable).

4.2.3.2 Permeability measurements of test drugs across the hCMEC/D3 *in vitro* blood-brain barrier model

Test drugs were used in permeability studies across the hCMEC/D3 *in vitro* BBB model. Tables 4.4 and 4.5 detail apparent and exact permeability respectively, with and without the P-gp inhibitor GF120918, for amprenavir, carbamazepine, chlorpromazine, citalopram, haloperidol, mesoridazine and risperidone. Percentage recoveries for all test drugs were similar.

Table 4.4 Apparent permeability and efflux ratio of test drugs across hCMEC/D3 *in vitro* blood-brain barrier model

	With out inhibitor			With inhibitor		
Test Drug	**P_{app} A-B**	**P_{app} B-A**	**ER**	**P_{app} A-B**	**P_{app} B-A**	**ER**
Amprenavir	30.1 ± 9.1	37.4 ± 16.1	1.2	20.6 ± 10.7	32.4 ± 9.6	1.6
Carbamazepine	385.0	559.9	1.5	510.8	766.3	1.5
Chlorpromazine	37.4 ± 16.3	48.3 ± 8.3	1.3	35.5 ± 9.6	50.4 ± 14.5	1.4
Citalopram	505.1	474.6	0.9	457.7	343.5	0.8
Haloperidol	88.0 ± 14.7	80.7 ± 18.2	0.9	72.0 ± 38.7	113.8 ± 13.4	1.6
Mesoridazine	33.4 ± 15.3	76.0 ± 40.8	2.3	39.1 ± 13.3	61.8 ± 17.9	1.6
Risperidone	28.2	200.0	7.1	57.3	96.0	1.7

Apparent permeability of amprenavir, carbamazepine, chlorpromazine, citalopram, haloperidol, mesoridazine and risperidone (3 µM) across the hCMEC/D3 *in vitro* BBB model in both A-B and B-A directions, with and without the potent P-gp inhibitor GF120918 (2 µM), was measured over 60 min. The apparent permeability (P_{app} nm.s^{-1}) and efflux ratio (ER) were calculated. Apparent permeability data are expressed as mean ± standard deviation of duplicates, n=3 independent experiments for all test drugs apart from carbamazepine, citalopram and risperidone where data are expressed as the mean of duplicates from one independent experiment. Efflux ratios (B-A/A-B) were calculated from mean apparent permeability values.

Table 4.5 Exact permeability and efflux ratio of test drugs across hCMEC/D3 *in vitro* blood-brain barrier model

	With out inhibitor			With inhibitor		
Test Drug	**P_{exact} A-B**	**P_{exact} B-A**	**ER**	**P_{exact} A-B**	**P_{exact} B-A**	**ER**
Amprenavir	47.6 ± 15.9	36.1 ± 15.9	0.8	22.0 ± 5.9	42.6 ± 8.1	1.9
Carbamazepine	632.3	829.2	1.3	876.1	1019.3	1.2
Chlorpromazine	46.3 ± 14.5	48.4 ± 10.3	1.1	43.7 ± 17.2	69.9 ± 17.0	1.6
Citalopram	747.8	1676.6	2.2	1297.8	618.9	0.5
Haloperidol	81.2 ± 7.9	72.4 ± 21.2	0.9	88.6 ± 50.0	121.6 ± 16.1	1.4
Mesoridazine	26.5 ± 7.5	53.7 ± 21.4	2.0	43.7 ± 15.9	64.2 ± 21.0	1.5
Risperidone	33.5	237.5	7.1	81.2	115.7	1.4

Exact permeability of amprenavir, carbamazepine, chlorpromazine, citalopram, haloperidol, mesoridazine and risperidone (3 µM) across the hCMEC/D3 *in vitro* BBB model in both A-B and B-A directions, with and without the potent P-gp inhibitor GF120918 (2 µM), was measured over 60 min. The exact permeability (Pexact nm.s^{-1}) and efflux ratio (ER) were calculated. Exact permeability data are expressed as mean ± standard deviation of duplicates, n=3 independent experiments for all test drugs apart from carbamazepine, citalopram and risperidone where data are expressed as the mean of duplicates from one independent experiment.

The P_{app} A-B ranged from 28.2–505.1 nm.s^{-1} and the P_{app} B-A ranged from 37.4-559.9 nm.s^{-1} without inhibitor. The P_{exact} A-B ranged from 26.5–747.8 nm.s^{-1} and P_{exact} B-A ranged from 36.1–1676.6 nm.s^{-1} without inhibitor. An appreciable difference between P_{app} B-A and P_{exact} B-A was observed.

The efflux ratios ranged from 0.9-7.1 (calculated using P_{app}) and 0.8-7.1 (calculated using P_{exact}). Risperidone and mesoridazine were shown to be substrates of efflux transporters using P_{app} to calculate efflux ratio (7.1 and 2.3 respectively), whereas citalopram and risperidone were shown to be substrates of efflux transporters using P_{exact} to calculate efflux ratio (2.2 and 7.1 respectively) and mesoridazine was shown to be a borderline substrate (efflux ratio 2.0).

These results suggest that the hCMEC/D3 *in vitro* BBB model exhibits functionally active efflux transporter(s), contradicting the data obtained for amprenavir (a known P-gp substrate) which was used as a marker of P-gp efflux function (Table 4.1 efflux ratio P_{app} 1.2, P_{exact} 0.8). The efflux ratios for all test drugs were less than 2 (P_{app} 0.8-1.7, P_{exact} 0.5-1.9) with the inhibitor GF120918 suggesting that the active efflux observed was due to P-gp or inhibition of another efflux transporter by GF120918.

4.2.3.3 Permeability measurements of test drugs across the MDR1-MDCKII *in vitro* blood-brain barrier model

Test drugs were used in permeability studies across the MDR1-MDCKII *in vitro* BBB model using a high throughput screening technique. Table 4.6 and 4.7 detail apparent permeability and exact permeability respectively, with and without the P-gp inhibitor GF120918, across the MDR1-MDCKII *in vitro* BBB model for amprenavir, carbamazepine, chlorpromazine, citalopram, clozapine, donepezil, haloperidol, mesoridazine, primidone, quetiapine, risperidone and ziprasidone. Percentage recoveries for all test drugs were similar for all cell types.

Table 4.6 **Apparent permeability and efflux ratio of test drugs across MDR1-MDCKII *in vitro* blood-brain barrier model**

	With out inhibitor			With inhibitor		
Test drugs	**P_{app} A-B**	**P_{app} B-A**	**ER**	**P_{app} A-B**	**P_{app} B-A**	**ER**
Amprenavir	53.5 ± 8.5	460.6 ± 70.0	8.6	307.8 ± 39.4	306.9 ± 61.8	1.0
Carbamazepine	910.7 ± 226.7	939.2 ± 105.2	1.0	776.0 ± 156.6	721.0 ± 78.5	0.9
Chlorpromazine	213.1 ± 52.8	136.4 ± 21.6	0.6	340.8 ± 96.3	185.3 ± 52.5	0.5
Citalopram	748.0 ± 188.7	918.9 ± 165.4	1.2	737.4 ± 131.0	706.6 ± 121.1	1.0
Clozapine	574.0 ± 162.7	502.6 ± 110.1	0.9	510.9 ± 123.5	399.8 ± 59.7	0.8
Donepezil	645.6 ± 169.6	604.0 ± 107.7	0.9	615.6 ± 176.6	554.5 ± 153.0	0.9
Haloperidol	481.2 ± 119.8	480.5 ± 143.9	1.0	424.5 ± 96.2	380.9 ± 82.1	0.9
Mesoridazine	306.7 ± 71.5	683.5 ± 126.9	2.2	598.5 ± 105.0	480.8 ± 87.5	0.8
Primidone	421.6 ± 74.9	237.0 ± 54.9	0.6	421.0 ± 72.5	223.8 ± 32.4	0.5
Quetiapine	1023.7 ± 168.5	823.0 ± 127.5	0.8	995.8 ± 242.6	816.5 ± 136.3	0.8
Risperidone	527.1 ± 129.3	705.7 ± 118.0	1.3	804.5 ± 226.8	561.4 ± 116.2	0.7
Ziprasidone	188.3 ± 57.2	192.9 ± 58.6	1.0	526.7 ± 102.3	121.1 ± 35.2	0.2

Apparent permeability of amprenavir, carbamazepine, chlorpromazine, citalopram, clozapine, donepezil, haloperidol, mesoridazine, primidone, quetiapine, risperidone and ziprasidone (3 µM) across the MDR1-MDCKII *in vitro* BBB model in both A-B and B-A directions, with and without the potent P-gp inhibitor GF120918 (2 µM), was measured over 90 min. The apparent permeability (P_{app} nm.s^{-1}) and efflux ratio (ER) were calculated. Apparent permeability data are expressed as mean ± standard deviation of duplicates, n=3 independent experiments for all test drugs. Efflux ratios (B-A/A-B) were calculated from mean apparent permeability values.

Table 4.7 **Exact permeability and efflux ratio of test drugs across MDR1-MDCKII *in vitro* blood-brain barrier model**

	With out inhibitor			With inhibitor		
Test drugs	**P_{exact} A-B**	**P_{exact} B-A**	**ER**	**P_{exact} A-B**	**P_{exact} B-A**	**ER**
Amprenavir	56.2 ± 11.2	570.4 ± 58.0	10.2	362.8 ± 39.7	363.1 ± 63.4	1.0
Carbamazepine	1037.1± 122.8	1078.2 ± 147.4	1.0	960.8 ± 128.4	897.1 ± 74.5	0.9
Chlorpromazine	511.9 ± 58.6	221.1 ± 64.3	0.4	756.1 ± 61.8	225.8 ± 62.1	0.3
Citalopram	822.7 ± 167.5	997.2 ± 168.6	1.2	898.9 ± 118.4	760.9 ± 110.2	0.9
Clozapine	763.3 ± 148.0	576.3 ± 138.7	0.8	745.9 ± 90.0	430.4 ± 51.9	0.6
Donepezil	814.5 ± 154.9	674.8 ± 79.9	0.8	746.9 ± 138.8	659.0 ± 162.6	0.9
Haloperidol	761.5 ± 90.3	517.1 ± 78.5	0.7	670.9 ± 49.6	446.1 ± 60.0	0.7
Mesoridazine	347.4 ± 74.5	737.2 ± 60.2	2.1	697.4 ± 112.0	512.4 ± 83.9	0.7
Primidone	479.1 ± 138.6	253.0 ± 46.8	0.5	417.5 ± 63.5	251.4 ± 50.01	0.6
Quetiapine	1135.5 ± 219.7	993.7 ± 127.8	0.9	1062.1 ± 215.0	986.1 ± 178.4	0.9
Risperidone	546.8 ± 118.5	778.0 ± 133.2	1.4	821.4 ± 197.7	659.6 ± 154.4	0.8
Ziprasidone	430.0 ± 82.8	333.9 ± 61.7	0.8	1055.0 ± 144.5	188.3 ± 41.9	0.2

Exact permeability of amprenavir, carbamazepine, chlorpromazine, citalopram, clozapine, donepezil, haloperidol, mesoridazine, primidone, quetiapine, risperidone and ziprasidone (3 µM) across the MDR1-MDCKII *in vitro* BBB model in both A-B and B-A directions, with and without the potent P-gp inhibitor GF120918 (2 µM), was measured over 90 min. The exact permeability (P_{exact} nm.s^{-1}) and efflux ratio (ER) were calculated. Exact permeability data are expressed as mean ± standard deviation of duplicates, n=3 independent experiments for all test drugs. Efflux ratios (B-A/A-B) were calculated from mean exact permeability values.

The P_{app} A-B ranged from 53.5-1023.7 $nm.s^{-1}$ and the P_{app} B-A from 136.4-939.2 $nm.s^{-1}$ without inhibitor. The P_{exact} A-B ranged from 56.2-1135.5 $nm.s^{-1}$ and P_{exact} B-A from 221.1-1078.2 $nm.s^{-1}$ without inhibitor. No appreciable difference between P_{app} B-A and P_{exact} B-A was observed. Eleven out of the 12 test drugs exhibited permeability values > 150 $nm.s^{-1}$ which has been documented in the literature to be characteristic of CNS indicated drugs using the MDR1-MDCKII *in vitro* BBB model (Mahar Doan et al. 2002; Reichel 2009).

The efflux ratios ranged from 0.6-8.6 (calculated using P_{app}) and 0.4-10.2 (calculated using P_{exact}) which returned to less than 2 with the P-gp inhibitor GF120918, 0.2-1.0 (calculated using P_{app}) and 0.2-1.0 (calculated using P_{exact}) indicating that the MDR1-MDCKII *in vitro* BBB model could identify P-gp substrates. Both P_{app} and P_{exact} used to calculate efflux ratios identified amprenavir and mesoridazine to be substrates of efflux transporters (P_{app} efflux ratio 8.6 and 2.2 respectively and P_{exact} 10.2 and 2.1 respectively).

4.2.3.4 Permeability measurements of test drugs across the MDCKwt *in vitro* blood-brain barrier model

Test drugs were used in permeability studies across MDCKwt *in vitro* BBB model using a high throughput screening technique. Tables 4.8 and 4.9 detail apparent permeability and exact permeability, with and without the P-gp inhibitor GF120918 across MDCKwt cell monolayers for amprenavir, carbamazepine, chlorpromazine, citalopram, clozapine, donepezil, haloperidol, mesoridazine, primidone, quetiapine, risperidone and ziprasidone. Percentage recoveries for all test drugs were similar.

Table 4.8 **Apparent permeability and efflux ratio of test drugs across MDCKwt *in vitro* blood-brain barrier model**

	With out inhibitor			With inhibitor		
Test drugs	**P_{app} A-B**	**P_{app} B-A**	**ER**	**P_{app} A-B**	**P_{app} B-A**	**ER**
Amprenavir	206.2 ± 24.7	416.3 ± 71.5	2.0	401.5 ± 68.3	369.7 ± 69.1	0.9
Carbamazepine	787.7 ± 119.7	776.4 ± 114.8	1.0	732.6 ± 107.6	688.1 ± 86.8	0.9
Chlorpromazine	303.2 ± 75.9	205.2 ± 38.0	0.7	414.9 ± 52.3	190.0 ± 35.1	0.5
Citalopram	880.9 ± 147.3	750.9 ± 46.1	0.9	860.1 ± 135.0	737.2 ± 85.0	0.9
Clozapine	490.2 ± 129.7	393.6 ± 93.7	0.8	416.6 ± 56.1	311.2 ± 74.4	0.8
Donepezil	662.5 ± 82.1	554.5 ± 52.8	0.8	650.8 ± 121.2	591.9 ± 108.8	0.9
Haloperidol	484.6 ± 66.9	377.9 ± 57.0	0.8	453.6 ± 86.7	405.8 ± 78.8	0.9
Mesoridazine	493.6 ± 84.4	474.5 ± 41.0	1.0	620.2 ± 77.7	515.3 ± 62.2	0.8
Primidone	305.9 ± 64.4	206.0 ± 50.6	0.7	417.3 ± 145.5	236.1 ± 65.5	0.6
Quetiapine	1722.7 ± 252.2	1312.0 ± 139.4	0.8	1386.4 ± 198.1	1008.5 ± 122.4	0.7
Risperidone	878.6 ± 169.1	722.9 ± 122.9	0.8	892.2 ± 147.1	729.8 ± 99.6	0.8
Ziprasidone	340.6 ± 89.1	140.0 ± 31.2	0.4	729.2 ± 141.1	124.6 ± 28.6	0.2

Apparent permeability of amprenavir, carbamazepine, chlorpromazine, citalopram, clozapine, donepezil, haloperidol, mesoridazine, primidone, quetiapine, risperidone and ziprasidone (3 µM) across the MDCKwt *in vitro* BBB model in both A-B and B-A directions, with and without the potent P-gp inhibitor GF120918 (2 µM), was measured over 90 min. The apparent permeability (P_{app} nm.s^{-1}) and efflux ratio (ER) were calculated. Apparent permeability data are expressed as mean ± standard deviation of duplicates, n=3 independent experiments for all test drugs. Efflux ratios (B-A/A-B) were calculated from mean apparent permeability values.

Table 4.9 **Exact permeability and efflux ratio of test drugs across MDCKwt *in vitro* blood-brain barrier model**

	With out inhibitor			With inhibitor		
Test drugs	**P_{exact} A-B**	**P_{exact} B-A**	**ER**	**P_{exact} A-B**	**P_{exact} B-A**	**ER**
Amprenavir	237.4 ± 26.8	485.0 ± 36.6	2.0	415.6 ± 27.5	395.9 ± 22.9	1.0
Carbamazepine	1001.1 ± 103.6	968.6 ± 76.7	1.0	906.6 ± 118.2	893.5 ± 89.5	1.0
Chlorpromazine	557.3 ± 69.4	275.7 ± 48.8	0.5	818.8 ± 73.3	253.0 ± 44.7	0.3
Citalopram	950.9 ± 79.4	885.8 ± 92.0	1.0	915.1 ± 102.9	806.2 ± 66.7	0.9
Clozapine	694.4 ± 111.5	472.7 ± 101.8	0.7	598.1 ± 52.9	360.4 ± 89.5	0.6
Donepezil	782.7 ± 137.5	644.6 ± 68.7	0.8	718.7 ± 136.1	660.2 ± 81.9	0.9
Haloperidol	674.3 ± 71.6	499.3 ± 92.3	0.7	613.4 ± 92.5	485.3 ± 92.0	0.8
Mesoridazine	757.4 ± 100.5	585.6 ± 38.3	0.8	731.4 ± 70.9	597.1 ± 80.4	0.8
Primidone	337.1 ± 47.3	240.7 ± 68.6	0.7	427.8 ± 147.6	228.4 ± 40.5	0.5
Quetiapine	1585.3 ± 212.9	1554.5 ± 140.7	1.0	1450.7 ± 148.4	1188.5 ± 95.9	0.8
Risperidone	903.4 ± 144.4	822.0 ± 121.6	0.9	989.2 ± 184.0	805.7 ±114.7	0.8
Ziprasidone	629.9 ± 96.9	335.8 ± 49.1	0.5	1521.7 ±178.1	204.8 ± 46.0	0.1

Exact permeability of amprenavir, carbamazepine, chlorpromazine, citalopram, clozapine, donepezil, haloperidol, mesoridazine, primidone, quetiapine, risperidone and ziprasidone (3 µM) across the MDCKwt *in vitro* BBB model in both A-B and B-A directions, with and without the potent P-gp inhibitor GF120918 (2 µM), was measured over 90 min. The exact permeability (P_{exact} nm.s^{-1}) and efflux ratio (ER) were calculated. Exact permeability data are expressed as mean ± standard deviation of duplicates, n=3 independent experiments for all test drugs. Efflux ratios (B-A/A-B) were calculated from mean exact permeability values.

The P_{app} A-B ranged from 206.2-1722.7 nm.s^{-1} and the P_{app} B-A from 205.2-1312.0 nm.s^{-1} without inhibitor. The P_{exact} A-B ranged from 237.4-1585.3 nm.s^{-1} and P_{exact} B-A from 240.7-

1554.5 $nm.s^{-1}$ without inhibitor. No appreciable difference between P_{app} B-A and P_{exact} B-A was observed. The efflux ratios ranged from 0.4-1.0 (calculated using P_{app}) and 0.5-1.0 (calculated using P_{exact}) for 11 of the 12 test drugs whilst amprenavir (a known P-gp substrate) was shown to be a borderline P-gp substrate (efflux ratio P_{app} 2.0, P_{exact} 2.0).

4.2.4 Relationship between *in vitro* blood-brain barrier model permeabilities

The permeability data (Tables 4.2-4.9) obtained from *in vitro* BBB models was compared in order to evaluate similarities between *in vitro* BBB models. The A-B permeability (P_{app} and P_{exact}) with and without the P-gp inhibitor GF120918 was compared between the porcine, hCMEC/D3, MDR1-MDCKII and MDCKwt *in vitro* BBB models (Figures 4.3-4.7).

Figure 4.3 Relationship between porcine and hCMEC/D3 *in vitro* blood-brain barrier model permeabilities

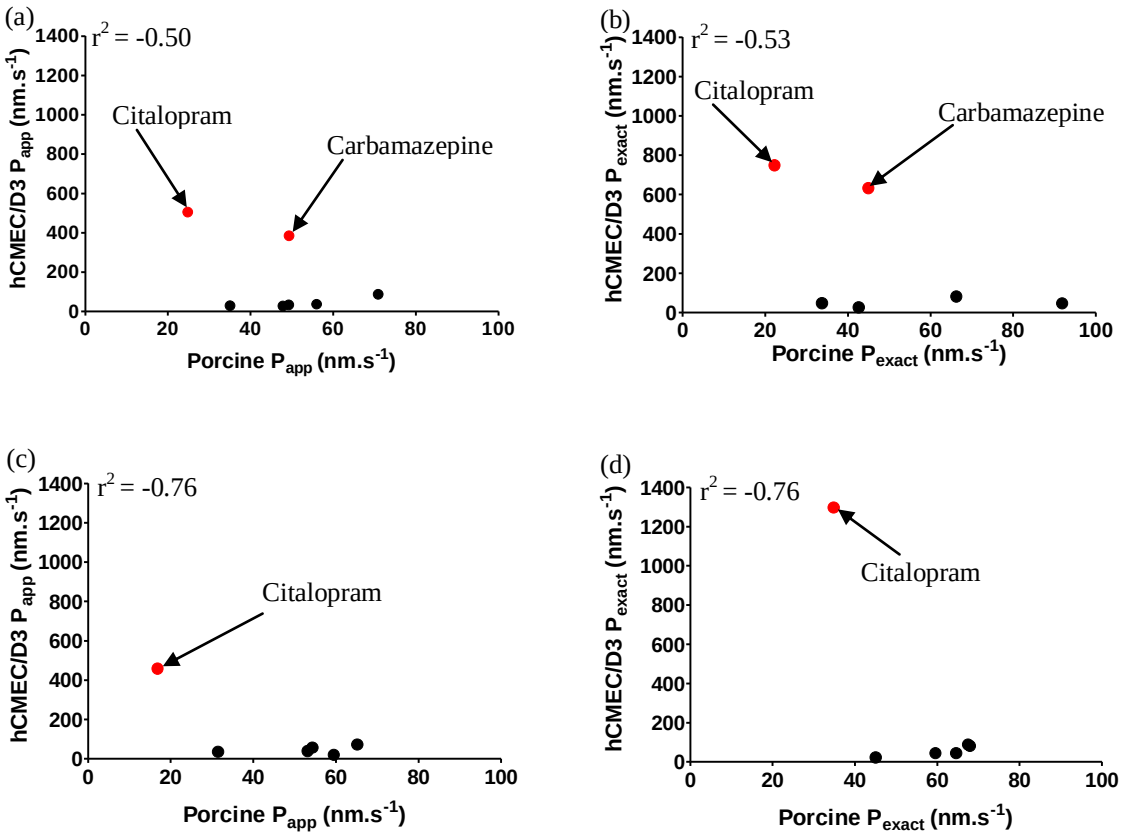

Relationship between porcine and hCMEC/D3 *in vitro* BBB model A-B permeabilities (P_{app} and P_{exact} nm.s^{-1}) without the P-gp inhibitor GF120918 (a and b) for amprenavir, carbamazepine, chlorpromazine, citalopram, haloperidol, mesoridazine and risperidone and with 2 µM of the P-gp inhibitor GF120918 (c and d) for amprenavir, chlorpromazine, citalopram, haloperidol, mesoridazine and risperidone. The data from the porcine *in vitro* BBB model are expressed as mean of duplicates, n=3 independent experiments for all test drugs except carbamazepine where data are expressed as the mean of duplicates from one independent experiment with and without the inhibitor GF120918. Data from the hCMEC/D3 *in vitro* BBB model are expressed as mean of duplicates, n=3 independent experiments for all test drugs apart from carbamazepine, citalopram and risperidone where data are expressed as the mean duplicates from one independent experiment with and without the inhibitor GF120918.

No relationship was observed between porcine and hCMEC/D3 *in vitro* BBB model A-B permeability (P_{app} and P_{exact}) for the test drugs without the inhibitor GF120918 (P_{app} r^2 = -0.50, P_{exact} r^2 = -0.53) (Figure 4.3a and 4.3b). For amprenavir, chlorpromazine, haloperidol, mesoridazine and risperidone both P_{app} and P_{exact} values from porcine and hCMEC/D3 *in vitro* BBB models were < 100 nm.s^{-1}. Carbamazepine (P_{app} 385.0 nm.s^{-1}, P_{exact} 632.3 nm.s^{-1}) and citalopram highlighted in red above (P_{app} 505.1 nm.s^{-1}, P_{exact} 747.8 nm.s^{-1})

both showed higher permeability across the hCMEC/D3 *in vitro* BBB model compared to the porcine model carbamazepine (P_{app} 49.3 $nm.s^{-1}$, P_{exact} 44.9 $nm.s^{-1}$) and citalopram highlighted in red above (P_{app} 24.8 $nm.s^{-1}$, P_{exact} 22.2 $nm.s^{-1}$) and compared to all other tests drugs across both models.

An efflux ratio > than 2 (P_{app} 2.6, P_{exact} 3.3) was observed for citalopram, suggesting it was a substrate of an efflux transporter, using the porcine *in vitro* BBB model. Although using hCMEC/D3 *in vitro* BBB model citalopram was only shown to be an efflux substrate when efflux ratio was calculated using P_{exact} (P_{app} 0.9, P_{exact} 2.2).

No appreciable change to the relationships between porcine and hCMEC/D3 *in vitro* BBB model A-B permeability (P_{app} and P_{exact}) for the test drugs was observed with the inhibitor GF120918 (P_{app} r^2 = -0.76, P_{exact} r^2 = -0.76) (Figure 4.3c and 4.3d) compared to the relationships without the inhibitor. Citalopram (P_{app} 457.7 $nm.s^{-1}$, P_{exact} 1297.8 $nm.s^{-1}$) again showed higher permeability across the hCMEC/D3 *in vitro* BBB model compared to the porcine model (P_{app} 16.8 $nm.s^{-1}$, P_{exact} 34.8 $nm.s^{-1}$).

Figure 4.4 Relationship between porcine and MDR1-MDCKII *in vitro* blood-brain barrier model permeabilities

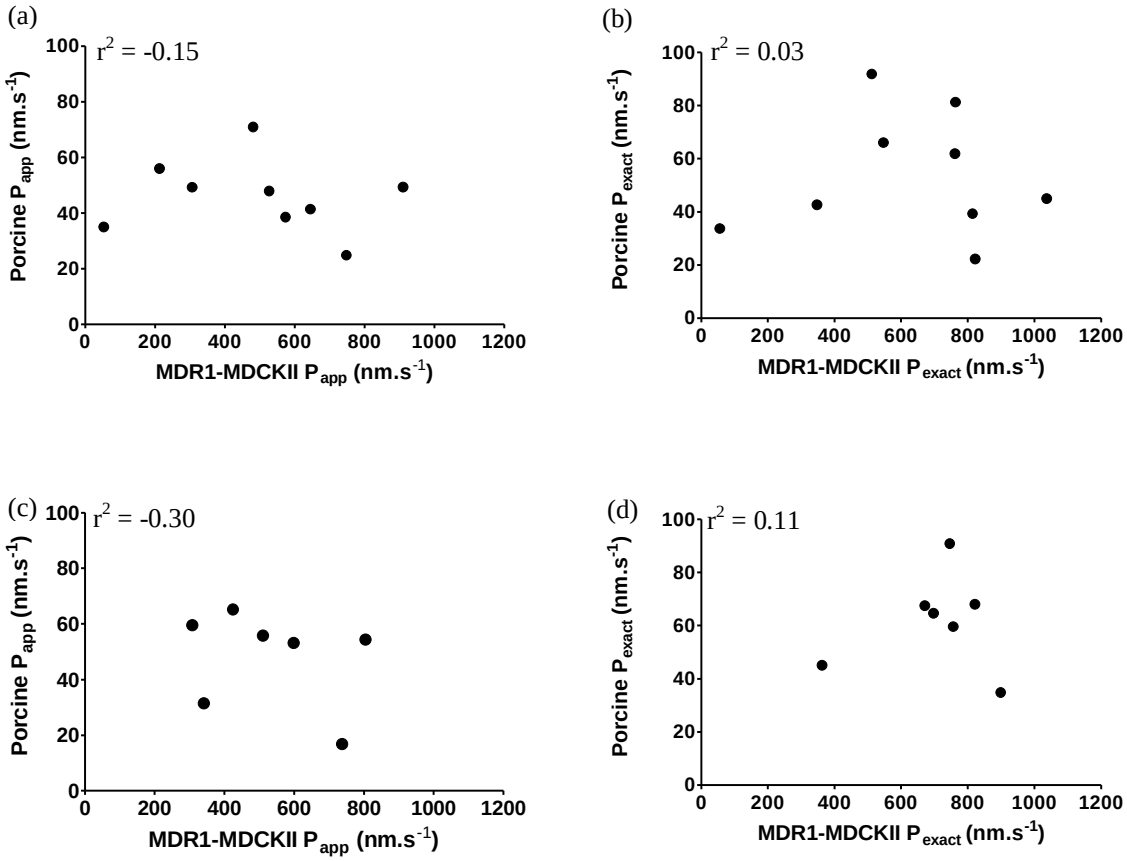

Relationship between porcine and MDR1-MDCKII *in vitro* BBB model A-B permeabilities (P_{app} and P_{exact} $nm.s^{-1}$) (a and b) without the P-gp inhibitor GF120918, for amprenavir, carbamazepine, chlorpromazine, citalopram, clozapine, donepezil, haloperidol, mesoridazine and risperidone and with 2 µM of the P-gp inhibitor GF120918 (c and d) for amprenavir, chlorpromazine, citalopram, clozapine, haloperidol, mesoridazine and risperidone. Data from the porcine *in vitro* BBB model are expressed as mean of duplicates, n=3 independent experiments for all test drugs except carbamazepine, clozapine and donepezil with out the inhibitor and except clozapine with the inhibitor where data are expressed as the mean of duplicates from one independent experiment. Data from the MDR1-MDCKII *in vitro* BBB model are expressed as mean of duplicates, n=3 independent experiments for all test drugs with and without the inhibitor GF120918.

No relationship was observed between the porcine and MDR1-MDCKII *in vitro* BBB model A-B permeability values (P_{app} r^2 = -0.15, P_{exact} r^2 = 0.03) without the inhibitor GF120918 (Figure 4.4a and 4.4b). The permeability rank order (lowest to highest based on P_{app}) of the test drugs from the porcine (citalopram, amprenavir, clozapine, donepezil,

risperidone, mesoridazine, carbamazepine, chlorpromazine and haloperidol) and MDR1-MDCKII (amprenavir, chlorpromazine, mesoridazine, haloperidol, risperidone, clozapine, donepezil, citalopram and carbamazepine) *in vitro* BBB models showed no similarity apart for with risperidone which held the median permeability value for both models.

No similarities were observed between the porcine and MDR1-MDCKII *in vitro* BBB model and A-B permeability values (P_{app} r^2 = -0.30, P_{exact} r^2 = 0.11) with the inhibitor GF120918 (Figure 4.4c and 4.4d). In general, the permeability values (both P_{app} and P_{exact}) obtained with the MDR1-MDCKII model were of an order of magnitude greater than the permeability values obtained with the porcine model. The permeability rank order (lowest to highest based on P_{app}) of the test drugs from the porcine (citalopram, chlorpromazine, mesoridazine, risperidone, clozapine, amprenavir and haloperidol) and MDR1-MDCKII (mesoridazine, chlorpromazine, risperidone, haloperidol, clozapine and citalopram) *in vitro* BBB model showed no similarity.

Figure 4.5 **Relationship between hCMEC/D3 and MDR1-MDCKII *in vitro* blood-brain barrier model permeabilities**

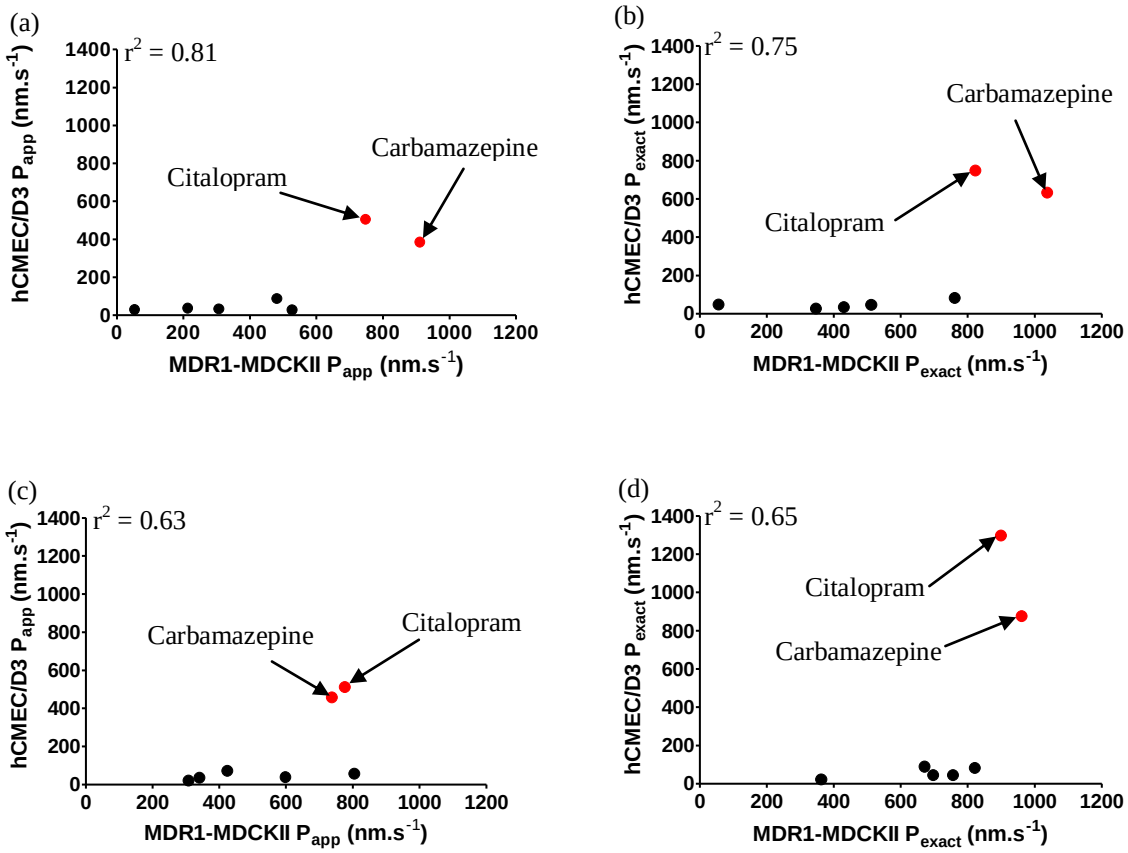

Relationship between hCMEC/D3 and MDR1-MDCKII *in vitro* BBB model A-B permeability (P_{app} and P_{exact} nm.s^{-1}) without the P-gp inhibitor GF120918 for amprenavir, carbamazepine, chlorpromazine, citalopram, haloperidol, mesoridazine and risperidone (a and b) and with 2 µM of the P-gp inhibitor GF120918. The data from the hCMEC/D3 *in vitro* BBB model are expressed as mean of duplicates, n=3 independent experiments for all test drugs apart from carbamazepine, citalopram and risperidone, with and without the inhibitor GF120918, where data are expressed as the mean of duplicates from one independent experiment. Data from the MDR1-MDCKII are expressed as mean of duplicates, n=3 independent experiments for all test drugs, with and without the inhibitor GF120918.

A stronger correlation (P_{app} r^2 = 0.81, P_{exact} r^2 = 0.75) was observed between the hCMEC/D3 and MDR1-MDCKII *in vitro* BBB models (Figure 4.5a and 4.5b). However, similarities between the actual permeability values for the test drugs were not observed between the models.

In general, the permeabilities values obtained from the MDR1-MDCKII *in vitro* BBB model were at least an order of magnitude greater (for 6/7 test drugs P_{app} 213.1-1023.7 nm.s^{-1},

P_{exact} 347.4-1135.5 $nm.s^{-1}$) than those obtained with the hCMEC/D3 (for 5/7 P_{app} 28.2-72.0 $nm.s^{-1}$, P_{exact} 22.0-88.8 $nm.s^{-1}$) except for carbamazepine (P_{app} 910.7 $nm.s^{-1}$ and P_{exact} 1037.1 $nm.s^{-1}$ from MDR1-MDCKII model, P_{app} 385.0 $nm.s^{-1}$ and P_{exact} 632.3 $nm.s^{-1}$ from hCMEC/D3 model) and citalopram (P_{app} 748.0 and P_{exact} 822.7 $nm.s^{-1}$ from MDR1-MDCKII model and P_{app} 505.1 and P_{exact} 747.8 $nm.s^{-1}$ from hCMEC/D3 model) which were of the same order of magnitude as the MDR1-MDCKII model permeabilities for these test drugs.

The relationship between A-B permeability of MDR1-MDCKII and hCMEC/D3 *in vitro* BBB models with inhibitor was not as strong (P_{app} $r^2 = 0.63$, P_{exact} $r^2 = 0.65$) (Figure 4.5c and 4.5d) as without the inhibitor (P_{app} $r^2 = 0.81$, P_{exact} $r^2 = 0.75$ (Figure 4.4a and 4.5b). Comparable with permeability values observed in Figures 4.5a and 4.5b the permeability values obtained from the MDR1-MDCKII *in vitro* BBB model were at least an order of magnitude greater than those obtained with the hCMEC/D3 model, exceptions to this being carbamazepine and citalopram, which had the highest permeability values with hCMEC/D3 cells.

Figure 4.6 **Relationship between MDR1-MDCKII and MDCKwt *in vitro* blood-brain barrier model permeabilities**

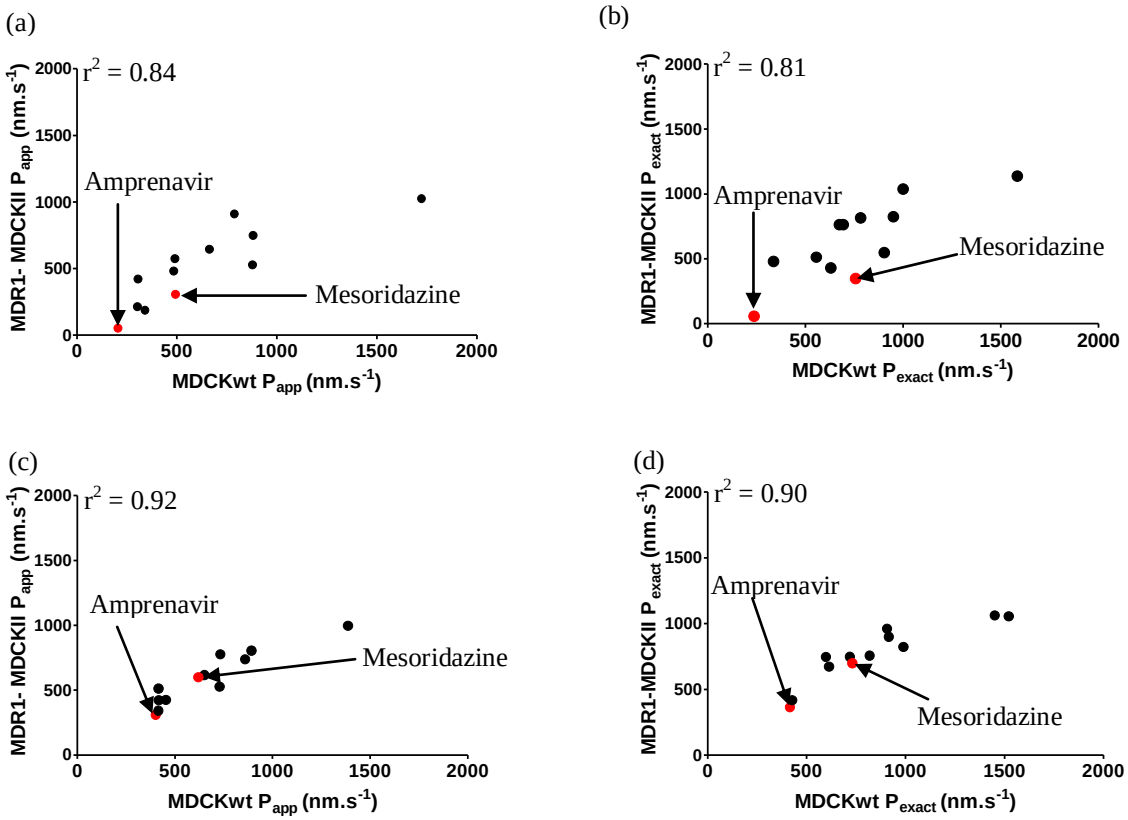

Relationship between MDR1-MDCKII and MDCKwt *in vitro* BBB model A-B permeability (P_{app} and P_{exact} nm.s^{-1}) without the P-gp inhibitor GF120918 (a and b) and with 2 µM of the P-gp inhibitor (c and d) for amprenavir, carbamazepine, chlorpromazine, citalopram, clozapine, donepezil, haloperidol, mesoridazine, primidone, quetiapine, risperidone and ziprasidone. The data from the MDR1-MDCKII *in vitro* BBB model are expressed as mean of duplicates, n=3 independent experiments for all test drugs with and without the inhibitor GF120918. Data from the MDCKwt control are expressed as mean of duplicates, n=3 independent experiments for all test drugs with and without the inhibitor GF120918.

The strongest relationship (P_{app} r^2 = 0.84 and P_{exact} r^2 = 0.81) was observed between MDCKwt and MDR1-MDCKII A-B permeability without the P-gp inhibitor GF120918 (Figure 4.6a and 4.6b) compared to the relationship between the other *in vitro* BBB models. Amprenavir (efflux ratio P_{app} 8.6 and P_{exact} 10.2) and mesoridazine (efflux ratio P_{app} 2.2 and P_{exact} 2.1) were the only 2 test drugs that were shown to be substrates of efflux transporters using the MDR1-MDCKII *in vitro* BBB model. Amprenavir was shown to be a borderline substrate using the MDCKwt model (efflux ratio P_{app} 2.0 and P_{exact} 2.0). The permeability values for each test drug using both *in vitro* BBB models were of the same magnitude of order

and the permeability rank order (lowest to highest based on P_{app}) of the test drugs from the MDR1-MDCKII (amprenavir, ziprasidone, chlorpromazine, mesoridazine, primidone, haloperidol, risperidone, clozapine, donepezil, citalopram carbamazepine and quetiapine) and MDR1-MDCKII control MDCKwt (amprenavir, chlorpromazine, primidone, ziprasidone, haloperidol, clozapine, mesoridazine, donepezil, carbamazepine, risperidone, citalopram and quetiapine) although not identical were similar.

The relationship was improved (P_{app} r^2 = 0.92, P_{exact} r^2 = 0.90) (Figure 4.6c and 4.6d) when A-B permeability was measured across MDR1-MDCKII *in vitro* BBB model and MDR1-MDCKII control MDCKwt cells with the P-gp inhibitor GF120918 in order to eliminate the effect of P-gp on permeability.

4.2.5 Relationship between *in vitro* and *in situ* permeability

The relationship between *in vitro* apparent and exact permeability determined using the porcine, hCMEC/D3 and MDR1-MDCKII *in vitro* BBB models and the *in situ* permeability measurement, permeability surface product (P) (values obtained from the literature), in rat was investigated in order to determine the *in vitro* BBB model that best predicted rat *in situ* BBB permeability. In brief, rats were anaesthetised, the left common artery was cannulated, the cardiac blood supply was cut off and the rat brains were perfused with Krebs-Ringer bicarbonate buffer, containing each test drug ($fu_{perfusate}$ =1), pH 7.4, oxygenated with a mixture of 95 % oxygen and 5 % CO_2 for 30 s. Each test drug was perfused in 3 rats.

Table 4.10 **Rat *in situ* permeability data for a series of centrally acting test drugs**

Test drug	Rat *in situ* permeability (P) nm.s^{-1}
Amprenavir	-
Carbamazepine	1066
Chlorpromazine	2900
Citalopram	645
Clozapine	2512
Donepezil	1757
Haloperidol	1864
Mesoridazine	930
Primidone	-
Quetiapine	2369
Risperidone	944
Ziprasidone	1109

Rat *in situ* permeability data (P) nm.s^{-1} sourced from the literature for 10 of the 12 test drugs (Summerfield et al. 2007) data unavailable for amprenavir and primidone.

Figure 4.7 **Relationship between porcine *in vitro* blood-brain barrier permeability and rat *in situ* permeability surface product**

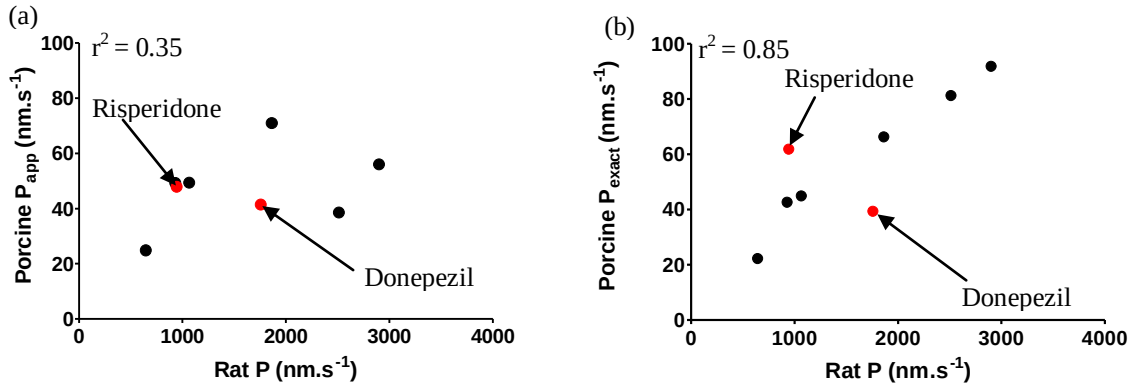

Relationship between *in vitro* A-B permeability (P_{app} and P_{exact} nm.s^{-1}) (Table 4.2 and 4.3) determined using porcine *in vitro* BBB model and rat *in situ* permeability surface product (P nm.s^{-1}) determined using a rat *in situ* brain perfusion model (Table 4.11) for carbamazepine, chlorpromazine, citalopram, clozapine, donepezil, haloperidol, mesoridazine and risperidone.

A strong correlation (Pearson's $r^2 = 0.85$) between exact permeability determined using the porcine *in vitro* BBB model and rat *in situ* permeability surface product was observed (Figure 4.7b). Although a weak correlation ($r^2 = 0.35$) between apparent permeability determined using the porcine *in vitro* BBB model and rat *in situ* permeability surface product (Figure 4.7a) was observed for the same test drugs. In Figure 4.7b risperidone and donepezil

have been highlighted as outliers to the correlation. Donepezil exhibited an efflux ratio > than 2 using the porcine *in vitro* BBB model (efflux ratio P_{exact} 9.8) suggesting that it was a substrate of an efflux transporter(s) whereas risperidone did not (efflux ratio P_{exact} 1.2). In addition, a Spearman's rank correlation (r=0.83) was performed on this data, which also showed a strong correlation between exact permeabilities, derived from the porcine *in vitro* BBB model, and rat *in situ* permeabilities.

Figure 4.8 **Relationship between hCMEC/D3 *in vitro* blood-brain barrier permeability and rat *in situ* permeability surface product**

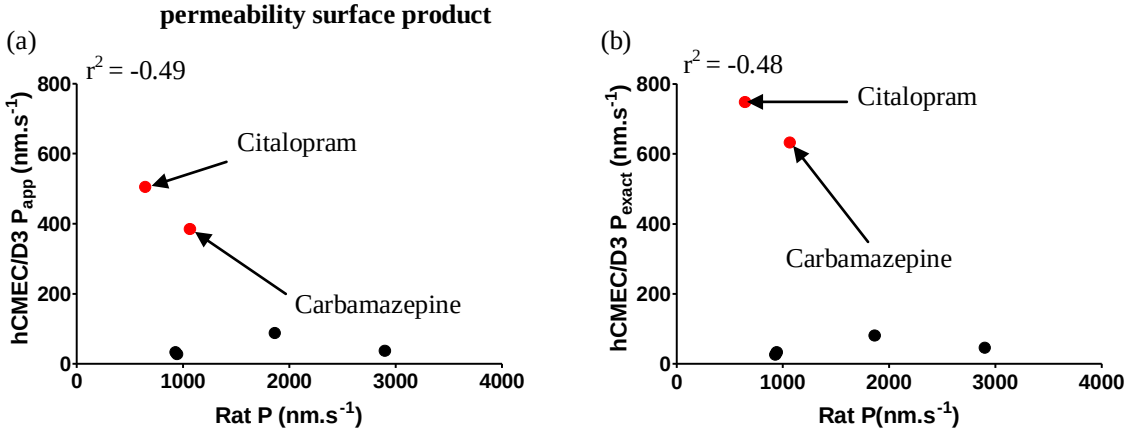

Relationship between *in vitro* A-B permeability (P_{app} and P_{exact} $nm.s^{-1}$) (Table 4.4 and 4.5) determined using hCMEC/D3 *in vitro* BBB model and rat *in situ* permeability surface product (P $nm.s^{-1}$) determined using a rat *in situ* brain perfusion model (Table 4.11) for carbamazepine, chlorpromazine, citalopram, haloperidol, mesoridazine and risperidone.

No relationship was observed between apparent or exact A-B permeability (P_{app} r^2=-0.49 and P_{exact} r^2= -0.48) using the hCMEC/D3 *in vitro* BBB model and rat *in situ* permeability for the test drugs (Figure 4.8a and 4.8b). Both carbamazepine and citalopram (P_{app} and P_{exact}) were shown to have the largest permeability values using hCMEC/D3 *in vitro* BBB models compared to the other test drugs. However, carbamazepine and citalopram were not shown to have the largest permeability values compared to the other test drugs using the rat *in situ* permeability model.

Figure 4.9 Relationship between MDR1-MDCKII *in vitro* blood-brain barrier permeability and rat *in situ* permeability surface product

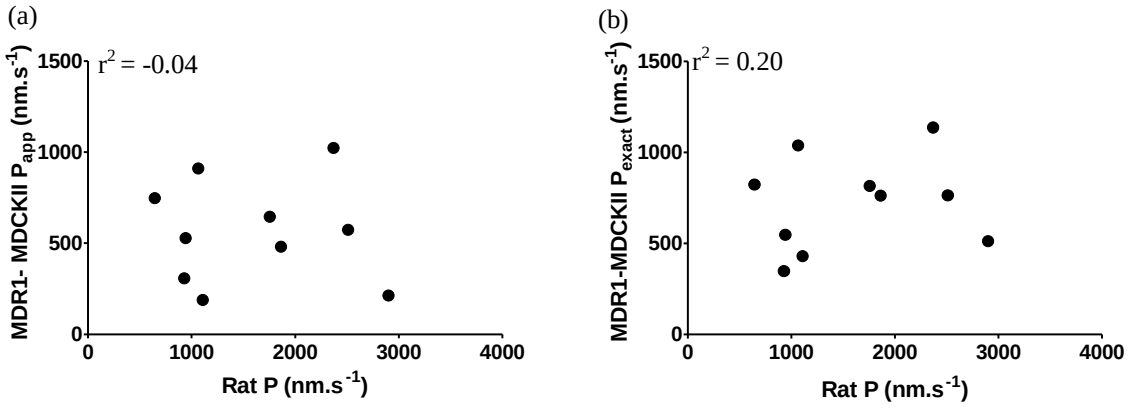

Relationship between *in vitro* A-B permeability (P_{app} and P_{exact} nm.s^{-1}) (Table 4.6 and 4.7) determined using MDR1-MDCKII *in vitro* BBB model and rat *in situ* permeability surface product (P nm.s^{-1}) determined using a rat *in situ* brain perfusion model (Table 4.11) for carbamazepine, chlorpromazine, citalopram, clozapine, donepezil, haloperidol, mesoridazine, quetiapine, risperidone and ziprasidone.

No relationship was observed between apparent or exact A-B permeability (Papp r^2 = -0.04 and P_{exact} r^2 = -0.20) (Figure 4.9a and 4.9b) using the MDR1-MDCKII *in vitro* BBB model and *in situ* rat permeability. There were also no similarities between the permeability rank order (P_{app} or P_{exact}) from the MDR1-MDCKII *in vitro* BBB model and rat *in situ* permeability.

4.3 Discussion

At present, there is no *in vitro* BBB model that is considered to be the 'gold standard' for the prediction of *in vivo* permeability. The literature documents a great variety of *in vitro* BBB models employing different cell types, from various species and tissues, developed using a range of culture techniques. Consequently, comparing permeability data between *in vitro* BBB models remains problematic.

However, the main aim of an *in vitro* BBB model, for transport studies, is to accurately predict *in vivo* BBB permeability. Therefore, it may not be a question of comparing permeability data across *in vitro* BBB models, but instead a question of finding an *in vitro* BBB model that best predicts *in vivo* BBB permeability.

Prior to commencing transport studies across each of the *in vitro* BBB models, it was necessary to determine a test drug concentration that did not affect the viability of the cells

employed as *in vitro* BBB models. The MTT assay was the assay of choice because of its rapidity, precision, high throughput and cost effectiveness (Mosmann 1983). Methylthiazolyldiphenyl-tetrazolium bromide is a yellow tetrazolium salt that is reduced to formazan, a purple water insoluble product, by mitochondrial succinate dehydrogenases which are only active in living cells (Liu et al. 1997). After solubilisation the formazan product can be quantified to determine the percentage of viable cells. The MTT assay demonstrates a linear relationship between cell number and MMT formazan product over a large range (200-50,000 cells per well)(Mosmann 1983).

Preliminary studies were carried out to determine the optimum cell seeding density (of each cell type employed as *in vitro* BBB models), for use in a subsequent cytotoxic MTT assay. Optimum sensitivity of the MTT assay is achieved using near confluent cells that are in the exponential growth phase to avoid underestimating drug toxicity. The seeding density that produced an absorbance of approximately 1 with cells maintained in culture for 48 h was chosen as the optimum cell seeding density.

None of the test drugs substantially decreased the viability of any cell type at 3 µM compared to control cells. A test drug concentration of 3 µM was desirable to remain consistent with studies performed routinely at GSK. The MTT assay was also performed with the potent P-gp inhibitor GF120918, because transport studies were to be conducted both with and without the inhibitor, in order to assess the possible effect of P-gp on drug transport across *in vitro* BBB models. None of the test drugs substantially decreased cell viability of any cell type at 3 µM in combination with GF120918 compared to control cells. In addition, the paracellular marker Lucifer yellow (with and without GF120918) had no substantially affect on cell viability at 100 µM. The test drug concentration of 3 µM was used in all subsequent transport studies.

The integrity of *in vitro* BBB model monolayers was characterised using Lucifer yellow as a paracellular permeability marker and TER measurements. Lucifer yellow permeabilities were shown to be comparable across hCMEC/D3, MDR1-MDCKII, MDCKwt and Caco-2 *in vitro* BBB models.

For MDR1-MDCKII and Caco-2 monolayers Lucifer yellow permeabilities were also in concordance with data reported in the literature (Madgula et al. 2007). However, for the hCMEC/D3 *in vitro* BBB model Lucifer yellow permeabilities reported in the literature

(221 $nm.s^{-1}$) (Poller et al. 2008) were approximately 4-fold greater than those obtained in this thesis (under similar experimental conditions), which may be explained by interlaboratory or inter-batch variation. Interlaboratory variation also makes the comparison of experimental drug permeability data, using the same *in vitro* BBB model, between laboratories difficult.

The Lucifer yellow permeability across the porcine *in vitro* BBB model was an order of magnitude greater than Lucifer yellow permeabilities across the other 4 *in vitro* BBB models used in the study. This suggests that the primary porcine *in vitro* BBB model monolayers were more permeable to Lucifer yellow than the other *in vitro* model monolayers used in the study, which all employed cells from continuous cell lines. This was not to be expected, because in general, continuous cell lines form less restrictive barriers than primary cultured CECs (Gumbleton et al. 2001). However, the permeability of Lucifer yellow across intact rat pial vessels has been reported in the literature to be 316 $nm.s^{-1}$ (Easton et al. 1994) which is comparable to the Lucifer yellow permeability obtained across the porcine *in vitro* BBB model (216 $nm.s^{-1}$) in these studies.

No appreciable differences were observed between apparent and exact Lucifer yellow permeabilities, obtained using any of the *in vitro* BBB models. Lucifer yellow demonstrated good mass balance (data not shown) which could explain why there were no differences between P_{app} and P_{exact} values. Other reasons could be that Lucifer yellow transport was linear with time and <10 % of Lucifer yellow was transported across the *in vitro* BBB monolayers.

Primary porcine *in vitro* BBB model monolayers exhibited the highest TER compared to all other *in vitro* BBB models in the study. The TER achieved across the monolayers of the primary porcine model (2000-2200 $\Omega.cm^2$) were comparable to reported *in vivo* TER values of 1490 $\Omega.cm^2$ and 1870 $\Omega.cm^2$ (Crone et al. 1982; Butt et al. 1990). Caco-2 monolayers also achieved high TER (1500-1800.cm^2) which was concordant with the literature (Garberg et al. 2005).

However, hCMEC/D3, MDR1-MDCKII and MDCKwt *in vitro* BBB models achieved relatively low TER which was not representative of *in vivo* BBB TER values (Crone et al. 1982; Butt et al. 1990). The TER values for the hCMEC/D3, MDR1-MDCKII and MDCKwt were consistent with those reported in previous studies (Garberg et al. 2005; Weksler et al. 2005).

Although, there is no direct correlation between the permeability of paracellular probes and TER (Deli et al. 2005), it is expected that the monolayers with the lowest paracellular permeability would also exhibit the highest TER which was not the case in these studies.

The reasons for the discrepancy observed during this would is still to be elucidated. Possible explanations for the differences in TER could be due to different sized Transwell® inserts were used for each of the *in vitro* BBB models. An insert size of 1.12 cm^2 was used for *in vitro* BBB models using PBEC, hCMEC/D3 and Caco-2 cells. Whereas an insert size of 0.33 cm^2 was used for *in vitro* BBB models using MDR1-MDCKII and MDCKwt cells. Future work should include taking TER measurements across all *in vitro* BBB models grown on the same insert type and size for more accurate comparison.

Lucifer yellow was used as a marker of paracellular permeability to remain consistent with studies performed at GSK. However, future work should include measuring sucrose permeability across all *in vitro* BBB models employed in this work for further comparison and better comparison with the literature as sucrose permeability measurements across *in vitro* BBB models are most widely reported in the literature.

Using amprenavir as a marker of functional P-gp efflux activity, the porcine and MDR1-MDCKII *in vitro* BBB models both showed functional P-gp activity (also see Chapter 3 section 3.2.9 and 3.2.10) as expected from reports in the literature (Pastan et al. 1988; Hunter et al. 1993). However, the hCMEC/D3 *in vitro* BBB model did not exhibit any functional P-gp activity which was contradictory to reports in the literature (Poller et al. 2008) from studies using Rhodamine 123. A reason for this could be variation between batches of hCMEC/D3.

The MDCKwt model exhibited borderline P-gp activity with amprenavir (ER= 2), which is consistent with reports that the MDCKwt cell line constitutively expresses low levels of P-gp (Horio et al. 1989), also substantiated by Luo et al., which has a negligible effect on drug transport (Luo et al. 2002). Luo at al. also showed expression of P-gp was similar between Caco-2 and MDR-MDCKII cell line which was much greater than the MDCKwt cell line (Luo et al. 2002).

Following characterisation of *in vitro* BBB model integrity and efflux function, test drugs were used in permeability studies across all of *in vitro* BBB models, with and without

the potent P-gp inhibitor GF120918, in order to determine permeability measurements and efflux ratios.

The porcine *in vitro* BBB model permeabilities of the test drugs demonstrated the lowest dynamic range compared to the other *in vitro* BBB models, despite exhibiting the highest Lucifer yellow permeability. In general, the hCMEC/D3 model also exhibited low permeabilities comparable to permeabilities obtained with the porcine model, with two exceptions, carbamazepine and citalopram, which were an order of magnitude greater than those obtained with the porcine model.

The MDR1-MDCKII and MDCKwt *in vitro* BBB models showed permeabilities of the same order of magnitude and were in general higher than those obtained with the porcine and hCMEC/D3 *in vitro* BBB models, despite the MDR1-MDCKII and MDCKwt *in vitro* BBB models demonstrating the lowest Lucifer yellow permeabilities in the study.

For the porcine, MDR1-MDCKII and MDCKwt *in vitro* BBB models no appreciable differences between the apparent and exact permeabilities was observed. However, with the hCMEC/D3 *in vitro* BBB model an appreciable difference between apparent and exact permeabilities was observed which was more obvious for some test drugs, for example, citalopram, compared to other test drugs. As percentage recoveries for all test drugs were good, the difference between P_{app} and P_{exact} was unlikely to be related to mass balance issues. Instead it is possible that differences between P_{app} and P_{exact} were due to > 10 % of the test drug being transported across the hCMEC/D3 cell monolayers or that the transport of the test drugs was not linear over time.

Different laboratories use different classification systems to determine substrates of efflux transporters. For example, Wang et al. consider a drug to be a substrate of an efflux transporters if it exhibits an efflux ratio >2 (Wang et al. 2005). In contrast, Mahar Doan et al. consider a drug to be a substrate of an efflux transporter if it displays an efflux ratio >2.5 (Mahar Doan et al. 2002). Tests drug were considered to be substrates of efflux transporters in this thesis when they exhibited an efflux ratio >2, in concordance with the US Food and Drug Administration (Zhang et al. 2008).

Identification of substrates of efflux transporters showed conflicting data across *in vitro* BBB models. Citalopram was shown to be a P-gp efflux substrate using the porcine

(using P_{app} and P_{exact}) and hCMEC/D3 (using P_{exact} only, as appreciable differences were observed between P_{app} and P_{exact} for this test drug) *in vitro* BBB models.

Previous studies including studies using knock out mice (Mahar Doan et al. 2002; Maurer et al. 2005; Summerfield et al. 2008) have suggested that citalopram is not subject to active efflux at the BBB. In addition, another previous studies using the MDR1-MDCKII *in vitro* BBB model obtained an efflux ratio of 20.1 (Summerfield et al. 2007) suggesting that citalopram is a substrate of P-gp, although citalopram exhibited an efflux ratio of <2 in this thesis using the MDR1-MDCKII *in vitro* BBB model.

Mesoridazine was shown to be a substrate of an efflux transporter (calculated with P_{app} and P_{exact}) using the hCMEC/D3 and MDR1-MDCKII *in vitro* BBB models. These data are in concordance with a previous study using an MDR1-MDCKII *in vitro* BBB model (ER 87.1) (Summerfield et al. 2007).

Risperidone was shown to be a substrate of an efflux transporter (calculated with P_{app} and P_{exact}) using only the hCMEC/D3 *in vitro* BBB model. Risperidone has been shown to be a P-gp efflux substrate in previous studies using the MDR1-MDCKII *in vitro* BBB model (Summerfield et al. 2007) and in studies using knock out mice (Doran et al. 2005; Summerfield et al. 2006). However, in another study, risperidone was not shown to be a P-gp substrate using MDR1-MDCKII and Md1a-MDCK monolayer efflux assays (Feng et al. 2008).

Carbamazepine was shown to be a substrate of an efflux transporter (efflux ratio P_{app} 4.0, P_{exact} 3.7) using only the porcine *in vitro* BBB model. However, this study was not performed in the presence of the potent P-gp inhibitor GF120918 so it is possible that the efflux ratio observed efflux could be due to P-gp and/or other transporter(s). It has been suggested from previous studies that carbamazepine is a substrate of the MRP2 transporter (Potschka et al. 2001), thus the ER of 4.0-3.7 observed in the present study could be explained if MRP2 is functionally active in the porcine *in vitro* BBB model.

Donepezil was shown to be an efflux substrate using only the porcine *in vitro* BBB model. As with carbamazepine this study was not performed in the presence of the potent P-gp inhibitor GF120918 making if difficult to determine if the efflux was due to P-gp. However, in a previous study using the MDR1-MDCKII *in vitro* BBB model (Summerfield et al. 2007) it

was suggested that donepezil was a P-gp efflux substrate as an efflux ratio of 2.3 was obtained. There are currently no *in vivo* studies to support this.

None of the other test drugs were shown to be substrates of efflux transporters with any of the *in vitro* BBB models used in these studies.

Examining the permeabilities and efflux ratios obtained with each of the *in vitro* BBB models highlights differences between the models and demonstrates difficulties in comparing permeability data obtained with different *in vitro* BBB models and in different laboratories. However, as the models are from different cell types (endothelial and epithelial, primary isolated cells and continuous cell lines), tissues (brain and kidney) and species (porcine, human and dog), it is not surprising that there is variation in the data obtained. In addition, it is likely that there will be differences in the types of transporters present in each model which may or may not have yet been characterised. There may also be differences in the abundances of transporters and possibly species differences in substrate specificity between the transporters (Ohe et al. 2003; Syvanen et al. 2009). In addition, some test drugs may be substrates for more than one efflux transporter and therefore may show differences in efflux ratios using models that express different types of transporters with different abundances.

The relationship between drug permeability obtained using the *in vitro* BBB models was further examined in order to investigate similarities between the *in vitro* BBB models.

No relationship was observed between the porcine and hCMEC/D3 or the porcine and MDR1-MDCKII *in vitro* BBB model permeabilities when they were plotted against each other. The relationship between the permeabilities was not improved in the presence of the potent P-gp inhibitor GF120918.

Although, the porcine and hCMEC/D3 *in vitro* BBB model both employ CECs, differences in Lucifer yellow permeabilities, TER values, P-gp functionality of the *in vitro* BBB models and species differences in transporter substrate identification could explain why there was no relationship between the model permeabilities. There may also be differences in active influx and efflux transporters that have not yet been characterised at these models.

Differences in cell architecture between PBECs and MDR1-MDCKII may explain differences between test drug permeabilities across porcine and MDR1-MDCKII *in vitro* BBB models. Porcine brain endothelial cells exhibit elongated, spindly, fusiform morphology

(Chapter 3), in contrast, MDR1-MDCKII (epithelial) cells are columnar in shape exhibiting micro villi (Udo et al. 2010) and originate from the dog kidney.

A relationship between drug permeabilities across the hCMEC/D3 and MDR1-MDCKII *in vitro* BBB models was observed, which was not improved in the presence of the potent P-gp inhibitor GF120918. However, the permeabilities obtained using the MDR1-MDCKII *in vitro* BBB model were greater for all test drugs than the permeabilities obtained using the hCMEC/D3 model. Although, both *in vitro* BBB models displayed comparable Lucifer yellow permeabilities and TER values.

A relationship was observed between the MDR1-MDCKII and the MDCKwt *in vitro* BBB model permeabilities. This was somewhat expected as both models employ the same cell type and demonstrate similar Lucifer yellow permeabilities and TER values. The main difference between the two models is that the MDR1-MDCKII model exhibits functional P-gp activity that has an appreciable effect on drug transport whereas the MDCKwt model does not. Since only 2 test drugs were classified as P-gp substrates using the MDR1-MDCKII model, the presence of functionally active P-gp did not appreciably affect the relationship between the MDR1-MDCKII and MDCKwt models.

However, the relationship was improved in the presence of the inhibitor GF120918, which demonstrated the effect of P-gp efflux on test drug transport even for test drugs that were not classified P-gp substrates. The presence of P-gp at the MDR1-MDCKII *in vitro* BBB model did not appreciably affect the permeabilities all the test drugs. However, the efflux ratios derived using the MDR1-MDCKII *in vitro* BBB model for most of the test drugs decreased in the presence of the potent P-gp inhibitor GF120918 even for test drugs that not been classified P-gp substrates.

Differences and inconsistencies between the permeability function of the porcine, hCMEC/D3, MDR1-MDCKII and MDCKwt *in vitro* BBB models have been observed, highlighting problems associated with comparing data between *in vitro* BBB models. However, the main aim of an *in vitro* BBB model is to predict *in vivo* BBB permeability. The relationship between *in vitro* BBB permeability and rat *in situ* permeability was therefore investigated in order to determine which *in vitro* BBB model best predicted rat *in situ* BBB permeability.

Exact permeabilities obtained using the porcine *in vitro* BBB model showed a strong relationship with rat *in situ* permeability (Pearson's correlation coefficient). The relationship was stronger than the relationship between; porcine (apparent permeabilities) and rat *in situ* permeability and both hCMEC/D3 and MDR1-MDCKII (apparent and exact permeabilities) and rat *in situ* permeability.

For the porcine model, in addition to the strong correlation observed using Pearson's correlation coefficient, a strong correlation was also observed using Spearman's rank correlation. Despite observing no appreciable differences between apparent and exact permeabilities using the porcine model (section 4.2.3), the exact permeability showed a stronger relationship with *in situ* rat permeability compared to the apparent permeability.

Although the differences between apparent and exact permeabilities did not appear to be appreciable, inaccuracies, however small, may be responsible for the poor relationship observed with the apparent permeabilities.

The porcine *in vitro* BBB model employs primary cultured cells which exhibit the closest phenotypic resemblance to the *in vivo* BBB cells (de Boer et al. 1999) unlike *in vitro* BBB models which employ cells from continuous cell lines that are often hindered by their insufficient barrier properties (Gumbleton et al. 2001; Reichel et al. 2003). The PBECs have been extensively characterised (Chapter 3) to confirm physiologically realistic cell architecture, the formation of tight junction protein complexes, a restrictive paracellular pathway, functional expression of efflux transporters and BBB-associated marker enzymes.

The findings of the present study are consistent with previous studies demonstrating a strong relationships between *in vitro* BBB permeability using a primary porcine BBB model and rat *in situ* permeability (Zhang et al. 2006). Additionally, primary bovine *in vitro* BBB models have also shown good correlations with *in vivo* permeability (Cecchelli et al. 1999). Hence, the porcine *in vitro* BBB model utilised in this thesis appears to be a valid model for predicting *in vivo* BBB permeability.

A poor correlation was observed with hCMEC/D3 and MDR1-MDCKII *in vitro* BBB model permeabilities and rat *in situ* permeability in this thesis. However, in contrast, a previous study reported a strong correlation (r=0.938) between *in vitro* permeability and rat *in situ* brain perfusion (Weksler et al. 2005). These studies were performed with different test drugs to those in this study. Furthermore, previous studies comparing *in vitro* permeability

using the MDR1-MDCKII model and *in vivo* mouse data did not show a strong relationship (Garberg et al. 2005) in agreement with *in vitro-in vivo* correlations in this thesis using the MDR1-MDCKII *in vitro* BBB model.

The *in vitro* BBB models employed in these studies demonstrated differences in terms of Lucifer yellow permeabilities and TER values as well as P-gp efflux function, suggesting that they would demonstrate differences regarding test drug permeabilities. Transport studies across each of the *in vitro* BBB models confirmed differences in model permeability function. This showed that the comparison of data between *in vitro* BBB models was not possible and highlighted the importance of an *in vitro* BBB model to be able to accurately predict *in vivo* BBB permeability. The *in vitro* porcine BBB model exact permeabilities demonstrated a strong relationship with rat *in situ* permeability suggesting the potential of this model to predict *in vivo* BBB permeability.

Chapter 5
Species Comparison of Nonspecific Drug Binding in Blood and Brain tissue

5.0 Chapter 5: Species comparison of nonspecific drug binding in blood and brain tissue

5.1 Background

This chapter focuses on determining the fraction of drug unbound in rat, dog, pig and human blood (fu_{blood}) and the fraction of drug unbound in rat, dog and pig brain (fu_{brain}), as currently there is limited understanding of the relationship of fu_{blood} and fu_{brain} across species (Summerfield et al. 2008; Read et al. 2010) and hence the utility of interspecies extrapolation.

The brain to blood partition coefficient (K_p Equation 5.1) is the most widely documented *in vivo* measure of the extent of brain penetration (Kalvass et al. 2002; Summerfield et al. 2006; Kalvass et al. 2007; Summerfield et al. 2007). The brain to blood partition coefficient (K_p) represents a combination of all processes that govern CNS brain penetration, BBB permeability, active influx and efflux mechanisms and drug binding in blood and brain tissue. However, more recently the unbound brain to blood partition coefficient ($K_{p,uu}$, Equation 5.2 and 5.3) has been introduced as a measure of the extent of brain penetration (Gupta et al. 2006) which also accounts for drug binding in blood and brain tissue.

Extrapolating preclinical data to predict clinical outcomes in humans has become a key component of modern drug discovery. A greater understanding of differences in drug binding in blood and brain tissue across species could lead to more accurate predictions of drug binding in humans and consequently aid predictions of the extent of drug penetration and improve understanding of differences in the extent of drug penetration across species.

The specific aims of the work in this chapter were to investigate species differences in fu_{blood} and fu_{brain} and measures of the extent of brain penetration and investigate the prediction of CNS drug penetration *in vivo* using *in vitro* parameters.

$$K_p = \frac{AUC_{brain}}{AUC_{blood}}$$ Equation 5.1

Where AUC_{brain} is the area under the concentration-time curve for total (bound and unbound) concentration in brain tissue and AUC_{blood} is the area under the concentration-time curve for total (bound and unbound) concentration in blood.

$$K_{p,uu} = \frac{AUC_{u,brain}}{AUC_{u,blood}}$$ Equation 5.2

Where $AUC_{u,brain}$ is the area under the concentration-time curve for unbound concentration in brain tissue and $AUC_{u,blood}$ is the area under the concentration-time curve for unbound concentration in blood.

$$K_{p,uu} = K_p \times \frac{fu_{brain}}{fu_{blood}}$$ Equation 5.3

Where K_p is the total brain to blood concentration ratio, fu_{brain} is the fraction unbound in brain tissue and fu_{blood} is the fraction unbound in blood.

5.2 Results

5.2.1 Nonspecific drug binding-preliminary studies

Nonspecific drug binding studies using pig and human blood and, pig brain tissue were conducted at the University of Manchester (Manchester, UK) for 12 centrally acting test drugs. Nonspecific drug binding studies using dog blood and brain tissue were conducted at GSK (New Frontiers Science Park, Harlow, Essex, UK) for the same 12 test drugs. Nonspecific drug binding studies using rat blood and brain tissue, for all 12 test drugs, were conducted at both the University of Manchester and GSK. The fraction of drug unbound in rat blood and rat brain tissue for all 12 test drugs was shown to be comparable between sites with no significant differences observed (Appendix 6). Therefore, interlaboratory variation was not considered to be an issue during these studies.

5.2.2 Species comparison of nonspecific drug binding in blood and brain tissue

Equilibrium dialysis is a technique that enables nonspecific drug binding in blood and brain tissue to be examined in isolation of the BBB. A greater understanding of how fu_{blood} and fu_{brain} varies across species could be used to understand and potentially predict human drug binding *in vivo*. *In vitro* drug binding of a set of 12 centrally acting test drugs was measured and compared across rat, dog, pig and human blood and rat, dog and pig brain tissue, using equilibrium dialysis, in order to investigate differences in fu_{blood} and fu_{brain} across species.

Table 5.1 Species comparison of unbound drug fraction in blood and brain tissue for twelve centrally acting test drugs

	Rat		Dog		Pig		Human	
Test drug	**fu_{blood}**	**fu_{brain}**	**fu_{blood}**	**fu_{brain}**	**fu_{blood}**	**fu_{brain}**	**fu_{blood}**	**fu_{brain}**
Amprenavir	0.164±0.027	0.186±0.046	0.206±0.040	0.157±0.040	0.192±0.055	0.166±0.035	0.080±0.018	
Carbamazepine	0.340±0.146	0.257±0.117	0.238±0.016	0.187±0.020	0.211±0.058	0.182±0.075	0.178±0.064	
Chlorpromazine	0.024±0.008	0.002±0.001	0.020±0.004	0.004±0.0004	0.018±0.007	0.002±0.001	0.016±0.003	
Citalopram	0.251±0.040	0.066±0.014	0.250±0.047	0.080±0.014	0.184±0.057	0.052±0.009	0.207±0.049	
Clozapine	0.119±0.075	0.014±0.004	0.073±0.015	0.014±0.003	0.044±0.016	0.014±0.004	0.043±0.005	
Donepezil	0.215±0.054	0.143±0.038	0.265±0.036	0.145±0.018	0.284±0.077	0.117±0.059	0.129±0.037	
Haloperidol	0.099±0.025	0.018±0.004	0.129±0.017	0.027±0.003	0.069±0.015	0.036±0.023	0.099±0.042	0.023±0.002*
Mesoridazine	0.195±0.048	0.041±0.015	0.146±0.010	0.039±0.006	0.122±0.055	0.029±0.008	0.059±0.015	
Primidone	0.690±0.129	0.634±0.044	0.500±0.110	0.489±0.157	0.641±0.244	0.447±0.285	0.673±0.139	0.733±0.171*
Quetiapine	0.132±0.031	0.047±0.006	0.159±0.012	0.052±0.012	0.142±0.046	0.031±0.009	0.079±0.014	
Risperidone	0.164±0.044	0.133±0.049	0.194±0.023	0.124±0.023	0.148±0.042	0.119±0.034	0.162±0.043	
Ziprasidone	0.015±0.002	0.017±0.006	0.054±0.020	0.032±0.024	0.027±0.010	0.016±0.005	0.019±0.007	

Data are expressed as mean ± standard deviation of 6 replicates, n= at least 3 independent experiments.
* (Summerfield et al. 2008)

The fu_{blood} of rat, dog, pig and human and fu_{brain} of rat, dog and pig were successfully determined for all 12 test drugs using equilibrium dialysis (Table 5.1). It was not possible to obtain fu_{brain} values for human tissue because of difficulties in obtaining human brain tissue so, where available, literature values have been used.

The fu_{brain} values for all species spanned over a larger range (rat 317-fold difference, dog 122-fold difference and pig 224-fold difference) than the fu_{blood} values (rat 46-fold difference, dog 25-fold difference and pig 36-fold difference).

5.2.2.1 Nonspecific drug binding across species –linear regression analysis

Figure 5.1 Species comparison of fu_{brain} in rat, dog and pig

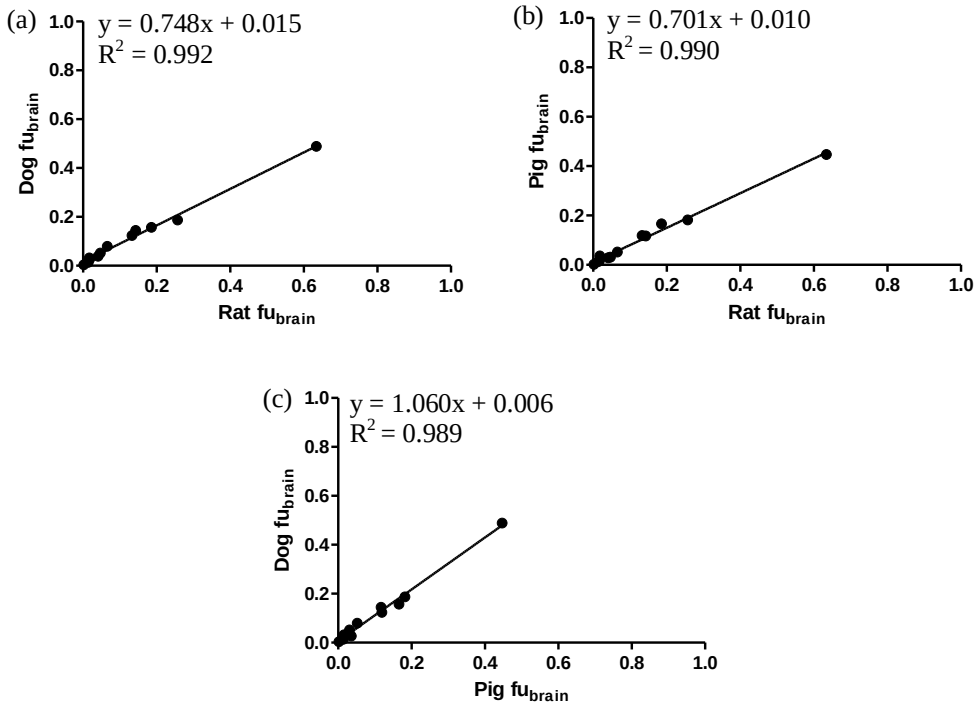

The fu_{brain} of rat, dog and pig was determined by equilibrium dialysis for amprenavir, carbamazepine, chlorpromazine, citalopram, clozapine, donepezil, haloperidol, mesoridazine, primidone, quetiapine, risperidone and ziprasidone, (a) comparison of rat fu_{brain} and dog fu_{brain}, (b) comparison of rat fu_{brain} and pig fu_{brain} and (c) comparison of pig fu_{brain} and dog fu_{brain}. Data are expressed as mean ± standard deviation of 6 replicates, n = at least 3 independent experiments.

Figure 5.2 Species comparison of fu_{blood} in rat, dog, pig and human

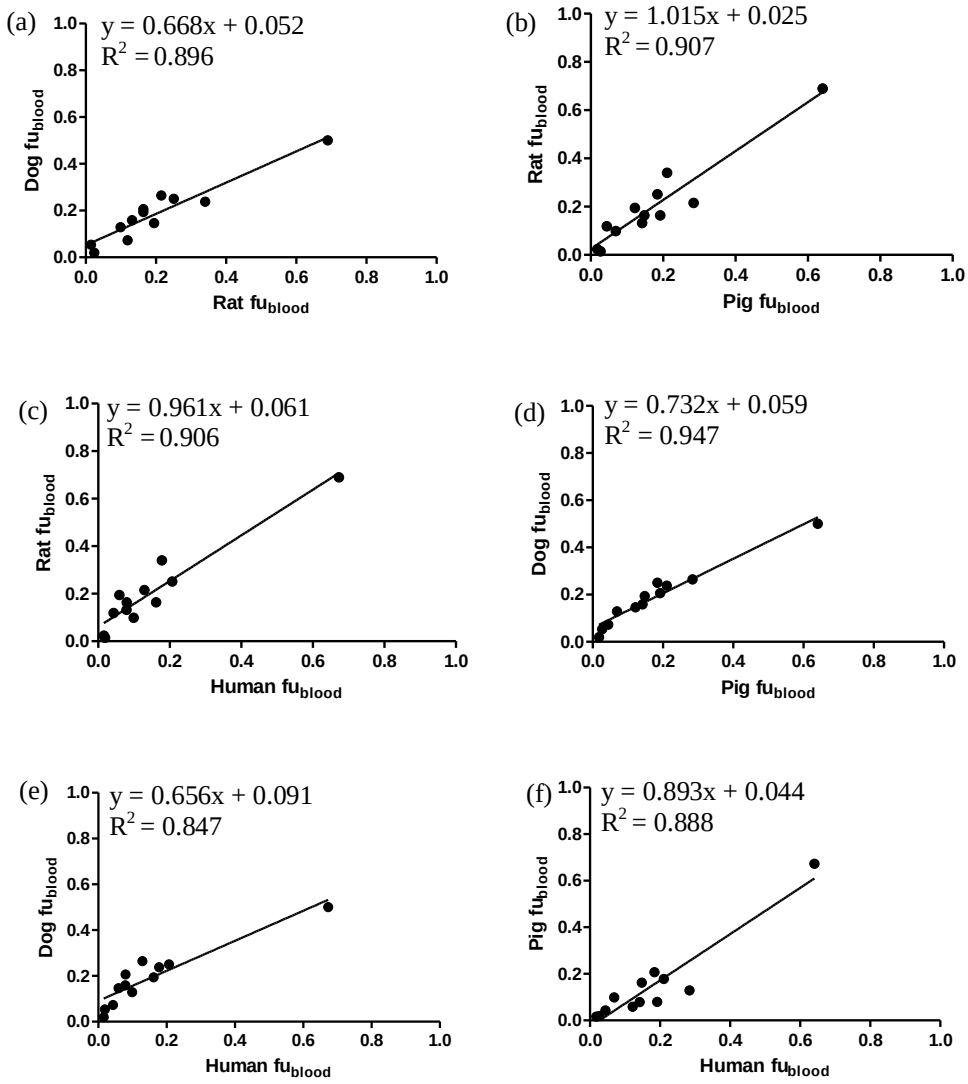

The fu_{blood} of rat, dog, pig and human was determined by equilibrium dialysis for amprenavir, carbamazepine, chlorpromazine, citalopram, clozapine, donepezil, haloperidol, mesoridazine, primidone, quetiapine, risperidone and ziprasidone, (a) comparison of rat fu_{blood} and dog fu_{blood}, (b) comparison of pig fu_{blood} and rat fu_{blood}, (c) comparison of human fu_{blood} and rat fu_{blood}, (d) comparison of pig fu_{blood} and dog fu_{blood}, (e) comparison of human fu_{blood} and dog fu_{blood} and (f) comparison of human fu_{blood} and pig fu_{blood}. Data are expressed as mean ± standard deviation of 6 replicates, n = at least 3 independent experiments.

Table 5.2 **Summary of linear regression analysis of fu_{brain} across species**

fu_{brain} comparison	R^2	Slope	y-intercept
Rat vs dog	0.992	0.748	0.015
Rat vs pig	0.990	0.701	0.010
Pig vs dog	0.989	1.060	0.006

Comparison of correlation, slope and y-intercept from linear regression analysis of fu_{brain} comparisons across rat, dog and pig.

Table 5.3 **Summary of linear regression analysis of fu_{blood} across species**

fu_{blood} comparison	R^2	Slope	y-intercept
Rat vs dog	0.896	0.668	0.052
Rat vs pig	0.907	1.015	0.025
Human vs rat	0.906	0.961	0.061
Pig vs dog	0.947	0.732	0.059
Human vs dog	0.847	0.656	0.091
Human vs pig	0.888	0.893	0.044

Comparison of correlation, slope and y-intercept from linear regression analysis of fu_{blood} comparisons across rat, dog, pig and human.

When, comparing fu_{brain} of the test drugs across species (Figure 5.1) a strong correlation was observed between all species. The strongest correlation was noted between rat and dog brain ($R^2 = 0.992$) (Figure 5.1 (a)), whilst the correlation coefficients for rat and pig brain (Figure 5.1 (b)) and pig and dog brain (Figure 5.1 (c)) were $R^2 = 0.990$ and $R^2 = 0.989$ respectively.

When comparing drug fu_{blood} across species the correlations, although strong, were not as strong as the correlations observed for fu_{brain} with the same 12 test drugs and more scatter of the points was observed compared to the correlations for fu_{brain}. Regarding human fu_{blood}, the strongest correlation was observed with rat fu_{blood}, $R^2 = 0.906$ (Figure 5.2(c)), whilst the correlation coefficients for fu_{blood} human and pig and fu_{blood} human and dog were $R^2 = 0.888$ (Figure 5.2 (f)) and $R^2 = 0.847$ (Figure 5.2 (e)) respectively. The strongest fu_{blood} correlation was observed between pig and dog, with a correlation coefficient of $R^2 = 0.947$ (Figure 5.2 (d)).

For fu_{brain} comparisons across species, the slopes of the regression lines ranged from 0.701 to 1.060 (Table 5.2) compared to 0.668-1.015 (Table 5.3) for fu_{blood} comparisons across species suggesting close agreement of both fu_{brain} and fu_{blood} across species. The y-intercepts of the regression lines for fu_{brain} (0.006 to 0.015) were closer to zero than those for fu_{blood} (0.025-0.095). These findings suggest that although, similarities between fu_{blood} across species have been shown drug, fu_{brain} is more consistent across species (rat, dog and pig) than fu_{blood}.

5.2.2.2 Nonspecific drug binding across species –Spearman's rank correlation

The rank order of fu_{blood} and fu_{brain} for the test drugs was investigated across species in order to identify trends in the data. The fu_{blood} (Table 5. 6) and fu_{brain} (Table 5.4) values for the test drugs for each species were ranked from 1 to 12, with 1 being the largest fu_{blood} or fu_{brain} value and 12 being the smallest. A Spearman's rank correlation coefficient was also calculated for each of the fu_{blood} (Table 5.7) and fu_{brain} (Table 5.5) comparisons.

Table 5.4 Rank order of fu_{brain} across rat, dog and pig

Rank	Rat		Dog		Pig	
order	Test drug	fu_{brain}	Test drug	fu_{brain}	Test drug	fu_{brain}
1	Primidone	0.634	Primidone	0.489	Primidone	0.447
2	Carbamazepine	0.257	Carbamazepine	0.187	Carbamazepine	0.182
3	Amprenavir	0.186	Amprenavir	0.157	Amprenavir	0.166
4	Donepezil	0.143	Donepezil	0.145	Risperidone	0.119
5	Risperidone	0.133	Risperidone	0.124	Donepezil	0.117
6	Citalopram	0.066	Citalopram	0.080	Citalopram	0.052
7	Quetiapine	0.047	Quetiapine	0.052	Haloperidol	0.036
8	Mesoridazine	0.041	Mesoridazine	0.039	Quetiapine	0.031
9	Haloperidol	0.018	Ziprasidone	0.032	Mesoridazine	0.029
10	Ziprasidone	0.017	Haloperidol	0.027	Ziprasidone	0.016
11	Clozapine	0.014	Clozapine	0.014	Clozapine	0.014
12	Chlorpromazine	0.002	Chlorpromazine	0.004	Chlorpromazine	0.002

Table 5.5 Spearman's rank correlation for fu_{brain} across rat, dog and pig

fu_{brain} comparison	Spearman r	P value
Rat vs dog	0.993	P<0.0001
Rat vs pig	0.972	P<0.0001
Pig vs dog	0.951	P<0.0001

The rank order of fu_{brain} for the 12 test drugs across rat, dog and pig was shown to be similar across all species (Spearman r, 0.951-0.993) (Table 5.5). The closest rank orders were observed between rat and dog (r=0.993), followed by rat and pig (r=0.972) and the rank orders that showed the largest difference were observed between pig and dog (r=0.951). All comparisons were shown to be statistically significant with P<0.0001.

When looking at fu_{brain} in terms of which species had the largest or smallest values, for carbamazepine, mesoridazine, and risperidone fu_{brain} pig<dog<rat and for primidone pig<dog<rat<human. For citalopram, donepezil, quetiapine and ziprasidone fu_{brain} pig<rat<dog. For, chlorpromazine pig=rat<dog and for clozapine pig=dog=rat. These trends suggest that in general pig fu_{brain} was smaller or the same compared to rat and dog fu_{brain}. Outliers were thought to be amprenavir where dog<pig<rat (although amprenavir was in the

same rank order across species) and haloperidol where rat<human<dog<pig (haloperidol had a different rank order in pig compared to rat and dog).

Table 5.6 Rank order of fu_{blood} across rat, dog, pig and human

Rank	Rat		Dog		Pig		Human	
order	Test drug	fu_{blood}	Test drug	fu_{blood}	Test drug	fu_{blood}	Test drug	fu_{blood}
1	Primidone	0.690	Primidone	0.500	Primidone	0.641	Primidone	0.673
2	Carbamazepine	0.340	Donepezil	0.265	Donepezil	0.284	Citalopram	0.207
3	Citalopram	0.251	Citalopram	0.250	Carbamazepine	0.211	Carbamazepine	0.178
4	Donepezil	0.215	Carbamazepine	0.238	Amprenavir	0.192	Risperidone	0.162
5	Mesoridazine	0.195	Amprenavir	0.206	Citalopram	0.184	Donepezil	0.129
6	Risperidone	0.164	Risperidone	0.194	Risperidone	0.148	Haloperidol	0.099
7	Amprenavir	0.164	Quetiapine	0.159	Quetiapine	0.142	Amprenavir	0.080
8	Quetiapine	0.132	Mesoridazine	0.146	Mesoridazine	0.122	Quetiapine	0.079
9	Clozapine	0.119	Haloperidol	0.129	Haloperidol	0.069	Mesoridazine	0.059
10	Haloperidol	0.099	Clozapine	0.073	Clozapine	0.044	Clozapine	0.043
11	Chlorpromazine	0.024	Ziprasidone	0.054	Ziprasidone	0.027	Ziprasidone	0.019
12	Ziprasidone	0.015	Chlorpromazine	0.020	Chlorpromazine	0.018	Chlorpromazine	0.016

Table 5.7 Spearman's rank correlation for fu_{blood} across rat, dog and pig

fu_{blood} comparison	Spearman r
Rat vs dog	0.914
Rat vs pig	0.897
Human vs rat	0.844
Pig vs dog	0.979
Human vs dog	0.895
Human vs pig	0.853

The rank order of fu_{blood} across rat, dog, pig and human was shown to be similar (Table 5.6), Spearman's rank correlation (r) ranged from 0.844 to 0.979 (Table 5.7) However, rat, dog and pig comparisons not as similar as those observed with fu_{brain} (Table 5.4) (fu_{blood} Spearman's r ranged from 0.891-0.979 and fu_{brain} ranged from 0.951-0.993). Regarding human fu_{blood} the closest rank orders were observed between human and dog (r=0.895), followed by

human and pig (r=0.853) and then human and rat (r=0.844). All comparisons were to shown to be statistically significant with P ranging from < 0.0001 to <0.001.

When looking at fu_{blood} in terms of which species had the largest or smallest values, trends in the data were less obvious than for fu_{brain}. For carbamazepine, chlorpromazine, clozapine and mesoridazine fu_{blood} human<pig<dog<rat, for amprenavir and quetiapine human<rat<pig<dog, for risperidone pig<human<rat<dog and haloperidol pig<human=rat<dog, for citalopram pig<human<dog<rat, for donepezil human<rat<dog<pig and for ziprasidone rat<human<pig<dog. Primidone was thought to be an outlier where dog<pig<human<rat because it exhibited the only rank order where dog had the smallest fu_{blood} value and human was the third smallest fu_{blood} value.

Where comparing fu_{blood} to fu_{brain} values there were only 3 cases where $fu_{blood} < fu_{brain}$ which were in rat for amprenavir and ziprasidone and human for primidone. For dog and pig $fu_{blood} > fu_{brain}$ for all 12 test drugs.

5.2.2.3 Nonspecific drug binding in human brain

Due to difficulties in obtaining human brain tissue, where available, literature values for fu_{brain} have been used. The literature only documents fu_{brain} for 2 of the test drugs used in these studies, namely haloperidol and primidone. Hence linear regression analysis and Spearman's rank correlation could not be performed on these data. Fraction unbound in brain was compared across rat, dog, pig and human for haloperidol and primidone in order to investigate similarities between fu_{brain} human and the other species used in this study.

Figure 5.3 Species comparison of fu_{brain} for haloperidol

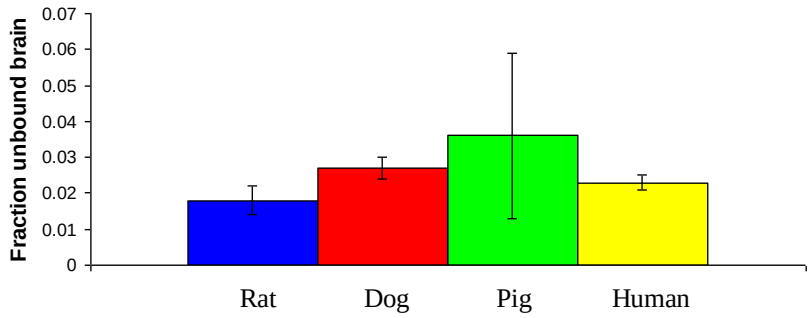

The fu_{brain} rat (blue), dog (red), pig (green) and yellow (human) were compared for haloperidol. Fraction unbound in brain for rat, dog and pig were determined by equilibrium dialysis, data are expressed as mean ± standard deviation of 6 replicates, n = at least 3 independent experiments. Fraction unbound in brain for human was obtained from the literature (Table 5.1).

Figure 5.4 Species comparison of fu_{brain} for primidone

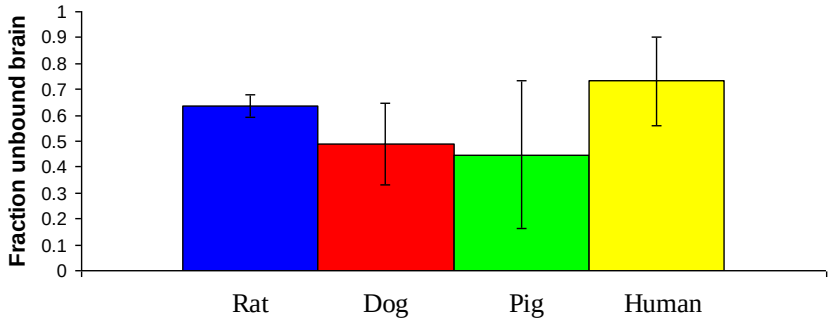

The fu_{brain} rat (blue), dog (red), pig (green) and yellow (human) were compared for primidone. Fraction unbound in brain for rat, dog and pig were determined by equilibrium dialysis, data are expressed as mean ± standard deviation of 6 replicates, n = at least 3 independent experiments. Fraction unbound in brain for human was obtained from the literature (Table 5.1).

Fraction of drug unbound in brain was comparable across all species for both haloperidol (0.018-0.036, Figure 5.3) and primidone (0.447-0.733, Figure 5.4). For haloperidol dog fu_{brain} was closest to human fu_{brain} and for primidone rat fu_{brain} was closest to human fu_{brain}. Haloperidol fraction unbound was thought to be an outlier to trends in rank order of fu_{brain} across species observed in section 5.2.2.2. These data suggest that fu_{brain} could be

consistent across rat, dog, pig and human. However, more human brain equilibrium dialysis data are required to validate this suggestion.

5.2.3 Comparison between rat *in vitro* blood to brain fraction unbound ratio and *in vivo* brain to blood concentration ratio

Stemming from the free drug hypothesis, for compounds that passively diffuse across the BBB the *in vitro* blood to brain fraction unbound ratio can used to predict the *in vivo* brain to blood concentration ratio under steady state conditions.

As

$$C_{u,blood} = C_{u,brain} \qquad \text{Equation 5.4}$$

And

$$C_u = fu \ x \ C_{total} \qquad \text{Equation 5.5}$$

Therefore

$$fu_{blood} \ x \ C_{blood} = fu_{brain} \ x \ C_{brain} \qquad \text{Equation 5.6}$$

And

$$\frac{C_{brain}}{C_{blood}} = \frac{fu_{blood}}{fu_{brain}} \qquad \text{Equation 5.7}$$

Where, C_u is the unbound concentration, C_{total} is the total concentration, $C_{u,blood}$ and $C_{u,brain}$ are the unbound concentration in blood and brain tissue respectively, C_{blood} and C_{brain} are the total concentration in blood and brain tissue respectively, fu is the fraction unbound, and fu_{blood} and fu_{brain} are the fractions unbound in blood and brain tissue respectively.

The relationship between the *in vitro* blood to brain faction unbound ratio (fu_{blood}:fu_{brain}, referred to as Kbb) was compared to the *in vivo* brain to blood concentration ratio (K_p) for rat, to investigate whether an *in vitro* parameter could be used to predict an *in vivo* measure of CNS penetration for the test drugs. Rat was the species chosen for this comparison because a more complete *in vivo* data set (for 11 of the 12 test drugs, no value available for amprenavir) was available for rat. The *in vivo* rat data are supplementary data,

provided by GSK (New Frontiers Science Park, Harlow, Essex, UK) and are the property of GSK.

Table 5.8 Comparison between rat *in vitro* Kbb and *in vivo* K_p

Test drug	Rat Kbb	Rat K_p	Fold difference
Amprenavir	0.88	-	-
Carbamazepine	1.32	1.39	1.0
Chlorpromazine	9.86	27.31	2.8
Citalopram	3.78	6.84	1.8
Clozapine	8.44	22.87	2.7
Donepezil	1.51	3.43	2.3
Haloperidol	5.48	16.79	**3.1**
Mesoridazine	4.80	1.04	**4.6**
Primidone	1.09	0.46	2.4
Quetiapine	2.78	4.00	1.4
Risperidone	1.23	0.29	**4.2**
Ziprasidone	0.84	1.51	1.8

Fraction unbound in rat blood and brain tissue were determined by equilibrium dialysis for amprenavir, carbamazepine, chlorpromazine, citalopram, clozapine, donepezil, haloperidol, mesoridazine, primidone, quetiapine, risperidone and ziprasidone (data are expressed as mean ± standard deviation of 6 replicates, n = at least 3 independent experiments) and used to calculate Kbb. Rat K_p data for carbamazepine, chlorpromazine, citalopram, clozapine, donepezil, haloperidol, mesoridazine, primidone, quetiapine, risperidone and ziprasidone are supplementary data, determined by GSK and are the property of GSK. The K_p value for amprenavir was not available from GSK.

Figure 5.5 **Relationship between rat *in vitro* Kbb and *in vivo* K_p**

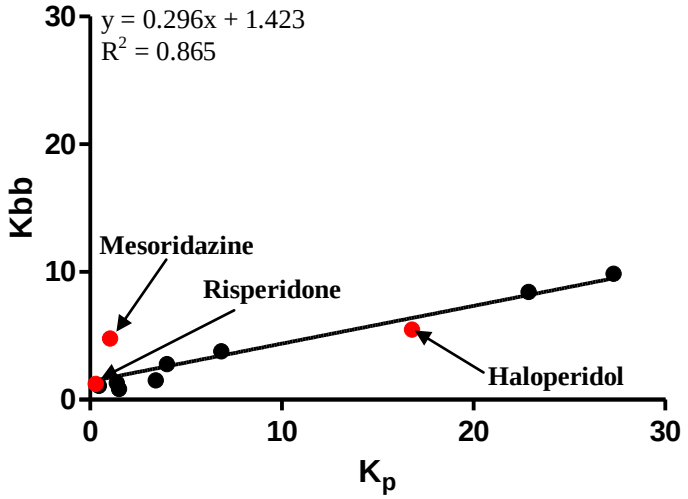

The relationship between rat Kbb and K_p for carbamazepine, chlorpromazine, citalopram, clozapine, donepezil, haloperidol, mesoridazine, quetiapine, risperidone and ziprasidone (Table 5.2). Brain to blood concentration ratio (K_p) was not available for amprenavir.

Figure 5.6 **Improved relationship between rat *in vitro* Kbb and *in vivo* K_p**

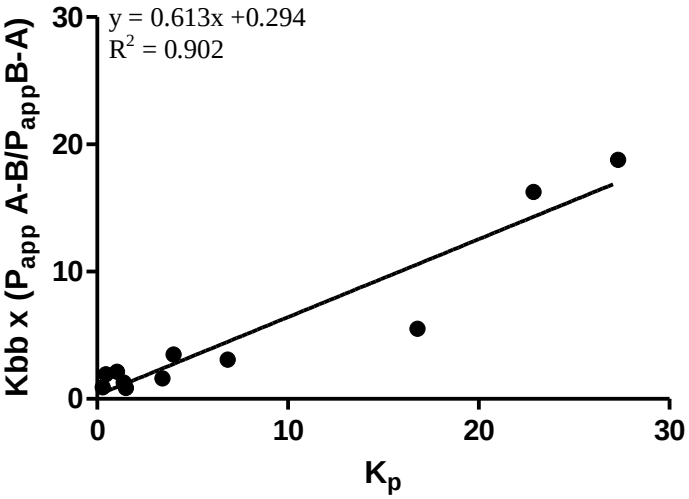

The relationship between rat Kbb and K_p for carbamazepine, chlorpromazine, citalopram, clozapine, donepezil, haloperidol, mesoridazine, quetiapine, risperidone and ziprasidone (Table 5.2). Brain to blood concentration ratio (K_p) was not available for amprenavir. was improved when efflux was incorporated into the prediction using data obtained from the MDR1-MDCKII *in vitro* BBB model Chapter 4.

A strong correlation using linear regression analysis was observed between rat *in vitro* Kbb and the *in vivo* measure of CNS penetration K_p, Figure 5.5 ($R^2 = 0.865$). The Kbb for 8 of

the 11 test drugs were within 3-fold of the K_p values (for individual test drug values see Table 5.8), suggesting a passive diffusion mechanism for these drugs across the BBB. Haloperidol, mesoridazine and risperidone were the only test drugs in the set where Kbb did not lie within 3-fold of K_p. The Kbb under predicted K_p for haloperidol suggesting an active influx mechanism across the BBB. *In vitro* Kbb over predicted *in vivo* K_p for both mesoridazine and risperidone suggesting active efflux mechanism across the BBB. The relationship between Kbb and K_p was improved (linear regression analysis) (R^2 = 0.985) when haloperidol, mesoridazine and risperidone were removed from the data set, data not shown.

Using Spearman's rank correlation, the correlation was also improved when haloperidol, mesoridazine and risperidone were removed from the data set, from r = 0.781 using all 11 test drugs in the analysis to r = 0.929 data not shown.

When the Kbb prediction of K_p incorporated efflux (using data obtained form the MDR1-MDCKII *in vitro* BBB model as a full data set was available) as apposed to Kbb alone the correlation was improved from R^2 = 0.865 (Figure 5.5) to R^2 = 0.902 (Figure 5.6). In addition, the gradient of the line was nearer to 1 (0.613) when the Kbb prediction incorporated efflux compared to Kbb alone (0.296) and the y intercept was also closer to zero (0.294 compared to 1.423 for Kbb alone).

5.2.4 Species comparison of *in vitro* Kbb for the prediction of *in vivo* K_p

The relationship between *in vitro* Kbb across rat, dog, pig and human (where values were available) and also the relationship between *in vitro* Kbb across rat, dog, pig and human and human K_p (values obtained from the literature, Table 5.9) was investigated to assess whether Kbb from any one species could be used as a predictor of human K_p. Human K_p values from the literature were only available for 5 of the test drugs.

Table 5.9 Rat, dog, pig and human *in vitro* Kbb and human *in vivo* K_p

Test drug	Rat Kbb	Dog Kbb	Pig Kbb	Human Kbb	Human K_p
Amprenavir	0.883	1.306	1.157		
Carbamazepine	1.324	1.271	1.159		1.100[a] 1.78[b]
Chlorpromazine	9.857	5.109	7.648		
Citalopram	3.782	3.126	3.508		1.320[c]
Clozapine	8.435	5.145	3.133		
Donepezil	1.505	1.824	2.420		
Haloperidol	5.476	4.784	1.916	4.304	10.000-30.000[d]
Mesoridazine	4.800	3.760	4.240		~ 2.500[e]
Primidone	1.088	1.023	1.433	0.918	0.870[f]
Quetiapine	2.784	3.050	4.624		
Risperidone	1.226	1.556	1.241		
Ziprasidone	0.837	1.714	1.667		

Rat, dog and pig Kbb was calculated from fu_{blood} and fu_{brain} determined by equilibrium dialysis (data are expressed as mean ± standard deviation of 6 replicates, n = at least 3 independent experiments) for amprenavir, carbamazepine, chlorpromazine, citalopram, clozapine, donepezil, haloperidol, mesoridazine, primidone, quetiapine, risperidone and ziprasidone. Human Kbb was calculated for haloperidol and primidone using fu_{blood} determined by equilibrium dialysis (data are expressed as mean ± standard deviation of 6 replicates, n = at least 3 independent experiments) and fu_{brain} from the literature. Human K_p values were reported in the literature for carbamazepine, citalopram, haloperidol, mesoridazine and primidone from post mortem data. Literature values for the remaining test drugs are currently unavailable.

[a](Morselli et al. 1977)
[b](Rambeck et al. 2006)
[c](Fu et al. 2000)
[d](Kornhuber et al. 1999)
[e](Svendsen et al. 1988), brain and plasma concentrations were from different subjects (Summerfield et al. 2008)
[f](Houghton et al. 1975) K_p was derived from linear regression analysis (Summerfield et al. 2008) original literature source quoted data as $1/K_p$.

Fraction unbound in blood and brain ratio (Kbb) was within 3-fold for all test drugs across rat, dog, pig and human (Table 5.9), although for some test drugs more variation between species was observed, for example, clozapine (highly variable) compared carbamazepine (very little variation).

Figure 5.7 Comparison of rat, dog, pig and human *in vitro* Kbb with human *in vivo* K_p

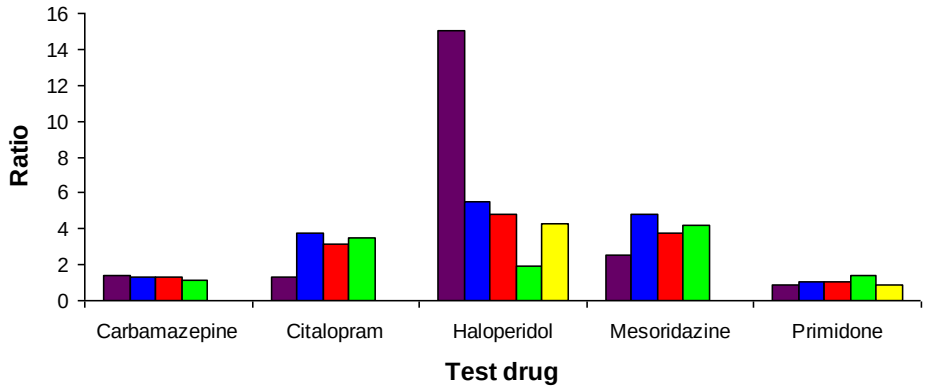

Comparison of human K_p (purple) from the literature with rat (blue), dog (red) and pig (green) Kbb for, carbamazepine, citalopram, haloperidol, mesoridazine and primidone and with human Kbb (yellow) for haloperidol and primidone (human Kbb values available only for these test drugs). Where more than one K_p value from the literature was available the mean K_p was used for comparisons.

Rat, dog, and pig Kbb was within 3-fold of human K_p for carbamazepine, citalopram and mesoridazine and rat, dog, pig and human (human values only available for haloperidol and primidone) Kbb was within 3-fold of human K_p for primidone (Figure 5.7). For haloperidol Kbb under predicted human K_p by more than 3-fold for all species including human (rat 3.1-fold, dog 3.1-fold, pig 7.8-fold, human 3.5-fold) (Figure 5.7) suggesting higher brain penetration than by passive diffusion and the possibility of an active influx mechanism (as suggested in section 5.2.3). No single species was shown to give a better prediction of human K_p for carbamazepine, citalopram, haloperidol, mesoridazine and primidone (test drugs where K_p values were available from the literature) compared to other species in the study.

5.2.5 Comparisons of *in vitro* predictions of human K_p

Studies in section 5.2.2 have shown that fu_{brain} is similar across rat, dog and pig for all 12 test drugs (and also similar in human for haloperidol and primidone). In order to investigate whether any one species in this study can be used to predict human K_p more accurately than the others, (for carbamazepine, citalopram, haloperidol, mesoridazine and primidone, the 5 test drugs where human K_p values were available from the literature) the ratio of fu_{blood} (human) to fu_{brain} of rat, dog and pig were compared to human K_p. The ratio of fu_{blood} human to fu_{brain} human for haloperidol and primidone was also compared to human K_p.

Figure 5.8 Comparisons of *in vitro* Kbb predictions of human *in vivo* K_p

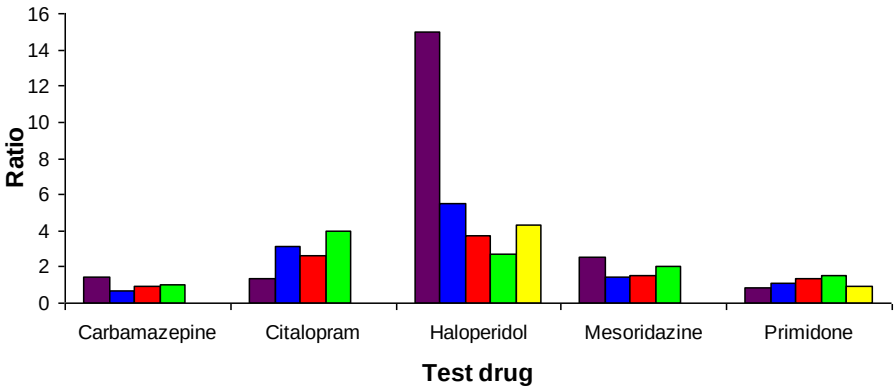

Human K_p obtained from the literature for carbamazepine, citalopram, haloperidol, mesoridazine and primidone was compared to the ratio of fu_{blood} (human) to fu_{brain} of rat (blue), dog (red), and pig (green) determined from equilibrium dialysis studies (data are expressed as mean ± standard deviation of 6 replicates, n = at least 3 independent experiments) and to the ratio of fu_{blood} (human) determined from equilibrium dialysis studies (data are expressed as mean ± standard deviation of 6 replicates, n = at least 3 independent experiments) to fu_{brain} of human from literature values (purple) for haloperidol and primidone. Where more than one K_p value from the literature was available the mean K_p was used for comparisons.

Predictions of human K_p using fu_{blood} human and fu_{brain} rat, dog, pig and human (i.e. Kbb) were within 3-fold of human K_p apart from the $fu_{blood,}$ human to fu_{brain}, (dog 4.1-fold, pig 5.5-fold and human 3.5-fold) for haloperidol (Figure 5.8) (also see section 5.2.3 and 5.2.4 relating to haloperidol). The results indicated that the use of fu_{blood} human instead of rat, dog or pig fu_{blood} and fu_{brain} (from the same species) to calculate Kbb did not improve the prediction of human $K_{p.}$ From these studies, use of human fu_{blood} in combination with either rat, dog or pig fu_{brain} yielded comparable predictions of the human K_p parameter.

Equilibrium dialysis is a valuable *in vitro* technique for the determination of fu_{blood} and fu_{brain}. Studies using equilibrium dialysis have shown fu_{brain} to be comparable across rat, dog and pig for the test drugs used in theses studies (section 5.2.2). This suggests that brain tissue from any of the species (rat, dog or pig) used in this study has the potential to be used as a surrogate for human brain. However, further validation using more test drugs in human brain tissue would help to confirm this.

5.2.6 Comparison of rat and human K_p

Human K_p values are available from the literature (Table 5.9) for 5 of the test drugs and were compared to rat K_p values to determine if any species differences in K_p were apparent between rat and human.

Figure 5.9 Comparison of rat and human K_p

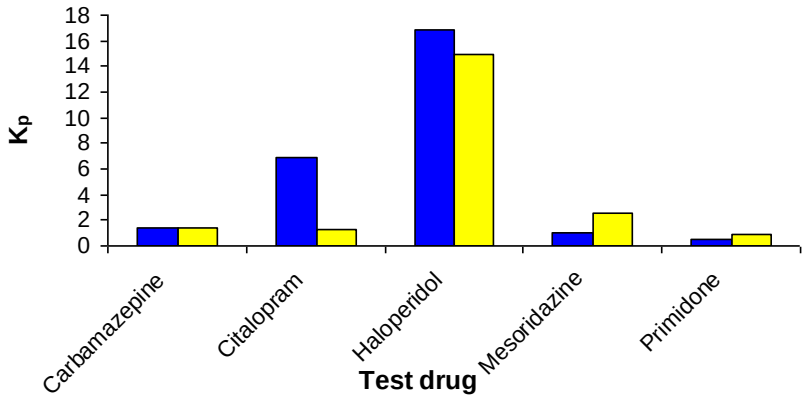

Rat (blue) K_p values for carbamazepine, citalopram, haloperidol, mesoridazine and primidone, (supplementary data, determined by GSK and are the property of GSK) were compared to human (yellow) K_p values obtained from the literature. Human K_p values were reported in the literature for carbamazepine, citalopram, haloperidol, mesoridazine and primidone. Literature values for the remaining test drugs are currently unavailable.

Rat and human K_p values were within 3-fold for carbamazepine, haloperidol, mesoridazine and primidone (Figure 5.9). For citalopram, rat and human K_p values were 5.2-fold apart suggesting a species difference between rat and human K_p, which was atypical when compared to the other 4 test drugs used in the comparison.

5.2.7 Comparison between measures of extent of drug brain penetration

Traditionally, K_p has been used as a measure of brain penetration, although more recently the use of K_p has been questioned. The brain to blood concentration ratio (K_p) is governed by drug permeability across the BBB, active influx and efflux mechanisms at the BBB and drug binding in blood and brain tissue. However, the ratio of unbound drug concentration in the brain to unbound drug concentration in the blood ($K_{p,uu}$) is independent of nonspecific drug binding in brain tissue and blood and is it now thought that $K_{p,uu}$ could be

better than K_p in assessing the extent of drug brain penetration, with a high $K_{p,uu}$ being most desirable (Liu et al. 2008; Hammarlund-Udenaes 2010).

$K_{p,uu}$ describes the effect of the BBB on drugs in terms of passive permeability and active transport processes (Gupta et al. 2006; Hammarlund-Udenaes et al. 2008; Reichel 2009). When $K_{p,uu}$ is close to unity passive diffusion across the BBB is assumed, when $K_{p,uu}<1$ active efflux at the BBB is assumed and when $K_{p,uu} > 1$ active influx at the BBB is assumed.

Rat K_p for 11 of the 12 test drugs (no rat K_p data was available for amprenavir) was compared to rat $K_{p,uu}$ which was calculated using rat K_p and rat fu_{blood} and fu_{brain} (Table 5.1 and Equation 5.3) determined from equilibrium dialysis to investigate the effect of nonspecific binding on K_p. Rat K_p are supplementary data, provided by GSK (Harlow Site, Essex, UK) and are the property of GSK.

Table 5.10 Comparison between rat K_p and $K_{p,uu}$ for a series of central nervous system targeted drugs

Test drug	Rat K_p	Rat $K_{p,uu}$	Fold-difference between K_p and $K_{p,uu}$
Carbamazepine	1.39	1.05	1.3
Chlorpromazine	27.31	2.77	9.9
Citalopram	6.84	1.81	3.8
Clozapine	22.87	2.71	8.4
Donepezil	3.43	2.28	1.5
Haloperidol	16.79	3.07	5.5
Mesoridazine	1.04	0.22	4.8
Primidone	0.46	0.42	1.1
Quetiapine	4.00	1.44	2.8
Risperidone	0.29	0.24	1.2
Ziprasidone	1.51	1.81	1.2

Rat K_p for carbamazepine, chlorpromazine, citalopram, clozapine, donepezil, haloperidol, mesoridazine, primidone, quetiapine, risperidone and ziprasidone, supplementary data, provided by GSK and the property of GSK was compared to $K_{p,uu}$ calculated using rat K_p and rat fu_{blood} and fu_{brain} determined by equilibrium dialysis Table 5.1.

Analogous to reports in the literature (Gupta et al. 2006; Hammarlund-Udenaes et al. 2008) the fold-difference between K_p values was found to be greater than the fold-difference between corresponding $K_{p,uu}$ values (94-fold and 13-fold respectively) for rat. The K_p values ranged from 0.29-27.31 whilst the $K_{p,uu}$ values ranged from 0.22-3.07 Table 5.10. The differences between K_p and $K_{p,uu}$ values for each test drug demonstrates the effect of

nonspecific drug binding on K_p and suggests that a high K_p may sometimes reflect a high degree of nonspecific binding to brain tissue, reducing the amount of free drug available to interact with receptors, and that $K_{p,uu}$ could be a better measure of the extent of drug brain penetration.

It was only possible to calculate human $K_{p,uu}$ values for 2 of the test drugs, namely haloperidol and primidone. The human $K_{p,uu}$ values for haloperidol and primidone were comparable to rat $K_{p,uu}$ values (haloperidol rat $K_{p,uu}$ = 3.07, human $K_{p,uu}$ = 3.48 and primidone rat $K_{p,uu}$ = 0.42, human $K_{p,uu}$ = 0.80).

5.2.8 Drug distribution in brain tissue

Drug distribution in the brain is predominantly dependent upon drug binding to brain tissue. Drug distribution can be described by the relationship between the total drug concentration in the brain and the unbound drug concentration in brain which is also known as the unbound volume of distribution in the brain ($V_{u,brain}$). As fu_{brain} has been shown to be consistent across rat, dog and pig for all test drugs and also across human for haloperidol and primidone (section 5.2.2) species differences would not be expected for this parameter. In addition other various brain properties have also been shown to be consistent across species (Stephan et al 1982).

However, $V_{u,brain}$ can instead can be used to give information on how a drug is distributed once it has entered the brain i.e. whether a drug is completely distributed in the interstitial fluid ($V_{u,brain}$ approximately 0.2 $ml.g^{-1}$) throughout the interstitial fluid and intercellular fluid ($V_{u,brain}$ approximately 0.8 $ml.g^{-1}$) or if the drug is in the main nonspecifically bound to brain tissue ($V_{u,brain}$ >0.8 $ml.g^{-1}$) (Hammarlund-Udenaes et al. 2008).

Drugs with similar $K_{p,uu}$ may show differences in distribution behaviour which becomes more relevant in terms of location of the target receptor and evoking a clinically significant response.

The unbound volume of distribution in the brain was calculated for all 12 test drugs across rat, dog, pig and human (for haloperidol and primidone) according to Equation 5.8 (Friden et al. 2007) in order to understand more about the distribution of the test drugs in the brain and to establish any species differences for the this parameter.

$$V_{u,brain} = 1 + D\left(\left(\frac{1}{fu(apparent)}\right) - 1\right) \qquad \text{Equation 5.8}$$

D = the dilution factor in diluted brain homogenate

$fu\ (apparent)$ = Measured unbound drug fraction in diluted brain homogenate

Table 5.11 **Unbound volume of distribution across rat, dog and pig for a series of central nervous system targeted drugs**

	$V_{u,brain}$ (ml.g^{-1})		
Test drug	**Rat**	**Dog**	**Pig**
Amprenavir	5.66±1.38	7.11±1.52	6.65±1.59
Carbamazepine	4.75±1.88	6.57±1.63	6.32±1.87
Chlorpromazine	535.52±106.34	348.45±45.20	633.58±142.87
Citalopram	21.20±2.17	16.25±3.11	21.96±5.70
Clozapine	94.10±27.28	97.75±16.04	96.99±24.57
Donepezil	8.49±2.00	8.22±1.21	8.94±2.87
Haloperidol	69.56±16.12	47.44±10.76	52.27±16.56
Mesoridazine	40.78±9.13	34.79±6.22	46.47±11.62
Primidone	0.78±0.15	1.85±0.78	2.53±1.64
Quetiapine	28.13±3.81	25.58±6.69	44.59±10.61
Risperidone	8.62±2.83	10.00±1.97	10.09±2.41
Ziprasidone	80.78±26.74	49.66±18.38	74.56±14.09

The unbound volume of distribution was calculated for all 12 test drugs across rat, dog and pig using $fu_{apparent}$ determined using equilibrium dialysis data are expressed as mean ± standard deviation of 6 replicates, n = at least 3 independent experiments.

The $V_{u,brain}$ values for the test drugs exhibited a large range of values across rat (0.78-535.52), dog (1.85-348.45) and pig (2.53-633.58) (Table 5.11). For 11 of the 12 test drugs $V_{u,brain} > 0.8$ ml.g^{-1} indicating that the test drugs were mainly nonspecifically bound to brain tissue and no species differences were observed for these test drugs. For primidone a species difference was observed where rat $V_{u,brain}$ (0.78) suggested that distribution of primidone was throughout the interstitial and intercellular fluid, whereas for dog and pig $V_{u,brain}$ (1.85, 2.53 respectively) suggested that primidone was mainly nonspecifically bound to brain tissue.

5.3 Discussion

Central nervous system drug penetration is governed by three main processes namely; BBB passive permeability, active transport processes at the BBB and relative drug binding between brain and blood.

To date, a key component in drug discovery programmes has been the use of *in vitro* BBB models to generate *in vitro* permeability and P-gp efflux measurements (Chapter 4) to predict the rate of CNS drug penetration. However, the relevance of determining the rate of penetration is debatable as most medication is administered under a regular dosing regimen and rapid rate of penetration may only be required when treating medical emergencies such as seizures and strokes or during anaesthesia.

The importance of determining fu_{blood} and fu_{brain} for the prediction of the extent of drug penetration in drug discovery programmes has more recently emerged. Due to ethical, practical and cost implications it was not possible to obtain human brain tissue for use in these studies, this is an obstacle faced by all researchers in this area of study. Hence, a surrogate animal species for use in this type of study in place of human brain tissue is highly desirable.

The focus of this chapter was to determine rat, dog, pig and human fu_{blood} and rat, dog and pig fu_{brain} in order to understand how drug fraction unbound varies across species and how this can be used to improve the prediction of human CNS drug penetration.

Nonspecific drug binding in blood and brain tissue for 12 centrally acting test drugs was examined using equilibrium dialysis. Fraction unbound in brain was found to be consistent across rat, dog and pig brain tissue (homogenate) for 10 of the 12 test drugs and rat, dog, pig and human brain tissue (homogenate) for the remaining 2 test drugs, where human fu_{brain} values were available from the literature (Summerfield et al. 2008). All vertebrate have a BBB which has been shown to be conserved across species (Cserr et al. 1984). It has been hypothosised that the protective nature of the BBB has resulted in conservation of morphology and composition of the brain across species (Summerfield et al. 2008). If brain composition is similar across species it is likely that nonspecific drug binding in the brain will also be consistent across species as demonstrated by data from these studies.

Since, commencing this work the literature has reported two other examples where fu_{brain} has been shown to be consistent across species, also using brain tissue homogenate.

The first example reports fu_{brain} to be consistent across rat, pig and human for 11 marketed drugs and 10 PET tracers (Summerfield et al. 2008) with correlation coefficients from linear regression analysis of $R^2 = 0.916$ for human vs rat and $R^2 = 0.929$ human vs pig.

The second example showed fu_{brain} to be consistent across mouse, rat, guinea pig, dog, pig, marmoset, cynomolgus monkey and human (Read et al. 2010) for 7 unnamed test compounds demonstrating a range of fu_{brain} values. The correlation coefficient R^2 (linear regression analysis) was not stated for all the comparisons, however, fu_{brain} in rat and human showed an excellent correlation ($R^2 = 0.98$).

From the work in this chapter and the data reported in the literature it could be suggested that fu_{brain} in any preclinical species could be used to predict fu_{brain} in humans. If this is the case then most fu_{brain} data to date that has been derived in rodents (Kalvass et al. 2002; Maurer et al. 2005; Summerfield et al. 2006; Summerfield et al. 2007) will still be of use to scientists. However, in terms of further research, the use of species with larger brains such as porcine (approximately 180 g compared to 2 g for rat, data not shown) could improve the throughput of the equilibrium dialysis technique.

The use of porcine tissue is more ethical, practical and cost effective than other preclinical species such as rodents and monkeys as it can be routinely obtained from abattoir after pigs are slaughtered for meat and where brain tissue would normally go to waste.

Fraction unbound in blood was shown to be similar across rat, dog, pig and human, although, not as similar as fu_{brain} across species. Differences in fu_{blood} across species may be explained by adaptation to environmental factors which would not affect the brain due to the protective nature of the BBB (Summerfield et al. 2008).

Variation in major drug binding plasma proteins albumin and $alpha_1$-acid glycoprotein levels has been documented across species. Albumin levels of 3.16 g.100 ml^{-1}, 2.63 g.100 ml^{-1}, 4.18 g.100 $ml^{-}1$ (Guarino et al. 1973) have been reported for rat, dog and human respectively and $alpha_1$-acid glycoprotein levels of 1.18 g.100 ml^{-1}, 0.37 g.100 ml^{-1} and 0.18 g.100 ml^{-1} (Guarino et al. 1973) have been reported for rat, dog and human respectively which may explain differences in nonspecific binding in blood across species.

Fraction unbound in blood of rat, pig and human has also been reported to show more variation across species compared to fu_{brain} (Summerfield et al. 2008). However, larger variation in fu_{blood} across species was documented (R^2 0.492-0.876) compared to this work (R^2

0.847-0.947) which may be attributed to differences in the compound sets chosen. The test drugs used in this work are all CNS active marketed drugs with similar physicochemical properties (Appendix 3), whereas, Summerfield et al. used a combination of marketed drugs (not all CNS active) and PET tracers.

In a recent study a species mismatch in fu_{blood} highlighted the effect of species differences on CNS brain penetration and efficacy (Summerfield et al. 2007). In rat, lower fu_{blood} and CNS brain penetration was reported compared to guinea pig which resulting in efficacy being observed only in guinea pig. The differences observed in efficacy were thought to be due lower fu_{blood} available to cross the BBB and also because nonspecific binding in blood was much greater than that in rat brain. Species difference in fu_{blood} is of less of a problem in drug discovery as human blood can be easily obtained and used for binding studies.

Fraction unbound in brain across species was shown to span a larger range than fu_{blood} which may be explained by the larger proportion of lipid in brain; weight fraction of 0.11 compared to 0.0065 in blood (Jeffrey et al. 2007) resulting in a higher degree of nonspecific binding in brain and the possibility of lower fu_{brain} values.

Fraction unbound in blood was greater than fu_{brain} for all test drugs in dog and pig and for rat with two exceptions (amprenavir and ziprasidone) and human for primidone. As all the test drugs in the study were marketed CNS active drugs $fu_{blood}>fu_{brain}$ may be a desirable property for CNS active drugs providing free drug in the blood to cross the BBB. Relative binding affinities in blood and brain may also be of importance for drugs with low fu_{blood} for example, chlorpromazine which has still been shown to penetrate (section 5.2.3 and 5.2.7) the brain and where binding in brain is greater than blood.

The rank order of the 12 test drugs in fu_{brain} across rat, dog and pig was shown to be similar across all species using Spearman's rank correlation. The rank order of fraction unbound in blood was also shown to be similar, although, not as similar as fu_{brain} which can be explained by a higher degree of conservation in brain across species compared to blood.

Pig fu_{brain} had the lowest values for 10 of the 12 test drugs compared to rat and dog. For fu_{blood} trends in the data were less obvious, although, in general human fu_{blood} was always the lowest or second lowest value across species apart from with primidone. The literature does not document any other studies that have looked at the rank order of test drug fu_{blood} and fu_{brain} across species.

The relationship between *in vitro* Kbb and *in vivo* K_p was investigated in order to determine whether an *in vitro* parameter could be used to predict an *in vivo* measure of the extent of brain penetration. Lack of human *in vivo* K_p data meant that this analysis was conducted using rat K_p data. The Kbb was considered predictive of K_p if the 2 values were within 3-fold of each other, 3-fold was chosen to remain consistent with similar work in the literature (Maurer et al. 2005; Summerfield et al. 2008) and to take into account experimental variation or actual differences of no significance.

For 8 of the 11 test drugs (no K_p data available for amprenavir) Kbb predicted K_p within 3-fold. This demonstrated that nonspecific binding in blood and brain tissue described as Kbb could be used to predict the extent of brain penetration for these 8 test drugs and suggested a passive diffusion mechanism across the BBB.

When haloperidol, mesoridazine and risperidone, the 3 test drugs where the Kbb did not lie within 3-fold of the K_p were removed from the data set, the correlation was improved. For haloperidol the Kbb under predicted the K_p suggesting an active influx mechanism across the BBB, which was consistent with reports in the literature (Ruiu et al. 2003).

For mesoridazine, Kbb over predicted *in vivo* K_p suggesting an active efflux mechanism at the BBB which was consistent with the literature, where a MDR1-MDCKII cell monolayer efflux assay had reported an efflux ratio of 87.1 (Summerfield et al. 2007).

For risperidone, the Kbb also over predicted K_p which was consistent with the literature where risperidone had been shown to be an efflux substrate in a MDR1-MDCKII cell monolayer assay (efflux ratio 20.8) (Summerfield et al. 2007) and in studies comparing K_p in wild type mice to K_p in *mdr1* knock out mice (Doran et al. 2005; Summerfield et al. 2006) (efflux ratio 10 and 21 respectively). Although, risperidone was not shown to be a P-gp efflux substrate in human MDR1-MDCKII or mouse Mdr1a-MDCK monolayer efflux assays documented in another study (Feng et al. 2008). It has also been noted in the literature that *in vitro* P-gp efflux data were not always consistent with *in vivo* mouse data (Doran et al. 2005).

The $K_{p,uu}$ values calculated in this work were also in agreement that haloperidol could be subject to active influx mechanisms at the BBB as the $K_{p,uu}$ >1. For mesoridazine and risperidone the $K_{p,uu}$ were both less than 1 suggesting active efflux at the BBB, which was also in agreement with Kbb over predicting K_p suggestive of active efflux mechanisms at the BBB for these test drugs. From transport studies, documented in Chapter 4 haloperidol was not

shown to be a substrate of an efflux transporter using any of the *in vitro* BBB models. However, mesoridazine was shown to be an efflux substrate in monolayer efflux assays using hCMEC/D3 cells and MDR1-MDCKII cells and risperidone was only shown to be an efflux substrate in monolayer efflux assays using the hCMEC/D3 *in vitro* BBB model.

To account for the influence of the BBB on test drug penetration the effect of efflux was incorporated into the Kbb prediction using the MDR1-MDCKII *in vitro* BBB model permeability data (only P_{app} was used for this analysis as no substantial differences between P_{app} and P_{exact} were observed Chapter 4).

When efflux was incorporated into Kbb (by multiplying Kbb by (P_{app} A-B/P_{app} B-A)) the prediction of K_p was improved. These studies have shown that Kbb, representing the extent of penetration into the brain, is an *in vitro* parameter that can be used to predict *in vivo* K_p for drugs that passively diffuse across the BBB. Further, combining the Kbb and efflux (by multiplying Kbb by (P_{app} A-B/P_{app} B-A)) to account for the effect of the BBB on drug penetration, in combination are two *in vitro* parameters that can be used to predict *in vivo* K_p for drugs that are subject to active transport mechanisms at the BBB.

These findings are consistent with reports in the literature for mice (Kalvass et al. 2002; Maurer et al. 2005) where Kbb has been shown to be predictive of K_p for test drugs that passively diffuse across the BBB including chlorpromazine, citalopram, clozapine and haloperidol (Maurer et al. 2005) and also for rat where Kbb and efflux ratio have been used to predict K_p for test compounds including the test drug risperidone. *In vitro* Kbb has also been shown to predict K_p for marketed CNS drugs and PET tracers that passively diffuse across the BBB in humans (Summerfield et al. 2008).

The Kbb for rat, dog, pig and human (where values were available) were compared to human K_p for the 5 test drugs where values were available from the literature in order to establish whether or not one species could give a better prediction of human K_p compared to the other species in the study. Human Kbb values were only available for haloperidol and primidone because of a lack of human fu_{brain} values and were calculated from fu_{blood} determined using equilibrium dialysis and human fu_{brain} documented in the literature (Summerfield et al. 2008).

The Kbb across species was shown to be within 3-fold of each other, which was to be expected because fu_{brain} has been shown to be consistent across species and fu_{blood} has shown

similarities across species for this set of test drugs. For rat, dog, pig and human (where available) Kbb was within 3-fold of human K_p for carbamazepine, citalopram, mesoridazine and primidone.

Haloperidol Kbb for all species under predicted human K_p by more than 3-fold suggesting the possibility of active influx mechanisms at the BBB in humans which is consistent with observations made in section 5.2.3 for rat and with $K_{p,uu}$ values for rat (section 5.2.7) and the literature. However, this observation was not consistent with the fold-differences between rat and human Kbb and human K_p documented in the literature (Summerfield et al. 2008) which were within 3-fold of each other.

The Kbb for citalopram and mesoridazine in rat, dog and pig were within 3-fold of human K_p, which was consistent with reports in the literature with rat and human Kbb and human K_p for both citalopram and mesoridazine (Summerfield et al. 2008). However, the Kbb for citalopram and mesoridazine in rat, dog and pig were greater than human K_p, also consistent with the literature for rat and human (Summerfield et al. 2008) which may suggest a very low propensity for active efflux which did not appreciably effect the predictions.

Additionally, this may show a species difference between rat and human in terms of active efflux at the BBB, as rat Kbb did not predict rat K_p for mesoridazine within 3-fold whereas rat, dog and pig Kbb for was within 3-fold of human K_p for mesoridazine.

There are conflicting reports in the literature regarding citalopram as an substrate of active efflux at the BBB (Doran et al. 2005) (Summerfield et al. 2007) as well as conflicting data from monolayer efflux assays (Chapter 4). Species differences in P-gp functionality between rat and human have been reported (Syvanen et al. 2009).

Blood to brain fraction unbound ratio (Kbb) for carbamazepine predicted human K_p for rat, dog and pig within 1.3-fold and Kbb for primidone predicted human K_p for rat, dog, pig and human within 1.7-fold suggesting passive diffusion mechanisms for these test drugs.

As human K_p values were available for only 5 of 12 test drugs it was not possible to establish whether one species gave a better prediction of human K_p compared to others species. However, as the Kbb values were within 3-fold of each other for all species for this test drug set it was unlikely that any significant differences between predictions would be observed.

As fu_{brain} has been shown to be consistent across species, it can be hypothesised that fu_{brain} values could be combined with human fu_{blood} to calculate Kbb in order to predict human K_p more accurately. Fraction unbound in brain from rat, dog, pig and human (where available) was combined with human fu_{blood} in order to establish whether the fu_{brain} values from one species can be used as a better prediction of human K_p compared to the other species. Kbb predictions for all test drugs were within 3-fold except for haloperidol. Haloperidol Kbb under predicted K_p in all species, as expected from previous reports in this thesis, that it could be subjected to active influx at the BBB (see above). Although, these Kbb predictions showed no improvement from Kbb predictions calculated from the same species, it is more accurate to combined human fu_{blood} with fu_{brain} from a preclinical species to make predictions of human K_p.

Rat and human K_p values were compared for the test drugs (carbamazepine, citalopram, haloperidol, mesoridazine and primidone) where human K_p values were available from the literature. A species mismatch was observed for citalopram only. Similarities have been shown (section 5.2.2) between rat and human fu_{blood} for citalopram and although no human fu_{brain} was available for citalopram similarities in rat, dog and pig fu_{brain} have been demonstrated (section 5.2.2). The differences between rat and human K_p could therefore be due to differences in transporter mechanism between the two species as previously mentioned. These results suggest that a rodent model may not always be representative of humans.

K_p describes the total concentration in brain relative to the total concentration in blood at steady state (Hammarlund-Udenaes et al. 2008). However, it is the unbound drug in blood that is able to cross the BBB and the unbound drug in brain that is pharmacologically active at the target site (Hammarlund-Udenaes 2010). A large K_p may just represent a large amount of nonspecific drug binding in brain tissue and hence drug that can not interact at the target site to evoke a response, explaining why K_p may be of limited use for predicting CNS drug effects (Hammarlund-Udenaes 2010) and the criticism that is emerging over the use of this parameter. However, $K_{p,uu}$ which describes the unbound concentration in brain relative to the unbound concentration in blood is independent of nonspecific binding in blood and brain tissue and is becoming increasingly accepted as a superior measure of brain penetration in drug discovery (Hammarlund-Udenaes et al. 2008).

When rat K_p was compared to $K_{p,uu,}$ the fold-difference between the K_p values was shown to be greater than the fold-difference between the $K_{p,uu}$ values and the $K_{p,uu}$ values for each test drug were less than the corresponding K_p values, demonstrating the effects of nonspecific drug binding on K_p. It was noted that test drugs with different K_p values, for example chlorpromazine (27.31) and clozapine (22.87), were shown to have similar $K_{p,uu}$ values 2.77 and 2.71 respectively. Using K_p as a measure of brain penetration for these test drugs would suggest that chlorpromazine exhibits a greater extent of brain penetration compared to clozapine, $K_{p,uu}$ would suggest a similar extent of brain penetration for both test drugs.

Routine determination of $K_{p,uu}$ in drug discovery programmes would offer several advantages. A high $K_{p,uu}$ is desirable when brain penetration is required, so knowledge of $K_{p,uu}$ could be useful for CNS drug discovery and also when CNS effects are undesirable when developing peripherally acting drugs.

Additionally, $K_{p,uu}$ can give quantitative information on transport processes at the BBB and quantitative information on the interaction potential of novel drugs at the BBB where a lower $K_{p,uu}$ indicates more potential for interaction (Hammarlund-Udenaes et al. 2008). A relationship between molecular structure and $K_{p,uu}$ in relation to hydrogen bonding has recently been described (Friden et al. 2009) which could also be used in the development of centrally and peripherally acting drugs. The addition of 2 hydrogen bond donors to centrally acting drugs was shown to reduce unbound brain exposure by 2-fold whereas adding 2 hydrogen bond donors to peripherally acting drugs with CNS side effects, decreased CNS side effects by reducing passive permeability and increasing the potential for interaction with efflux transporters at the BBB. Therefore it is beneficial for centrally acting drugs to have a low number of hydrogen bond donors which is exemplified using the test drugs in this study which are all centrally acting marketed drugs with a low number of hydrogen bond donors (range from 0-4).

Species differences in $K_{p,uu}$ still requires some investigation. From this work human $K_{p,uu}$ values were only available for 2 of the test drugs and were within 3-fold of rat $K_{p,uu}$ values. However, further validation with many more test drugs is required. Equilibrium dialysis is a useful technique for determining fu_{blood} and fu_{brain} to aid the predication of the extent of drug penetration. As human blood for determination of fu_{blood} can be easily obtained

and fu_{brain} has been shown to be consistent across species these parameters generated using equilibrium dialysis can be used to calculate $K_{p,uu}$ along with K_p (Equation 5.3). This would mean that the K_p parameter would not be entirely redundant. Further investigation into species differences is required to validate the abundance of rodent data available for use in this calculation.

Microdialysis is the only *in vivo* method to determine $K_{p,uu}$ but this method is limited in a drug discovery setting due to low throughput, high cost and poor recovery of lipophilic compounds (Liu et al. 2008). However, validation of $K_{p,uu}$ calculated using a combination of *in vivo* and *in vitro* parameters (fu_{blood} and fu_{brain} using equilibrium dialysis) (Ekblom et al. 1992) (Equation 5.3) means that this parameter is widely applicable in the drug discovery setting.

The distribution of test drugs in the brain described as the relationship between total and unbound drug concentration in the brain ($V_{u,brain}$) was calculated in order to understand more about the distribution of the test drugs in the brain using an *in vitro* parameter (fu_{brain}) and to establish any species differences in $V_{u,brain}$. For all 12 test drugs in dog and pig and, 11 of the 12 test drugs in rat $V_{u,brain} > 0.8$ $ml.g^{-1}$ suggesting that these test drugs were mainly nonspecifically bound to brain tissue. Whilst for primidone in rat $V_{u,brain}$ was close to the value of brain water volume (0.8 $ml.g^{-1}$) (Hammarlund-Udenaes et al. 2008) suggesting uniform distribution throughout the whole brain. Primidone also had the lowest $V_{u,brain}$ value in dog and pig which may be explained by primidone exhibiting the lowest lipophilicity out of the test drug set (Log D 0.4) and the highest fu_{brain} values.

As with any study there were several caveats associated with this work. The use of brain homogenate could be a potential caveat leading to an underestimation of fu_{brain} *in vitro* because homogenisation of brain tissue destroys cell membranes exposing intracellular binding sites. The brain homogenate technique has been validated with the brain slice technique (Becker et al. 2006) for determining fu_{brain}. However, the use of the brain slice technique is recommended for determining $V_{u,brain}$. This is because intracellular and extracellular concentrations of a drug may vary and the brain homogenate method can not distinguish between intracellular and extracellular drug distribution. When the brain slice method was compared to the brain homogenate method (Friden et al. 2007) $V_{u,brain}$ for 14 of the 15 compounds were within 3-fold of *in vivo* microdialysis for the brain slice method whilst for only 10 of the 15 compounds using the brain homogenate method.

Another drawback is the use data derived from post mortem because of the possibility of redistribution of drug in the tissue after death (Rodda et al. 2006).

Another limitation is, sourcing human fu_{brain} and K_p from the literature where there are not multiple sources of data for each test drug to make comparisons with and also methods of data collection may vary for each test drug.

During this work the importance of nonspecific binding in drug discovery has been highlighted and equilibrium dialysis has proven to be a useful *in vitro* technique for routinely determining fu_{blood} and fu_{brain}. Fraction unbound in brain has been shown to be comparable across species suggesting that species differences in brain penetration could be due to variation in fu_{blood} for drugs that cross the BBB by passive diffusion or species differences in transporter homology or affinity for drugs that are subject to active transport processes at the BBB (Baltes et al. 2007).

Fraction unbound in blood and fu_{brain} have been shown to be important parameters for predicting the extent of drug penetration in the CNS. For drugs that are thought to passively diffuse across the BBB fu_{blood} and fu_{brain} described as Kbb can be used to predict K_p. For drugs that are thought to be subjected to active transport processes at the BBB a combination of Kbb (to represent drug distribution into the brain) and efflux ratio (to account for the effect of the BBB on drug transport) can be used to describe K_p. The effect of nonspecific drug binding on K_p has been shown by the determination of $K_{p,uu}$, which is now thought to be a superior measure of the extent of brain penetration and can also provide information on transport processes at the BBB and interaction potential. Volume of distribution in the brain has been determined using fu_{brain} to provide information on drug distribution which could be used in drug discovery. Overall *in vitro* parameters have been shown to play a key role in the prediction of the extent of CNS drug penetration across species.

To further this work, more validation to establish if fu_{brain} across species is consistent with human fu_{brain} would be beneficial. Investigation of species differences in K_p would also be useful in order to use K_p in human $K_{p,uu}$ calculations. Further work to investigate species differences between active transport mechanisms at the BBB would help to improve *in vitro* predictions of the extent of *in vivo* drug brain penetration as rodent models may not always provide the best *in vitro* predictions.

Chapter 6
The Use of a Physiologically Based Pharmacokinetic Model of the Rat Central Nervous System to Predict Central Nervous System Drug Penetration

6.0 Chapter 6: The use of a physiologically based pharmacokinetic model of the rat central nervous system to predict central nervous system drug penetration

6.1 Background

Currently, there is a lack of effective drug treatments for diseases of the CNS. The prevalence of the majority of CNS diseases increases with age, for example dementia and Alzheimer's disease, which dramatically reduce quality of life. In a growing ageing population there is an urgent requirement for novel CNS active drugs. The formidable obstacle of the BBB, possessing tight junctions and efflux transporters, is an additional challenge to overcome when delivering drugs, to the brain. Consequently, the BBB contributes to higher attrition rates during development of novel CNS active drugs compared to rates in other therapeutic areas (Kola et al. 2004).

Poor success in CNS drug discovery may also be linked to uncertainty regarding how to interpret results from assays used in drug discovery programmes and the methods used to select novel drug candidates. The use of a physiologically based pharmacokinetic model (PBPK) of the CNS to accurately predict the extent of drug brain penetration in the early stages of drug discovery could be used to improve the selection of novel CNS active drugs without the need for complex, expensive and time consuming *in vivo* studies. For example, microdialysis to the quantify the extent of brain penetration, which tends to be conducted late in drug development, after considerable time, resources and expense have been invested

Work documented in Chapter 5 (section 5.2.3) has shown that *in vitro* Kbb can be used to predict an *in vivo* measure of the extent of brain penetration, namely K_p, where passive diffusion of test drugs across the BBB was assumed. However, more recently it has been suggested that $K_{p,uu}$ provides a better measure of the extent of brain penetration than K_p (Hammarlund-Udenaes et al. 2008).

The aim of this work was to use an in-house hybrid-PBPK rat CNS model (Appendix 7) developed and validated, using *in vivo* parameters, by Dr Raj Badhan (manuscript in preparation, Development of a Physiologically-Based Pharmacokinetic Model of the Rat Central nervous System) as a tool to predict rat *in vivo* $K_{p,uu}$ using *in vitro* input parameters, which could reduce the number of *in vivo* studies required in a drug discovery setting. The drug specific *in vitro* parameters used for the prediction of $K_{p,uu}$ were permeability measurements generated from transport studies (Chapter 4) and unbound drug fraction in blood and brain tissue generated by equilibrium dialysis (Chapter 5). Rat *in situ* permeability

(Summerfield et al. 2007) and knockout mouse data (Doran et al. 2005) were also used in simulations to make comparisons with predictions that used *in vitro* permeabilities.

6.2 Results

6.2.1 Drug-specific input parameters

Drug-specific input parameters (Table 6.1) for clearance (CL), volume of distribution (V_d) and fraction unbound in blood, brain tissue and CSF (fu_{CSF}) were used in all rat PBPK simulations.

Table 6.1 Drug-specific parameters used in all rat physiologically based pharmacokinetic central nervous system model simulations

Parameter	Unit	Chlorpromazine	Citalopram	Clozapine	Haloperidol	Risperidone
V_d	$ml.kg^{-1}$	29100[a]	24000[c]	7624[e]	9633[f]	1770[g]
CL	$ml.h^{-1}.kg^{-1}$	3660[b]	5550[d]	2549[e]	4984[f]	15240[g]
fu_{blood}	no unit	0.024	0.251	0.119	0.099	0.164
fu_{brain}	no unit	0.002	0.066	0.014	0.018	0.133

Rat volume of distribution (V_d) and clearance (CL) were obtained from the literature. Rat fu_{blood} and fu_{brain} were determined by equilibrium dialysis, data are expressed as mean of 6 replicates, n = at least 3 independent experiments. These values were used in all model simulations using chlorpromazine, citalopram, clozapine, haloperidol and risperidone.

[a] (Sawada et al. 1984)
[b] (Evans et al. 2006)
[c] (Poulin et al. 2002)
[d] (Fredricson Overo 1982)
[e] (Gershkovich et al.)
[f] (Cheng et al. 1992)
[g] (De Buck et al. 2007)

The permeability parameters were varied between simulations in order to investigate the effect of permeability (P_{app} and P_{exact}) generated from porcine (Table 6.2) and MDR1-MDCKII (Table 6.3) *in vitro* BBB models on predictions. In addition, permeability measurements, generated from rat *in situ* permeability studies with efflux measurements obtained from knock out mice studies, were employed in the hybrid-PBPK model (Table 6.4). Fraction unbound in cerebral spinal fluid was set at 1, due to low levels of drug binding protein in CSF (Shen et al. 2004), for all test drugs as it was not possible to determine this experimentally or obtain values from the literature.

Table 6.2 **Drug-specific permeability parameters used for physiologically based pharmacokinetic model simulations using the porcine *in vitro* blood-brain barrier model permeabilities**

In vitro BBB model	Parameter $ml.h^{-1}.kg^{-1}$	Chlorpromazine	Citalopram	Clozapine	Haloperidol	Risperidone
Porcine	PS_{bbb}	61	28	79	112	119
(P_{app})	PS_{cp}	607	281	791	1120	1190
	PSe_{bbb}	28	102	90	174	101
	PSe_{cp}	283	1021	901	1745	1006
Porcine	PS_{bbb}	85	70	107	106	140
(P_{exact})	PS_{cp}	847	699	1075	1063	1397
	PSe_{bbb}	28	117	93	110	120
	PSe_{cp}	275	1171	928	1095	1199

Drug-specific passive (PS_{bbb} and PS_{cp} $ml.h^{-1}.kg^{-1}$) and active (PSe_{bbb} and PSe_{cp} $ml.h^{-1}.kg^{-1}$) permeability parameters for chlorpromazine, citalopram, clozapine, haloperidol and risperidone calculated from apparent and exact permeabilities determined from transport studies using the porcine *in vitro* BBB model (chapter 4).

Table 6.3 **Drug-specific permeability parameters used for physiologically based pharmacokinetic model simulations using the MDR1-MDCKII *in vitro* blood-brain model permeabilities**

In vitro BBB model	Parameter $ml.h^{-1}.kg^{-1}$	Chlorpromazine	Citalopram	Clozapine	Haloperidol	Risperidone
MDR1-	PS_{bbb}	117	322	203	180	305
MDCKII	PS_{cp}	1174	3223	2033	1798	3049
(P_{app})	PSe_{bbb}	61	410	224	215	315
	PSe_{cp}	609	4102	2244	2145	3150
MDR1-	PS_{bbb}	219	370	263	249	331
MDCKII	PS_{cp}	2192	3705	2626	2493	3306
(P_{exact})	PSe_{bbb}	99	445	257	231	347
	PSe_{cp}	987	4452	2573	2308	3473

Drug-specific passive (PS_{bbb} and PS_{cp} $ml.h^{-1}.kg^{-1}$) and active (PSe_{bbb} and PSe_{cp} $ml.h^{-1}.kg^{-1}$) permeability parameters for chlorpromazine, citalopram, clozapine, haloperidol and risperidone calculated from apparent and exact permeabilities determined from transport studies using the MDR1-MDCKII *in vitro* BBB model (chapter 4).

Table 6.4 **Drug-specific permeability parameters used for physiologically based pharmacokinetic model simulations using rat *in situ* permeabilities**

Parameter	Unit	Chlorpromazine	Citalopram	Clozapine	Haloperidol	Risperidone
PS_{bbb}	$ml.h^{-1}.kg^{-1}$	322	72	279	207	104
PS_{cp}	$ml.h^{-1}.kg^{-1}$	3220	720	2790	2070	1040
Efflux ratio	$ml.h^{-1}.kg^{-1}$	1.3	1.9	0.95	1.4	10
PSe_{bbb}	$ml.h^{-1}.kg^{-1}$	419	136	265	290	1049
PSe_{cp}	$ml.h^{-1}.kg^{-1}$	4189	1362	2652	2900	10489

Drug-specific passive (PS_{bbb} and PS_{cp}) and active (PSe_{bbb} and PSe_{cp}) permeability parameters (calculated using passive permeabilities and efflux ratio from knockout mice (Doran et al. 2005) for chlorpromazine, citalopram, clozapine, haloperidol and risperidone using the rat *in situ* model (Summerfield et al. 2007). For clozapine an efflux ratio was not available from knockout mice, so an average efflux ratio determined from transport studies using MDR1-MDCKII and porcine *in vitro* BBB models was used.

6.2.2 Prediction of the extent of central nervous system drug penetration

The calculated $K_{p,uu}$ (Chapter 2, Equation 2.9 for details of calculation) were compared to the predicted $K_{p,uu}$ obtained from simulations using the rat hybrid-PBPK model with drug-specific permeability parameters from MDR1-MDCKII and porcine *in vitro* BBB models and rat *in situ* and knock out mice studies (Tables 6.1-6.4) detail the drug-specific permeability input parameters).

Figure 6.1 **Comparison of calculated and predicted $K_{p,uu}$ using drug-specific permeability parameters from porcine *in vitro* blood-brain barrier model permeabilities**

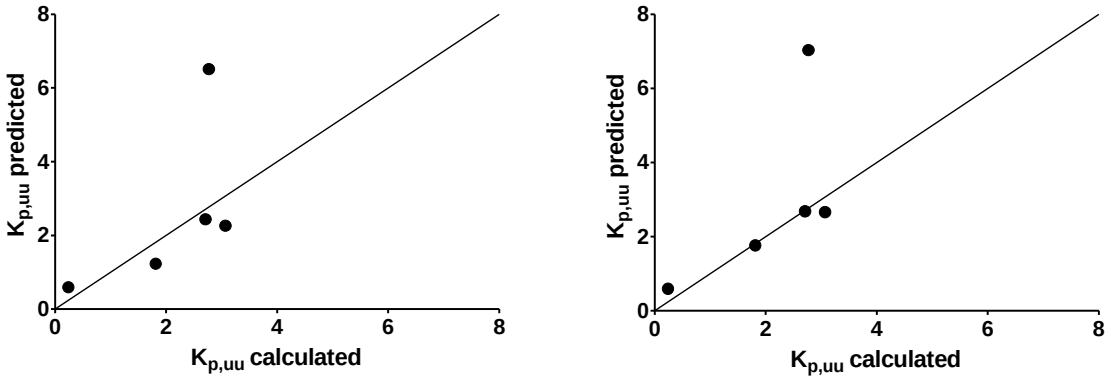

The calculated $K_{p,uu}$ were compared to the predicted $K_{p,uu}$ simulated by the rat hybrid-PBPK CNS model for chlorpromazine, citalopram, clozapine, haloperidol and risperidone using

permeability parameters (a) P_{app} and (b) P_{exact} from transport studies using the porcine *in vitro* BBB model. Solid line represents line of unity.

For simulations performed using drug-specific permeability parameters calculated from permeabilities (P_{app} and P_{exact}) obtained using the porcine *in vitro* BBB model, the predicted $K_{p,uu}$ was within 3-fold (for individual fold-differences see Table 6.5 and 6.6) of the calculated $K_{p,uu}$ for all 5 test drugs used in the simulations (chlorpromazine, citalopram, clozapine, haloperidol and risperidone) (Figure 6.1). Citalopram, clozapine and haloperidol provided excellent predictions using both P_{app} (within 1.5-fold of calculated) and P_{exact} (within 1.1-fold of calculated) permeability parameters. The greatest difference between predicted and calculated $K_{p,uu}$ was observed with risperidone (P_{app} and P_{exact} 3.0 fold-difference). No appreciable differences were observed in predicted $K_{p,uu}$ when either P_{app} and P_{exact} permeability parameters were used. This suggests that the rat CNS hybrid-PBPK model can accurately predict calculated $K_{p,uu}$ using *in vitro* permeability parameters from the porcine *in vitro* BBB model and *in vitro* drug binding data.

Table 6.5 **Predicted and calculated $K_{p,uu}$ using drug-specific apparent permeability parameters obtained using the porcine *in vitro* blood-brain barrier model permeabilities**

Test drug	Predicted $K_{p,uu}$	Calculated $K_{p,uu}$	Fold-difference
Chlorpromazine	6.5	2.8	2.3
Citalopram	1.2	1.8	1.5
Clozapine	2.4	2.7	1.1
Haloperidol	2.3	3.1	1.3
Risperidone	0.6	0.2	3.0

Table 6.6 **Predicted and calculated $K_{p,uu}$ values using drug-specific exact permeability parameters obtained using the porcine *in vitro* blood-brain barrier model permeabilities**

Test drug	Predicted $K_{p,uu}$	Calculated $K_{p,uu}$	Fold-difference
Chlorpromazine	7.0	2.8	2.5
Citalopram	1.8	1.8	1.0
Clozapine	2.7	2.7	1.0
Haloperidol	2.7	3.1	1.1
Risperidone	0.6	0.2	3.0

Figure 6.2 **Comparison of calculated and predicted $K_{p,uu}$ using drug-specific permeability parameters from the MDR1-MDCKII *in vitro* blood-brain barrier model permeabilities**

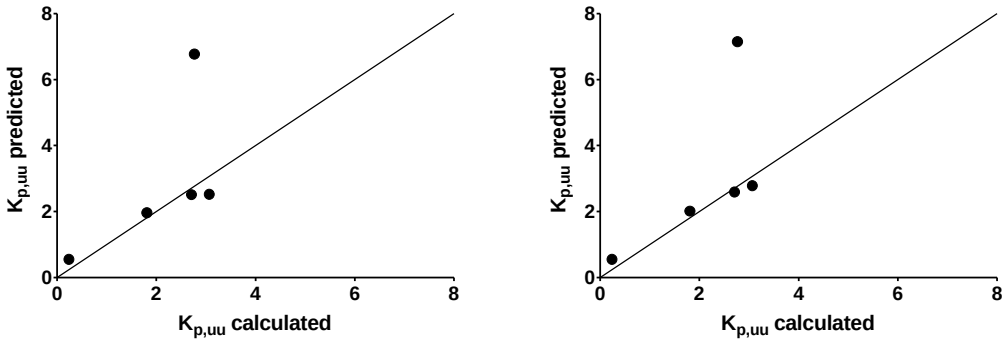

The calculated $K_{p,uu}$ were compared to the predicted $K_{p,uu}$ simulated by the rat hybrid-PBPK CNS model for chlorpromazine, citalopram, clozapine, haloperidol and risperidone using (a) P_{app} and (b) P_{exact} permeability parameters obtained from transport studies using the MDR1-MDCKII *in vitro* BBB model. Solid line represents line of unity.

For simulations performed using drug-specific permeability parameters calculated from MDR1-MDCKII *in vitro* BBB model permeabilities (P_{app} and P_{exact}), the predicted $K_{p,uu}$ was within 3-fold (for individual fold-differences see Table 6.7 and 6.8) of the calculated $K_{p,uu}$ for all 5 test drugs used in the simulation (chlorpromazine, citalopram, clozapine, haloperidol and risperidone) (Figure 6.2). For citalopram, clozapine and haloperidol excellent predictions were observed using both P_{app} (within 1.2-fold of calculated $K_{p,uu}$) and P_{exact} (within 1.1-fold of calculated $K_{p,uu}$). The greatest difference between predicted and calculated $K_{p,uu}$ was observed with risperidone (P_{app} and P_{exact} 3.0-fold difference). No appreciable differences were observed with predicted $K_{p,uu}$ and calculated $K_{p,uu}$ when either P_{app} or $P_{exact.}$ was used. The results from these simulations suggest that the rat CNS hybrid-PBPK model can accurately predict calculated $K_{p,uu}$ using *in vitro* permeability parameters from the MDR1-MDCKII *in vitro* BBB model and *in vitro* drug binding data.

Table 6.7 **Predicted and calculated $K_{p,uu}$ using drug-specific apparent permeability parameters obtained using the MDR1-MDCKII *in vitro* blood-brain barrier model permeabilities**

Test drug	Predicted $K_{p,uu}$	Calculated $K_{p,uu}$	Fold-difference
Chlorpromazine	6.6	2.8	2.4
Citalopram	2.0	1.8	1.1
Clozapine	2.5	2.7	1.1
Haloperidol	2.5	3.1	1.2
Risperidone	0.6	0.2	3.0

Table 6.8 **Predicted and calculated $K_{p,uu}$ using drug-specific exact permeability parameters obtained using the MDR1-MDCKII *in vitro* blood-brain barrier model permeabilities**

Test drug	Predicted $K_{p,uu}$	Calculated $K_{p,uu}$	Fold-difference
Chlorpromazine	7.2	2.8	2.6
Citalopram	2.0	1.8	1.1
Clozapine	2.6	2.7	1.0
Haloperidol	2.8	3.1	1.1
Risperidone	0.6	0.2	3.0

Figure 6.3 **Comparison of calculated and predicted $K_{p,uu}$ using drug-specific permeability parameters from the rat *in situ* model and *mdr1a/1b* knock out mice data**

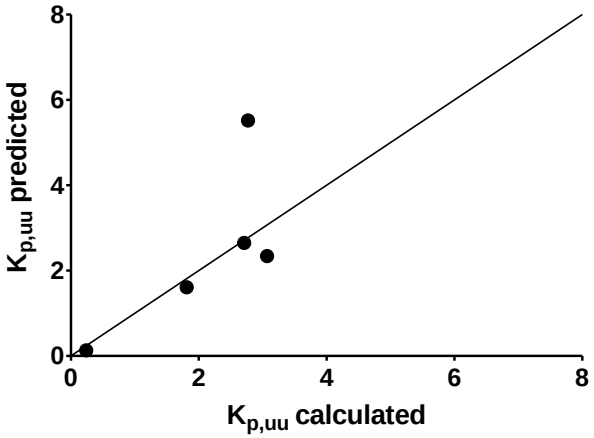

The calculated $K_{p,uu}$ was compared to the predicted $K_{p,uu}$ simulated by the rat hybrid-PBPK CNS model for chlorpromazine, citalopram, clozapine, haloperidol and risperidone using permeability parameters obtained from rat *in situ* model and efflux ratio obtained from knock out mice (Table 6.4). For clozapine an efflux ratio was not available from knockout mice so an average efflux ratio determined from transport studies using porcine and MDR1-MDCKII *in vitro* BBB models was used. Solid line shows line of unity.

For simulations performed using drug-specific permeability parameters calculated from permeability measurements obtained using the rat *in situ* model and knockout mice data, the predicted $K_{p,uu}$ was within 2-fold (for individual fold-differences see Table 6.9) of the calculated $K_{p,uu}$ for all 5 test drugs used in the simulation (chlorpromazine, citalopram, clozapine, haloperidol and risperidone) (Figure 6.3). Hence, provided marginally better predictions than predictions using permeability parameters from porcine and MDR1-MDCKII *in vitro* BBB models. Analogous to predictions obtained using the *in vitro* BBB models, citalopram, clozapine and haloperidol provided the best predictions (all within 1.3-fold). Comparable to predictions obtained using the and porcine MDR1-MDCKII *in vitro* BBB permeabilities the greatest difference between predicted and calculated $K_{p,uu}$ was observed for chlorpromazine and risperidone (2.0-fold). This suggests that the rat CNS hybrid-PBPK model can accurately predict calculated $K_{p,uu}$ using *in situ* rat, *in vivo* knockout mouse and *in vitro* drug binding data and although these predictions were marginally better than those using porcine and MDR1-MDCKII *in vitro* BBB models, they were not substantially better.

Table 6.9 **Predicted and calculated $K_{p,uu}$ values using drug-specific permeability parameters from rat *in situ* model and knock out mice data**

Test drug	Predicted $K_{p,uu}$	Calculated $K_{p,uu}$	Fold-difference
Chlorpromazine	5.5	2.8	2.0
Citalopram	1.6	1.8	1.1
Clozapine	2.7	2.7	1.0
Haloperidol	2.3	3.1	1.3
Risperidone	0.1	0.2	2.0

Discussion 6.3

The aim of this work was to use an in-house PBPK model of rat CNS developed and validated by Dr Raj Badhan (manuscript in preparation, Development of a Physiologically-Based Pharmacokinetic Model of the Rat Central nervous System) as a tool to predict rat *in vivo* $K_{p,uu}$ using *in vitro* input parameters. The rat CNS hybrid-PBPK model successfully predicted $K_{p,uu}$ within 3-fold of the calculated $K_{p,uu}$ for chlorpromazine, citalopram, clozapine, haloperidol and risperidone using drug-specific permeability parameters calculated from permeabilities (both P_{app} and P_{exact}) obtained using the porcine and MDR1-MDCKII *in vitro*

BBB models and *in vitro* drug binding data. The PBPK model also predicted $K_{p,uu}$ within 2-fold using rat *in situ*, knockout mice and *in vitro* drug binding data.

The permeability input parameters and the blood flow at the BCSFB was set at 10-fold compared to the permeability input parameter at the BBB due to validation studies performed by Dr Raj Badhan (manuscript in preparation, Development of a Physiologically-Based Pharmacokinetic Model of the Rat Central nervous System). These studies revealed that when the permeability and blood flow parameters where set at 10-fold greater than at the BBB that $K_{p,uu}$ and CSF:plasma$_u$ (used for model validation) model predictions for 7 model compounds were within 3-fold of *in vivo* values. These observations are consistent with reports in the literature where the blood flow to and permeability of, the choroidal epithelium of the choroid plexus are greater than those of the BBB (Del Bigio 1995; Saito el al. 1987).

These data suggest that the rat CNS hybrid-PBPK model could be used to accurately predict calculated $K_{p,uu}$ from *in vitro* and *in situ* drug specific permeability parameters and *in vitro* drug binding parameters.

The model simulations using the rat *in situ* permeabilities and knock out mice data provided slightly better predictions of $K_{p,uu}$ than the simulations using *in vitro* BBB model permeabilities from the porcine and MDR1-MDCKII *in vitro* BBB models. *In situ* permeability data is likely to be a more accurate permeability measurement than *in vitro* BBB model permeability because it accounts for the whole interplay of factors that influence drug permeability for example, blood and brain tissue drug binding, blood flow and the effect of a variety of efflux and influx transporters etc. In addition *in vivo* studies are experimentally complex, expensive and low throughput. However, the use of *in vitro* BBB model permeabilities still provided a prediction of $K_{p,uu}$ within 3-fold and could therefore be used as a surrogate for *in situ* permeability in order to increase throughput and reduce costs in drug development.

A strong relationship was observed between rat *in situ* permeability and porcine *in vitro* BBB model permeability (Chapter 4, Figure 4.8), although low concordance was observed between rat *in situ* permeability and MDR1-MDCKII *in vitro* BBB model permeability for the test drugs studied (Chapter 4, Figure 4.9). Despite this, incorporation of permeabilities obtained from the MDR1-MDCKII *in vitro* BBB model into the rat PBPK model provided a good prediction of $K_{p,uu}$. In addition, the actual permeability values from the

porcine and MDR1-MDCKII *in vitro* BBB models and rat *in situ* permeabilities were shown to be quite different. This would suggest that permeability is not the most important factor in determining extent of CNS drug penetration. Permeability measurements are most often used to predict the rate of CNS drug penetration. Most medication is administered under a regular doing regimen, where rate of penetration is not of high importance. Rapid rate of penetration is more important when treating condition such as seizure and stroke or during anaesthesia.

The importance of determining fu_{blood} and fu_{brain} for the prediction of the extent of drug penetration was highlighted in Chapter 5. Predicted $K_{p,uu}$ values were within 2-fold of the calculated $K_{p,uu}$ values for citalopram, clozapine and haloperidol whose fu_{brain} values ranged from 0.012-0.060. However, predicted $K_{p,uu}$ values were between 2 and 3-fold of the calculated $K_{p,uu}$ values for chlorpromazine whose fu_{brain} (0.002) was an order of magnitude lower than the fu_{brain} values of citalopram, clozapine and haloperidol and for risperidone whose fu_{brain} (0.144) was an order of magnitude higher than the fu_{brain} values of citalopram, clozapine and haloperidol. This suggests that fu_{brain} in the rat CNS PBPK model could have a greater impact of the prediction of $K_{p,uu}$ than permeability. However, it must be noted that the rat CNS hybrid-PBPK model can predict calculated $K_{p,uu}$ values within 3-fold for a range of fu_{blood} (0.028-0.264) and fu_{brain} (0.002-0.144) values.

There are shortages of predictive models in the literature for the quantification of CNS drug penetration. Non-physiological models are composed of either 1 compartment representing the brain or two compartments, of which one compartment represents the brain and the other compartment represents the body (Hammarlund-Udenaes et al. 1997) or blood/plasma (Liu et al. 2005). The literature recently described as semi-physiological model to predict CNS pharmacokinetics using *in vitro* and *in vivo* parameters (Liu et al. 2005). The model differed to the model used in this thesis as it utilised both *in vitro* and *in vivo* parameters and predicted time to achieve equilibrium unlike the model in this thesis which was used to predict the extent of CNS drug penetration. Liu et al concluded high BBB permeability and high fu_{brain} was required to achieve rapid brain equilibrium.

Currently all models in the literature are deficient of a distinct CSF component. The in-house hybrid-PBPK model of rat CNS described in this thesis is the most complex CNS rat model to date and the first model that incorporates a brain and detailed CSF compartment to accurately predict the extent of CNS drug penetration.

The rat PBPK model has the potential to be validated further with regard to fu_{CSF}. Fraction unbound in cerebrospinal fluid is not always available in the literature and is difficult to determine experimentally. In order to obtain an optimal fu_{CSF} value for use in the rat PBPK model when fu_{CSF} is unavailable, the impact of varying the fu_{CSF} value on the predicted $K_{p,uu}$ value could be investigated which could validate the model further.

Human $K_{p,uu}$ data (calculated using human K_p and human fu_{blood} and fu_{brain}, for details of calculation see Equation 2.9) was only available for 2 of the test drugs used throughout this work, namely haloperidol and primidone. Calculated human $K_{p,uu}$ for haloperidol and primidone were within 3-fold of calculated rat $K_{p,uu}$ (haloperidol: rat $K_{p,uu}$ = 3.07, human $K_{p,uu}$ = 3.48 and primidone: rat $K_{p,uu}$ = 0.42, human $K_{p,uu}$ = 0.80 Chapter 5). As calculated rat and human $K_{p,uu}$ were comparable for haloperidol and primidone, rat $K_{p,uu}$ could have the potential to act as a surrogate for human $K_{p,uu}$ and hence this model may have the potential to predict the extent of drug penetration in humans when using rat $K_{p,uu}$ as a surrogate for human. However, more human $K_{p,uu}$ values are required to validate this suggestion. In addition the model would need to be modified to incorporate other human input parameters, for example, blood flow to the BBB and bulk flow of interstitial fluid.

Future work could also include the development of a whole body PBPK human model containing a CNS component for the prediction of CNS pharmacokinetics. Incorporating the impact of disease on the prediction of CNS pharmacokinetics would be useful addition to this PBPK model.

This work demonstrates the potential of the rat CNS hybrid-PBPK model as a useful tool for drug discovery scientists to aid the prediction of the extent of drug penetration in the early stages of drug discovery thereby potentially reducing attrition rates and providing novel efficacious CNS drugs which are urgently required. Additionally, the rat CNS hybrid-PBPK model has potential use in non-CNS drug development to predict brain penetration of peripherally targeted drugs which could lead to CNS side effects limiting their use.

7.0 Chapter 7: Summary and Conclusion

The overall aim of this work was to use *in vitro* permeability and unbound drug fraction to predict CNS drug penetration. In order to investigate this, it was necessary to derive *in vitro* permeability and unbound drug fraction measurements.

The first part of the work in this thesis involved developing and characterising a primary porcine *in vitro* BBB model for use as a permeability screen. Optimised culture conditions for the model were determined. These included purification of PBECs with puromycin treatment, co-culture with CTX-TNA2 astrocyte cell line and the use of supplemented medium.

Characterisation of the primary porcine *in vitro* BBB model confirmed; physiologically realistic cell architecture, the formation of tight junction protein complexes, a restrictive paracellular pathway, functional expression of efflux transporters and BBB-associated marker enzymes. Characterisation concluded that the primary porcine *in vitro* BBB model possessed key features that were representative of the BBB *in vivo* and could be used in subsequent drug permeation studies.

In order to determine permeability measurements, the next part of this work involved comparing four *in vitro* BBB models regarding their potential for the prediction of *in vivo* BBB permeability. The *in vitro* BBB models employed in these studies demonstrated differences regarding barrier integrity and efflux function. Further differences between the *in vitro* BBB models were exhibited during drug permeation studies using a set of centrally-acting test drugs chosen by GSK. This showed that the permeability data between *in vitro* BBB models was not comparable and highlighted the importance of using an *in vitro* BBB model that could accurately predict *in vivo* BBB permeability. The *in vitro* porcine BBB model permeabilities demonstrated the strongest relationship with rat *in situ* permeability suggesting the potential of this model to predict *in vivo* BBB permeability.

To obtain unbound drug fraction, fu_{blood} and fu_{brain} were investigated across species. Fraction unbound in brain was shown to be comparable across species suggesting that any species could be used as a surrogate for human brain, as human brain tissue is difficult to obtain. Variation in fu_{blood} was observed across species. However human blood for use in binding studies is easily obtainable and therefore a surrogate is not required. This work suggested that species differences in brain penetration could be due to variation in fu_{blood} for

drugs that cross the BBB by passive diffusion and/or species differences in transporter homology or affinity for drugs that are subject to active transport processes at the BBB.

The final part of this work involved the use of an in-house hybrid-PBPK rat CNS model to predict the extent of drug penetration ($K_{p,uu}$) *in vivo* for rat, using *in vitro* parameters. The drug specific *in vitro* parameters used for the prediction of $K_{p,uu}$ were permeability measurements generated from transport studies and unbound drug fraction in blood and brain generated by equilibrium dialysis. The rat CNS hybrid-PBPK model was shown to accurately predict calculated $K_{p,uu}$ within 3-fold from *in vitro* drug specific permeability parameters and *in vitro* drug binding parameters.

In conclusion *in vitro,* permeability measurements and unbound drug fraction in blood and brain determined during this work have been shown to predict CNS drug penetration.

Appendix 1: Materials

Acetic acid	Fisher Scientific, Leicestershire, UK
Acetonitrile (HPLC grade)	Fisher Scientific, Leicestershire, UK
Acrylamide/bisacrylamide	Sigma-Aldrich Chemical Co, Poole, Dorset, UK
Amprenavir	Toronto Research Chemicals. Toronto, Canada
2-amino-2-methyl-1-propanol	Sigma-Aldrich Chemical Co, Poole, Dorset, UK
Bovine serum albumin	Sigma-Aldrich Chemical Co, Poole, Dorset, UK
Bradford reagent	BioRad Laboratories Ltd, Hertfordshire, UK
Bromophenol blue	Sigma-Aldrich Chemical Co, Poole,
(3′3 ′′5 ′5 ′′ tetrabromo phenolsulphonephthalein)	Dorset, UK
Calcein acetoxymethyl ester (Calcein-AM)	InVitrogen, Paisley, Scotland, UK
cAMP: (8-(4-chlorophenylthio) adenosine 3′, 5′-cyclic monophosphate sodium salt)	Sigma-Aldrich Chemical Co, Poole, Dorset, UK
CAPS: (3-(cyclohexylamino)-1-propane sulfonic Acid)	VWR International (Leicestershire, UK).
Carbamazepine	Sigma-Aldrich Chemical Co, Poole, Dorset, UK
Chlorpromazine hydrochloride	Sigma-Aldrich Chemical Co, Poole, Dorset, UK
Citalopram hydrobromide	Sigma-Aldrich Chemical Co, Poole, Dorset, UK
Clozapine	Sigma-Aldrich Chemical Co, Poole, Dorset, UK

Collagen type 1, rat tail 3.75 $mg.ml^{-1}$	BD Biosciences, Oxford, UK
Collagenase type III from *Clostridium histolycitcum.* Specific activity 130 $units.mg^{-1}$	Worthington Lorne Laboratories Twyford, Reading, UK
Coomassie blue stain	BioRad Laboratories Ltd, Hertfordshire, UK
Deoxyribonuclease I partially purified from bovine pancreas. Specific activity 2740 $units.mg^{-1}$	Worthington Lorne Laboratories, Twyford, Reading, UK
Donepezil > 99 % pure	Chemical Development GSK
Dulbecco's Modified Eagle Medium	Invitrogen, Paisley, Scotland, UK
Dulbecco's Modified Eagle Medium with Gluatmax	Invitrogen, Paisley, Scotland, UK
Dulbecco's PBS	Invitrogen, Paisley, Scotland, UK
ECL Plus western blotting reagent	GE Healthcare Life Sciences, Buckinghamshire, UK.
Ethanol HPLC grade	Fisher Scientific, Leicestershire, UK
Falcon^{TM} HTS 24-Mulitwell insert systems (polyethylene terphthalate, 1.0 µM pore size, diameter 6.5 mm, growth area 0.31 cm^2, 24 well clusters)	Becton Dickinson,. NJ, USA
Fibronectin (human)	BD Biosciences, Oxford UK
Fluorescein iso-thiocyanate (FITC)-labelled IB4	Invitrogen, Paisley, Scotland, UK
Fluorescein-labelled goat anti-rabbit IgG secondary antibody	Vector Laboratories Ltd, Peterborough, UK
Foetal Bovine Serum	Invitrogen, Paisley, Scotland, UK
GF120918	Gift from Chemical Development GSK, Harlow site, Essex, UK
Glycerol	Sigma-Aldrich Chemical Co, Poole, Dorset, UK
Glycine	Fisher Scientific, Leicestershire, UK

Glycylglycine	Sigma-Aldrich Chemical Co, Poole, Dorset, UK
GW633104X	Gift from Chemical Development GSK, Harlow site, Essex, UK
Haloperidol	Sigma-Aldrich Chemical Co, Poole, Dorset, UK
Heparin 170 USP unit.mg^{-1}	Sigma-Aldrich Chemical Co, Poole, Dorset, UK
HEPES 1M buffer solution	Invitrogen, Paisley, Scotland, UK
Horse serum	Zymed, Paisley, Scotland, UK
Hydrocortisone	Sigma-Aldrich Chemical Co, Poole, Dorset, UK
Leibovitz-15 medium	Sigma-Aldrich Chemical Co, Poole, Dorset, UK
L-glutamine 200mM 100 X	Invitrogen, Paisley, Scotland, UK
L-glutamyl-*p*-nitroanilide	Sigma-Aldrich Chemical Co, Poole, Dorset, UK
Lucifer Yellow CH dilithium salt	Sigma-Aldrich Chemical Co, Poole, Dorset, UK
M199	Sigma-Aldrich Chemical Co, Poole, Dorset, UK
Magnesium chloride	Sigma-Aldrich Chemical Co, Poole, Dorset, UK
Mesoridazine benenesulfonate	Sigma-Aldrich Chemical Co, Poole, Dorset, UK
Methanol	Fisher Scientific, Leicestershire, UK
Minimum Essential Medium Eagle modified with Earle's Salts and 20 mM HEPES x 1	MP Biomedicals, Illkirch, France
MTT (3-(4, 5-dimethylthiazol-2-yl)-2,5-diphenyl tetrazolium bromide	Invitrogen, Paisley, Scotland, UK

2-mercaptoethanol	Sigma-Aldrich Chemical Co, Poole, Dorset, UK
Non-essential amino acids 100 X	Invitrogen, Paisley, Scotland, UK
PAGE protein marker, broad range (2-212 kDa)	New England Biolabs, Hertfordshire, UK
Penicillin G sodium 10,000 units,ml^{-1} streptomycin sulphate 10,000 $\mu g.ml^{-1}$	Sigma-Aldrich Chemical Co, Poole, Dorset, UK
Plasma derived serum	First Link UK, Birmingham, UK
p-nitrophenyl phosphate	Sigma-Aldrich Chemical Co, Poole, Dorset, UK
Potassium chloride	Sigma-Aldrich Chemical Co, Poole, Dorset, UK
Potassium phosphate	Sigma-Aldrich Chemical Co, Poole, Dorset, UK
Primary antibody: rabbit anti-human occludin	Zymed, Paisley, Scotland, UK
Primary antibody: rabbit anti-human ZO-1	Zymed, Paisley, Scotland, UK
ProLong® mounting medium containing DAPI	InVitrogen, Paisley, Scotland, UK
Protease inhibitor cocktail	Sigma-Aldrich Chemical Co, Poole, Dorset, UK
Puromycin dihydrochloride	Sigma-Aldrich Chemical Co, Poole, Dorset, UK
RO20-1724 (4-(3-Butoxy-4-methoxybenzyl)-2-imidazolidinone)	Merck Bioscience, Nottingham, UK
SB243213	Gift from Chemical Development GSK, Harlow site, Essex, UK
Sodium chloride	Analab, Dorset, UK
Sodium phosphate	Sigma-Aldrich Chemical Co, Poole, Dorset, UK
TEMED (N,N,N′,N′-tetramethylethylenediamine)	Sigma-Aldrich Chemical Co, Poole, Dorset, UK,

T-Flask- 25 cm^2	Greiner Biosciences, Stonehouse, UK
T-Flask- 75 cm^2	Greiner Biosciences, Stonehouse, UK
T-Flask- 175 cm^2	Greiner Biosciences, Stonehouse, UK
Tissue culture-treated 6-well plates	Greiner Biosciences, Stonehouse, UK
Tissue culture-treated 96-well flat bottomed plate	Corning Costar, High Wycombe, UK
Transwell™ polycarbonate inserts (pore size 0.4 µm, diameter 12 mm, growth area 1.12 cm^2, 12-well cell culture cluster	Corning Costar, High Wycombe, UK
Tris (Tris [hydroxymethyl]aminomethane)	Sigma-Aldrich Chemical Co, Poole, Dorset, UK
Triton x-100	Sigma-Aldrich Chemical Co, Poole, Dorset, UK
Trypan Blue solution 0.4 % (w/v)	Sigma-Aldrich Chemical Co, Poole, Dorset, UK
Trypsin partially purified from bovine pancreas Specific activity 216 units.mg^{-1}	Worthington Lorne Laboratories, Twyford, Reading, UK
Trypsin-EDTA solution (1 x 500 Na-Benzoyl-Arginine Ethyl Ester units porcine trypsin and EDTA, 180 µg.ml^{-1})	Invitrogen, Paisley, Scotland, UK
Quetiapine > 99 % pure	Gift from Chemical Development GSK, Harlow site, Essex, UK
Risperidone > 99 % pure	Gift from Chemical Development GSK, Harlow site, Essex, UK
Ziprasisdone > 99 % pure	Gift from Chemical Development GSK, Harlow site, Essex, UK

Appendix 2: Solutions and Media Composition

Digest mix

Collagenase	210 $U.ml^{-1}$
Trypsin	91 $U.ml^{-1}$
DNase 1	114 $U.ml^{-1}$

Freshly prepare on the day of isolation. Dissolve enzymes in M199 containing 10 % (v/v) FBS and penicillin G sodium (100 $units.ml^{-1}$) and streptomycin sulphate (100 $\mu g.ml^{-1}$) and filter sterilise. Correct each enzyme batch for differences in activity ($U.mg^{-1}$).

Phosphate buffered saline pH 7.4.

NaCl	137.0 mM
KCl	2.7 mM
Na_2HPO_4	10.0 mM
KH_2PO_4	2.0 mM

Dissolved in distilled water and adjusted to pH 7.4. Autoclave to sterilise when required for cell culture.

Culture media

Astrocyte

DMEM	
FBS	10 % (v/v)
Penicillin G sodium	100 $u.ml^{-1}$
Streptomycin sulphate	100 $\mu g.ml^{-1}$

Caco-2

DMEM	
FBS	10 % (v/v)
L-glutamine	2 mM
NEAA	1 % (v/v)
Penicillin G sodium	100 $u.ml^{-1}$
Streptomycin sulphate	100 $\mu g.ml^{-1}$

hCMEC/D3 advised by INSERM

EBM2 basal media	500 ml
FBS	2.5 % (v/v)
Penicillin G sodium	100 $u.ml^{-1}$
Streptomycin sulphate	100 $\mu g.ml^{-1}$
VEGF	125 µl (from EGM-2 MV bullet kit)
IGF	125 µl (from EGM-2 MV bullet kit)
EGF	125 µl (from EGM-2 MV bullet kit)
Hydrocortisone	50 µl (from EGM-2 MV bullet kit)
HEPES	1 mM
bFGF	200 $ng.ml^{-1}$

MDCK	
DMEM + Glutamax	
FBS	10 % (v/v)
Penicillin G sodium	100 $u.ml^{-1}$
Streptomycin sulphate	100 $\mu g.ml^{-1}$
PBEC	
DMEM	
Penicillin G sodium	100 $u.ml^{-1}$
Streptomycin sulphate	100 $\mu g.ml^{-1}$
L-glutamine	2 mM
PDS	10 % (v/v)
Heparin	125 mM
Transport media/solution	
Caco-2	
HBSS	
HEPES	1 mM
hCMEC/D3 advised by INSERM	
EBM2 basal media	500 ml
FBS	2.5 % (v/v)
Penicillin G sodium	100 $u.ml^{-1}$
Streptomycin sulphate	100 $\mu g.ml^{-1}$
Hydrocortisone	2.8 mM
HEPES	1mM
bFGF	200 $ng.ml^{-1}$
MDCK	
DPBS	
HEPES	1 mM
PBEC	
DMEM	500 ml
Heparin	125 µM
L-glutamine	2 mM
Penicillin G sodium	100 $u.ml^{-1}$
Streptomycin sulphate	100 $\mu g.ml^{-1}$
cAMP	312.5 µM
RO-20-1724	17.5 µM
Hydrocortisone	550 nM

Reagents for Western Blotting

Lysis buffer without protease inhibitor
50 mM Tris-HCl pH 7.8
5 mM EDTA

Sonicate and heat if required. For lysis buffer with protease inhibitor, add protease inhibitor cocktail (2 $\mu l.ml^{-1}$) to the above solution.

1.5M Tris - pH 8.8
Tris Base 340 $mg.ml^{-1}$
Adjust pH with HCl and store at 4 °C

0.5M Tris –pH 6.8
Tris base 76.25 $mg.ml^{-1}$
Adjust pH with HCl and store at 4 °C

SDS Sample buffer (8 ml)

Tris base 0.025M	1.0 ml
dH_2O	3.8 ml
Glycerol	0.8 ml
10% SDS	1.6 ml
Mercaptoethanol	0.4 ml
bromophenol blue 1 %	0.4ml

5 X Running buffer
dH_2O

Tris base	15 $mg.ml^{-1}$
Glycine	72 $\mu l.ml^{-1}$
SDS	5 $mg.ml^{-1}$

Store at 4°C and dilute with dH_2O to 1X when required

De-staining solution (40% methanol, 7% acetic acid)
dH_2O

Methanol	40 % (v/v)
Acetic acid	7 % (v/v)

Store at room temperature

Transfer buffer
CAPS-pH 11 10 mM

TBS-T

Tris base	10 mM
NaCl	150 mM
Tween-20	0.05 % (v/v)

Blocking buffer

CAPS Marvel milk	50 $mg.ml^{-1}$
TBS-T	

Appendix 3: Physicochemical Properties of Test Drugs

Test drug	Molecular weight	acd-clogP	acd-clogD (pH7.4)	PSA	Hydrogen bond donors	Hydrogen bond acceptors	Ion class
Amprenavir	505.6	4.2	4.2	139.4	4	9	Neutral
Carbamazepine	236.3	2.7	2.7	46.33	2	3	Neutral
Chlorpromazine	318.9	5.2	3.2	6.48	0	2	Basic
Citalopram	324.4	2.5	0.4	36.26	0	3	Basic
Clozapine	326.8	3.5	3.3	30.87	1	4	Basic
Donepezil	379.5	4.7	3.3	38.77	0	4	Basic
Haloperidol	375.9	3.0	2.1	40.54	1	3	Basic
Mesoridazine	386.6	6.1	3.9	6.48	0	4	Basic
Primidone	218.3	0.4	0.4	58.20	2	2	Basic
Quetiapine	383.5	1.6	1.6	48.30	1	6	Basic
Risperidone	410.5	2.9	2.3	64.16	0	6	Basic
Ziprazidone	412.9	4.0	3.0	48.47	1	4	Basic

Appendix 4: Mass Spectroscopy

Amprenavir

MS set up

Electrospray interface +ve mode

Source temp: 125 ºC Desolvation temp: 350 ºC

Cone gas: 150 $L.hr^{-1}$ Desolvation gas: 600 $L.hr^{-1}$

Capillary voltage: 3.5 kV

Amprenavir

Mass transitions: 506.35>245.25

Cone voltage: 50 V Collision voltage: 15 eV

SB243213(IS)

Mass transitions: 429.15>228.15

Cone voltage: 90 V Collision voltage: 225 eV

LC set up

Luna 5u C18 50x4.6 mm column from Phenomenex

Gradient elution at $1ml.min^{1}$

	A	B	C	D	Curve
0 min	-	-	100	-	1
1 min	-	-	100	-	11
3 min	15	-	10	75	1
4 min	-	15	-	85	1
5 min	-	-	100	-	1

Where A = 90 % H2O, 10 % MeCN + 0.05 % formic acid

B = 10 % H2O, 90 % MeCN + 0.05 % formic acid

C = 90 % H2O, 10 % MeCN + 1 mM ammonium acetate

D = 10 % H2O, 90 % MeCN + 1 mM ammonium acetate

Retention times: Amprenavir = 3.0

IS = 4.4

Carbamazepine

MS set up

Electrospray interface +ve mode

Source temp: 125 ºC Desolvation temp: 350 ºC

Cone gas: 150 $L.hr^{-1}$ Desolvation gas: 600 $L.hr^{-1}$

Capillary voltage: 3.5 kV

Carbamazepine
Mass transitions: 237.05>194.1
Cone voltage: 90 V Collision voltage: 220 eV

SB243213(IS)
Mass transitions: 429.15>228.15
Cone voltage: 90 V Collision voltage: 225 eV

LC set up
Luna 5u C18 50x4.6 mm column from Phenomenex

Gradient elution at 1ml.min^{-1}

	A	B	C	D	Curve
0 min	-	-	100	-	1
1 min	-	-	100	-	11
3 min	15	-	35	50	1
4 min	-	15	-	85	1
5 min	-	-	100	-	1

Where A = 90 % H2O, 10 % MeCN + 0.05 % formic acid
B = 10 % H2O, 90 % MeCN + 0.05 % formic acid
C = 90 % H2O, 10 % MeCN + 1 mM ammonium acetate
D = 10 % H2O, 90 % MeCN + 1 mM ammonium acetate

Retention times: Carbamazepine = 2.9
IS = 4.4

Chlorpromazine

MS set up
Electrospray interface +ve mode
Source temp: 125 ºC Desolvation temp: 350 ºC
Cone gas: 150 L.hr^{-1} Desolvation gas: 600 L.hr^{-1}
Capillary voltage: 3.5 kV

Chlorpromazine
Mass transitions: 319.15>86.25
Cone voltage: 50 V Collision voltage: 20 eV

SB243213(IS)
Mass transitions: 429.15>228.15
Cone voltage: 90 V Collision voltage: 25 eV

LC set up
Luna 5u C18 50x4.6 mm column from Phenomenex

Gradient elution at 1ml.min^{-1}

	A	B	C	D	Curve
0 min	-	-	100	-	1
1 min	-	-	100	-	11
3 min	15	-	10	75	1
4 min	-	15	-	85	1
5 min	-	-	100	-	1

Where A = 90 % H2O, 10 % MeCN + 0.05 % formic acid
B = 10 % H2O, 90 % MeCN + 0.05 % formic acid
C = 90 % H2O, 10 % MeCN + 1 mM ammonium acetate
D = 10 % H2O, 90 % MeCN + 1 mM ammonium acetate

Retention times: Chlorpromazine = 2.4
IS = 3.3

Citalopram

MS set up
Electrospray interface +ve mode
Source temp: 125 ºC Desolvation temp: 350 ºC
Cone gas: 150 L.hr^{-1} Desolvation gas: 600 L.hr^{-1}
Capillary voltage: 3.5 kV

Citalopram
Mass transitions: 325.35>109.1
Cone voltage: 60 V Collision voltage: 25 eV

SB243213(IS)
Mass transitions: 429.15>228.15
Cone voltage: 90 V Collision voltage: 25 eV

LC set up
Luna 5u C18 50x4.6 mm column from Phenomenex

Gradient elution at 1ml.min^{-1}

	A	B	C	D	Curve
0 min	-	-	100	-	1
1 min	-	-	100	-	11
3 min	15	-	10	75	1
4 min	-	15	-	85	1
5 min	-	-	100	-	1

Where A = 90 % H2O, 10 % MeCN + 0.05 % formic acid
B = 10 % H2O, 90 % MeCN + 0.05 % formic acid
C = 90 % H2O, 10 % MeCN + 1 mM ammonium acetate
D = 10 % H2O, 90 % MeCN + 1 mM ammonium acetate

Retention times: Citalopram = 2.4
IS = 4.4

Clozepine

MS set up
Electrospray +ve mode
Source temp: 125 ºC Desolvation temp: 350ºC
Cone gas: 150 $L.hr^{-1}$ Desolvation gas: 600 $L.hr^{-1}$
Capillary voltage: 3.5 kV

Clozepine
Mass transitions: 327.15>270.2
Cone voltage: 50 V Collision voltage: 225 eV

SB243213(IS)
Mass transitions: 429.15>228.15
Cone voltage: 90 V Collision voltage: 225 eV

LC set up
Luna 5u C18 50x4.6 mm column from Phenomenex

Gradient elution at 1$ml.min^{-1}$

	A	B	C	D	Curve
0 min	-	-	100	-	1
1 min	-	-	100	-	11
3 min	15	-	10	75	1
4 min	-	15	-	85	1
5 min	-	-	100	-	1

Where A = 90 % H2O, 10 % MeCN + 0.05 % formic acid
B = 10 % H2O, 90 % MeCN + 0.05 % formic acid
C = 90 % H2O, 10 % MeCN + 1 mM ammonium acetate
D = 10 % H2O, 90 % MeCN + 1 mM ammonium acetate

Retention times: Clozapine = 2.4
IS = 3.3

Control (GW633104)

MS set up
Electrospray interface +ve mode
Source temp: 125ºC Desolvation temp: 350ºC
Cone gas: 150 L/hr Desolvation gas: 600 L/hr
Capillary voltage: 3.5 KV

Control
Mass transitions: 409.15>92.2
Cone voltage: 90 V Collision voltage: 30eV

SB243213(IS)
Mass transitions: 429.15>228.15
Cone voltage: 90 V Collision voltage: 225 eV

LC set up
Luna 5u C18 50x4.6 mm column from Phenomenex

Gradient elution at 1ml.min^{-1}

	A	B	C	D	Curve
0 min	-	-	100	-	1
1 min	-	-	100	-	11
3 min	15	-	35	50	1
4 min	-	15	-	85	1
5 min	-	-	100	-	1

Where A = 90 % H2O, 10 % MeCN + 0.05 % formic acid
B = 10 % H2O, 90 % MeCN + 0.05 % formic acid
C = 90 % H2O, 10 % MeCN + 1 mM ammonium acetate
D = 10 % H2O, 90 % MeCN + 1 mM ammonium acetate

Retention times: Control = 4.0
IS = 4.4

Donepezil

MS set up
Electrospray interface +ve mode
Source temp: 125 ºC Desolvation temp: 350 ºC
Cone gas: 150 L.hr^{-1} Desolvation gas: 600 L.hr^{-1}
Capillary voltage: 3.5 kV

Donepezil
Mass transitions: 380.25>91.25
Cone voltage: 100 V Collision voltage: 35 eV

SB414796(IS)
Mass transitions: 537.2>334.25
Cone voltage: 140 V Collision voltage: 25 eV

LC set up
Luna 5u C18 50x4.6 mm column from Phenomenex

Gradient elution at 1ml.min^{-1}

	A	B	C	D	Curve
0 min	-	-	100	-	1
1 min	-	-	100	-	11
3 min	-	-	-	100	6
4 min	-	-	-	100	1
5 min	-	-	100	-	1

Where A = 90 % H2O, 10 % MeCN + 0.05 % formic acid
B = 10 % H2O, 90 % MeCN + 0.05 % formic acid
C = 90 % H2O, 10 % MeCN + 1 mM ammonium acetate
D = 10 % H2O, 90 % MeCN + 1 mM ammonium acetate

Retention times: Donepezil = 3.9
IS = 3.7

Haloperidol

MS set up
Electrospray interface +ve mode
Source temp: 125 ºC Desolvation temp: 350 ºC
Cone gas: 150 L.hr^{-1} Desolvation gas: 600 L.hr^{-1}
Capillary voltage: 3.5 kV

Haloperidol
Mass transitions: 376.05>165.05
Cone voltage: 60 V Collision voltage: 25 eV

SB243213(IS)
Mass transitions: 429.15>228.15
Cone voltage: 90 V Collision voltage: 25 eV

LC set up
Luna 5u C18 50x4.6 mm column from Phenomenex

Gradient elution at 1ml.min^{-1}

	A	B	C	D	Curve
0 min	-	-	100	-	1
1 min	-	-	100	-	11
3 min	15	-	10	75	1
4 min	-	15	-	85	1
5 min	-	-	100	-	1

Where A = 90 % H2O, 10 % MeCN + 0.05 % formic acid
B = 10 % H2O, 90 % MeCN + 0.05 % formic acid
C = 90 % H2O, 10 % MeCN + 1 mM ammonium acetate
D = 10 % H2O, 90 % MeCN + 1 mM ammonium acetate

Retention times: Haloperidol = 2.3
IS = 3.3

Mesoridazine

MS set up
Electrospray interface +ve mode
Source temp: 125 ºC Desolvation temp: 350ºC
Cone gas: 150 L.hr^{-1} Desolvation gas: 600 L.hr^{-1}
Capillary voltage: 3.5 KV

Mesoridazine
Mass transitions: 387.3>126.15
Cone voltage: 60 V Collision voltage: 25 eV

SB243213(IS)
Mass transitions: 429.15>228.15
Cone voltage: 90 V Collision voltage: 25 eV

LC set up
Luna 5u C18 50x4.6 mm column from Phenomenex

Gradient elution at 1ml.min^{-1}

	A	B	C	D	Curve
0 min	-	-	100	-	1
1 min	-	-	100	-	11
3 min	15	-	10	75	1
4 min	-	15	-	85	1
5 min	-	-	100	-	1

Where A = 90 % H2O, 10 % MeCN + 0.05 % formic acid
B = 10 % H2O, 90 % MeCN + 0.05 % formic acid
C = 90 % H2O, 10 % MeCN + 1 mM ammonium acetate
D = 10 % H2O, 90 % MeCN + 1 mM ammonium acetate

Retention times: Mesoridazine = 2.5
IS = 4.4

Primidone

MS set up
Electrospray interface +ve mode
Source temp: 125 ºC Desolvation temp: 350 ºC
Cone gas: 150 $L.hr^{-1}$ Desolvation gas: 600 $L.hr^{-1}$
Capillary voltage: 3.5 KV

Primidone
Mass transitions: 218.95>162.05
Cone voltage: 60 V Collision voltage: 12eV

SB243213(IS)
Mass transitions: 429.15>228.15
Cone voltage: 90 V Collision voltage: 225 eV

LC set up
Luna 5u C18 50x4.6 mm column from Phenomenex

Gradient elution at 1$ml.min^{-1}$

	A	B	C	D	Curve
0 min	-	-	100	-	1
1 min	-	-	100	-	11
3 min	15	-	25	60	1
4 min	-	15	-	85	1
5 min	-	-	100	-	1

Where A = 90 % H2O, 10 % MeCN + 0.05 % formic acid
B = 10 % H2O, 90 % MeCN + 0.05 % formic acid
C = 90 % H2O, 10 % MeCN + 1 mM ammonium acetate
D = 10 % H2O, 90 % MeCN + 1 mM ammonium acetate

Retention times: Primidone = 2.4
IS = 4.2

Quetiapine

MS set up
Electrospray interface +ve mode
Source temp: 125ºC Desolvation temp: 350ºC
Cone gas: 150 $L.hr^{-1}$ Desolvation gas: 600 $L.hr^{-1}$
Capillary voltage: 3.5 KV

Quetiapine
Mass transitions: 384.15>253.1
Cone voltage: 100 V Collision voltage: 20eV

SB243213(IS)
Mass transitions: 429.15>228.15
Cone voltage: 90 V Collision voltage: 25 eV

LC set up
Luna 5u C18 50x4.6 mm column from Phenomenex

Gradient elution at 1ml.min^{-1}

	A	B	C	D	Curve
0 min	-	-	100	-	1
1 min	-	-	100	-	11
3 min	15	-	10	75	1
4 min	-	15	-	85	1
5 min	-	-	100	-	1

Where A = 90 % H2O, 10 % MeCN + 0.05 % formic acid
B = 10 % H2O, 90 % MeCN + 0.05 % formic acid
C = 90 % H2O, 10 % MeCN + 1 mM ammonium acetate
D = 10 % H2O, 90 % MeCN + 1 mM ammonium acetate

Retention times: Quetiapine = 2.6
IS = 3.3

Risperidone

MS set up
Electrospray interface +ve mode
Source temp: 125 ºC Desolvation temp: 350 ºC
Cone gas: 150 $L.hr^{-1}$ Desolvation gas: 600 $L.hr^{-1}$
Capillary voltage: 3.5 kV

Risperidone
Mass transitions: 411.25>191.15
Cone voltage: 100 V Collision voltage: 30eV

SB243213(IS)
Mass transitions: 429.15>228.15
Cone voltage: 90 V Collision voltage: 225 eV

LC set up
Luna 5u C18 50x4.6 mm column from Phenomenex

Gradient elution at 1ml/min

	A	B	C	D	Curve
0 min	-	-	100	-	1
1 min	-	-	100	-	11
3 min	15	-	10	75	1
4 min	-	15	-	85	1
5 min	-	-	100	-	1

Where A = 90 % H2O, 10 % MeCN + 0.05 % formic acid
B = 10 % H2O, 90 % MeCN + 0.05 % formic acid
C = 90 % H2O, 10 % MeCN + 1 mM ammonium acetate
D = 10 % H2O, 90 % MeCN + 1 mM ammonium acetate

Retention times: Risperidone = 2.4
IS = 3.3

Ziprasidone

MS set up
Electrospray interface +ve mode
Source temp: 125 ºC Desolvation temp: 350 ºC
Cone gas: 150 $L.hr^{-1}$ Desolvation gas: 600 $L.hr^{-1}$
Capillary voltage: 3.5 KV

Ziprazidone
Mass transitions: 413.2>194.15
Cone voltage: 100 V Collision voltage: 225 eV

SB243213(IS)
Mass transitions: 429.15>228.15
Cone voltage: 90 V Collision voltage: 225 eV

LC set up
Luna 5u C18 50x4.6 mm column from Phenomenex

Gradient elution at 1ml.min^{-1}

	A	B	C	D	Curve
0 min	-	-	100	-	1
1 min	-	-	100	-	11
3 min	5	-	20	75	1
4 min	-	15	-	85	1
5 min	-	-	100	-	1

Where A = 90 % H2O, 10 % MeCN + 0.05 % formic acid
B = 10 % H2O, 90 % MeCN + 0.05 % formic acid
C = 90 % H2O, 10 % MeCN + 1 mM ammonium acetate
D = 10 % H2O, 90 % MeCN + 1 mM ammonium acetate

Retention times: Ziprasidone = 2.8
IS = 3.3

Appendix 5: Caco-2 Transport Studies

A5.1 Assessment of test drug concentration for use in transport studies across *in vitro* blood-brain barrier models

Figure A5.1 Effect of test drug concentration on cell viability

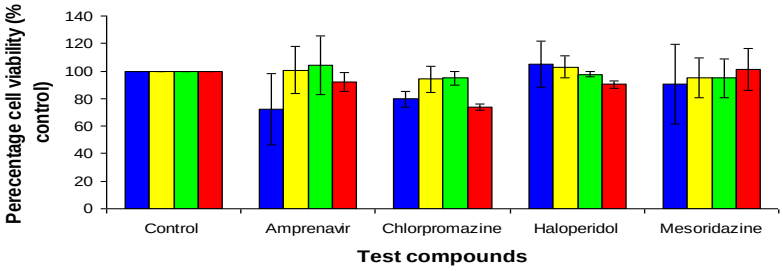

Caco-2 were seeded onto 96-well plates at a pre-determined cell density (17,500 cells.cm^{-2}) and incubated for 24 h. Cells were then incubated with test drugs at 0.03 µM (blue), 0.3 µM (yellow), 3 µM (green) and 30 µM (red) for 60 min, washed with PBS and incubated for 24 h in growth medium. Methylthiazolyldiphenyl-tetrazolium bromide in PBS (5 mg.ml^{-1}) was added to all wells (10 µl per 100 µl medium) and the cells were incubated for 4 h. The MTT-formazan produced was solubilised and quantified colourmetrically using a spectrophotometer. The control (cells exposed to solvent at the same concentration as all test drug solutions) corresponded to a cell viability of 100 %. Data are expressed as mean ± standard deviation of one independent experiment, with 4 replicate determinants.

Figure A5.2 Effect of test drug concentration and GF120918 on cell viability

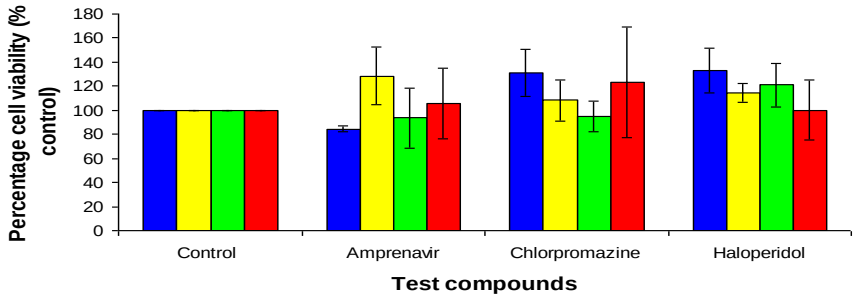

Caco-2 cells were seeded at a pre-determined density of 17,500 cells.cm^{-2} (and incubated for 24 h. The cells were then co-incubated with the test drugs that were to be used in subsequent transport studies at a range of concentrations (blue 0.03 µM, yellow 0.30 µM, green 3.00 µM and red 30.00 µM) and GF120918 (2 µM) for 60 min. The cells were washed and incubated for 24 h in growth medium. Methylthiazolyldiphenyl-tetrazolium bromide in PBS (5 mg.ml^{-1}), was added to all wells (10 µl per 100 µl medium) and the cells were incubated for 4 h. The MTT-formazan produced was solubilised and quantified colourmetrically using a spectrophotometer. The control (cells exposed to solvent at the same concentration as all test drugs solutions) corresponded to a cell viability of 100 %. Data are expressed as mean ± standard deviation of 4 replicates from one independent experiment.

Lucifer yellow (100 µM) alone, employed in all studies to monitor cell monolayer integrity, did not appreciably affect Caco-2 cell viability (101.99 %) compared to control cells (100 %). Similarly, there was no appreciable effect on cell viability when cells were exposed to GF120918 (2 µM) alone (99.20%) or exposed to a combination of Lucifer yellow (100 µM) and GF120918 (100.94 %) compared to control cells. This study confirmed that a test drug concentration of 3 µM, the P-gp inhibitor GF120918 (2 µM) and the paracellular marker Lucifer yellow (100 µM) did not substantially decrease cell viability of Caco-2 cell type and were therefore suitable to be used in subsequent transport studies.

A5.2 Characterisation of Caco-2 *in vitro* blood-brain barrier model integrity and efflux function

Table A5.1 Markers of monolayer integrity and efflux function

***In vitro* BBB model**	**Lucifer yellow P_{app} ($nm.s^{-1}$)**	**Lucifer yellow P_{exact} ($nm.s^{-1}$)**	**TER ($\Omega.cm^2$)**	**Efflux ratio (P_{app})**	**Efflux ratio (P_{exact})**
Caco-2	37.2±13.3	39.3±14.0	1500-1800	8.6	10.2

The table shows A-B apparent permeability (P_{app} $nm.s^{-1}$) and exact permeability (P_{exact} $nm.s^{-1}$) of Lucifer yellow (100 µM), transcellular electrical resistance ($\Omega.cm^2$) and efflux ratio (B-A/A-B) of amprenavir determined from both apparent permeability (P_{app} $nm.s^{-1}$) and exact permeability (P_{exact} $nm.s^{-1}$) across Caco-2 *in vitro* BBB model. Lucifer yellow data are expressed as mean ± standard deviation of at least 6 replicates, n=3 independent experiments, transcellular electrical resistance data are expressed as range of at least 12 replicates, n=3 independent experiments and efflux ratios (B-A/A-B) (P_{app} and P_{exact}) for amprenavir are calculated from mean of duplicates, n=3 independent experiments.

A5.3 Permeability measurements of test drugs across the Caco-2 *in vitro* BBB model

Four of the 12 test drugs were used in permeability studies across the Caco-2 *in vitro* BBB model. Table A5.2 and A5.3 detail apparent permeability and exact permeability respectively, with and without the P-gp inhibitor GF120918, across the Caco-2 *in vitro* BBB model for amprenavir, chlorpromazine, haloperidol and mesoridazine.

Table A5.2 Apparent permeability and efflux ratio of test drugs across the Caco-2 *in vitro* blood-brain barrier model

	With out inhibitor			With inhibitor		
Test Drug	**P_{app} A-B**	**P_{app} B-A**	**ER**	**P_{app} A-B**	**P_{app} B-A**	**ER**
Amprenavir	19.4 ± 10.4	248.5± 89.4	12.8	43.1 ± 10.6	225.8± 24.9	5.2
Chlorpromazine	54.0 ± 21.1	82.6± 25.7	1.5	45.6 ± 8.2	95.8 ± 16.9	2.1
Haloperidol	60.0 ± 9.3	221.7 ± 35.5	3.7	48.9 ± 1.6	122.3 ± 21.5	2.5
Mesoridazine	40.0	58.8	1.5			

Apparent permeability of amprenavir, chlorpromazine, haloperidol and mesoridazine (3 µM) across the Caco-2 *in vitro* BBB model in both A-B and B-A directions, with and without the potent P-gp inhibitor GF120918 (2 µM), was measured over 60 min. The apparent permeability (P_{app} nm.s^{-1}) and efflux ratio (ER) were calculated. Apparent permeability data are expressed as mean ± standard deviation of duplicates, n=3 independent experiments for all test drugs apart from mesoridazine where data are expressed as the mean of duplicates from one independent experiment. Efflux ratios (B-A/A-B) were calculated from mean apparent permeability values.

Table A5.3 Exact permeability and efflux ratio of test drugs across the Caco-2 *in vitro* blood-brain barrier model

	With out inhibitor			With inhibitor		
Test Drug	**P_{exact} A-B**	**P_{exact} B-A**	**ER**	**P_{exact} A-B**	**P_{exact} B-A**	**ER**
Amprenavir	21.2 ± 12.4	252.4± 95.6	11.9	50.7 ± 12.5	237.6 ± 38.5	4.7
Chlorpromazine	93.0± 25.8	105.8 ± 36	1.1	68.9 ± 22.6	98.0 ± 26.2	1.4
Haloperidol	72.1 ± 10.7	211.0 ± 43.2	2.9	54.1 ± 12.3	110.7 ± 24.0	2.1
Mesoridazine	48.8	65.8	1.4			

Exact permeability of amprenavir, chlorpromazine, haloperidol and mesoridazine (3 µM) across the Caco-2 *in vitro* BBB model in both A-B and B-A directions, with and without the potent P-gp inhibitor GF120918 (2 µM), was measured over 60 min. The exact permeability (P_{exact} nm.s^{-1}) and efflux ratio (ER) were calculated. Exact permeability data are expressed as mean ± standard deviation of duplicates, n=3 independent experiments for all test drugs apart from mesoridazine where data are expressed as the mean of duplicates from one independent experiment. Efflux ratios (B-A/A-B) were calculated from mean exact permeability values.

A5.4 Relationship between *in vitro* blood-brain barrier model permeabilities

Figure A5.3 Relationship between porcine and Caco-2 *in vitro* BBB model permeabilities

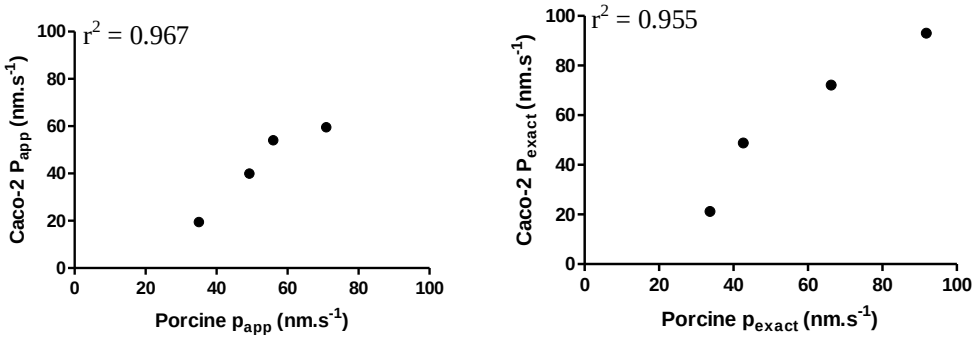

Relationship between Caco-2 and porcine *in vitro* BBB model A-B permeabilities (P_{app} and P_{exact} $nm.s^{-1}$) without the P-gp inhibitor GF120918 for amprenavir, chlorpromazine, haloperidol and mesoridazine. The data from the Caco-2 *in vitro* BBB model are expressed as mean of duplicates, n=3 independent experiments for all test drugs apart from mesoridazine where data are expressed as the mean of duplicates from one independent experiment. Data from the porcine *in vitro* BBB model are expressed as mean of duplicates, n=3 independent experiments for all test drugs.

Figure A5.4 Relationship between Caco-2 and porcine *in vitro* blood-brain barrier model passive permeabilities

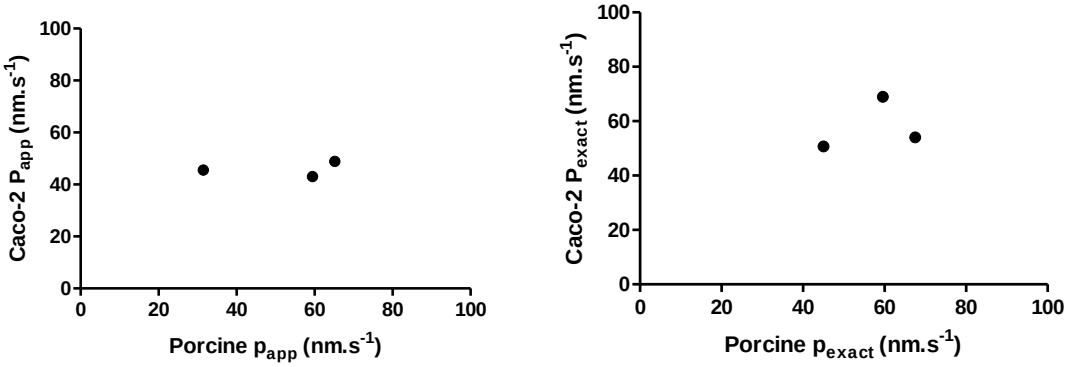

Caco-2 and porcine *in vitro* BBB model A-B passive permeabilities (P_{app} and P_{exact} $nm.s^{-1}$) for amprenavir, chlorpromazine and haloperidol. Studies were carried out with 2 µM of the P-gp inhibitor GF120918. Data from the both Caco-2 and porcine *in vitro* BBB model are expressed as mean of duplicates, n=3 independent experiments for all test drugs.

Figure A5.5 Relationship between Caco-2 and hCMEC/D3 *in vitro* BBB model permeabilities

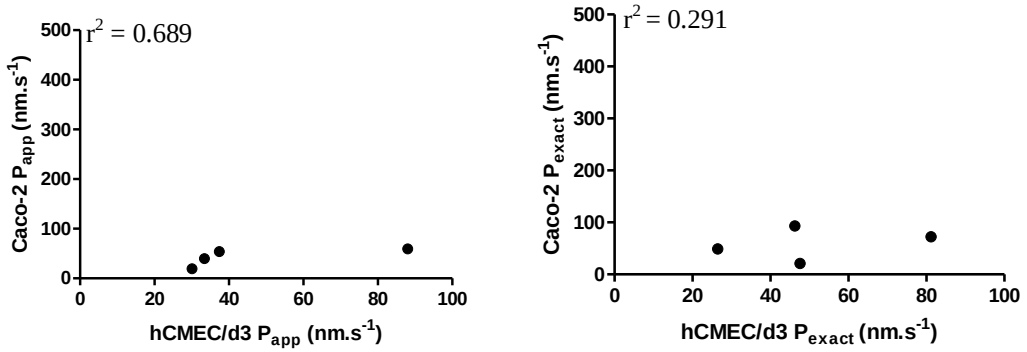

Relationship between Caco-2 and porcine *in vitro* BBB model A-B permeabilities (P_{app} and P_{exact} $nm.s^{-1}$) without the P-gp inhibitor GF120918 for amprenavir, chlorpromazine, haloperidol and mesoridazine. The data from the Caco-2 *in vitro* BBB model are expressed as mean of duplicates, n=3 independent experiments for all test drugs apart from mesoridazine where data are expressed as the mean of duplicates from one independent experiment. Data from the h|CMEC/d3 *in vitro* BBB model are expressed as mean of duplicates, n=3 independent experiments for all test drugs.

Figure A5.6 Relationship between Caco-2 and hCMEC/D3 *in vitro* blood-brain barrier model passive permeabilities

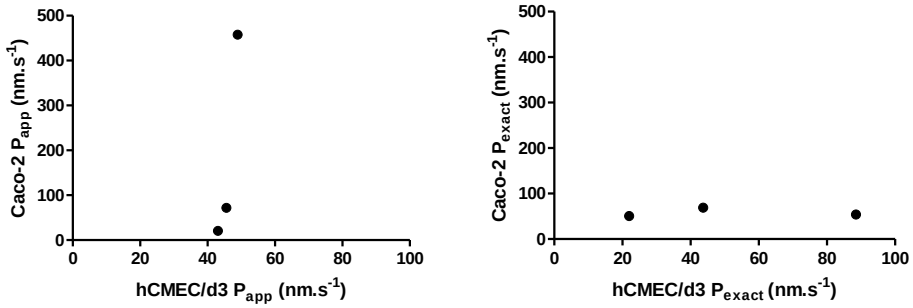

Caco-2 and hCMEC/d3 *in vitro* BBB model A-B passive permeabilities (P_{app} and P_{exact} $nm.s^{-1}$) for amprenavir, chlorpromazine and haloperidol. Studies were carried out with 2 µM of the P-gp inhibitor GF120918. Data from the both Caco-2 and hCMEC/d3 *in vitro* BBB model are expressed as mean of duplicates, n=3 independent experiments for all test drugs.

Figure A5.7 Relationship between Caco-2 and MDR1-MDCKII *in vitro* BBB model permeabilities

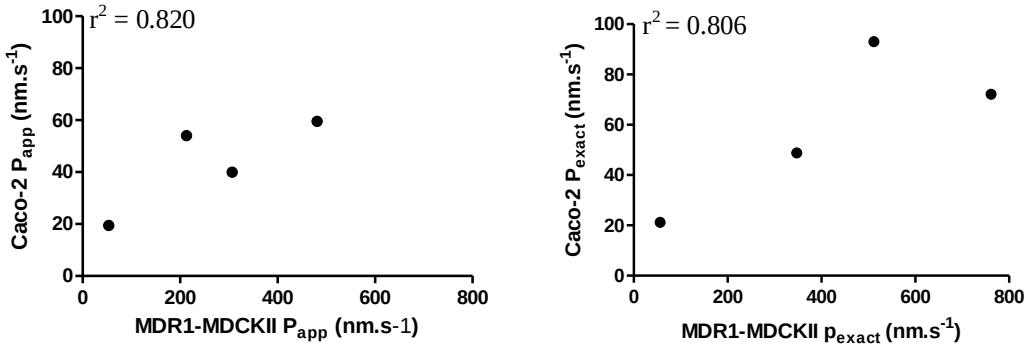

Relationship between Caco-2 and MDR1-MDCKII *in vitro* BBB model A-B permeabilities (P_{app} and P_{exact} $nm.s^{-1}$) without the P-gp inhibitor GF120918 (2 µM) for amprenavir, chlorpromazine, haloperidol and mesoridazine. The data from the Caco-2 *in vitro* BBB model are expressed as mean of duplicates, n=3 independent experiments for all test drugs apart from mesoridazine where data are expressed as the mean of duplicates from one independent experiment. Data from the MDR1-MDCKII *in vitro* BBB model are expressed as mean of duplicates, n=3 independent experiments for all test drugs.

Figure A5.8 Relationship between Caco-2 and MDR1-MDCKII *in vitro* blood-brain barrier model passive permeabilities

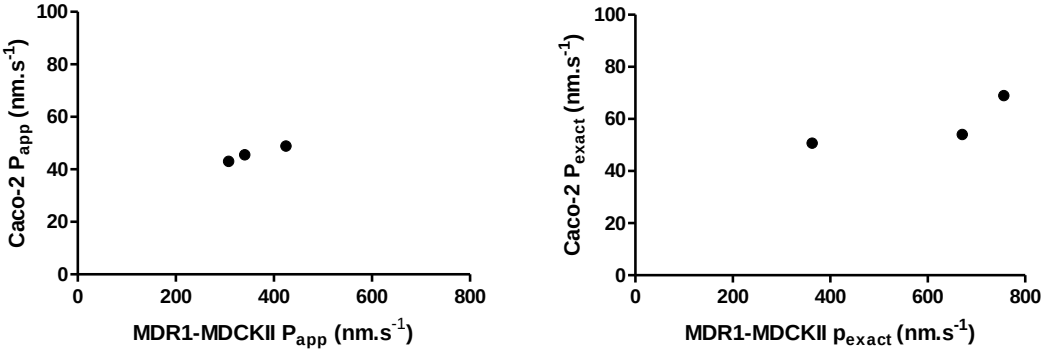

Caco-2 and MDR1-MDCKII *in vitro* BBB model A-B passive permeabilities (P_{app} and P_{exact} $nm.s^{-1}$) for amprenavir, chlorpromazine and haloperidol. Studies were carried out with 2 µM of the P-gp inhibitor GF120918. Data from the both Caco-2 and MDR1-MDCKII *in vitro* BBB model are expressed as mean of duplicates, n=3 independent experiments for all test drugs.

A5.5 Relationship between *in vitro* and *in situ* permeability

Figure A5.9 Relationship between Caco-2 *in vitro* blood-brain barrier permeability and *in sit* rat permeability surface product

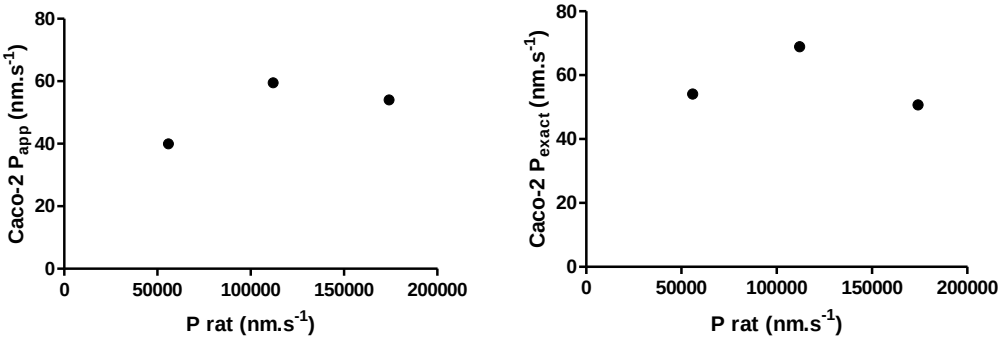

Relationship between *in vitro* A-B permeability (P_{app} and P_{exact} nm.s^{-1}) (Table A5.2 and A5.3) determined using Caco-2 *in vitro* BBB model and *in situ* rat permeability surface product (P nm.s^{-1}) determined using a rat *in situ* brain perfusion model (Table 4.11) for chlorpromazine, haloperidol and mesoridazine.

Appendix 6: Nonspecific Drug Binding Preliminary Studies

A6.1 Nonspecific drug binding-preliminary studies

Table A6.1 **Rat fu_{blood} determined for test drugs at GlaxoSmithKline and The University of Manchester**

Test drug	fu_{blood} GSK	fu_{blood} Manchester
Amprenavir	0.179±0.006	0.178±0.031
Carbamazepine	0.239±0.015	0.197±0.049
Chlorpromazine	0.026±0.002	0.030±0.006
Citalopram	0.227±0.015	0.236±0.049
Clozapine	0.232±0.043	0.127±0.030
Donepezil	0.224±0.017	0.223±0.056
Haloperidol	0.110±0.011	0.087±0.031
Mesoridazine	0.178±0.031	0.222±0.051
Primidone	0.690±0.129	0.636±0.151
Quetiapine	0.160±0.012	0.103±0.005
Risperidone	0.200±0.046	0.153±0.024
Ziprasidone	0.015±0.002	0.017±0.006

Data are expressed as mean ± standard deviation of 6 replicates, n= 1 independent experiment.

Table A6.2 **Rat fu_{brain} determined for test drugs at GlaxoSmithKline and The University of Manchester**

Test drug	fu_{brain} GSK	fu_{brain} Manchester
Amprenavir	0.169±0.019	0.174±0.057
Carbamazepine	0.169±0.021	0.283±0.200
Chlorpromazine	0.003±0.0002	0.002±0.001
Citalopram	0.085±0.014	0.060±0.002
Clozapine	0.012±0.001	0.015±0.004
Donepezil	0.135±0.033	0.139±0.008
Haloperidol	0.021±0.002	0.019±0.004
Mesoridazine	0.046±0.008	0.041±0.022
Primidone	0.634±0.044	0.626±0.044
Quetiapine	0.051±0.008	0.046±0.002
Risperidone	0.116±0.034	0.107±0.019
Ziprasidone	0.016±0.005	0.015±0.006

Data are expressed as mean ± standard deviation of 6 replicates, n= 1 independent experiment.

Appendix 7: Physiologically-Based Pharmacokinetic Model of the Rat Central Nervous System

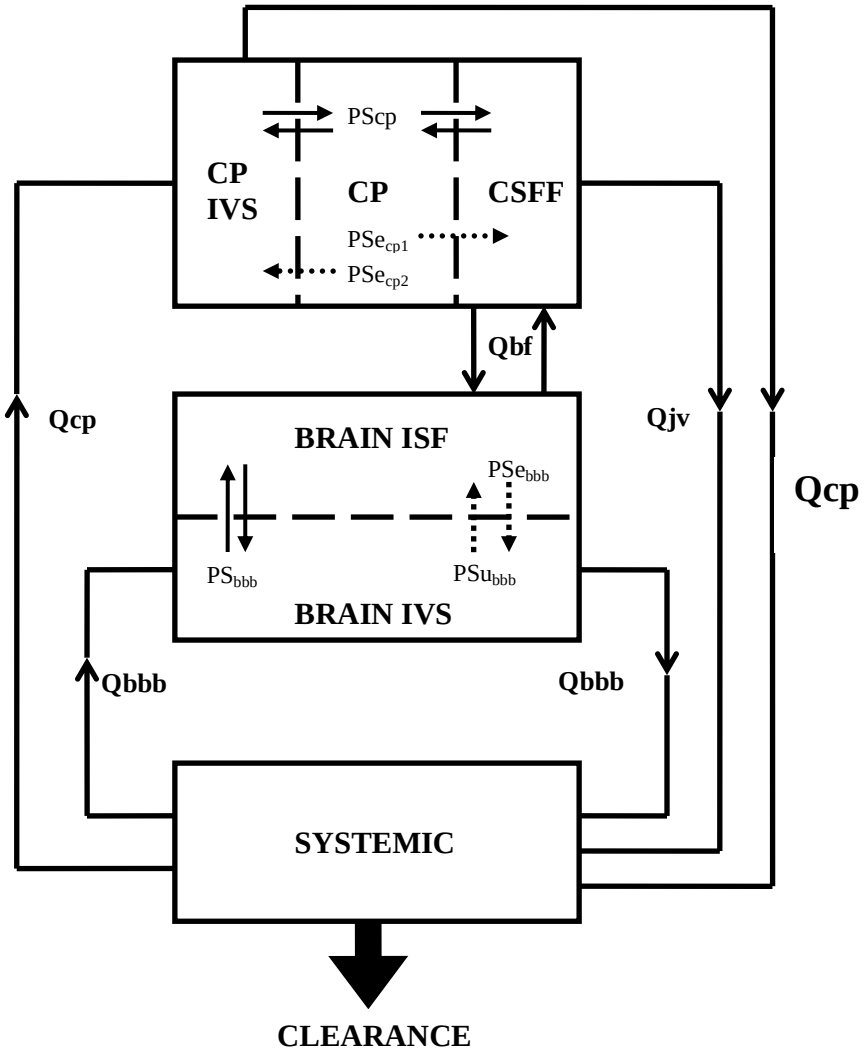

Figure A7.1 **Rat hybrid central nervous system physiologically based pharmacokinetic model**

The rat hybrid central nervous system physiologically based pharmacokinetic model. CP: Choroid plexus epithelium, ISF: intravascular space, ISF: interstitial fluid, PS_{bbb} bi-directional permeability –surface area product for the blood-brain barrier, PSe_{bbb}: permeability-surface area product for efflux at the blood-brain barrier, PS_{cp}: permeability-surface area product for the choroidal epithelium of the choroid plexus, PSe_{cp1}: permeability surface area product for drug efflux into the systemic circulation from the choroidal epithelium of the choroid plexus, PSe_{cp2}: permeability surface area product for drug efflux into the systemic circulation from the choroidal epithelium of the choroid plexus into the CSF, Q_{bbb}: flow through the blood-brain barrier, $Q_{bf:}$ bulk flow of ISF, $Q_{cp:}$ flow through the CP.

References

Abbott, J. N. (2005). "Physiology of the blood-brain barrier and its consequences for drug transport to the brain." International Congress Series **1277**: 3-18.

Abbott, N. J. (2002). "Astrocyte-endothelial interactions and blood-brain barrier permeability." J Anat **200**(6): 629-38.

Abbott, N. J., D. E. Dolman and A. K. Patabendige (2008). "Assays to predict drug permeation across the blood-brain barrier, and distribution to brain." Curr Drug Metab **9**(9): 901-10.

Abbott, N. J., C. C. Hughes, P. A. Revest and J. Greenwood (1992). "Development and characterisation of a rat brain capillary endothelial culture: towards an in vitro blood-brain barrier." J Cell Sci **103 (Pt 1)**: 23-37.

Abbott, N. J., A. A. Patabendige, D. E. Dolman, S. R. Yusof and D. J. Begley (2009). "Structure and function of the blood-brain barrier." Neurobiol Dis **37**(1): 13-25.

Abbott, N. J., L. Ronnback and E. Hansson (2006). "Astrocyte-endothelial interactions at the blood-brain barrier." Nat Rev Neurosci **7**(1): 41-53.

Andlin-Sobocki, P., B. Jonsson, H. U. Wittchen and J. Olesen (2005). "Cost of disorders of the brain in Europe." Eur J Neurol **12 Suppl 1**: 1-27.

Bachmeier, C. J., W. J. Trickler and D. W. Miller (2006). "Comparison of drug efflux transport kinetics in various blood-brain barrier models." Drug Metab Dispos **34**(6): 998-1003.

Ballabh, P., A. Braun and M. Nedergaard (2004). "The blood-brain barrier: an overview: structure, regulation, and clinical implications." Neurobiol Dis **16**(1): 1-13.

Baltes, S., A. M. Gastens, M. Fedrowitz, H. Potschka, V. Kaever and W. Loscher (2007). "Differences in the transport of the antiepileptic drugs phenytoin, levetiracetam and carbamazepine by human and mouse P-glycoprotein." Neuropharmacology **52**(2): 333-46.

Bandopadhyay, R., C. Orte, J. G. Lawrenson, A. R. Reid, S. De Silva and G. Allt (2001). "Contractile proteins in pericytes at the blood-brain and blood-retinal barriers." J Neurocytol **30**(1): 35-44.

Bangsow, T., E. Baumann, C. Bangsow, M. H. Jaeger, B. Pelzer, P. Gruhn, S. Wolf, H. von Melchner and D. B. Stanimirovic (2008). "The epithelial membrane protein 1 is a novel tight junction protein of the blood-brain barrier." J Cereb Blood Flow Metab **28**(6): 1249-60.

Banker, M. J., T. H. Clark and J. A. Williams (2003). "Development and validation of a 96-well equilibrium dialysis apparatus for measuring plasma protein binding." J Pharm Sci **92**(5): 967-74.

Banks, W. A. (1999). "Physiology and pathology of the blood-brain barrier: implications for microbial pathogenesis, drug delivery and neurodegenerative disorders." J Neurovirol **5**(6): 538-55.

Bauer, B., D. S. Miller and G. Fricker (2003). "Compound profiling for P-glycoprotein at the blood-brain barrier using a microplate screening system." Pharm Res **20**(8): 1170-6.

Bauer, F., C. Kuntner, J. P. Bankstahl, T. Wanek, M. Bankstahl, J. Stanek, S. Mairinger, B. Dorner, W. Loscher, M. Muller, T. Erker and O. Langer (2010). "Synthesis and in vivo

evaluation of [11C]tariquidar, a positron emission tomography radiotracer based on a third-generation P-glycoprotein inhibitor." Bioorg Med Chem **18**(15): 5489-97.

Bauer, H. C. and H. Bauer (2000). "Neural induction of the blood-brain barrier: still an enigma." Cell Mol Neurobiol **20**(1): 13-28.

Becker, S. and X. Liu (2006). "Evaluation of the utility of brain slice methods to study brain penetration." Drug Metab Dispos **34**(5): 855-61.

Begley, D. J. (2003). "Understanding and circumventing the blood-brain barrier." Acta Paediatr Suppl **92**(443): 83-91.

Begley, D. J. (2004). "ABC transporters and the blood-brain barrier." Curr Pharm Des **10**(12): 1295-312.

Begley, D. J. (2004). "Delivery of therapeutic agents to the central nervous system: the problems and the possibilities." Pharmacol Ther **104**(1): 29-45.

Begley, D. J. and M. W. Brightman (2003). "Structural and functional aspects of the blood-brain barrier." Prog Drug Res **61**: 39-78.

Bernas, M. J., F. L. Cardoso, S. K. Daley, M. E. Weinand, A. R. Campos, A. J. Ferreira, J. B. Hoying, M. H. Witte, D. Brites, Y. Persidsky, S. H. Ramirez and M. A. Brito (2010). "Establishment of primary cultures of human brain microvascular endothelial cells to provide an in vitro cellular model of the blood-brain barrier." Nat Protoc **5**(7): 1265-72.

Birkett, D. J. (2006). Pharmacokinetics Made Easy. Australia,
Mcgraw-Hill Australia Pty Limited.

Bowman, P. D., S. R. Ennis, K. E. Rarey, A. L. Betz and G. W. Goldstein (1983). "Brain microvessel endothelial cells in tissue culture: a model for study of blood-brain barrier permeability." Ann Neurol **14**(4): 396-402.

Bradford, M. M. (1976). "A rapid and sensitive method for the quantitation of microgram quantities of protein utilizing the principle of protein-dye binding." Anal Biochem **72**: 248-54.

Butt, A. M., H. C. Jones and N. J. Abbott (1990). "Electrical resistance across the blood-brain barrier in anaesthetized rats: a developmental study." J Physiol **429**: 47-62.

Calabria, A. R., C. Weidenfeller, A. R. Jones, H. E. de Vries and E. V. Shusta (2006). "Puromycin-purified rat brain microvascular endothelial cell cultures exhibit improved barrier properties in response to glucocorticoid induction." J Neurochem **97**(4): 922-33.

Cantrill, C. (2009). Interactions of Interleukin-1 receptor antagonist with primary porcine brain endothelial cells. School of Pharmacy and Pharmaceutical Sciences. Manchester, University of Manchester. **PhD:** 175.

Cardoso, F. L., D. Brites and M. A. Brito (2010). "Looking at the blood-brain barrier: molecular anatomy and possible investigation approaches." Brain Res Rev.

Caspers, M. L. and C. A. Diglio (1984). "Expression of gamma-glutamyltranspeptidase in a transformed rat cerebral endothelial cell line." Biochim Biophys Acta **803**(1-2): 1-6.

Cecchelli, R., B. Dehouck, L. Descamps, L. Fenart, V. V. Buee-Scherrer, C. Duhem, S. Lundquist, M. Rentfel, G. Torpier and M. P. Dehouck (1999). "In vitro model for evaluating drug transport across the blood-brain barrier." Adv Drug Deliv Rev **36**(2-3): 165-178.

Cheng, Y. F. and L. K. Paalzow (1992). "Linear pharmacokinetics of haloperidol in the rat." Biopharm Drug Dispos **13**(1): 69-76.

Citi, S., H. Sabanay, R. Jakes, B. Geiger and J. Kendrick-Jones (1988). "Cingulin, a new peripheral component of tight junctions." Nature **333**(6170): 272-6.

Clausen, J. and M. H. Bickel (1993). "Prediction of drug distribution in distribution dialysis and in vivo from binding to tissues and blood." J Pharm Sci **82**(4): 345-9.

Cohen-Kashi Malina, K., I. Cooper and V. I. Teichberg (2009). "Closing the gap between the in-vivo and in-vitro blood-brain barrier tightness." Brain Res **1284**: 12-21.

Cole, S. P., G. Bhardwaj, J. H. Gerlach, J. E. Mackie, C. E. Grant, K. C. Almquist, A. J. Stewart, E. U. Kurz, A. M. Duncan and R. G. Deeley (1992). "Overexpression of a transporter gene in a multidrug-resistant human lung cancer cell line." Science **258**(5088): 1650-4.

Cooray, H. C., C. G. Blackmore, L. Maskell and M. A. Barrand (2002). "Localisation of breast cancer resistance protein in microvessel endothelium of human brain." Neuroreport **13**(16): 2059-63.

Cordon-Cardo, C., J. P. O'Brien, D. Casals, L. Rittman-Grauer, J. L. Biedler, M. R. Melamed and J. R. Bertino (1989). "Multidrug-resistance gene (P-glycoprotein) is expressed by endothelial cells at blood-brain barrier sites." Proc Natl Acad Sci U S A **86**(2): 695-8.

Correale, J. and A. Villa (2009). "Cellular elements of the blood-brain barrier." Neurochem Res **34**(12): 2067-77.

Crone, C. and S. P. Olesen (1982). "Electrical resistance of brain microvascular endothelium." Brain Res **241**(1): 49-55.

Cserr, H. F. and M. Bundgaard (1984). "Blood-brain interfaces in vertebrates: a comparative approach." Am J Physiol **246**(3 Pt 2): R277-88.

Cucullo, L., P. O. Couraud, B. Weksler, I. A. Romero, M. Hossain, E. Rapp and D. Janigro (2008). "Immortalized human brain endothelial cells and flow-based vascular modeling: a marriage of convenience for rational neurovascular studies." J Cereb Blood Flow Metab **28**(2): 312-28.

Culot, M., S. Lundquist, D. Vanuxeem, S. Nion, C. Landry, Y. Delplace, M. P. Dehouck, V. Berezowski, L. Fenart and R. Cecchelli (2008). "An in vitro blood-brain barrier model for high throughput (HTS) toxicological screening." Toxicol In Vitro **22**(3): 799-811.

Cunningham, V. J., R. N. Gunn and J. C. Matthews (2004). "Quantification in positron emission tomography for research in pharmacology and drug development." Nucl Med Commun **25**(7): 643-6.

Cutler, L., C. Howes, N. J. Deeks, T. L. Buck and P. Jeffrey (2006). "Development of a P-glycoprotein knockout model in rodents to define species differences in its functional effect at the blood-brain barrier." J Pharm Sci **95**(9): 1944-53.

Dauchy, S., F. Dutheil, R. J. Weaver, F. Chassoux, C. Daumas-Duport, P. O. Couraud, J. M. Scherrmann, I. De Waziers and X. Decleves (2008). "ABC transporters, cytochromes P450 and their main transcription factors: expression at the human blood-brain barrier." J Neurochem **107**(6): 1518-28.

Dauchy, S., F. Miller, P. O. Couraud, R. J. Weaver, B. Weksler, I. A. Romero, J. M. Scherrmann, I. De Waziers and X. Decleves (2009). "Expression and transcriptional regulation of ABC transporters and cytochromes P450 in hCMEC/D3 human cerebral microvascular endothelial cells." Biochem Pharmacol **77**(5): 897-909.

de Boer, A. G., P. J. Gaillard and D. D. Breimer (1999). "The transference of results between blood-brain barrier cell culture systems." Eur J Pharm Sci **8**(1): 1-4.

De Buck, S. S., V. K. Sinha, L. A. Fenu, R. A. Gilissen, C. E. Mackie and M. J. Nijsen (2007). "The prediction of drug metabolism, tissue distribution, and bioavailability of 50 structurally diverse compounds in rat using mechanism-based absorption, distribution, and metabolism prediction tools." Drug Metab Dispos **35**(4): 649-59.

de Klerk, O. L., A. T. Willemsen, M. Roosink, A. L. Bartels, N. Harry Hendrikse, F. J. Bosker and J. A. den Boer (2009). "Locally increased P-glycoprotein function in major depression: a PET study with [11C]verapamil as a probe for P-glycoprotein function in the blood-brain barrier." Int J Neuropsychopharmacol: 1-10.

de Vries, H. E., J. Kuiper, A. G. de Boer, T. J. Van Berkel and D. D. Breimer (1997). "The blood-brain barrier in neuroinflammatory diseases." Pharmacol Rev **49**(2): 143-55.

Dean, M., Y. Hamon and G. Chimini (2001). "The human ATP-binding cassette (ABC) transporter superfamily." J Lipid Res **42**(7): 1007-17.

DeBault, L. E. and P. A. Cancilla (1980). "gamma-Glutamyl transpeptidase in isolated brain endothelial cells: induction by glial cells in vitro." Science **207**(4431): 653-5.

Dehouck, M. P., S. Meresse, P. Delorme, J. C. Fruchart and R. Cecchelli (1990). "An easier, reproducible, and mass-production method to study the blood-brain barrier in vitro." J Neurochem **54**(5): 1798-801.

Del Bigio, M. R. (1995). "The ependyma: a protective barrier between brain and cerebrospinal fluid." Glia **14**(1): 1-13.

Deli, M. A., C. S. Abraham, Y. Kataoka and M. Niwa (2005). "Permeability studies on in vitro blood-brain barrier models: physiology, pathology, and pharmacology." Cell Mol Neurobiol **25**(1): 59-127.

Demeule, M., A. Regina, J. Jodoin, A. Laplante, C. Dagenais, F. Berthelet, A. Moghrabi and R. Beliveau (2002). "Drug transport to the brain: key roles for the efflux pump P-glycoprotein in the blood-brain barrier." Vascul Pharmacol **38**(6): 339-48.

Doran, A., R. S. Obach, B. J. Smith, N. A. Hosea, S. Becker, E. Callegari, C. Chen, X. Chen, E. Choo, J. Cianfrogna, L. M. Cox, J. P. Gibbs, M. A. Gibbs, H. Hatch, C. E. Hop, I. N. Kasman, J. Laperle, J. Liu, X. Liu, M. Logman, D. Maclin, F. M. Nedza, F. Nelson, E. Olson, S. Rahematpura, D. Raunig, S. Rogers, K. Schmidt, D. K. Spracklin, M. Szewc, M. Troutman, E. Tseng, M. Tu, J. W. Van Deusen, K. Venkatakrishnan, G. Walens, E. Q. Wang, D. Wong, A. S. Yasgar and C. Zhang (2005). "The impact of P-glycoprotein on the disposition of drugs targeted for indications of the central nervous system: evaluation using the MDR1A/1B knockout mouse model." Drug Metab Dispos **33**(1): 165-74.

Dorner, B., C. Kuntner, J. P. Bankstahl, M. Bankstahl, J. Stanek, T. Wanek, G. Stundner, S. Mairinger, W. Loscher, M. Muller, O. Langer and T. Erker (2009). "Synthesis and small-animal positron emission tomography evaluation of [11C]-elacridar as a radiotracer to assess the distribution of P-glycoprotein at the blood-brain barrier." J Med Chem **52**(19): 6073-82.

Doyle, L. A., W. Yang, L. V. Abruzzo, T. Krogmann, Y. Gao, A. K. Rishi and D. D. Ross (1998). "A multidrug resistance transporter from human MCF-7 breast cancer cells." Proc Natl Acad Sci U S A **95**(26): 15665-70.

Durieu-Trautmann, O., N. Foignant-Chaverot, J. Perdomo, P. Gounon, A. D. Strosberg and P. O. Couraud (1991). "Immortalization of brain capillary endothelial cells with maintenance of structural characteristics of the blood-brain barrier endothelium." In Vitro Cell Dev Biol **27A**(10): 771-8.

Easton, A. S. and P. A. Fraser (1994). "Variable restriction of albumin diffusion across inflamed cerebral microvessels of the anaesthetized rat." J Physiol **475**(1): 147-57.

Ederoth, P., K. Tunblad, R. Bouw, C. J. Lundberg, U. Ungerstedt, C. H. Nordstrom and M. Hammarlund-Udenaes (2004). "Blood-brain barrier transport of morphine in patients with severe brain trauma." Br J Clin Pharmacol **57**(4): 427-35.

Ehrlich, P. (1885). "Das sauerstoff-Bedurfnis des Organismus." eine farbenanalyishe Studie.

Ekblom, M., M. Hammarlund-Udenaes, T. Lundqvist and P. Sjoberg (1992). "Potential use of microdialysis in pharmacokinetics: a protein binding study." Pharm Res **9**(1): 155-8.

El-Bacha, R. S. and A. Minn (1999). "Drug metabolizing enzymes in cerebrovascular endothelial cells afford a metabolic protection to the brain." Cell Mol Biol (Noisy-le-grand) **45**(1): 15-23.

El Hafny, B., J. M. Bourre and F. Roux (1996). "Synergistic stimulation of gamma-glutamyl transpeptidase and alkaline phosphatase activities by retinoic acid and astroglial factors in immortalized rat brain microvessel endothelial cells." J Cell Physiol **167**(3): 451-60.

El Hafny, B., O. Chappey, M. Piciotti, M. Debray, B. Boval and F. Roux (1997). "Modulation of P-glycoprotein activity by glial factors and retinoic acid in an immortalized rat brain microvessel endothelial cell line." Neurosci Lett **236**(2): 107-11.

Elsinga, P. H., N. H. Hendrikse, J. Bart, A. van Waarde and W. Vaalburg (2005). "Positron emission tomography studies on binding of central nervous system drugs and P-glycoprotein function in the rodent brain." Mol Imaging Biol **7**(1): 37-44.

Eneroth, A., E. Astrom, J. Hoogstraate, D. Schrenk, S. Conrad, H. M. Kauffmann and K. Gjellan (2001). "Evaluation of a vincristine resistant Caco-2 cell line for use in a calcein AM extrusion screening assay for P-glycoprotein interaction." Eur J Pharm Sci **12**(3): 205-14.

Evans, C. A., L. J. Jolivette, R. Nagilla and K. W. Ward (2006). "Extrapolation of preclinical pharmacokinetics and molecular feature analysis of "discovery-like" molecules to predict human pharmacokinetics." Drug Metab Dispos **34**(7): 1255-65.

Feng, B., J. B. Mills, R. E. Davidson, R. J. Mireles, J. S. Janiszewski, M. D. Troutman and S. M. de Morais (2008). "In vitro P-glycoprotein assays to predict the in vivo interactions of P-glycoprotein with drugs in the central nervous system." Drug Metab Dispos **36**(2): 268-75.

Franke, H., H. Galla and C. T. Beuckmann (2000). "Primary cultures of brain microvessel endothelial cells: a valid and flexible model to study drug transport through the blood-brain barrier in vitro." Brain Res Brain Res Protoc **5**(3): 248-56.

Fredricson Overo, K. (1982). "Kinetics of citalopram in test animals; drug exposure in safety studies." Prog Neuropsychopharmacol Biol Psychiatry **6**(3): 297-309.

Friden, M., F. Ducrozet, B. Middleton, M. Antonsson, U. Bredberg and M. Hammarlund-Udenaes (2009). "Development of a high-throughput brain slice method for studying drug distribution in the central nervous system." Drug Metab Dispos **37**(6): 1226-33.

Friden, M., A. Gupta, M. Antonsson, U. Bredberg and M. Hammarlund-Udenaes (2007). "In vitro methods for estimating unbound drug concentrations in the brain interstitial and intracellular fluids." Drug Metab Dispos **35**(9): 1711-9.

Friden, M., S. Winiwarter, G. Jerndal, O. Bengtsson, H. Wan, U. Bredberg, M. Hammarlund-Udenaes and M. Antonsson (2009). "Structure-brain exposure relationships in rat and human using a novel data set of unbound drug concentrations in brain interstitial and cerebrospinal fluids." J Med Chem **52**(20): 6233-43.

Fu, K., R. J. Konrad, R. W. Hardy, R. M. Brissie and C. A. Robinson (2000). "An unusual multiple drug intoxication case involving citalopram." J Anal Toxicol **24**(7): 648-50.

Furuse, M., K. Fujita, T. Hiiragi, K. Fujimoto and S. Tsukita (1998). "Claudin-1 and -2: novel integral membrane proteins localizing at tight junctions with no sequence similarity to occludin." J Cell Biol **141**(7): 1539-50.

Furuse, M., T. Hirase, M. Itoh, A. Nagafuchi, S. Yonemura, S. Tsukita and S. Tsukita (1993). "Occludin: a novel integral membrane protein localizing at tight junctions." J Cell Biol **123**(6 Pt 2): 1777-88.

Gaillard, P. J., I. C. van der Sandt, L. H. Voorwinden, D. Vu, J. L. Nielsen, A. G. de Boer and D. D. Breimer (2000). "Astrocytes increase the functional expression of P-glycoprotein in an in vitro model of the blood-brain barrier." Pharm Res **17**(10): 1198-205.

Gaillard, P. J., C. C. Visser and A. G. de Boer (2005). "Targeted delivery across the blood-brain barrier." Expert Opin Drug Deliv **2**(2): 299-309.

Gaillard, P. J., L. H. Voorwinden, J. L. Nielsen, A. Ivanov, R. Atsumi, H. Engman, C. Ringbom, A. G. de Boer and D. D. Breimer (2001). "Establishment and functional characterization of an in vitro model of the blood-brain barrier, comprising a co-culture of brain capillary endothelial cells and astrocytes." Eur J Pharm Sci **12**(3): 215-22.

Garberg, P., M. Ball, N. Borg, R. Cecchelli, L. Fenart, R. D. Hurst, T. Lindmark, A. Mabondzo, J. E. Nilsson, T. J. Raub, D. Stanimirovic, T. Terasaki, J. O. Oberg and T. Osterberg (2005). "In vitro models for the blood-brain barrier." Toxicol In Vitro **19**(3): 299-334.

Gershkovich, P., O. Sivak, A. Sharma, A. M. Barr, R. Procyshyn and K. M. Wasan "Effect of hypertriglyceridemia on the pharmacokinetics and blood-brain barrier penetration of clozapine and norclozapine following administration to rats." Eur Neuropsychopharmacol **20**(8): 545-52.

Ghosh, C., J. Gonzalez-Martinez, M. Hossain, L. Cucullo, V. Fazio, D. Janigro and N. Marchi (2010). "Pattern of P450 expression at the human blood-brain barrier: Roles of epileptic condition and laminar flow." Epilepsia.

Goadsby, P. J. (2000). "The pharmacology of headache." Prog Neurobiol **62**(5): 509-25.

Goldmann, E. E. (1913). "vitalfarbung am Zentralnervensystem."

Grosu, A. L. and W. A. Weber (2010). "PET for radiation treatment planning of brain tumours." Radiother Oncol **96**(3): 325-327.

Guarino, A. M., J. B. Anderson, D. K. Starkweather and C. F. Chignell (1973). "Pharmacologic studies of camptothecin (NSC-100880): distribution, plasma protein binding, and biliary excretion." Cancer Chemother Rep **57**(2): 125-40.

Gumbiner, B., T. Lowenkopf and D. Apatira (1991). "Identification of a 160-kDa polypeptide that binds to the tight junction protein ZO-1." Proc Natl Acad Sci U S A **88**(8): 3460-4.

Gumbleton, M. and K. L. Audus (2001). "Progress and limitations in the use of in vitro cell cultures to serve as a permeability screen for the blood-brain barrier." J Pharm Sci **90**(11): 1681-98.

Gupta, A., P. Chatelain, R. Massingham, E. N. Jonsson and M. Hammarlund-Udenaes (2006). "Brain distribution of cetirizine enantiomers: comparison of three different tissue-to-plasma partition coefficients: K(p), K(p,u), and K(p,uu)." Drug Metab Dispos **34**(2): 318-23.

Gupta, A., M. Hammarlund-Udenaes, P. Chatelain, R. Massingham and E. N. Jonsson (2006). "Stereoselective pharmacokinetics of cetirizine in the guinea pig: role of protein binding." Biopharm Drug Dispos **27**(6): 291-7.

Gutmann, H., G. Fricker, M. Torok, S. Michael, C. Beglinger and J. Drewe (1999). "Evidence for different ABC-transporters in Caco-2 cells modulating drug uptake." Pharm Res **16**(3): 402-7.

Gutmann, H., M. Torok, G. Fricker, J. Huwyler, C. Beglinger and J. Drewe (1999). "Modulation of multidrug resistance protein expression in porcine brain capillary endothelial cells in vitro." Drug Metab Dispos **27**(8): 937-41.

Hammarlund-Udenaes, M. (2000). "The use of microdialysis in CNS drug delivery studies. Pharmacokinetic perspectives and results with analgesics and antiepileptics." Adv Drug Deliv Rev **45**(2-3): 283-94.

Hammarlund-Udenaes, M. (2010). "Active-site concentrations of chemicals - are they a better predictor of effect than plasma/organ/tissue concentrations?" Basic Clin Pharmacol Toxicol **106**(3): 215-20.

Hammarlund-Udenaes, M., M. Friden, S. Syvanen and A. Gupta (2008). "On the rate and extent of drug delivery to the brain." Pharm Res **25**(8): 1737-50.

Hammarlund-Udenaes, M., L. K. Paalzow and E. C. de Lange (1997). "Drug equilibration across the blood-brain barrier--pharmacokinetic considerations based on the microdialysis method." Pharm Res **14**(2): 128-34.

Haseloff, R. F., I. E. Blasig, H. C. Bauer and H. Bauer (2005). "In search of the astrocytic factor(s) modulating blood-brain barrier functions in brain capillary endothelial cells in vitro." Cell Mol Neurobiol **25**(1): 25-39.

Haskins, J., L. Gu, E. S. Wittchen, J. Hibbard and B. R. Stevenson (1998). "ZO-3, a novel member of the MAGUK protein family found at the tight junction, interacts with ZO-1 and occludin." J Cell Biol **141**(1): 199-208.

Hellstrom, M., H. Gerhardt, M. Kalen, X. Li, U. Eriksson, H. Wolburg and C. Betsholtz (2001). "Lack of pericytes leads to endothelial hyperplasia and abnormal vascular morphogenesis." J Cell Biol **153**(3): 543-53.

Hilgers, A. R., R. A. Conradi and P. S. Burton (1990). "Caco-2 cell monolayers as a model for drug transport across the intestinal mucosa." Pharm Res **7**(9): 902-10.

Hirohashi, T., H. Suzuki, X. Y. Chu, I. Tamai, A. Tsuji and Y. Sugiyama (2000). "Function and expression of multidrug resistance-associated protein family in human colon adenocarcinoma cells (Caco-2)." J Pharmacol Exp Ther **292**(1): 265-70.

Hoheisel, D., T. Nitz, H. Franke, J. Wegener, A. Hakvoort, T. Tilling and H. J. Galla (1998). "Hydrocortisone reinforces the blood-brain properties in a serum free cell culture system." Biochem Biophys Res Commun **247**(2): 312-5.

Hori, S., S. Ohtsuki, K. Hosoya, E. Nakashima and T. Terasaki (2004). "A pericyte-derived angiopoietin-1 multimeric complex induces occludin gene expression in brain capillary endothelial cells through Tie-2 activation in vitro." J Neurochem **89**(2): 503-13.

Horio, M., K. V. Chin, S. J. Currier, S. Goldenberg, C. Williams, I. Pastan, M. M. Gottesman and J. Handler (1989). "Transepithelial transport of drugs by the multidrug transporter in cultured Madin-Darby canine kidney cell epithelia." J Biol Chem **264**(25): 14880-4.

Houghton, G. W., A. Richens, P. A. Toseland, S. Davidson and Falconer (1975). "Brain concentrations of phenytoin, phenobarbitone and primidone in epileptic patients." Eur J Clin Pharmacol **9**(1): 73-8.

Hughes, H. C. (1986). "Swine in cardiovascular research." Lab Anim Sci **36**(4): 348-50.

Hunter, J., M. A. Jepson, T. Tsuruo, N. L. Simmons and B. H. Hirst (1993). "Functional expression of P-glycoprotein in apical membranes of human intestinal Caco-2 cells. Kinetics of vinblastine secretion and interaction with modulators." J Biol Chem **268**(20): 14991-7.

Igarashi, Y., H. Utsumi, H. Chiba, Y. Yamada-Sasamori, H. Tobioka, Y. Kamimura, K. Furuuchi, Y. Kokai, T. Nakagawa, M. Mori and N. Sawada (1999). "Glial cell line-derived neurotrophic factor induces barrier function of endothelial cells forming the blood-brain barrier." Biochem Biophys Res Commun **261**(1): 108-12.

Janzer, R. C. and M. C. Raff (1987). "Astrocytes induce blood-brain barrier properties in endothelial cells." Nature **325**(6101): 253-7.

Jeffrey, P. and S. Summerfield (2010). "Assessment of the blood-brain barrier in CNS drug discovery." Neurobiol Dis **37**(1): 33-7.

Jeffrey, P. and S. G. Summerfield (2007). "Challenges for blood-brain barrier (BBB) screening." Xenobiotica **37**(10-11): 1135-51.

Joo, F. (1993). "The blood-brain barrier in vitro: the second decade." Neurochem Int **23**(6): 499-521.

Joo, F. and I. Karnushina (1973). "A procedure for the isolation of capillaries from rat brain." Cytobios **8**(29): 41-8.

Juliano, R. L. and V. Ling (1976). "A surface glycoprotein modulating drug permeability in Chinese hamster ovary cell mutants." Biochim Biophys Acta **455**(1): 152-62.

Kacem, K., P. Lacombe, J. Seylaz and G. Bonvento (1998). "Structural organization of the perivascular astrocyte endfeet and their relationship with the endothelial glucose transporter: a confocal microscopy study." Glia **23**(1): 1-10.

Kalaria, R. N. and S. I. Harik (1987). "Blood-brain barrier monoamine oxidase: enzyme characterization in cerebral microvessels and other tissues from six mammalian species, including human." J Neurochem **49**(3): 856-64.

Kalvass, J. C. and T. S. Maurer (2002). "Influence of nonspecific brain and plasma binding on CNS exposure: implications for rational drug discovery." Biopharm Drug Dispos **23**(8): 327-38.

Kalvass, J. C., T. S. Maurer and G. M. Pollack (2007). "Use of plasma and brain unbound fractions to assess the extent of brain distribution of 34 drugs: comparison of unbound concentration ratios to in vivo p-glycoprotein efflux ratios." Drug Metab Dispos **35**(4): 660-6.

Kariv, I., H. Cao and K. R. Oldenburg (2001). "Development of a high throughput equilibrium dialysis method." J Pharm Sci **90**(5): 580-87.

Kartner, N., M. Shales, J. R. Riordan and V. Ling (1983). "Daunorubicin-resistant Chinese hamster ovary cells expressing multidrug resistance and a cell-surface P-glycoprotein." Cancer Res **43**(9): 4413-9.

Katoh, M., N. Suzuyama, T. Takeuchi, S. Yoshitomi, S. Asahi and T. Yokoi (2006). "Kinetic analyses for species differences in P-glycoprotein-mediated drug transport." J Pharm Sci **95**(12): 2673-83.

Kelder, J., P. D. Grootenhuis, D. M. Bayada, L. P. Delbressine and J. P. Ploemen (1999). "Polar molecular surface as a dominating determinant for oral absorption and brain penetration of drugs." Pharm Res **16**(10): 1514-9.

Ketabi-Kiyanvash, N., C. Herold-Mende, F. Kashfi, S. Caldeira, M. Tommasino, W. E. Haefeli and J. Weiss (2007). "NKIM-6, a new immortalized human brain capillary endothelial cell line with conserved endothelial characteristics." Cell Tissue Res **328**(1): 19-29.

Kido, Y., I. Tamai, T. Nakanishi, T. Kagami, I. Hirosawa, Y. Sai and A. Tsuji (2002). "Evaluation of blood-brain barrier transporters by co-culture of brain capillary endothelial cells with astrocytes." Drug Metab Pharmacokinet **17**(1): 34-41.

Kido, Y., I. Tamai, M. Okamoto, F. Suzuki and A. Tsuji (2000). "Functional clarification of MCT1-mediated transport of monocarboxylic acids at the blood-brain barrier using in vitro cultured cells and in vivo BUI studies." Pharm Res **17**(1): 55-62.

Kim, I. W., C. Booth-Genthe and S. V. Ambudkar (2008). "Relationship between drugs and functional activity of various mammalian P-glycoproteins (ABCB1)." Mini Rev Med Chem **8**(3): 193-200.

Kola, I. and J. Landis (2004). "Can the pharmaceutical industry reduce attrition rates?" Nat Rev Drug Discov **3**(8): 711-5.

Kornhuber, J., A. Schultz, J. Wiltfang, I. Meineke, C. H. Gleiter, R. Zochling, K. W. Boissl, F. Leblhuber and P. Riederer (1999). "Persistence of haloperidol in human brain tissue." Am J Psychiatry **156**(6): 885-90.

Kosel, M., M. Amey, A. C. Aubert and P. Baumann (2001). "In vitro metabolism of citalopram by monoamine oxidase B in human blood." Eur Neuropsychopharmacol **11**(1): 75-8.

Kreisl, W. C., J. S. Liow, N. Kimura, N. Seneca, S. S. Zoghbi, C. L. Morse, P. Herscovitch, V. W. Pike and R. B. Innis (2010). "P-glycoprotein function at the blood-brain barrier in humans can be quantified with the substrate radiotracer 11C-N-desmethyl-loperamide." J Nucl Med **51**(4): 559-66.

Kusch-Poddar, M., J. Drewe, I. Fux and H. Gutmann (2005). "Evaluation of the immortalized human brain capillary endothelial cell line BB19 as a human cell culture model for the blood-brain barrier." Brain Res **1064**(1-2): 21-31.

Lauer, R., R. Bauer, B. Linz, F. Pittner, G. A. Peschek, G. Ecker, P. Friedl and C. R. Noe (2004). "Development of an in vitro blood-brain barrier model based on immortalized porcine brain microvascular endothelial cells." Farmaco **59**(2): 133-7.

Lennington, J. B., Z. Yang and J. C. Conover (2003). "Neural stem cells and the regulation of adult neurogenesis." Reprod Biol Endocrinol **1**: 99.

Levin, V. A. (1980). "Relationship of octanol/water partition coefficient and molecular weight to rat brain capillary permeability." J Med Chem **23**(6): 682-4.

Liminga, G., P. Nygren and R. Larsson (1994). "Microfluorometric evaluation of calcein acetoxymethyl ester as a probe for P-glycoprotein-mediated resistance: effects of cyclosporin A and its nonimmunosuppressive analogue SDZ PSC 833." Exp Cell Res **212**(2): 291-6.

Linton, K. J. (2007). "Structure and function of ABC transporters." Physiology (Bethesda) **22**: 122-30.

Liow, J. S., S. Lu, J. A. McCarron, J. Hong, J. L. Musachio, V. W. Pike, R. B. Innis and S. S. Zoghbi (2007). "Effect of a P-glycoprotein inhibitor, Cyclosporin A, on the disposition in rodent brain and blood of the 5-HT1A receptor radioligand, [11C](R)-(-)-RWAY." Synapse **61**(2): 96-105.

Liu, X., C. Chen and B. J. Smith (2008). "Progress in brain penetration evaluation in drug discovery and development." J Pharmacol Exp Ther **325**(2): 349-56.

Liu, X., B. J. Smith, C. Chen, E. Callegari, S. L. Becker, X. Chen, J. Cianfrogna, A. C. Doran, S. D. Doran, J. P. Gibbs, N. Hosea, J. Liu, F. R. Nelson, M. A. Szewc and J. Van Deusen (2005). "Use of a physiologically based pharmacokinetic model to study the time to reach brain equilibrium: an experimental analysis of the role of blood-brain barrier permeability, plasma protein binding, and brain tissue binding." J Pharmacol Exp Ther **313**(3): 1254-62.

Liu, X., M. Tu, R. S. Kelly, C. Chen and B. J. Smith (2004). "Development of a computational approach to predict blood-brain barrier permeability." Drug Metab Dispos **32**(1): 132-9.

Liu, Y., D. A. Peterson, H. Kimura and D. Schubert (1997). "Mechanism of cellular 3-(4,5-dimethylthiazol-2-yl)-2,5-diphenyltetrazolium bromide (MTT) reduction." J Neurochem **69**(2): 581-93.

Liu, Y. H., Y. M. Di, Z. W. Zhou, S. L. Mo and S. F. Zhou (2010). "Multidrug resistance-associated proteins and implications in drug development." Clin Exp Pharmacol Physiol **37**(1): 115-20.

Lundquist, S., M. Renftel, J. Brillault, L. Fenart, R. Cecchelli and M. P. Dehouck (2002). "Prediction of drug transport through the blood-brain barrier in vivo: a comparison between two in vitro cell models." Pharm Res **19**(7): 976-81.

Luo, F. R., P. V. Paranjpe, A. Guo, E. Rubin and P. Sinko (2002). "Intestinal transport of irinotecan in Caco-2 cells and MDCK II cells overexpressing efflux transporters Pgp, cMOAT, and MRP1." Drug Metab Dispos **30**(7): 763-70.

Madgula, V. L., B. Avula, V. L. N. Reddy, I. A. Khan and S. I. Khan (2007). "Transport of decursin and decursinol angelate across Caco-2 and MDR-MDCK cell monolayers: in vitro models for intestinal and blood-brain barrier permeability." Planta Med **73**(4): 330-5.

Mahar Doan, K. M., J. E. Humphreys, L. O. Webster, S. A. Wring, L. J. Shampine, C. J. Serabjit-Singh, K. K. Adkison and J. W. Polli (2002). "Passive permeability and P-glycoprotein-mediated efflux differentiate central nervous system (CNS) and non-CNS marketed drugs." J Pharmacol Exp Ther **303**(3): 1029-37.

Martin-Padura, I., S. Lostaglio, M. Schneemann, L. Williams, M. Romano, P. Fruscella, C. Panzeri, A. Stoppacciaro, L. Ruco, A. Villa, D. Simmons and E. Dejana (1998). "Junctional adhesion molecule, a novel member of the immunoglobulin superfamily that distributes at intercellular junctions and modulates monocyte transmigration." J Cell Biol **142**(1): 117-27.

Maurer, T. S., D. B. Debartolo, D. A. Tess and D. O. Scott (2005). "Relationship between exposure and nonspecific binding of thirty-three central nervous system drugs in mice." Drug Metab Dispos **33**(1): 175-81.

McCarthy, K. D. and J. de Vellis (1980). "Preparation of separate astroglial and oligodendroglial cell cultures from rat cerebral tissue." J Cell Biol **85**(3): 890-902.

Miller, D. S., B. Bauer and A. M. Hartz (2008). "Modulation of P-glycoprotein at the blood-brain barrier: opportunities to improve central nervous system pharmacotherapy." Pharmacol Rev **60**(2): 196-209.

Morselli, P. L., A. Baruzzi, M. Gerna, L. Bossi and M. Porta (1977). "Carbamazepine and carbamazepine-10, 11-epoxide concentrations in human brain." Br J Clin Pharmacol **4**(5): 535-40.

Mosmann, T. (1983). "Rapid colorimetric assay for cellular growth and survival: application to proliferation and cytotoxicity assays." J Immunol Methods **65**(1-2): 55-63.

Muruganandam, A., L. M. Herx, R. Monette, J. P. Durkin and D. B. Stanimirovic (1997). "Development of immortalized human cerebromicrovascular endothelial cell line as an in vitro model of the human blood-brain barrier." Faseb J **11**(13): 1187-97.

Nakagawa, S., M. A. Deli, H. Kawaguchi, T. Shimizudani, T. Shimono, A. Kittel, K. Tanaka and M. Niwa (2009). "A new blood-brain barrier model using primary rat brain endothelial cells, pericytes and astrocytes." Neurochem Int **54**(3-4): 253-63.

Neuhaus, W., V. E. Plattner, M. Wirth, B. Germann, B. Lachmann, F. Gabor and C. R. Noe (2008). "Validation of in vitro cell culture models of the blood-brain barrier: tightness characterization of two promising cell lines." J Pharm Sci **97**(12): 5158-75.

Nitz, T., T. Eisenblatter, K. Psathaki and H. J. Galla (2003). "Serum-derived factors weaken the barrier properties of cultured porcine brain capillary endothelial cells in vitro." Brain Res **981**(1-2): 30-40.

Ohe, T., M. Sato, S. Tanaka, N. Fujino, M. Hata, Y. Shibata, A. Kanatani, T. Fukami, M. Yamazaki, M. Chiba and Y. Ishii (2003). "Effect of P-glycoprotein-mediated efflux on cerebrospinal fluid/plasma concentration ratio." Drug Metab Dispos **31**(10): 1251-4.

Olesen, J. and M. Leonardi (2003). "The burden of brain diseases in Europe." Eur J Neurol **10**(5): 471-7.

Ott, M., G. Fricker and B. Bauer (2009). "Pregnane X receptor (PXR) regulates P-glycoprotein at the blood-brain barrier: functional similarities between pig and human PXR." J Pharmacol Exp Ther **329**(1): 141-9.

Palmer, A. M. (2009). "The role of the blood-CNS barrier in CNS disorders and their treatment." Neurobiol Dis **37**(1): 3-12.

Palmer, A. M. and F. A. Stephenson (2005). "CNS drug discovery: challenges and solutions." Drug News Perspect **18**(1): 51-7.

Pangalos, M. N., L. E. Schechter and O. Hurko (2007). "Drug development for CNS disorders: strategies for balancing risk and reducing attrition." Nat Rev Drug Discov **6**(7): 521-32.

Pardridge, W. M. (1983). "Brain metabolism: a perspective from the blood-brain barrier." Physiol Rev **63**(4): 1481-535.

Pardridge, W. M. (1998). "CNS drug design based on principles of blood-brain barrier transport." J Neurochem **70**(5): 1781-92.

Pardridge, W. M. (2007). "Blood-brain barrier delivery." Drug Discov Today **12**(1-2): 54-61.

Parkinson, F. E. and C. Hacking (2005). "Pericyte abundance affects sucrose permeability in cultures of rat brain microvascular endothelial cells." Brain Res **1049**(1): 8-14.

Pastan, I., M. M. Gottesman, K. Ueda, E. Lovelace, A. V. Rutherford and M. C. Willingham (1988). "A retrovirus carrying an MDR1 cDNA confers multidrug resistance and polarized expression of P-glycoprotein in MDCK cells." Proc Natl Acad Sci U S A **85**(12): 4486-90.

Perriere, N., P. Demeuse, E. Garcia, A. Regina, M. Debray, J. P. Andreux, P. Couvreur, J. M. Scherrmann, J. Temsamani, P. O. Couraud, M. A. Deli and F. Roux (2005).

"Puromycin-based purification of rat brain capillary endothelial cell cultures. Effect on the expression of blood-brain barrier-specific properties." J Neurochem **93**(2): 279-89.

Poller, B., H. Gutmann, S. Krahenbuhl, B. Weksler, I. Romero, P. O. Couraud, G. Tuffin, J. Drewe and J. Huwyler (2008). "The human brain endothelial cell line hCMEC/D3 as a human blood-brain barrier model for drug transport studies." J Neurochem **107**(5): 1358-68.

Polli, J. W., T. M. Baughman, J. E. Humphreys, K. H. Jordan, A. L. Mote, L. O. Webster, R. J. Barnaby, G. Vitulli, L. Bertolotti, K. D. Read and C. J. Serabjit-Singh (2004). "The systemic exposure of an N-methyl-D-aspartate receptor antagonist is limited in mice by the P-glycoprotein and breast cancer resistance protein efflux transporters." Drug Metab Dispos **32**(7): 722-6.

Polli, J. W., J. L. Jarrett, S. D. Studenberg, J. E. Humphreys, S. W. Dennis, K. R. Brouwer and J. L. Woolley (1999). "Role of P-glycoprotein on the CNS disposition of amprenavir (141W94), an HIV protease inhibitor." Pharm Res **16**(8): 1206-12.

Polli, J. W., S. A. Wring, J. E. Humphreys, L. Huang, J. B. Morgan, L. O. Webster and C. S. Serabjit-Singh (2001). "Rational use of in vitro P-glycoprotein assays in drug discovery." J Pharmacol Exp Ther **299**(2): 620-8.

Potschka, H. (2009). "Targeting regulation of ABC efflux transporters in brain diseases: a novel therapeutic approach." Pharmacol Ther **125**(1): 118-27.

Potschka, H., M. Fedrowitz and W. Loscher (2001). "P-glycoprotein and multidrug resistance-associated protein are involved in the regulation of extracellular levels of the major antiepileptic drug carbamazepine in the brain." Neuroreport **12**(16): 3557-60.

Potschka, H., M. Fedrowitz and W. Loscher (2003). "Multidrug resistance protein MRP2 contributes to blood-brain barrier function and restricts antiepileptic drug activity." J Pharmacol Exp Ther **306**(1): 124-31.

Poulin, P. and F. P. Theil (2002). "Prediction of pharmacokinetics prior to in vivo studies. 1. Mechanism-based prediction of volume of distribution." J Pharm Sci **91**(1): 129-56.

Rambeck, B., U. H. Jurgens, T. W. May, H. W. Pannek, F. Behne, A. Ebner, A. Gorji, H. Straub, E. J. Speckmann, B. Pohlmann-Eden and W. Loscher (2006). "Comparison of brain extracellular fluid, brain tissue, cerebrospinal fluid, and serum concentrations of antiepileptic drugs measured intraoperatively in patients with intractable epilepsy." Epilepsia **47**(4): 681-94.

Read, K. D. and S. Braggio (2010). "Assessing brain free fraction in early drug discovery." Expert Opin Drug Metab Toxicol **6**(3): 337-44.

Reese, T. S. and M. J. Karnovsky (1967). "Fine structural localization of a blood-brain barrier to exogenous peroxidase." J Cell Biol **34**(1): 207-17.

Regina, A., A. Koman, M. Piciotti, B. El Hafny, M. S. Center, R. Bergmann, P. O. Couraud and F. Roux (1998). "Mrp1 multidrug resistance-associated protein and P-glycoprotein expression in rat brain microvessel endothelial cells." J Neurochem **71**(2): 705-15.

Regina, A., I. A. Romero, J. Greenwood, P. Adamson, J. M. Bourre, P. O. Couraud and F. Roux (1999). "Dexamethasone regulation of P-glycoprotein activity in an immortalized rat brain endothelial cell line, GPNT." J Neurochem **73**(5): 1954-63.

Reichel, A. (2009). "Addressing central nervous system (CNS) penetration in drug discovery: basics and implications of the evolving new concept." Chem Biodivers **6**(11): 2030-49.

Reichel, A., D. J. Begley and N. J. Abbott (2003). "An overview of in vitro techniques for blood-brain barrier studies." Methods Mol Med **89**: 307-24.

Rodda, K. E. and O. H. Drummer (2006). "The redistribution of selected psychiatric drugs in post-mortem cases." Forensic Sci Int **164**(2-3): 235-9.

Rubin, L. L., D. E. Hall, S. Porter, K. Barbu, C. Cannon, H. C. Horner, M. Janatpour, C. W. Liaw, K. Manning, J. Morales and et al. (1991). "A cell culture model of the blood-brain barrier." J Cell Biol **115**(6): 1725-35.

Ruiu, S., G. Marchese, P. L. Saba, R. Satta, G. Gessa, A. Vaccari and L. Pani (2003). "In vitro evidence for the presence of [3H]-haloperidol uptake in rat brain." Br J Pharmacol **138**(1): 188-92.

Saito, Y. and E. M. Wright (1987). "Regulation of intracellular chloride in bullfrog choroid plexus." Brain Res **417**(2): 267-72.

Sawada, Y., M. Hanano, Y. Sugiyama, H. Harashima and T. Iga (1984). "Prediction of the volumes of distribution of basic drugs in humans based on data from animals." J Pharmacokinet Biopharm **12**(6): 587-96.

Scherrmann, J. M. (2002). "Drug delivery to brain via the blood-brain barrier." Vascul Pharmacol **38**(6): 349-54.

Schinkel, A. H. (1999). "P-Glycoprotein, a gatekeeper in the blood-brain barrier." Adv Drug Deliv Rev **36**(2-3): 179-194.

Schinkel, A. H., U. Mayer, E. Wagenaar, C. A. Mol, L. van Deemter, J. J. Smit, M. A. van der Valk, A. C. Voordouw, H. Spits, O. van Tellingen, J. M. Zijlmans, W. E. Fibbe and P. Borst (1997). "Normal viability and altered pharmacokinetics in mice lacking mdr1-type (drug-transporting) P-glycoproteins." Proc Natl Acad Sci U S A **94**(8): 4028-33.

Shen, D. D., A. A. Artru and K. K. Adkison (2004). "Principles and applicability of CSF sampling for the assessment of CNS drug delivery and pharmacodynamics." Adv Drug Deliv Rev **56**(12): 1825-57.

Simon, G. A. and H. I. Maibach (2000). "The pig as an experimental animal model of percutaneous permeation in man: qualitative and quantitative observations--an overview." Skin Pharmacol Appl Skin Physiol **13**(5): 229-34.

Smith, M., Y. Omidi and M. Gumbleton (2007). "Primary porcine brain microvascular endothelial cells: biochemical and functional characterisation as a model for drug transport and targeting." J Drug Target **15**(4): 253-68.

Smith, M. W. and M. Gumbleton (2006). "Endocytosis at the blood-brain barrier: from basic understanding to drug delivery strategies." J Drug Target **14**(4): 191-214.

Sobue, K., N. Yamamoto, K. Yoneda, M. E. Hodgson, K. Yamashiro, N. Tsuruoka, T. Tsuda, H. Katsuya, Y. Miura, K. Asai and T. Kato (1999). "Induction of blood-brain barrier properties in immortalized bovine brain endothelial cells by astrocytic factors." Neurosci Res **35**(2): 155-64.

Soontornmalai, A., M. L. Vlaming and J. M. Fritschy (2006). "Differential, strain-specific cellular and subcellular distribution of multidrug transporters in murine choroid plexus and blood-brain barrier." Neuroscience **138**(1): 159-69.

Stephan, H., G. Baron and H. D. Frahm (1982). "Comparison of brain structure volumes in Insectivora and Primates. II. Accessory olfactory bulb (AOB)." J Hirnforsch **23**(5): 575-91.

Stewart, P. A. and M. J. Wiley (1981). "Developing nervous tissue induces formation of blood-brain barrier characteristics in invading endothelial cells: a study using quail--chick transplantation chimeras." Dev Biol **84**(1): 183-92.

Summerfield, S. G., A. J. Lucas, R. A. Porter, P. Jeffrey, R. N. Gunn, K. R. Read, A. J. Stevens, A. C. Metcalf, M. C. Osuna, P. J. Kilford, J. Passchier and A. D. Ruffo (2008). "Toward an improved prediction of human in vivo brain penetration." Xenobiotica **38**(12): 1518-35.

Summerfield, S. G., K. Read, D. J. Begley, T. Obradovic, I. J. Hidalgo, S. Coggon, A. V. Lewis, R. A. Porter and P. Jeffrey (2007). "Central nervous system drug disposition: the relationship between in situ brain permeability and brain free fraction." J Pharmacol Exp Ther **322**(1): 205-13.

Summerfield, S. G., A. J. Stevens, L. Cutler, M. del Carmen Osuna, B. Hammond, S. P. Tang, A. Hersey, D. J. Spalding and P. Jeffrey (2006). "Improving the in vitro prediction of in vivo central nervous system penetration: integrating permeability, P-glycoprotein efflux, and free fractions in blood and brain." J Pharmacol Exp Ther **316**(3): 1282-90.

Sun, H., E. C. Chow, S. Liu, Y. Du and K. S. Pang (2008). "The Caco-2 cell monolayer: usefulness and limitations." Expert Opin Drug Metab Toxicol **4**(4): 395-411.

Svendsen, C. N., C. C. Hrbek, M. Casendino, R. D. Nichols and E. D. Bird (1988). "Concentration and distribution of thioridazine and metabolites in schizophrenic post-mortem brain tissue." Psychiatry Res **23**(1): 1-10.

Syvanen, S., O. Lindhe, M. Palner, B. R. Kornum, O. Rahman, B. Langstrom, G. M. Knudsen and M. Hammarlund-Udenaes (2009). "Species differences in blood-brain barrier transport of three positron emission tomography radioligands with emphasis on P-glycoprotein transport." Drug Metab Dispos **37**(3): 635-43.

Takasato, Y., S. I. Rapoport and Q. R. Smith (1984). "An in situ brain perfusion technique to study cerebrovascular transport in the rat." Am J Physiol **247**(3 Pt 2): H484-93.

Tatsuta, T., M. Naito, T. Oh-hara, I. Sugawara and T. Tsuruo (1992). "Functional involvement of P-glycoprotein in blood-brain barrier." J Biol Chem **267**(28): 20383-91.

Thiebaut, F., T. Tsuruo, H. Hamada, M. M. Gottesman, I. Pastan and M. C. Willingham (1989). "Immunohistochemical localization in normal tissues of different epitopes in the multidrug transport protein P170: evidence for localization in brain capillaries and crossreactivity of one antibody with a muscle protein." J Histochem Cytochem **37**(2): 159-64.

Tiberghien, F. and F. Loor (1996). "Ranking of P-glycoprotein substrates and inhibitors by a calcein-AM fluorometry screening assay." Anticancer Drugs **7**(5): 568-78.

Tontsch, U. and H. C. Bauer (1991). "Glial cells and neurons induce blood-brain barrier related enzymes in cultured cerebral endothelial cells." Brain Res **539**(2): 247-53.

Tran, N. D., J. Correale, S. S. Schreiber and M. Fisher (1999). "Transforming growth factor-beta mediates astrocyte-specific regulation of brain endothelial anticoagulant factors." Stroke **30**(8): 1671-8.

Tran, T. T., A. Mittal, T. Gales, B. Maleeff, T. Aldinger, J. W. Polli, A. Ayrton, H. Ellens and J. Bentz (2004). "Exact kinetic analysis of passive transport across a polarized confluent MDCK cell monolayer modeled as a single barrier." J Pharm Sci **93**(8): 2108-23.

Udo, K., S. Aoki, K. Uchihashi, M. Kawasaki, A. Matsunobu, Y. Tokuda, A. Ootani, S. Toda and J. Uozumi (2010). "Adipose tissue explants and MDCK cells reciprocally regulate their morphogenesis in coculture." Kidney Int **78**(1): 60-8.

van de Waterbeemd, H., D. A. Smith and B. C. Jones (2001). "Lipophilicity in PK design: methyl, ethyl, futile." J Comput Aided Mol Des **15**(3): 273-86.

van Waarde, A., N. K. Ramakrishnan, A. A. Rybczynska, P. H. Elsinga, F. Berardi, J. R. de Jong, C. Kwizera, R. Perrone, M. Cantore, J. W. Sijbesma, R. A. Dierckx and N. A. Colabufo (2009). "Synthesis and preclinical evaluation of novel PET probes for P-glycoprotein function and expression." J Med Chem **52**(14): 4524-32.

Veronesi, B. (1996). "Characterization of the MDCK cell line for screening neurotoxicants." Neurotoxicology **17**(2): 433-43.

Vlaming, M. L., J. S. Lagas and A. H. Schinkel (2009). "Physiological and pharmacological roles of ABCG2 (BCRP): recent findings in Abcg2 knockout mice." Adv Drug Deliv Rev **61**(1): 14-25.

Volk, H. A. and W. Loscher (2005). "Multidrug resistance in epilepsy: rats with drug-resistant seizures exhibit enhanced brain expression of P-glycoprotein compared with rats with drug-responsive seizures." Brain **128**(Pt 6): 1358-68.

von Tell, D., A. Armulik and C. Betsholtz (2006). "Pericytes and vascular stability." Exp Cell Res **312**(5): 623-9.

Vorbrodt, A. W. (1989). "Ultracytochemical characterization of anionic sites in the wall of brain capillaries." J Neurocytol **18**(3): 359-68.

Wang, Q., J. D. Rager, K. Weinstein, P. S. Kardos, G. L. Dobson, J. Li and I. J. Hidalgo (2005). "Evaluation of the MDR-MDCK cell line as a permeability screen for the blood-brain barrier." Int J Pharm **288**(2): 349-59.

Ward, P. (2008). "Importance of drug transporters in pharmacokinetics and drug safety." Toxicol Mech Methods **18**(1): 1-10.

Weksler, B. B., E. A. Subileau, N. Perriere, P. Charneau, K. Holloway, M. Leveque, H. Tricoire-Leignel, A. Nicotra, S. Bourdoulous, P. Turowski, D. K. Male, F. Roux, J. Greenwood, I. A. Romero and P. O. Couraud (2005). "Blood-brain barrier-specific properties of a human adult brain endothelial cell line." Faseb J **19**(13): 1872-4.

William B, J., Ed. (1981). Methods in Enzymology. Detoxificcation and Drug Metabolism:Conjugation and Related Systems. New York, Academic Press.

Wolburg, H. and A. Lippoldt (2002). "Tight junctions of the blood-brain barrier: development, composition and regulation." Vascul Pharmacol **38**(6): 323-37.

Xia, C. Q., N. Liu, D. Yang, G. Miwa and L. S. Gan (2005). "Expression, localization, and functional characteristics of breast cancer resistance protein in Caco-2 cells." Drug Metab Dispos **33**(5): 637-43.

Xia, C. Q., G. Xiao, N. Liu, S. Pimprale, L. Fox, C. J. Patten, C. L. Crespi, G. Miwa and L. S. Gan (2006). "Comparison of species differences of P-glycoproteins in beagle dog, rhesus monkey, and human using Atpase activity assays." Mol Pharm **3**(1): 78-86.

Xie, R. and M. Hammarlund-Udenaes (1998). "Blood-brain barrier equilibration of codeine in rats studied with microdialysis." Pharm Res **15**(4): 570-5.

Yamazaki, M., W. E. Neway, T. Ohe, I. Chen, J. F. Rowe, J. H. Hochman, M. Chiba and J. H. Lin (2001). "In vitro substrate identification studies for p-glycoprotein-mediated transport: species difference and predictability of in vivo results." J Pharmacol Exp Ther **296**(3): 723-35.

Yasuno, F., S. S. Zoghbi, J. A. McCarron, J. Hong, M. Ichise, A. K. Brown, R. L. Gladding, J. D. Bacher, V. W. Pike and R. B. Innis (2006). "Quantification of serotonin 5-HT1A receptors in monkey brain with [11C](R)-(-)-RWAY." Synapse **60**(7): 510-20.

Yee, S. (1997). "In vitro permeability across Caco-2 cells (colonic) can predict in vivo (small intestinal) absorption in man--fact or myth." Pharm Res **14**(6): 763-6.

Youdim, K. A., A. Avdeef and N. J. Abbott (2003). "In vitro trans-monolayer permeability calculations: often forgotten assumptions." Drug Discov Today **8**(21): 997-1003.

Zhang, E. Y., G. T. Knipp, S. Ekins and P. W. Swaan (2002). "Structural biology and function of solute transporters: implications for identifying and designing substrates." Drug Metab Rev **34**(4): 709-50.

Zhang, L., Y. D. Zhang, J. M. Strong, K. S. Reynolds and S. M. Huang (2008). "A regulatory viewpoint on transporter-based drug interactions." Xenobiotica **38**(7-8): 709-24.

Zhang, X. Y., F. Yasuno, S. S. Zoghbi, J. S. Liow, J. Hong, J. A. McCarron, V. W. Pike and R. B. Innis (2007). "Quantification of serotonin 5-HT1A receptors in humans with [11C](R)-(-)-RWAY: radiometabolite(s) likely confound brain measurements." Synapse **61**(7): 469-77.

Zhang, Y., C. S. Li, Y. Ye, K. Johnson, J. Poe, S. Johnson, W. Bobrowski, R. Garrido and C. Madhu (2006). "Porcine brain microvessel endothelial cells as an in vitro model to predict in vivo blood-brain barrier permeability." Drug Metab Dispos **34**(11): 1935-43.

Zhou, S. F. (2008). "Structure, function and regulation of P-glycoprotein and its clinical relevance in drug disposition." Xenobiotica **38**(7-8): 802-32.